

CRANFIELD UNIVERSITY

ANDREW MCLEOD

BIOGAS ENHANCEMENT WITH MEMBRANES

SCHOOL OF APPLIED SCIENCES
Cranfield Water Science Institute

PhD
Academic Year: 2010 - 2014

Supervisor: Dr Ewan McAdam & Prof. Bruce Jefferson
April 2014

CRANFIELD UNIVERSITY

SCHOOL OF APPLIED SCIENCES
Cranfield Water Science Institute

PhD

Academic Year 2010 - 2014

ANDREW MCLEOD

Biogas Enhancement with Membranes

Supervisor: Dr Ewan McAdam & Prof. Bruce Jefferson
April 2014

© Cranfield University 2014. All rights reserved. No part of this publication may be reproduced without the written permission of the copyright owner.

Abstract

Biogas is generated during anaerobic digestion (AD) of sewage sludge at wastewater treatment works (WWTW) and consists of approximately 50-70 % methane (CH_4) balanced primarily by carbon dioxide (CO_2). It is commonly used directly as a fuel gas for the renewable generation of electricity on-site by combined heat and power (CHP) engines. However, as a result of governmental incentivisation, biogas possesses a greater value when applied to the national gas grid as a natural gas substitute. However, this requires enhancement of the CH_4 content to that comparable to natural gas by selective removal of CO_2 ; a process known as biogas upgrading.

This thesis explores the potential of hydrophobic micro-porous hollow fibre membrane contactors (HFMCs) to biogas upgrading. HFMCs allow non-dispersive contact between the biogas and a liquid solvent for the preferential absorption of CO_2 , which is conventionally facilitated by packed-column gas scrubbing technology. However, recent gas absorption literature has demonstrated many practical and operational advantages of HFMCs, which suggests they may be effective for biogas upgrading at WWTW.

In this thesis, HFMCs were used to explore the mechanism and controllability of the undesirable co-absorption of CH_4 , known as methane slip. This was found to be attributable to the phase limiting mass transfer, with liquid-limited physical absorption in water exhibited 5.2 % slip whereas gas-limited chemical absorption displayed just 0.1 %. Ammonia-rich wastewaters were investigated as sustainable chemical absorbents using HFMCs and exhibited comparable chemically enhanced absorption to analogue synthetic ammonia solutions. The recovery of the subsequent reaction product (ammonium bicarbonate) by crystallisation facilitated by the membrane was also examined. The potential of this approach was summarised within two hypothetical wastewater flowsheets, where upgrading using a return liquor absorbent acts as a return liquor treatment and where ion exchange allows 100 % application of wastewater derived ammonia to biogas upgrading. These both offered potential economic advantages versus conventional flowsheets with 100 % biogas application to CHP.

Acknowledgements

My gratitude must first be extended to my supervisor Dr. Ewan McAdam for his guidance and encouragement throughout the project and for providing me with the opportunity to develop towards a prospective career in academia. I very much enjoyed our regular tangential discussions about semi-relevant minutia only a fraction of which may be directly found within the thesis. I must also thank my co-supervisor Prof. Bruce Jefferson for directing the thesis towards its full potential whilst consistently maintaining a practical perspective. I thank both Ewan and Bruce for help editing my thesis chapters and unrelenting suggestions for their improvement.

I must extend my gratitude to my sponsors at Anglian Water, Northumbrian Water, Severn Trent Water and Yorkshire Water for their financial support and particularly thank their representatives at my regular meetings: Adam Brookes; Rheanne White, Bernie Glanville and Andrew Moore; Pete Vale; and Liz Wood for their heartening enthusiasm for the project and willingness to let it proceed along its most fruitful path. Thank you also to the Engineering and Physical Sciences Research Council (EPSRC) for their financial support.

I would like to thank all of the technical staff in building 39 for their technical support, in particular Nigel Janes, for all his help with my experimental rigs at the pilot hall and for making that place feel a little bit less dispiriting than it surely is, and Christine Kimpton for her assistance with the microscopy and diffractive analytical techniques. I would like to thank Pompilia Buzatu for her contributions with MATLAB® and Olivier Autin for his help with my surface tension data.

Finally I would like to thank all of my friends and family for their love and support. Cheers to my Mum, Dad, Natalie and Joff in particular, not least for their help with proof reading in the final weeks, my Grandparents for their constant enthusiasm and encouragement and to my uncles Jim Smith and Stephen Staines for their initial advice about careers in wastewater and at Cranfield University respectively. Thanks to Bruce Petrie, Francisco Simões and Ellie Butterworth for their supportive friendship and to anyone else who has pulled on that coveted British Virgin Islands Jersey at the Cranfield World Cup (we was robbed).

List of Figures

Chapter 1.	
Figure 1.1	<i>Schematic of a conventional wastewater treatment works (WWTW) including biogas production directed to combined heat and power (CHP) generation.</i> 1
Figure 1.2	<i>Global biogas upgrading facilities operating a variety of technologies quantified by number of individual plants (a) and by total volumetric flow of raw biogas processed ($\text{m}^3 \text{h}^{-1}$) (b).</i> 2
Figure 1.3	<i>Anticipated flow sheet including a water scrubber receiving secondary effluent as a solvent and retaining CHP only to maintain supply heat to the AD.</i> 3
Figure 1.4	<i>Cross-section of a hydrophobic micro-porous hollow fibre membrane supporting non-dispersive liquid-gas contact for preferential absorption of CO_2 to form a CH_4 enriched biomethane.</i> 5
Figure 1.5	<i>Thesis plan.</i> 9
Chapter 2.	
Figure 2.1	<i>Sketch of gas dissolution. A solvent is expanded to form a cavity to accommodate a solute and solute-solvent interactions are then initiated, where α, μ and H_α / H_δ denote dispersion, polar, and hydrogen bond donor/acceptor interactions respectively.</i> 18
Figure 2.2	<i>Schematic of the equilibria established for a gas solute between the gas phase and the solvent boundary layer, and the solvent boundary layer and the solvent bulk. The dotted line represents the concentration gradient across the phases.</i> 26
Figure 2.3	<i>The contrasting relationships between free energy of cavity formation (G_{cav}, kJ mol^{-1}) and solubility for non-polar and polar gases, and large volatiles (inset) in water.</i> 29
Figure 2.4	<i>Gas solubility in water compared to common organic solvents for non-polar solutions (a) commercial and specialist solvents in non-polar solutions (b) and commercial and specialist solvents in polar solutions (c).</i> 33
Figure 2.5	<i>Negative log-linear correlation of individual gas solubilities in various physical solvents requiring progressively increased work for cavity formation (G_{cav}, kJ mol^{-1}).</i> 34
Figure 2.6	<i>Parity between experimentally derived Henry's constants for several gases in several solvents and corresponding Henry's constants calculated by SPT (Brückl and Kim, 1981).</i> 35
Figure 2.7	<i>Gas diffusivity in solutions with only non-polar solute-solvent interactions (a) and comparison with solutions divergent to the non-polar trend (b).</i> 37
Chapter 3.	
Figure 3.1	<i>Schematic of the experimental set-up used for determining 'slip' from a polypropylene micro-porous hollow fibre membrane contactor.</i> 64

Figure 3.2	<i>Impact of liquid velocity (V_L 0.0054 m s⁻¹ to 0.024 m s⁻¹) with fixed initial gas velocity (V_G 0.0047 m s⁻¹) on CO₂ flux in DI, NaCl, and NaOH solvents (24-26 °C) (a) and impact of V_G (0.0017 m s⁻¹ to 0.031 m s⁻¹) at fixed V_L (0.0089 m s⁻¹) on CO₂ flux in NaOH and NaOH + NaCl solvents (24-26 °C) (b).</i>	68
Figure 3.3	<i>The impact of liquid velocity (V_L 0.0046 m s⁻¹ to 0.024 m s⁻¹) on CH₄ flux in four solvents DI, NaCl, NaOH, and NaOH/NaCl (24-26 °C).</i>	69
Figure 3.4	<i>Influence of hydrodynamic conditions on CO₂ selectivity. Liquid velocity (V_L) varied from 0.0074 m s⁻¹ to 0.024 m s⁻¹ for DI and NaCl solvents and (gas velocity, V_G, fixed to 0.0047 m s⁻¹). For NaOH and NaOH + NaCl, V_G varied between 0.0046 m s⁻¹ and 0.031 m s⁻¹ (V_L fixed at 0.0089 m s⁻¹).</i>	70
Figure 3.5	<i>Methane losses over multiple solvent recirculations using DI or NaOH solvents. Methane losses normalised to CO₂ removed during gas separation. DI water V_L 0.024 m s⁻¹ and V_G 0.0031 m s⁻¹ (L/G 7.7); NaOH solvent V_L 0.032 m s⁻¹ and V_G 0.058 m s⁻¹ (L/G 0.42).</i>	72
Figure 3.6	<i>Outlet gas composition measured during sequential solvent recirculations using DI and NaOH absorption solvents (24-26 °C). V_L 0.024 m s⁻¹ and V_G 0.0031 m s⁻¹ for DI (L/G 7.7) and V_L 0.032 m s⁻¹ and V_G 0.058 m s⁻¹ for NaOH (L/G 0.42).</i>	73
Figure 3.7	<i>Energy and carbon balance based on methane slip during single pass (SP) and multi-pass (MP) solvent recirculation. A net energy gain is determined once solvent is recirculated more than once. Carbon neutrality requires greater than five solvent recirculations based on the modelled hydrodynamic conditions (assumptions 0.52 kg_{CO2} kWh⁻¹; 40 % electrical efficiency).</i>	77

Chapter 4.

Figure 4.1	<i>Schematic of the membrane degas apparatus, including liquid saturation aspirator, sweep gas generation equipment and degassing membrane module (HFMC).</i>	86
Figure 4.2	<i>CH₄ removal efficiency from water saturated by a 75/25 CH₄/CO₂ gas mixture (1 atm, 25 °C) for sweep gas Q_G of increasing orders of magnitude (1.67×10^{-7} m³ s⁻¹ - 1.67×10^{-4} m³ s⁻¹) with variable Q_L (0.017×10^{-5} m³ s⁻¹ - 1.28×10^{-5} m³ s⁻¹) using a HFMC.</i>	90
Figure 4.3	<i>Comparison of experimental CH₄ removal efficiencies at respective values of G/L ratio with removal efficiencies at the 'minimum G/L', determined on the basis of equilibrium obeying Henry's law.</i>	91
Figure 4.4	<i>Impact of variable Q_G (1.67×10^{-7} m³ s⁻¹ to 1.67×10^{-4} m³ s⁻¹) upon out-gas methane purity (% vol. CH₄) at fixed Q_L (0.17×10^{-5} m³ s⁻¹, 0.33×10^{-5} m³ s⁻¹, 0.67×10^{-5} m³ s⁻¹ and 1.23×10^{-5} m³ s⁻¹) (a) and single correlation of out-gas methane purity the respective values of G/L (b).</i>	92

Figure 4.5	<i>Effect of increasing the Reynolds number (Re) in the liquid upon mass transfer of CH_4, represented by Sherwood number (Sh), for Q_G of increasing orders of magnitude ($1.67 \times 10^{-7} \text{ m}^3 \text{ s}^{-1}$ to $1.67 \times 10^{-4} \text{ m}^3 \text{ s}^{-1}$) and comparison with the Sh predicted by the Graetz-L��v��que equation (dashed line).</i>	93
Figure 4.6	<i>Comparison of CH_4 mass transfer (present study) with data adapted for O_2 degas in a micro-porous HFMC (black filled crossed shapes, adapted from Tai et al., 1998) and the Graetz-L��v��que equation (dashed line).</i>	94
Figure 4.7	<i>Wilson plot used to estimate the mass transfer coefficient of the membrane.</i>	95
Figure 4.8	<i>Trade-off between removal efficiency and purity of recovered CH_4.</i>	99
<hr/> Chapter 5. <hr/>		
Figure 5.1	<i>Effect of pH and temperature upon the empirically determined percentage free NH_3, via influence of the NH_4^+ / NH_3 equilibrium, in pure solution.</i>	109
Figure 5.2	<i>Set-up used for gas absorption in a polypropylene micro-porous hollow fibre membrane contactor (a); ion exchange column for removal of ammoniacal nitrogen from raw sewage by clinoptilolite and subsequent production ion exchange regenerant. SP indicates sampling point (b).</i>	111
Figure 5.3	<i>Effect of pH and temperature upon CO_2 flux (J_{CO_2}) in pure NH_3 solutions with concentrations of $10000 \text{ g}_{NH_4-N} \text{ m}^{-3}$ (a), $1000 \text{ g}_{NH_4-N} \text{ m}^{-3}$ (b), $100 \text{ g}_{NH_4-N} \text{ m}^{-3}$ (c) and $10 \text{ g}_{NH_4-N} \text{ m}^{-3}$ (d) under fixed Q_L and Q_G ($1.67 \times 10^{-6} \text{ m}^3 \text{ s}^{-1}$ and $1.25 \times 10^{-5} \text{ m}^3 \text{ s}^{-1}$ respectively).</i>	114
Figure 5.4	<i>Effect of variable gas flow rate (Q_G, 0.05×10^{-5}-$2.8 \times 10^{-5} \text{ m}^3 \text{ s}^{-1}$) upon methane purity in the gas exiting the HFMC (a) and CO_2 flux at a fixed liquid flow rate (Q_L, $6.7 \times 10^{-6} \text{ m}^3 \text{ s}^{-1}$) in synthetic ammonia solutions at four distinct concentrations (10, 100, 5000, & 10000 $\text{g}_{NH_4-N} \text{ m}^{-3}$) (b).</i>	115
Figure 5.5	<i>Effect of variable liquid flow rate (Q_L, 0.17×10^{-5}-$1.7 \times 10^{-5} \text{ m}^3 \text{ s}^{-1}$) upon enhancement factor (E, dimensionless), determined by ratio of CO_2 flux for each distinct NH_3 concentration (10, 100, 1000, & 10000 $\text{g}_{NH_4-N} \text{ m}^{-3}$) against CO_2 flux in DI water.</i>	116
Figure 5.6	<i>Effect of increasing NH_3 concentration upon stripping of NH_3 in to the with fixed liquid and initial gas flow rates (Q_L, $1.67 \times 10^{-6} \text{ m}^3 \text{ s}^{-1}$; Q_G, $1.25 \times 10^{-5} \text{ m}^3 \text{ s}^{-1}$), where the dotted line represents the concentration limit for ammonia in biomethane for gas-to-grid and vehicular use ($0.020 \text{ g}_{NH_3} \text{ m}^{-3}$).</i>	117
Figure 5.7	<i>Effect of variable liquid flow rate (Q_L, 0.17×10^{-5}-$1.7 \times 10^{-5} \text{ m}^3 \text{ s}^{-1}$) upon enhancement factor (E, dimensionless), determined by ratio of CO_2 flux for return liquor and IEX regenerant ($2325 \text{ g}_{NH_4-N} \text{ m}^{-3}$ and $477 \text{ g}_{NH_4-N} \text{ m}^{-3}$ respectively) against CO_2 flux in DI water</i>	118

(a) and parity between enhancement determined for return liquor and IEX regenerant that expected for like synthetic NH_3 solutions (b).

Chapter 6.

Figure 6.1	<i>Operational mechanism of a membrane crystalliser through removal of solvent vapour to induce supersaturation (a) and proposed novel mechanism with supersaturation induced by rapid reaction of the solvent with absorbed gas (CO_2) (b).</i>	140
Figure 6.2	<i>Schematic of experimental apparatus.</i>	143
Figure 6.3	<i>Pore structure analysis of the PTFE hollow fibre membrane used: Stretched pore geometry illustrated using SEM (2000x) (a) and statistical determination of pore radius using log-normal distribution (b).</i>	145
Figure 6.4	<i>Effect of variable gas velocity (V_G) upon CO_2 removal efficiency and CO_2 flux, during absorption from a 50:50 CO_2:CH_4 gas mixture using $7 \text{ mol}_{\text{NH}_3} \text{ L}^{-1}$ aqueous solution at fixed liquid velocity (V_L, 0.02 m s^{-1}) in a single fibre PTFE HFMC. Error bars indicate standard error.</i>	146
Figure 6.5	<i>SEM surface analysis of: the virgin PTFE hollow fibre membrane surface (x5000) (a); and nucleation of ABC crystals is observed at the membrane-absorbent interface (shell-side) following CO_2 absorption using a $7 \text{ mol}_{\text{NH}_3} \text{ L}^{-1}$ ammonia solution in single pass operation (x5000) (b). Sample in image (b) observed at higher magnification (x10000) (c).</i>	147
Figure 6.6	<i>CO_2 flux observed with the PTFE membrane following NH_3 solvent recirculation (2 M, 3 M and 5 M) through the shell-side. Hydrodynamic conditions: G/L 10; V_G 0.93 m s^{-1}; V_L 0.02 m s^{-1}. Lumen-side blockage observed for 3 M and 5 M solutions. Error bars indicate standard error.</i>	148
Figure 6.7	<i>Dissected section of the PTFE hollow fibre membrane used for 5 M NH_3 absorbent recirculation. The experiment was stopped after 6 recirculations due to gas-side blockage. SEM analysis shows formation of ABC. Hydrodynamic conditions: G/L 10; V_G 0.93 m s^{-1}; V_L 0.02 m s^{-1}.</i>	148
Figure 6.8	<i>CO_2 flux observed with the nonporous PDMS hollow fibre membrane using 5 M NH_3 solvent recirculated through the module shell-side. Gas-side (lumen side) blockage noted following 800 solvent recirculations. Hydrodynamic conditions: G/L 0.4; V_L 0.1 m s^{-1}. Error bars indicate standard error.</i>	150
Figure 6.9	<i>Nonporous PDMS hollow fibre membrane following >800 recirculations of 5 M NH_3 absorbent: crystals formed inside the fibre lumen (a); an example crystal formed on the outside of the fibre (b) and the PDMS fibre dissected reveals crystals formed within the fibre lumen (c).</i>	151

Figure 6.10	<i>Impact of sodium chloride (5 % wt.) and glycerol (1 % wt.) on CO₂ flux when used as additives to 3 M NH₃ absorbent recirculated through the module shell-side. Hydrodynamic conditions: G/L 10; V_G 0.93 m s⁻¹; V_L 0.02 m s⁻¹.</i>	152
Figure 6.11	<i>Changes in surface tension relative to deionised water driven by aqueous ammonia and sodium chloride solute concentration within the concentration range examined (NH₃, 2-7 M; NaCl 5 % wt. or 0.85 M) (Weissenborn and Pugh, 1995).</i>	153
Figure 6.12	<i>Impact of liquid-surface contact angle on the thermodynamic favourability of heterogeneous vs. homogeneous nucleation calculated for the non-porous PDMS membrane and PTFE micro-porous membrane used (Appendix, A1).</i>	154
Figure 6.13	<i>An illustration of NH₃ depletion by chemical reaction with CO₂, where volatile free ammonia concentration at the interface with the gas is exceptionally low across the membrane length (z) due to rapid reaction, thereby inhibiting NH₃ volatilisation in to the gas phase.</i>	156

Chapter 7.

Figure 7.1	<i>Breakdown of several key capital and operational expenditures and monetary gains associated with a conventional WWTW with 100 % biogas application to CHP, and hypothetical WWTW with 13 % biogas applied to upgrading for return liquor treatment and 100 % applied to upgrading necessitating investment in ion exchange technology.</i>	178
------------	---	-----

List of Tables

Chapter 2.

Table 2.1	<i>Parameters determining solvent classification and for practical use as physical absorbents.</i>	21
Table 2.2a	<i>Operational characteristics, mass transfer performance and removal efficiencies for physical absorption processes using column-type contactors.</i>	23
Table 2.2b	<i>Operational characteristics, mass transfer performance and removal efficiencies for physical absorption processes using hollow fibre membrane contactors.</i>	25
Table 2.3	<i>Equilibrium constants for gases ostensibly physically absorbed in water.</i>	31
Table 2.A1a	<i>Scaled particle theory gas solute parameters.</i>	46
Table 2.A1b	<i>Scaled particle theory solvent parameters.</i>	47
Table 2.A2	<i>Solubility and diffusivity references for figures not included within the text.</i>	48

Chapter 3.

Table 3.1	<i>Methane slip in DI, NaCl, NaOH, and NaOH + NaCl solvents (24-26 °C) under conditions affording an output gas composition of 85 % CH₄.</i>	71
-----------	---	----

Chapter 4.		
Table 4.1	<i>Water solubility (mole fraction), dimensionless Henry's constant and diffusivity for O₂ and CH₄ in water and respective molecular size.</i>	84
Table 4.2	<i>Individual mass transfer coefficients for variable magnitudes of Q_G at fixed Q_L.</i>	95
Chapter 5.		
Table 5.1	<i>Scanning electron microscope (SEM) and energy dispersive X-ray (EDX) spectra of NH₄HCO₃ formed in situ by bubbling gas through bulk solvent and by nucleation on the membrane surface (a & b respectively), in situ CaCO₃ from IEX regenerant (c), and NaHCO₃ from dehydration of return liquor saturated by CO₂ (d).</i>	120
Table 5.2	<i>Characterisation of raw wastewater matrices and subsequently derived absorbents.</i>	124
Table 5.3	<i>Molecular masses and pure water solubilities of several binary carbonate and bicarbonate salts.</i>	126
Table 5.4	<i>Operational costs and net benefit of several scenarios versus the current baseline case with 100 % NH₄-N by nitrification and 100 % biogas to CHP.</i>	127
Table 5.A1	<i>Values and assumptions used for cost calculations.</i>	131
Chapter 6.		
Table 6.1	<i>Dimensions and surface characteristics of the single membrane fibres.</i>	142
Table 6.2	<i>SEM images and EDX analyses of ammonium bicarbonate crystals grown on the PTFE membrane at the membrane-absorbent interface (shell-side) during recirculation of aqueous ammonia absorbents ranging 2 to 5 mol_{NH3} L⁻¹ in concentration.</i>	149
Chapter 7.		
Table 7.1	<i>Typical specific surface areas for several liquid-gas contactors (adapted from Reed et al., 2003).</i>	169
Table 7.2	<i>Mass transfer and G/L data for CO₂ absorption by water in HFMCs and packed columns.</i>	170
Table 7.3	<i>Total costs for known return liquor treatments compared to the potential gain by using ABC recovery.</i>	177

Abbreviations

ABC	Ammonium bicarbonate	PTFE	Polytetrafluoroethylene
atm	atmospheres	PVDF	Polyvinylidene fluoride
BV	Bed volumes	<i>Re</i>	Reynolds number
BV h ⁻¹	Bed volumes per hour	RHI	Renewable heat incentive
cal	calories	SAR	Surface aeration reactor
CAPEX	Capital expenditure	<i>Sc</i>	Schmidt number
CCS	Carbon capture and storage	SEM	Scanning electron microscopy
CHP	Combined heat and power	<i>Sh</i>	Sherwood number
CV	Calorific value	SP	Single pass
DI	De-ionised	SPT	Scaled particle theory
EDX	Energy dispersive spectroscopy	STP	Standard temperature and pressure
GC	Gas chromatography	TCD	Thermal conductivity detector
GHG	Greenhouse gas	wt.	weight
GIR	Gas induction reactor	WWTW	Wastewater treatment works
G/L	Gas to liquid ratio	XRD	x-ray diffraction
<i>Gz</i>	Graetz number		
HFMC	Hollow fibre membrane contactor		
ID	Outer diameter		
kJ	Kilo Joules		
kWh	kilowatt hour		
L/G	Liquid to gas ratio		
L-J	Lennard Jones		
MJ	Mega Joules		
mol	moles		
MP	Multi-pass		
MS	Mass spectrometry		
OD	Inner diameter		
NO _x	Any nitrogen oxide gas		
OPEX	Operational expenditure		
PDMS	polydimethylsiloxane		
PP	Polypropylene		
ppmv	Parts per million by volume		
PSA	Pressure swing adsorption		

Chemical formulae

NaCl	Sodium chloride
NaOH	Sodium hydroxide
BaCl ₂	Barium chloride
NH ₄ HCO ₃	Ammonium bicarbonate
CaCO ₃	Calcium carbonate
NaHCO ₃	Sodium bicarbonate
α -Al ₂ O ₃	Ceramic membrane
HOCl	Hypochlorous acid
H ₂ SO ₄	Sulfuric acid
HCl	Hydrochloric acid
H ₂ CO ₃	Carbonic acid
HNO ₃	Nitric acid

Cations

H ⁺	Hydron
Na ⁺	Sodium
Ca ²⁺	Calcium
NH ₄ ⁺	Ammonium

Anions

OH ⁻	Hydroxide
Cl ⁻	chloride
HS ⁻	bisulfide
HSO ₃ ⁻	bisulfite
HCO ₃ ⁻	bicarbonate
CO ₃ ²⁻	carbonate

Gases

H ₂	Hydrogen
H ₂ O	Water
CH ₄	Methane
N ₂	Nitrogen
C ₂ H ₆	Ethane
O ₂	Oxygen
C ₃ H ₈	Propane
<i>n</i> -C ₄ H ₁₀	<i>n</i> -Butane
NH ₃	Ammonia
C ₂ H ₂	Acetylene
CO	Carbon monoxide
C ₂ H ₄	Ethylene
NO	Nitric oxide
H ₂ S	Hydrogen sulfide
CO ₂	Carbon dioxide
N ₂ O	Nitrous oxide
SO ₂	Sulfur dioxide
Cl ₂	Chlorine
He	Helium
Ne	Neon
Ar	Argon
Kr	Krypton
Xe	Xenon
Rn	Radon
L2	Hexamethyldisiloxane
L3	Octamethyltrisiloxane
L4	Decamethyltetrasiloxane
D3	Hexamethylcyclotrisiloxane
D4	Octamethylcyclotetrasiloxane
D5	Decamethylcyclopentasiloxane
C2	Ethane
C6	Hexane

Solvents

[BMIM][PF ₆]	1-butyl-3-methyl-imidazolium hexafluoro-phosphate
[EMIM][EtSO ₄]	1-ethyl-3-methyl-imidazolium ethyl-sulfate
PEG	polyethylene glycol
NMP	<i>N</i> -methyl-2-pyrrolidone
C5	<i>n</i> -pentane
C7	<i>n</i> -heptane
C9	<i>n</i> -nonane
C10	<i>n</i> -decane
C12	<i>n</i> -dodecane

Greek symbols

α	Polarizability	cm ³
γ	Surface tension	mN m ⁻¹
ε	Lennard-Jones energy parameter	erg
θ	Contact angle / packing fraction	° / -
μ	Dipole moment / dynamic viscosity	Debyes / mPa s
ρ	Mass density	g cm ³
σ	Lennard-Jones size parameter	cm
Ω	Electrical resistance	Volts per amp

Notation

a	Specific surface area	m ² m ⁻³
A_m	Membrane surface area	m ²
C	Celsius	
d_h	Characteristic length	m
D	Diffusivity	m ² s ⁻¹
E	Enhancement factor	-
G	Gibb's free energy	kJ mol ⁻¹
G_{cav}	Free energy of cavity formation	cal mol ⁻¹ / kJ mol ⁻¹
G_{int}	Free energy of interaction	cal mol ⁻¹ / kJ mol ⁻¹
H	Enthalpy	kJ mol ⁻¹
H	Henry's constant (dimensionless)	-

H_{α}	Hydrogen bond donating parameter	-
H_{β}	Hydrogen bond accepting parameter	-
J	Joules	
J	Flux	$\text{mol m}^{-2} \text{s}^{-1}$
k	Boltzmann constant	$\text{J K}^{-1} / \text{erg K}^{-1}$
k_G	Gas mass transfer coefficient	m s^{-1}
k_H	Henry's constant	$\text{mol L}^{-1} \text{atm}^{-1} / \text{atm}$
k_L	Liquid mass transfer coefficient	m s^{-1}
k_m	Membrane mass transfer coefficient	m s^{-1}
K	Kelvin	
L	Litre / contactor length	
M_r	Relative molecular mass	g mol^{-1}
n	Normal (straight chain) alkane	
N	Newton	
N	Avogadro's number	
P	Pressure / Permeability	Bar / Barrers
P_{vap}	Vapour pressure	Bar
P_g	Partial pressure	atm
Q_G	Gas flow rate	$\text{m}^3 \text{s}^{-1}$
Q_L	Liquid flow rate	$\text{m}^3 \text{s}^{-1}$
R	Molar gas constant	$\text{m}^3 \text{Pa K}^{-1} \text{mol}^{-1} / \text{cal K}^{-1} \text{mol}^{-1}$
S	Entropy / Solubility coefficient	$\text{J K}^{-1} \text{mol}^{-1} / \text{cm}^3 (\text{STP}) \text{cm}^{-3} \text{cmHg}$
T	Temperature	$^{\circ}\text{C} / \text{K}$
V_G	Gas velocity	m s^{-1}
V_L	Liquid velocity	m s^{-1}
V_m	Molar volume	$\text{cm}^3 \text{mol}^{-1}$
x	Mole fraction	-

Table of contents

Abstract	i
Acknowledgements	ii
List of Figures	iii
List of Tables	vii
Abbreviations and notations	ix
Chapter 1. Introduction	1
1.1 Project background	1
1.2 Project development	4
1.3 Hypothesis	6
1.4 Aims and objectives	7
1.5 Thesis structure	7
Chapter 2. A framework to identify physical solvents for gas separations in environmental gas-liquid absorption applications	13
2.1 Introduction	14
2.2 A physical description of dissolved gas within a solvent	17
2.3 A review of published literature on physical absorption for environmental applications	22
2.4 The role of solvent and solute physical chemistry on solubility and diffusivity	28
2.4.1. <i>Dissolution of gas within a water solvent</i>	28
2.4.2. <i>Comparison of solubility in water and organic solvents</i>	32
2.4.3. <i>Extension of G_{cav} analysis for the prediction of Henry's constants</i>	35
2.4.4. <i>Influence of solvent selection on gas solute diffusivity</i>	36
2.5 Discussion	37
2.6 Conclusions	43
Appendix	43
Chapter 3. Quantifying the loss of methane through secondary gas mass transport (or 'slip') from a micro-porous membrane contactor applied to biogas upgrading	61
3.1 Introduction	62
3.2 Materials and methods	64
3.2.1. <i>Equipment setup and operation</i>	64
3.2.2. <i>Preparation and sampling</i>	65
3.2.3. <i>Analysis</i>	67
3.3 Results	67
3.3.1. <i>Impact of solvent chemistry on biogas component flux</i>	67

3.3.2.	<i>Application of solvent recirculation to minimise slip</i>	71
3.4	Discussion	73
3.5	Conclusions	77
Chapter 4. Removal of dissolved methane from aqueous solution using a micro-porous hollow fibre membrane contactor (HFMC)		83
4.1	Introduction	84
4.2	Materials and methods	86
4.2.1.	<i>Equipment setup and operation</i>	86
4.2.2.	<i>Sampling and analysis</i>	87
4.2.3.	<i>Mass transfer and minimum G/L calculations</i>	88
4.3	Results	89
4.3.1.	<i>Removal of dissolved CH₄</i>	89
4.3.2.	<i>Purity of recovered CH₄</i>	91
4.3.3.	<i>CH₄ mass transfer</i>	93
4.4	Discussion	93
4.5	Conclusions	101
Chapter 5. Biogas upgrading by chemical absorption using ammonia rich absorbents derived from wastewater		107
5.1	Introduction	108
5.2	Materials and methods	110
5.2.1.	<i>Equipment setup and operation</i>	110
5.2.2.	<i>Chemical preparation, sampling and analysis</i>	112
5.3	Results	113
5.3.1.	<i>Assessment of CO₂ absorption using analogue ammonia absorbents</i>	113
5.3.2.	<i>Measurement of ammonia volatility within process boundary conditions</i>	117
5.3.3.	<i>Efficacy of real ammonia rich wastewaters to deliver enhanced CO₂ absorption</i>	118
5.3.4.	<i>Identifying the products formed in real solutions</i>	119
5.4	Discussion	121
5.5	Conclusions	129
	Appendix	130
Chapter 6. Controlling shell-side crystal nucleation in a gas-liquid membrane contactor for simultaneous ammonium bicarbonate recovery and biogas upgrading		138
6.1	Introduction	140
6.2	Experimental	143

6.2.1.	<i>Fabrication, setup and operation of equipment</i>	143
6.2.2.	<i>Sampling and analyses</i>	145
6.3	Results	146
6.3.1.	<i>Characterisation of the PTFE and PDMS membranes</i>	146
6.3.2.	<i>Removal of CO₂ using NH₃ as a chemical absorbent</i>	147
6.3.3.	<i>Identification of heterogeneous crystal growth</i>	148
6.3.4.	<i>Using membrane type to control lumen-side crystallisation</i>	151
6.3.5.	<i>Manipulating solvent chemistry to promote shell-side nucleation on PTFE fibres</i>	152
6.4	Discussion	154
6.5	Conclusions	159
	Appendix A	161
	Appendix B	161
	Chapter 7. Discussion	169
7.1	Discussion	169
	Chapter 8. Conclusions and further work	185
8.1	Conclusions	186
8.2	Further work	187

Chapter 1

Introduction

1. Introduction

1.1 Project background

Anaerobic digestion (AD) is used as a method for stabilising the organic solids generated during wastewater treatment to allow safe disposal (e.g. to land) and biogas is produced as a result of the breakdown of this organic matter by various microbial processes. Biogas is a 50:50 – 75:25 mixture of methane (CH_4) and carbon dioxide (CO_2) gases respectively, with additional hydrogen sulfide (H_2S) and volatile siloxane polymer trace components. It is produced during AD at wastewater treatment works (WWTW). Historically the biogas was emitted or flared without utilising its energetic value; however biogas is presently directed towards combined heat and power (CHP) that generates electricity on-site to the WWTW whilst providing heat to maintain the operation of the AD (Figure 1.1).

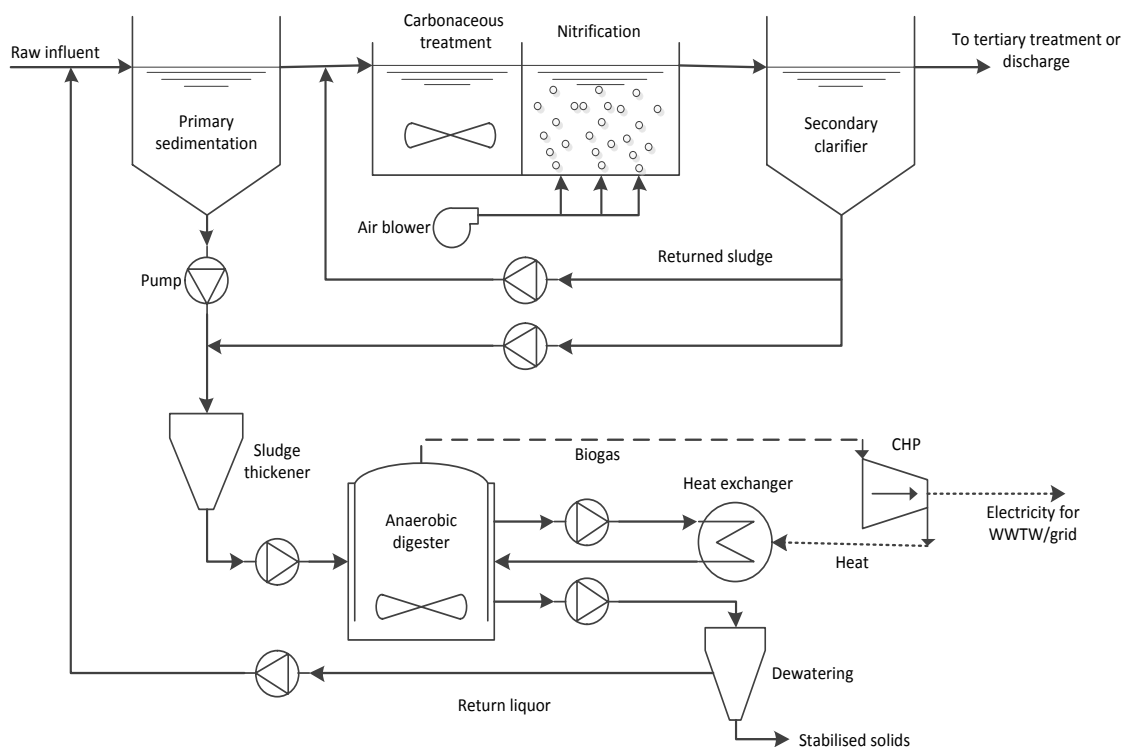


Figure 1.1 Schematic of a conventional wastewater treatment works (WWTW) including biogas production directed to combined heat and power (CHP) generation.

CHP engines are designed to operate efficiently at the moderate CO₂ content of biogas, requiring only removal of the trace components prior to combustion. However the CH₄ content of the biogas can be upgraded by removal of the CO₂ component, allowing the gas to be applied to the national gas grid as a natural gas substitute, known as biomethane. Currently in the UK incentivisation schemes place a greater value upon biogas directed towards the gas grid as biomethane (0.49 £ m⁻³) compared to biogas used for electricity generation by CHP (0.14 £ m⁻³), which has increased the interest of Water utilities towards biogas upgrading due to its greater profitability (Read and Hofmann, 2011).

There are several established biogas upgrading technologies, including pressure swing adsorption (PSA), cryogenic separation and separation by a selective dense, permeable membrane (Figure 1.2a and 1.2b).

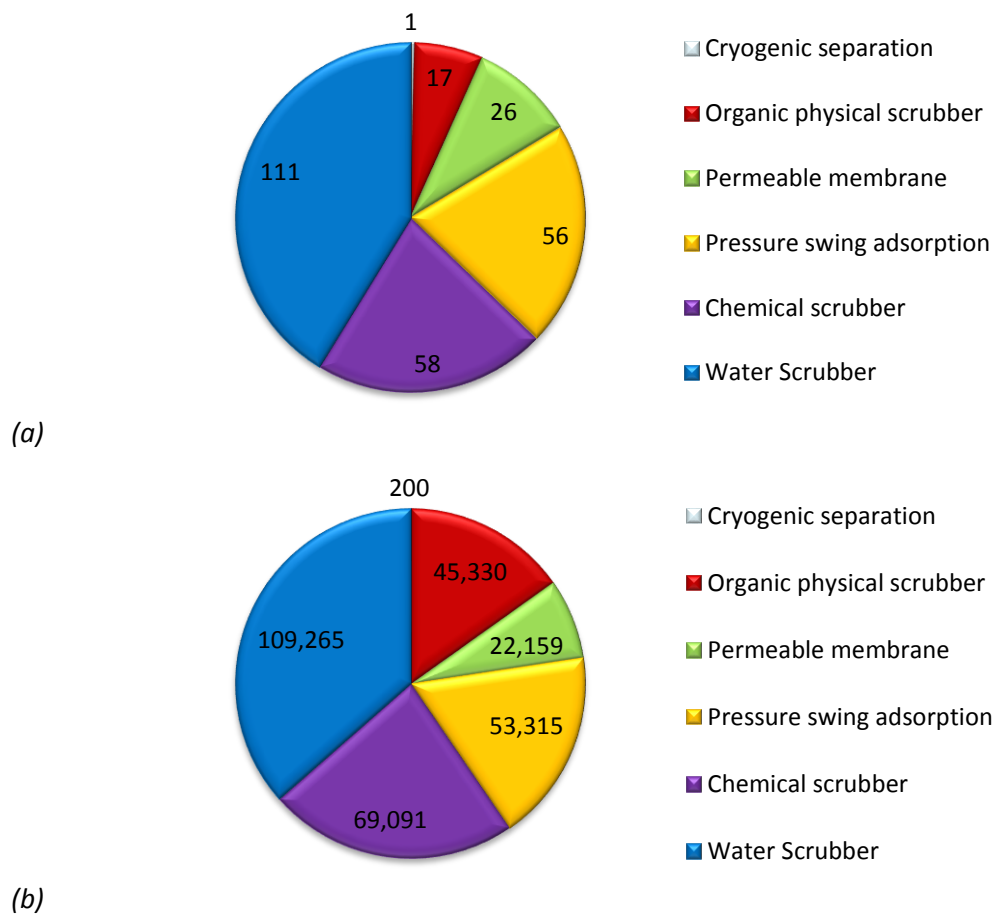


Figure 1.2 Global biogas upgrading facilities operating a variety of technologies quantified by number of individual plants (a) and by total volumetric flow of raw biogas processed (m³ h⁻¹) (b).

The technologies possesses various advantages and disadvantages, for example varying levels of fugitive CH_4 due to non-absolute selectivity for CO_2 (also known as methane slip) (Patterson *et al.*, 2011). However selective absorption within a liquid solvent is the most widely applied method, with 69 % of established biogas upgrading facilities (Figure 1.2a) and 74 % of total raw biogas flow (Figure 1.2b) processed using an absorption technique (Persson *et al.*, 2007; IEA bioenergy Task 37). Absorption can operate by either physical or chemical mechanisms. Chemical scrubbers typically use amine solutions to preference CO_2 absorption by chemical reaction, which inert CH_4 does not undergo. Physical absorption selectively removes CO_2 from the biogas due to its greater solubility within the solvent used, i.e. water or organic solvent. Water scrubbing is the most widely used physical absorption system and most popular individual technique, accounting for 41 % of upgrading facilities, due to the ready availability of solvent and relative simplicity of the technology. For instance, water scrubbers have been selected as the first UK upgrading installations within existing wastewater flow sheets because of the high throughput of potential solvent (i.e. secondary effluent) through individual WWTW, with the first already commissioned by Thames Water (Vale, 2013; IEA bioenergy Task 37) (Figure 1.3).

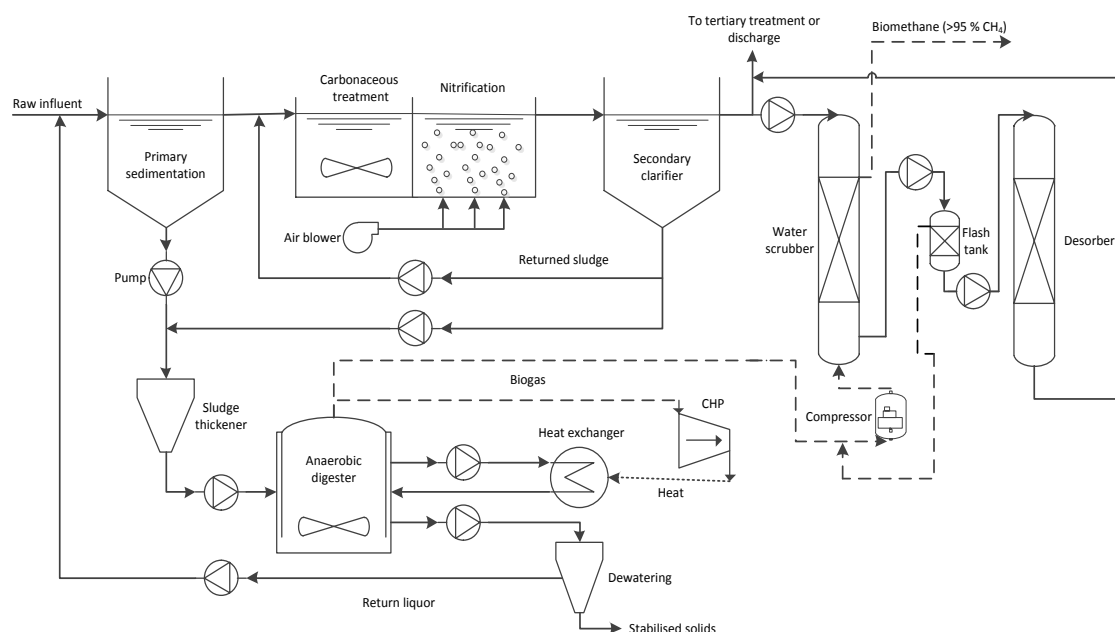


Figure 1.3 Anticipated flow sheet including a water scrubber receiving secondary effluent as a solvent and retaining CHP only to maintain supply heat to the AD.

However, known drawback of water scrubbing technology and the promise of alternative membrane technology has resulted in the desire to investigate alternative liquid-gas contacting technology to facilitate absorption.

1.2 Project development

Packed column technology has been applied across a broad range of industrial processes and is a relatively simple technology (Kohl and Nielsen, 1997). Liquid solvent, e.g. water, is sprayed over a bed of random packing material, which provides surface area for liquid-gas contact. The gas mixture is fed from the foot of the column and the most soluble component(s) absorb upon contact with the liquid film covering the packing material. Upon exiting the column the soluble component of the gas phase has been preferentially removed, thereby enriching the remaining component(s) that are less soluble within the applied solvent. However, this simple approach, where liquid-gas contact is facilitated by mutual dispersion of the phases presents several practical problems during operation such as (Feron and Jansen, 2002):

- Foaming – the formation of a foam layer above the random packing material that disrupts free fluid flow
- Entrainment – the formation of small bubbles within the liquid phase that reduces the contact between large volumes of the gas, within the bulk of the bubble, and the solvent
- Flooding – the formation of a fixed volume of solvent within the column that prevents free solvent flow within a film across the packing material (caused by excessive liquid flow rate)
- Channelling – the formation of non-uniform solvent flow through the random packing bed, due to low liquid flow rate, which prevents the full surface area from being used thereby reducing mass transfer.

In order to circumvent these disadvantages, alternative liquid-gas contacting technology is desirable. A particularly effective alternative technology is the hydrophobic micro-porous hollow fibre

membrane contactor (HFMC) (Figure 1.4). HFMCs provide non-dispersive contact between liquid and gas phases at the mouths of the gas-filled micro-pores, where the hydrophobicity and small pore size of the polymeric membrane material (i.e. polypropylene, PP), coupled to the surface tension of aqueous solvents, prevent penetration of the liquid to the gas side of the membrane (Feron and Jansen, 2002).

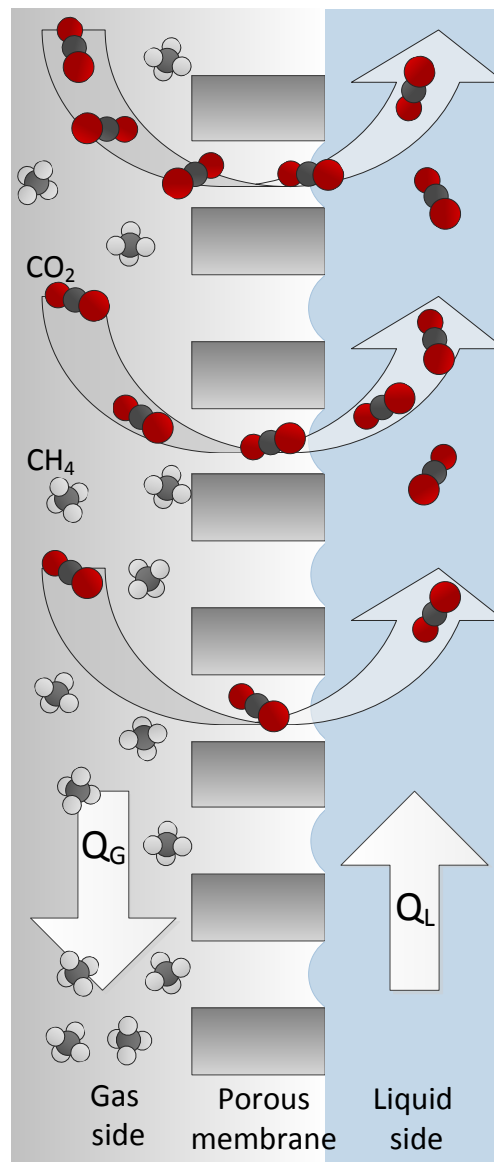


Figure 1.4 Cross-section of a hydrophobic micro-porous hollow fibre membrane supporting non-dispersive liquid-gas contact for preferential absorption of CO₂ to form a CH₄ enriched biomethane.

Similarly, a marginally greater pressure on the liquid side prevents the formation of gas bubbles in to the liquid phase. As a consequence the practical issues of foaming and entrainment arising in column

contactors are resolved by HFMCs. The problems of flooding and channelling arise from the inability of column contactors to alter solvent flow rate (Q_L) to suit demand in response to variable gas phase composition or gas flow rate (Q_G) (Feron and Jansen, 2002). Therefore large variation of Q_L cannot be performed in columns without sacrificing surface area for mass transfer. This failure is critical because when the mass transfer of gases (i.e. CO_2) is liquid-phase limited, as typically exhibited during physical absorption, the rate of gas absorption is highly dependent upon Q_L (Qi and Cussler, 1985). Therefore, for example, columns cannot respond well to changes in the CO_2 content or flow rate of biogas to maintain a fixed biomethane quality output. In contrast, HFMCs have an excellent capability to turn-up/turn-down Q_L to rapidly respond to variation in the gas-side without loss of surface area for mass transfer (Qi and Cussler, 1985). This can be achieved even at full scale, where liquid flows outside of the fibres and a baffle forces liquid flow across the entire surface area of the fibres independently of Q_L (Gabelman and Hwang, 1999). The regulated design of HFMCs enables a significant membrane surface area within a compact contactor volume, allowing high specific surface areas (a , $m^2 m^{-3}$). For HFMCs, ' a ' may be in the order of $1000 m^2 m^{-3}$ versus in the order of $100 m^2 m^{-3}$ for columns (Reed *et al.*, 1995). This suggests that integration of HFMCs as upgrading technology within existing wastewater treatment flow sheets will be substantially easier than integration of column-based water scrubbers. Further, direct comparative studies have shown the greater solvent efficiency and mass transfer performance of HFMCs versus packed columns (DeMontigney *et al.*, 2005; Nii *et al.*, 1992).

1.3 Hypothesis

The regulated design and non-dispersive liquid-gas contact of HFMCs, shown to offer excellent specific surface area very high mass transfer, can be applied to biogas upgrading to provide an effective, viable and potentially preferable alternative to existing upgrading technologies in a wastewater treatment context.

1.4 *Aims and objectives*

The aim of this thesis is to demonstrate the efficacy of HFMCs applied to biogas upgrading within a wastewater treatment context with respect to mass transfer of CO₂, whole life carbon and economic costs. In order to address this overall aim several objectives have been developed:

1. Determine the underlying mechanism governing the physical absorption of gases within a given liquid solvent from a first principles perspective and illustrate how this knowledge can rationalise the identity of the most suitable solvent(s) for a given gas separation
2. Develop procedures for the management of methane slip and demonstrate how their execution using HFMCs are uniquely capable of maintaining low residual CH₄ within the liquid solvent
3. Demonstrate the selective desorption of CH₄ using HFMCs to produce a viable concentration within the recovered gas whilst further maintaining a low residual CH₄ content within the solvent
4. Explore the chemical potential of wastewaters available on-site at WWTW when coupled with HFMC technology and determine their combined ability to enhance the worth of biogas beyond its direct energetic value and the subsequently impact upon conventional wastewater flow sheets.

1.5 *Thesis structure*

The chapters of this thesis have been formatted as journal papers that collectively address the established research objectives and include a literature review (Chapter 2) and four technical papers (Chapters 3, 4, 5 and 6) (Figure 1.5). Chapter 2 reviews the broad physical absorption literature pertaining to columns contactors and HFMCs. Using first principle modelling this review provides a framework by which the suitable physical solvents for any given gas separation can be identified, which is presently lacking within the literature. Chapter 3 investigates the mechanism by which CH₄

is lost during the upgrading process (known as methane slip) using both physical and chemical solvents in a HFMC and demonstrates how this may be controlled to reduce methane slip. Chapter 4 examines HFMCs applied to the recovery of dissolved CH_4 as a high concentration gas, thereby providing a low energy method of minimising methane slip whilst recovering a useful gas phase that may be directed to energy generation. Chapter 5 investigates the potential of ammonia-rich wastewater as an economically favourable and sustainable chemical solvent for biogas upgrading in a HFMC, thereby circumventing the disadvantages associated with chemical solvents, such as high chemical costs and high solvent regeneration energy. Also the concept of recovering the ammonium bicarbonate (ABC) product generated through the reaction between ammonia (NH_3) and CO_2 is introduced. Chapter 6 examines the heterogeneous nucleation and growth of ABC on the surface of hollow fibre membranes applied to biogas upgrading. Chapter 7 includes an overall discussion of the thesis chapters and consolidates the key findings relevant to the benefits of HFMCs within a wastewater treatment context.

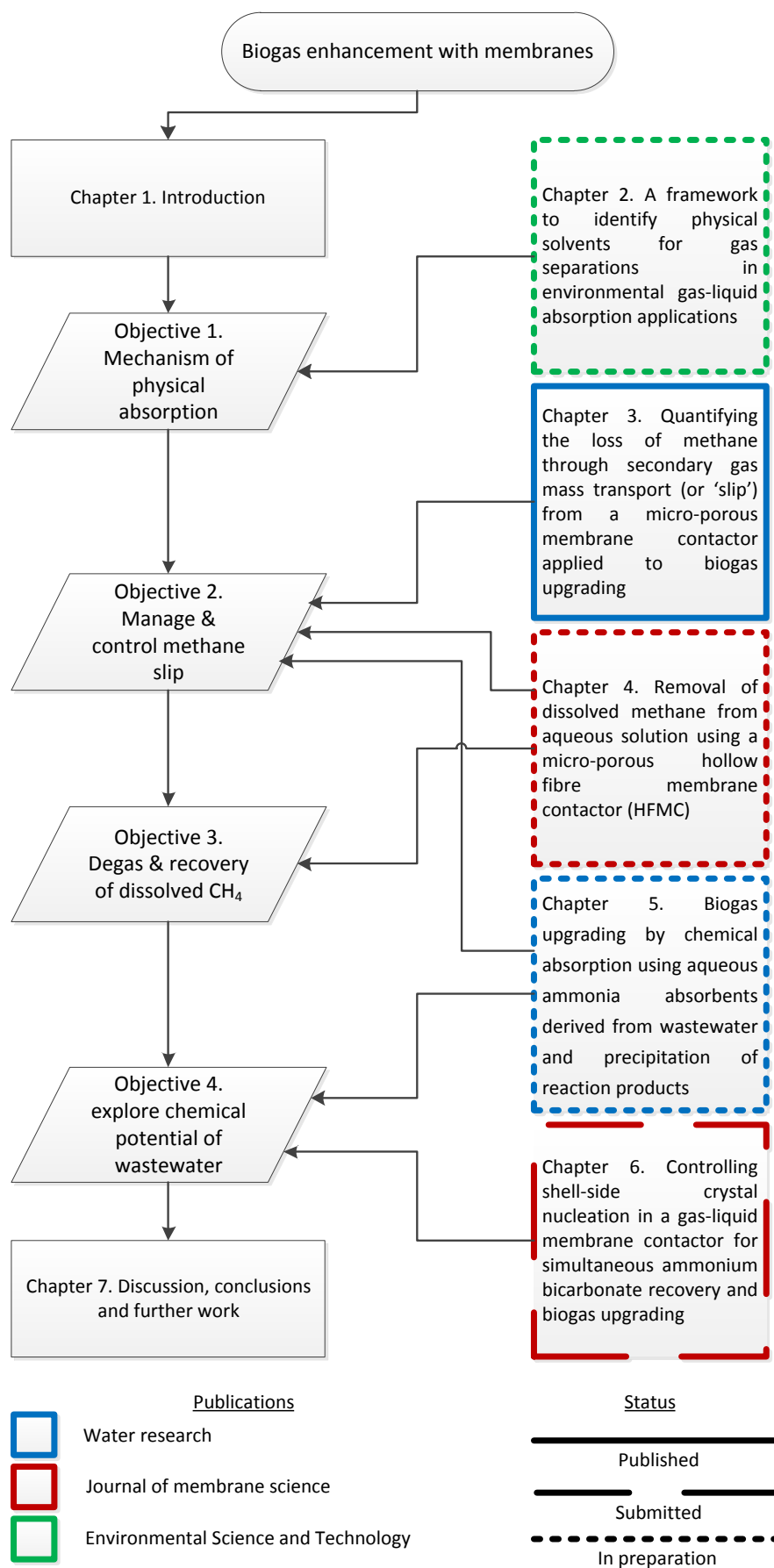


Figure 1.5 Thesis plan

References

Demontigny, D., Tontiwachwuthikul, P. and Chakma, A. (2005), "Comparing the absorption performance of packed columns and membrane contactors", *Industrial and Engineering Chemistry Research*, vol. 44, no. 15, pp. 5726-5732.

Feron, P. H. M. and Jansen, A. E. (2002), "CO₂ separation with polyolefin membrane contactors and dedicated absorption liquids: Performances and prospects", *Separation and Purification Technology*, vol. 27, no. 3, pp. 231-242.

Gabelman, A. and Hwang, S. -. (1999), "Hollow fiber membrane contactors", *Journal of Membrane Science*, vol. 159, no. 1-2, pp. 61-106.

IEA Bioenergy Task 37, "http://www.iea-biogas.net/plant-list.html?file=files/daten-redaktion/download/Up-grading_Plant_List.xls", (accessed 25th March 2014).

Kohl, A. and Nielsen, R. (1997), "Gas Purification, Fifth Edition", *Gulf Publishing Company*.

Nii, S., Takeuchi, H. and Takahashi, K. (1992), "Removal of CO₂ by gas absorption across a polymeric membrane", *Journal of Chemical Engineering of Japan*, vol. 25, no. 1, pp. 67-72.

Ofgem (2014), <https://www.ofgem.gov.uk/publications-and-updates/full-tariff-tables> (accessed 1st September 2014).

Patterson, T., Esteves, S., Dinsdale, R. and Guwy, A. (2011) "An evaluation of the policy and techno-economic factors affecting the potential for biogas upgrading for transport fuel use in the UK", *Energy Policy*, vol. 39, no. 3, pp. 1806-1816.

Persson M., Jonsson, O. and Wellinger, A. (2007), "Task 37 – Biogas upgrading to vehicle fuel standards and grid injection", *IEA Bioenergy*, "www.iea-biogas.net/files/daten-redaktion/download/publi-task37/upgrading_report_final.pdf", (accessed 25th March 2014).

Reed, W. B., Semmens, M. J. and Cussler, E. L. (1995), "Membrane contactors", in *Membrane Separations Technology Principles and Applications*, Elsevier.

Vale, P., Severn Trent Water, 9th December 2013, *Cranfield University*.

Qi, Z. and Cussler, E. L. (1985), "Microporous hollow fibers for gas absorption. I. Mass transfer in the liquid", *Journal of Membrane Science*, vol. 23, no. 3, pp. 321-332.

Chapter 2

Literature review - A framework to identify physical solvents for gas separations in environmental gas-liquid absorption applications

For submission to: Environmental Science and Technology

A framework to identify physical solvents for gas separations in environmental gas-liquid absorption applications

Andrew McLeod, Bruce Jefferson and Ewan J. McAdam*

Cranfield Water Science Institute, Building 39, Cranfield University, Bedfordshire, MK43 0AL, UK

*Corresponding author e-mail: e.mcadam@cranfield.ac.uk

Abstract

The physical absorption of gas within a solvent is a vital process for gas separations, such as fuel gas purification or to control environmentally harmful emissions. The selective absorption of a target gas from a gaseous mixture is critically dependent upon the chemical properties and subsequent interactions of gas solute and solvent, which determine the solubility (as described by Henry's law) and diffusivity parameters heavily influencing mass transfer. Therefore the selection of a suitable solvent is a fundamentally important aspect of any given gas separation. However, any rationale regarding solvent selection within the physical absorption literature is often limited to secondary, practical considerations, e.g. vapour pressure. There is presently no widely applicable theoretical treatment of solvent-solute interaction chemistry capable of assessing the relative suitability of physical solvents. In this review, a theoretical framework is developed using established first principles models. This approach dissects gas dissolution into two stages: the formation of an adequately sized cavity within the solvent for occupation by the gas solute (yielding a positive free energy); the activation of solute-solvent interactions (liberating free energy). The net free energy determines the phase equilibrium position of the solute, allowing a Henry's constant to be predicted. A good parity between predicted and empirical Henry's constants for a wide range of solutes and solvents validated this approach. This framework was successfully applied to gas separations found within the scientific literature and from full-scale operations, enabling solvent selection and subsequent mass transfer/separation performances to be retrospectively rationalised.

Keywords: physical absorption; mass transfer; selectivity; gas separation

2.1 Introduction

The separation of mixed gases is a critical operation for industrial processes generating pure gas products. For example hydrogen gas (H_2) generated by gasification of coal or during natural gas processing is purified by selective removal of carbon dioxide (CO_2), hydrogen sulfide (H_2S) and methane (CH_4) (Padurean *et al.*, 2012; Sweny, 1973; Wood and Mehra, 1995). Separation of industrial flue gases is also required to limit the emission of environmentally damaging gases. For example the greenhouse gases (GHG) CO_2 and nitrous oxide (N_2O), in addition to acid-rain-producing sulfur dioxide (SO_2), are released in vast quantities during coal-fired power generation, with 2180 Mt_{CO_2} , 3.4 Mt_{N_2O} and 10 Mt_{SO_2} emitted by the USA in 2005 (Cohan and Douglass, 2011). N_2O is 310 times more potent than CO_2 as a GHG and is a by-product of industrial scale nitric acid (HNO_3) production, where emissions of 0.4 $Mt_{N_2O} \text{ y}^{-1}$ (120 $Mt_{CO_2 \text{ eq.}} \text{ y}^{-1}$) equate to a third of the GHG reduction target for the European Union under the Kyoto Protocol (Groves *et al.*, 2006; Groves and Frank, 2009). Gas separations are also required at local scales for the management of air quality. For example hydrogen sulfide (H_2S) emitted during wastewater treatment causes odour problems and chronic illness from extended exposure to low concentrations and is fatal above concentrations of 700 $mg_{H_2S} \text{ m}^{-3}$ (Jefferson *et al.*, 2005; Lebrero *et al.*, 2011).

Gas separation can be facilitated by techniques such as pressure-swing adsorption (PSA) or membrane separation; however absorption within a solvent is the most widely applied method, operating by either a physical or chemical mechanism (Kohl and Nielsen, 1997). Chemical reaction of the target gas solute within the solvent during chemical absorption produces high capacity and selectivity over chemically inert gases, although this limits chemical absorption applications to reactive gas solutes only. Also high chemical costs and an energy intensive solvent regeneration step due to the heat needed to reverse the chemical reactions are undesirable aspects of chemical absorption. In contrast, physical absorption does not operate using chemical reactions and therefore offers a lower energy demand for solvent regeneration. As a result physical absorption can be more economically viable than chemical absorption in many circumstances (Kohl and Nielsen, 1997). For

example, the operational energy (e.g. for solvent cooling and heat for regeneration) for commercial physical solvents Selexol® (polyethylene glycol dimethyl ether) and Rectisol® (methanol) were calculated as approximately one order of magnitude lower ($0.54 \text{ MJ kg}_{\text{CO}_2}^{-1}$ and $0.58 \text{ MJ kg}_{\text{CO}_2}^{-1}$ respectively) than reactive amine solution ($5.9 \text{ MJ kg}_{\text{CO}_2}^{-1}$) for separation of CO_2 from syngas (Padurean *et al.*, 2012). Physical solvents achieve gas separation through preferential absorption of the most soluble gaseous component. The solubility of a gas solute in a physical solvent is defined through Henry's law, where the Henry's constant (k_H , $\text{mol L}^{-1} \text{ atm}^{-1}$) describes the partitioning of the gas solute between the gas phase and physical solvent. This enables the dissolved concentration of the gas solute to be determined when at equilibrium with the gas phase ($C_{2,\text{sat}}$, mol L^{-1}), provided the partial pressure of the target gas in the gas phase is known (P_2 , atm) (1):

$$C_{2,\text{sat}} = P_2 H \tag{1}$$

The equilibrium gas solute concentration in the physical solvent is dependent upon both temperature and pressure. As a consequence, the general trend is for increased gas solute dissolution at lower temperatures and higher partial pressures or, if the overall system is pressurised.

The difference in Henry's constants that can be imparted by a physical solvent on two gas solutes is dependent on the individual gas molecular properties and specific solvent-solute interaction and is critical in determining effective separation. Whilst water is a common physical solvent, e.g. for effective separation of carbon dioxide and methane, a host of proprietary physical solvents are also readily available for a range of applications and include Fluor-solvent®, Rectisol® and Selexol® (Kohl and Nielsen, 1997) which comprise either propylene carbonate, polyethylene glycol dimethyl ether, or chilled methanol respectively as the active physical solvent. Although used extensively on a commercial basis, the appropriate absorbent is often selected based on previous commercial success or practical considerations such as vapour pressure, surface tension or material compatibility (Dindore *et al.*, 2004; Burr and Lyddon, 2008; Aschenbrenner and Styring, 2010; Miller *et al.*, 2010) rather than through an explicit understanding of the role of solvent chemistry in

determining an effective solute-solute separation. The lack of a theoretical framework within the absorption literature has been recognised previously, resulting in development of semi-empirical theory-based approaches to identify suitable solvents for selective absorption of CO₂ over N₂ and SO₂ over CO₂ (Gwinner *et al.*, 2006; Van Dam *et al.*, 1997). In each case, established parameters pertaining to the solvent (Hildebrand solubility parameter and Gutmann donor parameter for CO₂ and SO₂ respectively) are correlated with the respective Henry's constants for CO₂ or SO₂, enabling behavioural patterns within broad chemically distinctive solvent families to be resolved and their suitability as solvents determined accordingly. However, the established solubility models adopted by each study demonstrated reasonable correlation with empirical Henry's constants only for the specific gas separation examined in each case. When the application of Hildebrand and Gutmann parameters was exchanged between the two gas separations, lesser parity was observed between theory and experiment. As a consequence, application of this approach to a broader range of possible gas separations is limited. This failure likely originates from the macroscopic perspective of the respective models used. For example, the Hildebrand parameter uses the heat of vaporisation of both solvent and solute to indicate solvent-solvent and solute-solute affinity and generate a single parameter value for each (Hildebrand and Scott, 1950; Hildebrand *et al.*, 1970). Solubility is then inferred by proximity of the values for the solvent and solute parameters, using a simplistic like-dissolves-like argument. The full role of the gas solute and solvent chemistry is not examined, yielding an incomplete theoretical treatment (e.g. Hildebrand solubility parameters are not applicable to solutions containing strong polar intermolecular interactions). A theoretical framework from a first principles perspective could better elucidate the specific molecular properties and interactions responsible for the behaviours of the solvent-solute system sufficiently to be applicable to any gas separation. This review aims to provide a theoretical framework from first principles, within the context of environmentally significant gas absorption processes, to enable rigorous justification for the selection of physical solvents. To achieve this, the review will satisfy several objectives:

- (1) Identify a suitable model, capable of adequately describing solvent-solute systems from a molecular perspective such that predictions of solubility and diffusivity can be made
- (2) Validate the accuracy of the model by correlating predicted and empirical values for gas solubility and diffusivity within respective solvents
- (3) Collate physical absorption literature and apply the framework to the solute-solvent systems to retrospectively assess the suitability of solvents chosen

2.2 A physical description of dissolved gas within a solvent

The Henry's constant describes the partitioning of a gaseous species between the gas phase and the solvent, however each Henry's constant is specific to each gas solute-solvent system and does not provide a physical description of the mechanisms governing solubility. A clearer physical representation of solubility has previously been described in the literature, where dissolution of a gas solute first requires a cavity to be produced within the solvent to accommodate the solute before solute-solvent interactions are considered (Eley, 1939). This is intuitive because the intermolecular spaces within solvents are usually insufficiently sized to accommodate even the smallest gas solutes and physical matter cannot overlap to occupy the same spatial position. However, because the solvent is dynamic, random motions allow for sizeable transient cavities to form in isolation, which occur sufficiently frequently from a macroscopic perspective to allow measurable dissolution of gases. The probability of cavity formation is dependent upon the cavity size required (i.e. the solute molecular size) and the molecular size and the molar volume of the solvent (V_m , $\text{cm}^3 \text{mol}^{-1}$). Once formed, the cavity allows for a solute to be inserted and solute-solvent interactions can be initiated, establishing intermolecular associations and thereby liberating free energy (Figure 2.1) (Eley, 1939). The scaled particle theory (SPT) solubility model enables the probability of a cavity forming within the solvent to be quantified and expressed as a free energy (or work) of cavity formation (G_{cav} , kJ mol^{-1}) by approximating solvent and solute molecules as hard spheres with diameters used as size parameters (σ_1 and σ_2 respectively), known as Lennard-Jones

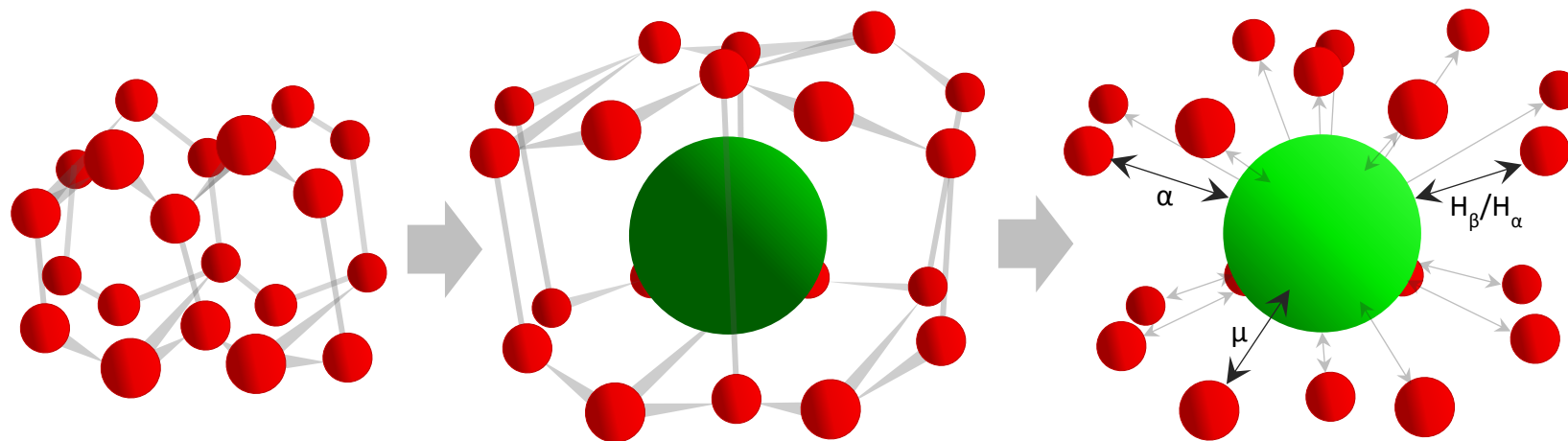


Figure 2.1 Sketch of gas dissolution. A solvent is expanded to form a cavity to accommodate a solute and solute-solvent interactions are then initiated, where α , μ and H_α/H_β denote dispersion, polar, and hydrogen bond donor/acceptor interactions respectively.

size parameters (See Appendix A for the full theory) (Pierotti, 1963, 1968 and 1975). G_{cav} is calculated using geometric arguments, with only σ_1 and σ_2 and the molar volume of the solvent (V_m) required for calculation. The cavity must have a diameter equivalent to the sum of the solvent and solute diameters to prevent overlapping of the spheres. SPT then calculates the free energy liberated by initiation of solute-solvent intermolecular interactions (G_{int} , kJ mol^{-1}). The extent to which solute-solvent interactions can compensate for the work of cavity formation is essentially the basis upon which SPT predicts partitioning behaviour, expressed in the form of a Henry's constant (k_H , atm). The advantage of the first principle approach by SPT is a molecular scale mechanistic interpretation of dissolution in addition to an ability to make predictions for a combination of systems on the basis of six easily obtainable parameters for both solute and solvent.

The value of G_{int} depends upon the type of interactions expressed within the specific solution and their respective absolute strength. Molecules influence each other through electrostatic interactions between negative and positive charges. These charges occur on molecules due to asymmetrical distributions of negatively charged electrons, which may be involved in the bonding between constituent atoms or exist as lone pairs upon electron-rich atoms, such as nitrogen (N), oxygen (O) and sulfur (S). The symmetry of electron distribution, and therefore the interactivity of a given molecule, is dependent upon molecular shape and the nature of the constituent atoms. For example, the noble gas series can be considered spherical, with an even average distribution of electrons. Consequently there is no permanent disparity of charge across the noble gases, which are therefore described as non-polar. Non-polar gases and solvents can only interact through momentary disruption to charge distribution that are induced when electrons are moved from their average even distributions under the influence of neighbouring molecules, forming transient attractive intermolecular forces (Israelachvili, 2011). These are known as dispersion or London forces and the susceptibility of a molecule to this phenomenon is represented by its polarizability (α_i , cm^3), which is readily available parameter (Tables 2.A1a and 2.A1b). This applies to any solute or solvent species possessing sufficient molecular symmetry and typically lacking electron rich constituent

atoms. In contrast, polar molecules possess a permanent asymmetrical distribution of electrons, through which they can interact, due to a lesser order of molecular symmetry and inclusion of electron rich atoms. Therefore in addition to dispersion forces, polar species can also interact through a permanent separation of charge across the molecule, which is reflected by the value of its dipole moment (μ_i , Debyes) (Table 2.1). The absolute value of G_{int} for solutions of polar solutes and solvents is typically larger than for non-polar solutions, and therefore possess a greater capability to compensate for large G_{cav} , resulting in higher solubility for respective like-sized gas solutes. It must be noted that several gases, including CO_2 , ethylene (C_2H_4) and acetylene (C_2H_2), exhibit polar-type interactions despite a nominal zero dipole moment. These relatively exceptional cases can be anticipated by recognition of the double or triple bonds where electron density is higher than on carbon, creating a net positive polarity on carbon but no overall μ_i due to the linear symmetry of these molecules. Another important intermolecular interaction is hydrogen bonding (H-bonding), where a hydrogen atom with particularly low local electron density (usually directly bound to O or N) associates electrostatically with electron-rich sites of neighbouring molecules (Israelachvili, 2011). Molecules possessing these electron deficient hydrogen atoms, e.g. methanol, can H-bond donate (H_α) whereas molecules possessing electron-rich sites, e.g. dimethylsulfoxide, can H-bond accept (H_β). Some molecules, such as water or ammonia (NH_3) can both donate and accept. Individual hydrogen bonds between solute and solvent are strong and therefore respective values of G_{int} for such solutions allow considerable compensation for G_{cav} and therefore generally high solubility. Whilst SPT does not take account of H-bonding, alternative models include H_α and H_β parameters that can be used to gauge the relative H-bonding properties of gases and solvents (Abraham, 1993; Abraham *et al.*, 1994; Ahmed *et al.*, 2007). For example, whilst H_α and H_β for *n*-alkanes are zero water has a H_α and H_β of 0.82 and 0.35 respectively (Table 2.1). Similarly whilst non-polar gases have zero H-bonding capability, polar NH_3 has H_α and H_β of 0.14 and 0.62 respectively.

Table 2.1 Parameters determining solvent classification and for practical use as physical absorbents.

	Molecular mass M_r g mol^{-1}	Dipole moment μ Debyes	H-bond donating H_α	H-bond accepting H_β	Viscosity η mPa s	Surface tension γ mN m^{-1}	Vapour pressure P_{vap} bar
Non-polar solvents							
Benzene	78.11		0	0.14	0.60	28.2	0.1271
Cyclohexane	84.16	0	0	0	0.89	24.7	0.1301
<i>n</i> -Hexane	86.18	0	0	0	0.313	17.9	0.2020
Toluene	92.14		0	0.14	0.56	27.9	0.0379
Methyl-cyclohexane	98.19	0	0	0	0.679	23.3	0.0618
<i>n</i> -Heptane	100.20	0	0	0	0.390	19.8	0.0609
<i>n</i> -Octane	114.23	0	0	0	0.546	21.1	0.0186
<i>n</i> -Nonane	128.26	0	0	0	0.666	22.3	
<i>n</i> -Decane	142.28	0	0	0	0.838	23.4	
Carbon tetrachloride	153.82	0	0	0	0.91	26.3	0.1520
Bromo-cyclohexane	163.06		0	0.16		33.3	
<i>n</i> -Dodecane	170.34	0	0	0	1.378	24.9	
<i>n</i> -Tetradecane	198.39	0	0	0	2.128	26.1	
Perfluoro- <i>n</i> -heptane	388.05	0					0.1364
Polar aprotic solvents							
Acetonitrile	41.05	3.38	0.07	0.32	0.37	28.7	0.1180
Acetone	58.08	2.78	0.05	0.49	0.31	23.0	0.3080
Dimethylsulfoxide	78.13	3.90	0	0.88	1.99	42.9	0.0008
Propylene carbonate	102.1	4.98			2.5	41.5	0.0001
[EMIM][EtSO ₄]	236.29				91.85	47.0	6.1×10^{-17}
Genosorb (Selexol)	1753 339.9	2.82			5.8	33.5	9.7×10^{-7}
Polar protic solvents							
Water	18.01	1.86	0.82	0.35	0.89	72.7	0.0317
Methanol	32.04	1.72	0.43	0.47	0.54	22.1	0.1692
Ethanol	46.07	1.70	0.337	0.48	1.07	22.0	0.0787
Ethylene glycol	62.07	2.34			16.1	48.4	0.0001

The terminology used for solvents herein reflects the ability to exhibit the above interaction types. All solvents possess dispersion force capability, however non-polar solvents limited exclusively to dispersion-type interactions (e.g. the *n*-alkane series). In contrast polar aprotic and polar protic solvents exhibit additional polar interactions. Whilst polar aprotic solvents are generally capable of accepting H-bonds from solutes (e.g. dimethylsulfoxide and acetonitrile), only polar protic solvents are capable of reciprocal donation of H-bonding with gas solutes (e.g. water and methanol).

2.3 A review of published literature on physical absorption for environmental applications

Scientific investigations of physical absorption processes may be categorised by the polar/non-polar characteristics of the given binary gas targeted for separation and by the nature of the solvent selected, i.e. non-polar, polar aprotic or polar protic (Table 2.2a and 2.2b). Commonly, the separation of non-polar gases involves fuel gas processing, such as the separation of hydrogen (H_2) from natural gas (primarily CH_4), the purification of CH_4 by selective removal of heavier hydrocarbon impurities, or the removal of problematic volatile siloxane polymers from raw biogas (Wood and Mehra, 1995; Mehra *et al.*, 1983; Ajhar *et al.*, 2010; Wheless and Pierce, 2004; Rasi *et al.*, 2008). Interestingly, both non-polar (hydrocarbons up to C_5) and polar aprotic solvents (Selexol) were both successfully applied to non-polar/non-polar separation of fuel gases. Other non-polar/non-polar separations involved the absorption of oxygen (O_2) to facilitate subsequent biological or chemical reactions within or with the physical solvents (Grund *et al.*, 1992; Tekie *et al.*, 1997; Kies *et al.*, 2006; Cote *et al.*, 1989). Consequently, in these cases, the physical solvent is not selected on the basis of optimised O_2 absorption but is necessarily fixed based on the desired application. The majority of the remaining cases involve the selective separation of polar and nonpolar gases. Multiple studies are devoted to the physical absorption of CO_2 , which is important industrially to reduce GHG emissions by carbon capture and storage (CCS) and for the removal from fuel gas streams such as biogas.

Table 2.2a Operational characteristics, mass transfer performance and removal efficiencies for physical absorption processes using column-type contactors.

Physical solvent (298.15 K)	Gas phase Target gas / balancing gases	Column type	Height/diameter m	Liquid velocity V_L 10^3 m s^{-1}	Gas velocity V_G m s^{-1}	Flow	Volumetric mass trans. coeff. $K_L a$ 10^3 s^{-1}	Removal %	Reference
Non-polar solvent – non-polar target gas									
Hydrocarbons $>C_5$	H_2 (20 %) / N.G.	Packed bed	-	-	-	counter	-	-	Wood and Mehra
Toluene	O_2 / air	Bubble	4.3 / 0.15	n/a	~0.18	n/a	~180	-	Grund <i>et al.</i>
Ligroin	O_2 / air	Bubble	4.3 / 0.15	n/a	~0.20	n/a	~80	-	Grund <i>et al.</i>
Cyclohexane	O_2 / N_2	Stirred cell (GIR)	0.18 / -	-	-	-	~1000	-	Tekie <i>et al.</i>
Cyclohexane	N_2 / O_2	Stirred cell (GIR)	0.18 / -	-	-	-	~1000	-	Tekie <i>et al.</i>
Cyclohexane	O_2 / N_2	Stirred cell (SAR)	0.18 / -	-	-	-	~100	-	Tekie <i>et al.</i>
Cyclohexane	N_2 / O_2	Stirred cell (SAR)	0.18 / -	-	-	-	~50	-	Tekie <i>et al.</i>
Mineral oil	Siloxanes / Landfill gas	-	-	-	-	-	-	<50	Ajhar <i>et al.</i>
Tetradecane	D_4 / CO_2	-	-	-	-	-	-	97	Huppmann <i>et al.</i>
Polar aprotic solvent – non-polar target gas									
Selexol	CH_4 (88 %), C_2H_6 (11 %) / C_3+	-	-	-	-	counter	-	-	Mehra
Selexol	Siloxanes / Landfill gas	Tray tower	-	-	2550*	counter	-	99	Wheless and Pierce
Polar protic solvent – non-polar target gas									
Water	O_2 / air	Droplet	3 / 0.15	9.4-18.9	10-11.5	co	0.41-1.40	-	Kies <i>et al.</i>
Water	O_2 / air	Bubble	4.3 / 0.15	n/a	~0.17	n/a	~70	-	Grund <i>et al.</i>
Methanol	O_2 / air	Bubble	4.3 / 0.15	n/a	~0.20	n/a	~120	-	Grund <i>et al.</i>
Water	Siloxanes / Landfill gas	Packed bed	-	-	6	-	-	0	Rasi <i>et al.</i>
Non-polar solvent – polar target gas									
PP10	CO_2	Stirred cell	-	-	-	-	~100	-	Heintz <i>et al.</i>

Table 2.2a Continued

Polar aprotic solvent – polar target gas									
PEG	H ₂ O (humidity) / air	Spray column	0.65 / 0.15	0.72-1.72	0.47-3.95	counter	-	> 37 %	Tanda <i>et al.</i>
Propylene carbonate	CO ₂	Stirred cell	-	-	-	-	4.46-6.3	-	K-Pawlak and Chacuk
NMP	CO ₂	Stirred cell	-	-	-	-	3.85-6.2	-	K-Pawlak and Chacuk
Selexol	CO ₂	Stirred cell	-	-	-	-	1.71-2.57	-	K-Pawlak and Chacuk
Selexol	CO ₂ / Raw biogas (CH ₄)	Full-scale column	-	-	4170*	-	-	-	Deed <i>et al.</i>
Selexol	CO ₂ (50 %) / N ₂	-	-	-	-	-	-	-	Aschenbrenner <i>et al.</i>
PEG 200	CO ₂ (50 %) / N ₂	-	-	-	-	-	-	-	Aschenbrenner <i>et al.</i>
PEG 300	CO ₂ (50 %) / N ₂	-	-	-	-	-	-	-	Aschenbrenner <i>et al.</i>
PEG 600	CO ₂ (50 %) / N ₂	-	-	-	-	-	-	-	Aschenbrenner <i>et al.</i>
[BMIM][PF ₆]	CO ₂ (10 %) / N ₂	Packed bed	0.2 / 0.025	-	-	counter	0.63-1.9	-	Zhang <i>et al.</i>
[BMIM][PF ₆]	CO ₂ (10 %) / N ₂	Rotating packed bed	-	-	-	-	9.5-39	-	Zhang <i>et al.</i>
PEG	NO _x (200,000 ppm) / O ₂	Spray column	0.74 / 0.8	0.56-1.7	1.8-5.6x10 ⁻⁴	cross	-	100	Li <i>et al.</i>
Polar protic solvent – polar target gas									
Water	NH ₃ (1 %) / air	Spray column	1.25 / 0.1	4.2-10.6	0.43-1.7	counter	-	< 95 %	Javed <i>et al.</i>
Methanol	H ₂ S (0.5 %) / H ₂ / CO ₂	-	-	-	-	counter	-	> 99 %	Ranke
Water	CO ₂	Packed bed	-	75-245	-	-	85-185	-	Sherwood and Holloway
Water	CO ₂ (10 %) / CO / H ₂	Packed bed	5.5 / 0.69	45	1.45x10 ⁻⁵	-	14.0	94 %	Rixon
Water	CO ₂ (20 %)/air	Packed bed	1.2 / 0.08	16.6-29.8	0.12	counter	12.7-19.5	-	Evren and Özdural
Water	CO ₂ / Raw biogas (CH ₄)	Full-scale column	-	-	2000*	-	-	-	Deed <i>et al.</i>
Methanol	CO ₂ (33 %) / H ₂	-	-	-	-	counter	-	> 99 %	Ranke
Glycerol	CO ₂ (50 %) / N ₂	-	-	-	-	-	-	-	Aschenbrenner <i>et al.</i>
Glycerol carbonate	CO ₂ (50 %) / N ₂	-	-	-	-	-	-	-	Aschenbrenner <i>et al.</i>
Water	NO _x (200,000 ppm) / O ₂	Spray column	0.74 / 0.8	0.56-1.7	1.8-5.6x10 ⁻⁴	cross	-	99.1	Li <i>et al.</i>
Water	SO ₂	Packed bed	-	6.7-8.8	-	-	67-105	-	Whitney and Vivian (1949)

PP10 is a perfluorinated hydrocarbon analogue; PEG is polyethylene glycol, where approximate molecular mass may be specified ; NMP is *N*-methyl-2-pyrrolidone; [BMIM][PF₆] is 1-Butyl-3-methyl-imidazolium hexafluorophosphate

Table 2.2b Operational characteristics, mass transfer performance and removal efficiencies for physical absorption processes using hollow fibre membrane contactors.

Physical solvent	Gas phase	Material	Dimensions	Relevant contact area	Eff. length	Liquid velocity (gas pressure)	Flow	Volumetric mass trans. coeff.	Reference
(298.15 K)	Target gas / balancing gases		ID/OD/pore size 10 ⁶ m	A _m (ID or OD) m ²	L m	V _L (P _g) m s ⁻¹ (bar)		K _L a 10 ³ s ⁻¹	
Polar protic solvent – non-polar target gas									
Water	CH ₄ (60 %) / CO ₂	PP	220/300/0.4	0.58 (ID)	0.113	0.005-0.024	counter	0.009-0.048	McLeod <i>et al.</i>
Water	O ₂ / air	Silicon rubber	305/635/-	0.0258 (OD)	0.30	0.1 - 7.72 (2.0)	cross	0.22-0.57	Cote <i>et al.</i>
Polar aprotic solvent – polar target gas									
Propylene carbonate	CO ₂	PP	600/800/ 0.64	0.00013 (ID)	0.07	0.05-0.38	counter	0.11-0.22	Dindore <i>et al.</i>
Propylene carbonate	CO ₂	PTFE	1000/1500/1	0.00022 (ID)	0.07	0.03-0.142	counter	0.16-0.29	Dindore <i>et al.</i>
N-Formyl morpholine	CO ₂	PP	600/800/ 0.64	0.00013 (ID)	0.07	0.024-0.134	counter	0.6-0.11	Dindore <i>et al.</i>
Dimethyl aniline	SO ₂ (3.3%) / air	α-Al ₂ O ₃	3000/4000/ 0.87	0.8 (ID)	0.44	0.0047	counter	3.17	Luis <i>et al.</i> (2007)
Dimethyl aniline	SO ₂ (3.3%) / CO ₂ (10%) / air	α-Al ₂ O ₃	3000/4000/ 0.88	0.8 (ID)	0.44	0.0047	counter	3.17	Luis <i>et al.</i> (2007)
[EMIM][EtSO ₄]	SO ₂ (3.3%) / air	α-Al ₂ O ₃	3000/4000/ 0.87	0.8 (ID)	0.44	0.0005	counter	0.967	Luis <i>et al.</i> (2009)
[EMIM][EtSO ₄]	SO ₂ (3.3%) / CO ₂ (10%) / air	α-Al ₂ O ₃	3000/4000/ 0.88	0.8 (ID)	0.44	0.0005	counter	0.724	Luis <i>et al.</i> (2009)
[EMIM][EtSO ₄]	CO ₂ (18%)-N ₂	PP	220/300/0.04	0.01 (ID)	0.015	0.0125	cross	2.79	Albo <i>et al.</i>
Polar protic solvent – polar target gas									
Water	CO ₂	PVDF	550/1000/ 0.0023	0.026 (ID)	0.15	0.16-1.0	counter	20.0-29.03	Mansourizadeh <i>et al.</i>
Water	CO ₂	PVDF	650/1000/0.2	0.019 (ID)	0.27	0.36-2.5	counter	27-42	Atcharyawut <i>et al.</i>
Water	CO ₂	PP	600/800/ 0.64	0.00013 (ID)	0.07	0.17-0.85	counter	0.25-0.45	Dindore <i>et al.</i>
Water	CO ₂	PTFE	1000/1500/1	0.00022 (ID)	0.07	0.012-0.098	counter	0.25-0.46	Dindore <i>et al.</i>
Water	CO ₂ (40 %) / CH ₄	PP	220/300/0.4	0.58 (ID)	0.113	0.005-0.024	counter	10.1-47.9	McLeod <i>et al.</i>
Water	CO ₂	PP	240/300/0.03	0.03	0.3	0.02-0.21	counter	130-250	Karoor and Sirkar
Water	SO ₂	PP	240/300/0.03	0.01	0.18	0.009-0.024	counter	95-114	Karoor and Sirkar

[EMIM][EtSO₄] is 1-Ethyl-3-methyl-imidazolium ethyl-sulfate; PP is polypropylene; PTFE is polytetrafluoroethylene; PVDF is Polyvinylidene fluoride

These include a full range of polar protic (Sherwood and Holloway, 1940; Ranke, 1973; Karoor and Sirkar, 1993; Evren and Özdural, 1995; Deed *et al.*, 2004; Dindore *et al.*, 2004; Atchariyawut *et al.*, 2007; Aschenbrenner *et al.*, 2010; Mansourizadeh *et al.*, 2010; McLeod *et al.*, 2013), polar aprotic (Deed *et al.*, 2004; Dindore *et al.*, 2004; Aschenbrenner *et al.*, 2010; Kierzkowska-Pawlak and Chacuk, 2010; Albo *et al.*, 2011; Zhang *et al.*, 2011; Li *et al.*, 2014), and non-polar solvents (Heintz *et al.*, 2008). The absorption of other important polar gases, including H_2S , SO_2 , nitrogen oxides (NO_x), ammonia (NH_3) and water vapour was investigated using both protic and aprotic polar solvents (Whitney and Vivian, 1949; Ranke, 1973; Karoor and Sirkar, 1993; Javed *et al.*, 2006; Luis *et al.*, 2007; Luis *et al.*, 2009; Tanda *et al.*, 2011; Li *et al.*, 2014).

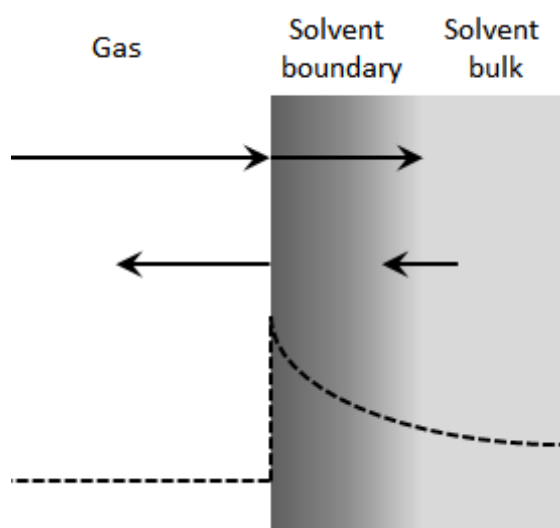


Figure 2.2 Schematic of the equilibria established for a gas solute between the gas phase and the solvent boundary layer, and the solvent boundary layer and the solvent bulk. The dotted line represents the concentration gradient across the phases.

The process of transporting a gas solute in to the solvent can be broken down to follow a sequential process (Figure 2.2) (Schwartz, 1986). The gas solute is transported within the gas phase to the gas-solvent interface. Then mass transfer of the gas across the interface can occur and a local equilibrium is established on the solvent side of the interface in the region known as the boundary layer. Mass transfer between the boundary layer at the gas-solvent interface and the greater solvent bulk can then occur and an equilibrium achieved. It is important to note that a gradient of gas solute concentration between the solvent boundary layer and the solvent bulk will occur when a disparity

between the established equilibria exists because saturation of the solvent bulk may not be approached if impeded by saturation in the boundary layer, thereby inhibiting the effective gas solubility within the solvent as a whole (A boundary layer also exists at the gas-side of the interface but this does not typically limit mass transfer during physical absorption and so can be neglected for simplicity). The rate of absorption through this process is typically characterised by the overall mass transfer coefficient, which describes the driving force for mass transport between the gas and solvent phases (2):

$$k_L = \frac{J_2}{\Delta C_2} = \frac{n_2}{A \Delta C_2} \quad 2$$

where J_2 is the flux of gas solute '2' ($\text{mol m}^{-2} \text{s}^{-1}$), ΔC_2 is the concentration difference between solvent and the solute '2' in the gas phase (mol m^{-3}), n_2 is the molar rate of mass transfer (mol s^{-1}), A is the area through which mass is being transferred (m^2), and k_L is the overall mass transfer coefficient (m s^{-1}). Coefficients are commonly normalised by specific surface area (a , $\text{m}^2 \text{m}^{-3}$), which allows the mass transfer to be evaluated within the context of process scale ($k_L a$, s^{-1}). Conventional packed-bed-type column contactors typically possess specific surface area in the order of $10^2 \text{ m}^2 \text{m}^{-3}$ and operate by dispersion of the gas within the solvent (Reed *et al.*, 1995). However hollow fibre membrane contactors (HFMC) are a maturing alternative technology, facilitating gas-solvent contact by non-dispersive contact at the mouths of micro-pores through the membrane wall, and may possess over an order of magnitude greater specific surface area (Reed *et al.*, 1995). This high specific surface area for HFMCs is the result of a highly regulated design, which has been demonstrated to significantly increase the solvent efficiency for HFMCs during gas absorption application. This allows enhanced selectivity and mass transfer versus column-type contactors in real terms (Nii *et al.*, 1992; McLeod *et al.*, 2013; deMontigny *et al.*, 2005). For comparison, physical mass transfer studies using column contactors and HFMCs have been separately tabulated (Table 2.2a and 2.2b respectively).

Expansion of the mass transfer equation (2) emphasises the critical role of solubility in bracketing the physical limits of the developing concentration gradient required to drive high flux but also introduces the significant role of gas solute diffusivity (D , $\text{m}^2 \text{s}^{-1}$), which can be regarded as analogous to the rate of solute transport from the gas-solvent interface to the greater solvent bulk (when turbulent mixing is absent) and is also governed by gas solute-solvent interactions (3a and b):

$$J_2 = k_L(C_{2,\text{sat}} - C_{2,\text{bulk}}) \quad 3a$$

$$J_2 = (ShD/d)[(P_{2,g} - H) - C_{2,\text{bulk}}] \quad 3b$$

where $C_{2,\text{sat}}$ is the absolute saturation concentration for solute 2 within the solvent, $C_{2,\text{bulk}}$ is the current concentration of solute 2 within the solvent bulk and d is the characteristic length (m). The Sherwood number (Sh) is a dimensionless quantity that expresses the ratio of convective to diffusive mass transport due to its definition as a function of the Reynolds number (Re), expressing whether the solvent flow regime is either laminar or turbulent, and the Schmidt number (Sc), which expresses the relative contributions of advective and molecular diffusion. Therefore Sh determines the importance of the solute diffusivity to mass transfer within the given physical absorption system, where turbulent flow and high advection diminish the critical impact of solute diffusivity to mass transfer.

2.4 The role of solvent and solute physical chemistry on solubility and diffusivity

2.4.1 Dissolution of gas within a water solvent

The experimentally determined polarizability of non-polar gas solutes can be approximated using the gas solute size parameter (σ_2). Typically, larger non-polar gases possessing a greater σ_2 also exhibit a higher polarizability (Table 2.A1a). For example, the increasing value of σ_2 down the noble gas group from helium, He ($\sigma_2 = 2.68 \times 10^{-8}$ cm), to radon, Rn ($\sigma_2 = 4.36 \times 10^{-8}$ cm), corresponds to enhanced polarizability ($\alpha_2 = 0.204 \times 10^{-24}$ cm³ and $\alpha_2 = 5.86 \times 10^{-24}$ cm³ respectively) due to the occupation of successively higher electron orbitals, which are more shielded from the influence of the atomic

nucleus. Any increase in this shielding effect better enables neighbouring molecules to exhibit a polarising effect upon them in comparison to the electrons in close proximity to the respective atomic nucleus. The polarizability of environmentally significant gases of such as H_2 , CH_4 and Cl_2 can be similarly estimated by a relationship with σ_2 that extends up to the broad range of cyclic (D3-D5) and linear (L2-L4) siloxanes, which are an environmentally relevant group of large volatile gas solutes. The correlation between polarizability and solubility has been previously acknowledged, although it was suggested that water did not exhibit this behaviour (Campanell *et al.*, 2010). In fact correlations are identified in all solvents, including water, if non-polar and polar gas solutes are treated separately. Polar gases can interact with polar solvents via their permanent dipole moment in addition to dispersion forces due to polarizability. As a result their solubility in water is enhanced above the trend exhibited for non-polar gases. This relationship is maintained for non-polar and polar gases in water if polarizability is substituted for calculated G_{cav} as a correlating parameter for gas solubility (Figure 2.3).

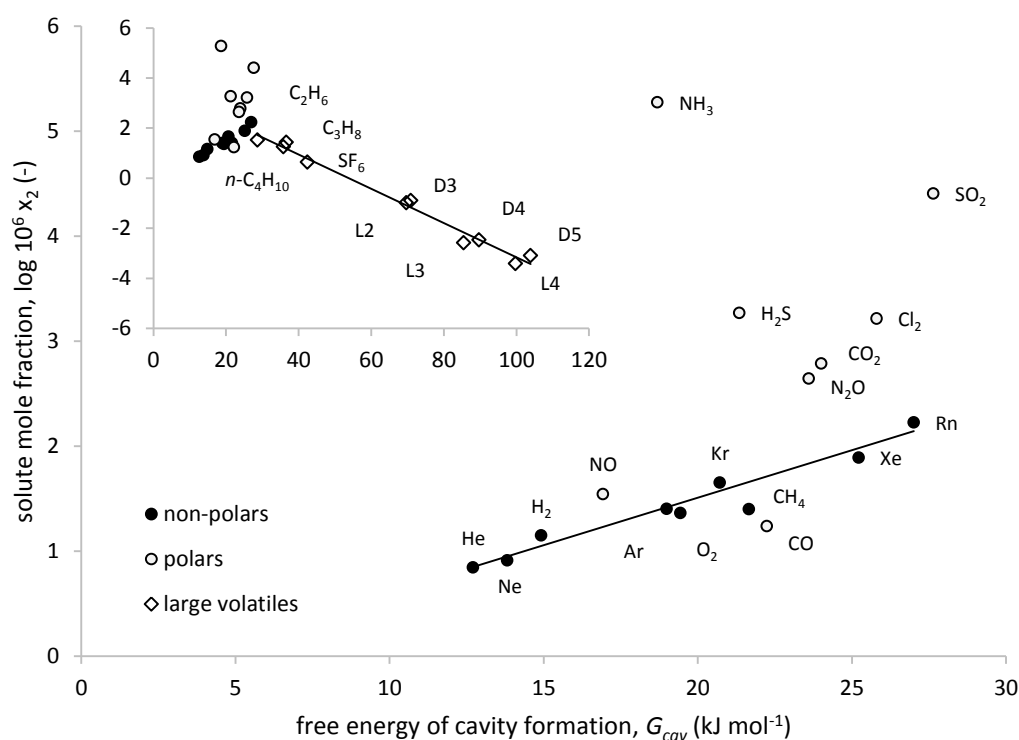


Figure 2.3 The contrasting relationships between free energy of cavity formation (G_{cav} , kJ mol⁻¹) and solubility for non-polar and polar gases, and large volatiles (inset) in water.

A simple correlation of non-polar gas solubility with respective gas polarizability would fix the position of each gas along the x-axis, with the solubility y-value apparently determined by the solvent alone. This provides a false impression of the factors influencing solubility, which can be considered more reciprocal in nature. Substitution of solute polarizability for the model value G_{cav} better reflects the influence of both the solvent and the solute by incorporating σ_1 and σ_2 in to its calculation. This fits directly with the physical interpretation of dissolutions, where G_{cav} represents the work required to form a suitably sized cavity within the solvent to accommodate the solute, but also corresponds to the dispersion interactivity between solvent and solute due to the relationship between σ_1 and σ_2 and respective polarizabilities. As a result, although in direct opposition to dissolution, the solubility of non-polar gases in water increases as G_{cav} is increased, in a log linear fashion. This reflects the increasing ability of greater interactivity to compensate for the increased work of cavity formation required for larger solutes. The use of empirically derived gas solubility data provides the clear theoretical link between the model value G_{cav} and experimental observation. The enhancement of experimentally determined polar gas water solubilities above the non-polar baseline trend set against G_{cav} is the result of additional polar interactions with the water solvent. For ammonia (NH_3) and hydrogen sulfide (H_2S) H-bonding with the protic water solvent further enhances solubility so that the size and polarizability of NH_3 and H_2S do not correspond to the same solubility trend as other environmental gases. Despite being nominally non-polar CO_2 and Cl_2 also exhibit above non-polar solubility behaviour. At saturation, these examples are expected to obey Henry's law, since their ionisation constants are below that of CO_2 , which is considered to be physically absorbed in water (Table 2.3) (Karoor and Sirkar, 1993). This reflects a non-dispersive interaction component with the protic water solvent.

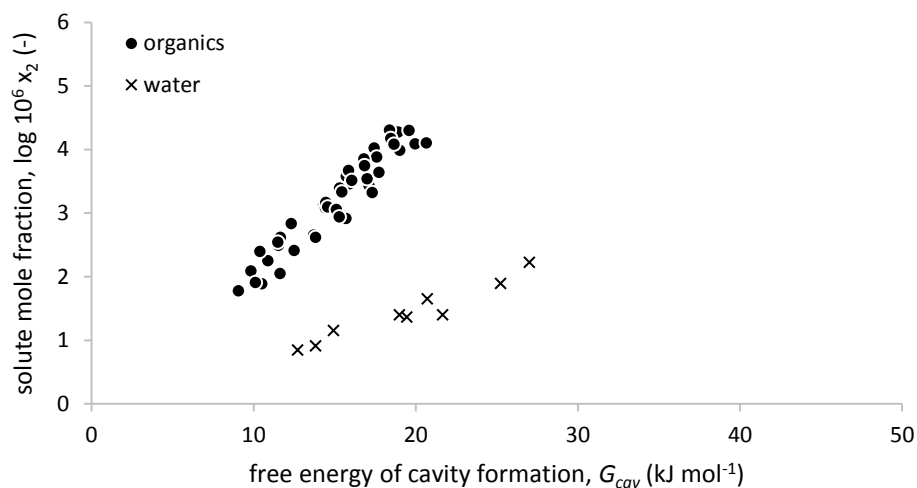
Table 2.3 Equilibrium constants for gases ostensibly physically absorbed in water.

Gas solute	equation	Equilibrium constant K_e	Units	Reference
Cl_2	$K_e = \frac{[\text{HOCl}][\text{H}^+][\text{Cl}^-]}{[\text{Cl}_2(\text{aq.})]}$	3.48×10^{-6}	M^2	Whitney and Vivian (1941)
NH_3	$K_e = \frac{[\text{NH}_4^+][\text{OH}^-]}{[\text{NH}_3(\text{aq.})]}$	1.74×10^{-5}	mol L^{-1}	Tan <i>et al.</i>
H_2S	$K_e = \frac{[\text{HS}^-][\text{H}^+]}{[\text{H}_2\text{S}(\text{aq.})]}$	8.9×10^{-8}	mol L^{-1}	
SO_2	$K_e = \frac{[\text{HSO}_4^-][\text{H}^+]}{[\text{SO}_2(\text{aq.})]}$	1.4×10^{-2}	mol L^{-1}	Karoor and Sirkar
CO_2	$K_e = \frac{[\text{H}_2\text{CO}_3]}{[\text{CO}_2(\text{aq.})]}$	2.58×10^{-3}	-	Loerting <i>et al.</i>

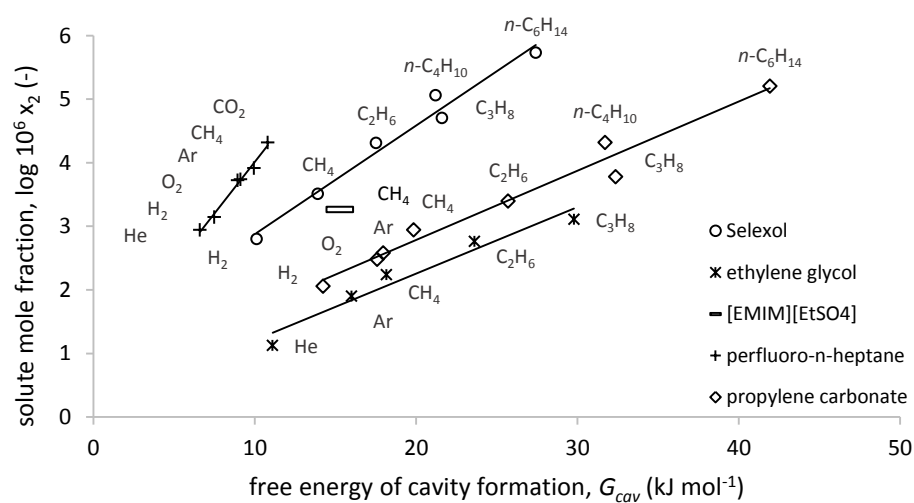
The trend of enhanced solubility with increasing G_{cav} is abruptly counteracted in water for the volatile category of solutes larger than Rn , which includes normal alkanes from C_2 to C_4 and the linear and cyclic short-chain siloxane polymers (Figure 2.3, inset). To demonstrate, an increase in G_{cav} of 45 % from H_2 to CH_4 in water yields a 77 % enhanced solubility for CH_4 , however a greater increase in G_{cav} of 140 % from H_2 to butane ($n\text{-C}_4\text{H}_{10}$) yields only a 29 % greater water solubility for $n\text{-C}_4\text{H}_{10}$. Further increase in G_{cav} exhibited by siloxanes due to their large σ_2 results in solubilities from 2 to 5 orders of magnitude less than that of H_2 . This phenomenon has been recognised previously in water and was historically attributed to a hydrophobic effect, where large non-polar solutes disrupt the hydrogen bonding network between water molecules without the capacity to positively contribute with solute-solvent H-bonding, thereby inhibiting high solubility (Frank and Evans, 1945; Lazaridis, 2001). However arguments from SPT suggest that it is the anomaly of the small σ_1 for water (Lee, 1985; Graziano, 2002), compared with other solvents, which exacerbates the values of G_{cav} to an extent that high solubility is irredeemable through dispersion interactions alone.

2.4.2 Comparison of solubility in water and organic solvents

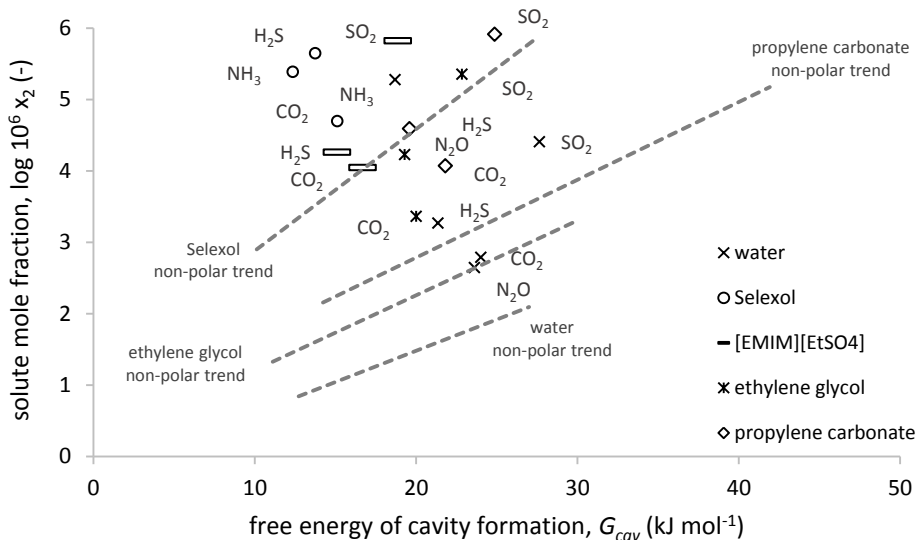
A positive log-linear trend was observed between the experimentally derived solubilities of a range of non-polar gases measured in several organic solvents (carbon tetrachloride, cyclohexane, benzene, *n*-heptane and methanol) and increased G_{cav} (Figure 2.4a). The solubility of non-polar gases for this range of organic solvents was markedly higher than that in water. Importantly, despite a substantial variation in chemical properties within this selection of organic solvents (including linear and cyclic alkanes, aromatic hydrocarbons, an alcohol and a chlorinated solvent), the closely grouped data further indicates that non-polar gases can be described by the size parameters (σ_1 and σ_2) of the solute-solvent system. A similar positive log-linear trend between G_{cav} and non-polar gas solubility was also established for several polar solvents (Selexol®, propylene carbonate, ethylene glycol), commonly applied to absorption, as well as for a perfluorinated solvent (perfluoro-*n*-heptane) and an ionic liquid ([EMIM][EtSO₄]) used in absorption investigations due to unique physical properties (Figure 2.4b) (Heintz *et al.*, 2008; Luis *et al.*, 2009). Whilst analysis by G_{cav} was able to correlate the empirical non-polar gas solubilities for each polar solvent independently, each solvent presented different solubilities for individual gas solutes. As a result respective non-polar solubility trends ranged between that established for water (low solubilities) and perfluoro-*n*-heptane (high solubilities). Interestingly the non-polar solubilities for perfluoro-*n*-heptane exceeded respective solubilities observed in the fully hydrogenated *n*-heptane analogue. Also, relatively large volatile solutes (alkanes from C2 to C6) were included within the solubility trends of Selexol®, propylene carbonate and ethylene glycol without that same sharp decline in solubility observed in water despite high solvent polarity, indicating this to be a water specific phenomenon.



(a)



(b)



(c)

Figure 2.4 Gas solubility in water compared to common organic solvents for non-polar solutions (a) commercial and specialist solvents in non-polar solutions (b) and commercial and specialist solvents in polar solutions (c).

Less ordered correlation between G_{cav} and solubility were observed for polar gases in the polar solvents, which were plotted alongside polar solubility data in water, and were similarly attributed to the additional polar interactions available in these solvents (Figure 2.4c). To illustrate, CO_2 exhibits solubility mole fractions of $x = 0.049$ and $x = 0.012$ in Selexol® and propylene carbonate respectively, which are markedly above that predicted for non-polar gas solutes of equivalent G_{cav} in these solvents ($x = 0.006$ and $x = 0.001$ respectively). Both Selexol® and propylene carbonate (also [EMIM][EtSO₄]) possess sizable dipole moments, enabling very strong interactions with polar gases (including CO_2). Of the solvents evaluated Selexol® possessed the highest solubility of polar gases, whilst water exhibited the lowest, with the exception of NH_3 in water, which was comparable to NH_3 in Selexol®. Interestingly perfluoro-*n*-heptane exhibited a CO_2 solubility ($x = 0.021$) comparable to that of Selexol® and greater than that of other polar solvents, despite ostensibly interacting purely via non-polar dispersion interactions. Perfluoro-*n*-heptane also exhibited the lowest absolute values of G_{cav} respectively for each gas. Whilst increasing G_{cav} is demonstrated to correspond to an enhancement in non-polar gas solubility within a fixed solvent, assessment of individual non-polar gas solubilities across a range of solvents established a log-linear reduction in respective gas solubility (Figure 2.5).

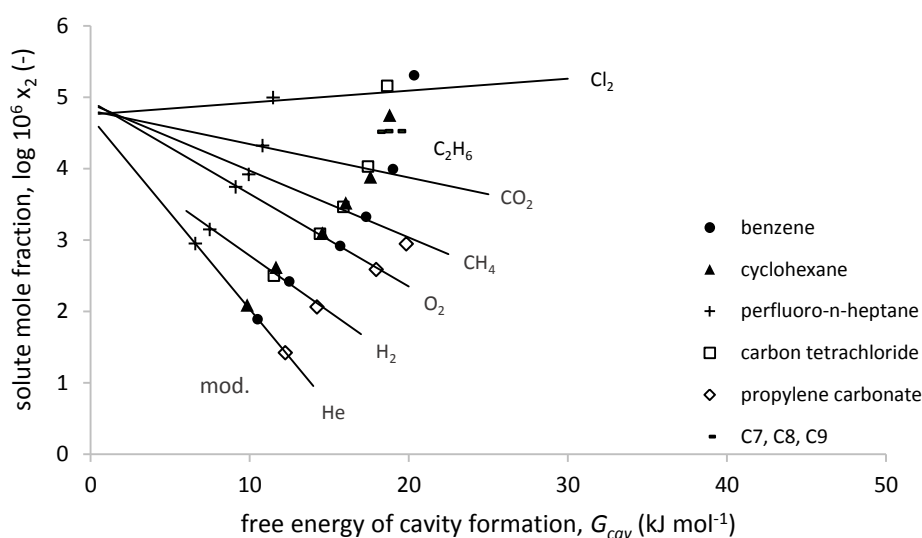


Figure 2.5 Negative log-linear correlation of individual gas solubilities in various physical solvents requiring progressively increased work for cavity formation (G_{cav} , $kJ\ mol^{-1}$).

The gradient of these relationships is increased as respective σ_2 are reduced, such that the solubility of CO_2 (in non-polar solvents) is less detrimentally impacted by G_{cav} within the different solvents than the smallest gas, He.

2.4.3 Extension of G_{cav} analysis for the prediction of Henry's constants

Through the incorporation of G_{int} (which provides a description of wider interaction forces) with G_{cav} , a theoretical Henry's constant (of the form k_{H} , atm) can be calculated to describe solubility of gases in gas solute-solvent systems. The parity between empirical Henry's constants and those calculated by SPT is very good for many solutions of many non-polar and polar gases in a wide range of solvents, which strongly supports the theoretical representation of dissolution depicted by SPT and enables accurate prediction of solubility when empirical values are not readily obtainable (Figure 2.6). The solubility of CO_2 and C_2H_2 and C_2H_4 in some solvents is the result of the polar interactivity exhibited by these solutes without possessing a dipole moment. This is disparity particularly large in water but also in solvents such as benzene and carbon tetrachloride, where values for polarizability and dipole moment do not completely accommodate the interactions exhibited between delocalised electron charge in these solvents and solutes.

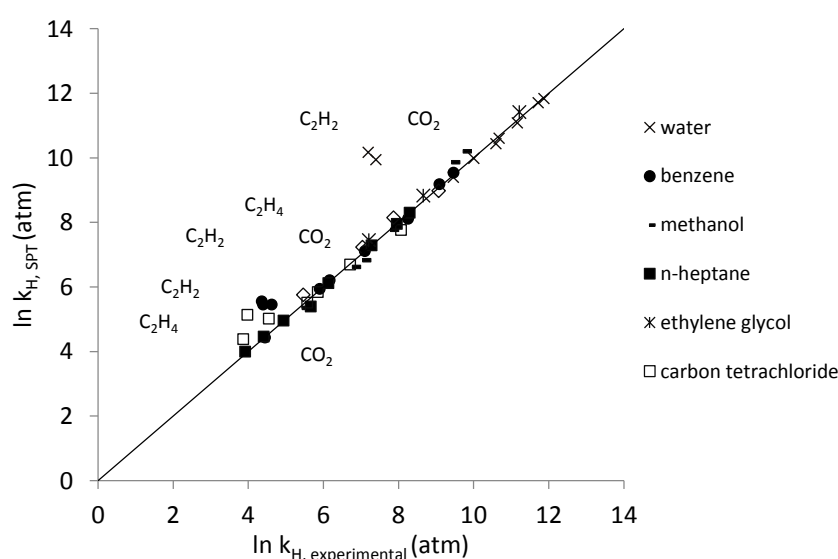


Figure 2.6 Parity between experimentally derived Henry's constants for several gases in several solvents and corresponding Henry's constants calculated by SPT (Brückl and Kim, 1981).

2.4.4 Influence of solvent selection on gas solute diffusivity

An exponential decline in experimental diffusivity is evidenced for non-polar gases in several solvents as G_{cav} is increased. Interestingly this is independent of the solvent used and dependent upon G_{cav} (Figure 2.7a). This can be attributed to the physical interpretation of G_{cav} , where a lesser work requirement to form a cavity within the solvent (low G_{cav}) results in a greater likelihood that a cavity neighbouring the solute will form, allowing more rapid diffusion through the condensed solvent medium. This intuitive concept is in agreement with previous studies of non-polar gaseous diffusion, where it was concluded that solvent specific interactions did not influence diffusivity (Ross and Hildebrand, 1964). This includes values for non-polar gases in water, since non-polar solutes cannot interact with the permanent dipole of water. Similarly the polar gas SO_2 is able to follow the non-polar trend in solutions of *n*-heptane, *n*-nonane, *n*-decane and *n*-dodecane (C7, C9, C10 and C12 respectively) because these solvents cannot interact with the permanent dipole of polar gases. Whilst the highest diffusivity found was that of H_2 in *n*-hexane ($16.36 \times 10^{-9} \text{ m}^2 \text{ s}^{-1}$) the lowest values were for the siloxane polymers in carbon tetrachloride and bromo-cyclohexane, obtained by interpolation from larger datasets (Edwards *et al.*, 1982), as a result of their large σ_2 and correspondingly large G_{cav} . For comparison, whilst polar gas solutes were broadly characterised by the same exponential trend with G_{cav} as for non-polar solutes (solid line), larger deviation from this trend indicates a contributing influence of the specified solvent through solute-solvent interactions (Figure 2.7b). Whilst the experimental diffusivity of CO_2 in Selexol® and propylene carbonate is lower than the values predicted by G_{cav} , a range of diffusivities in the aromatic solvents benzene and toluene are enhanced above the non-polar trend, indicating a complexity of contrasting mechanisms. However, measured diffusivity can also be concentration dependent for highly soluble gases such as NH_3 and SO_2 in water and NH_3 in methanol. Whilst diffusivity is enhanced at increased water concentrations, SO_2 diffusivity decreases with rising concentration, which complicates interpretation (Frank *et al.*, 1996; Leaist, 1984).

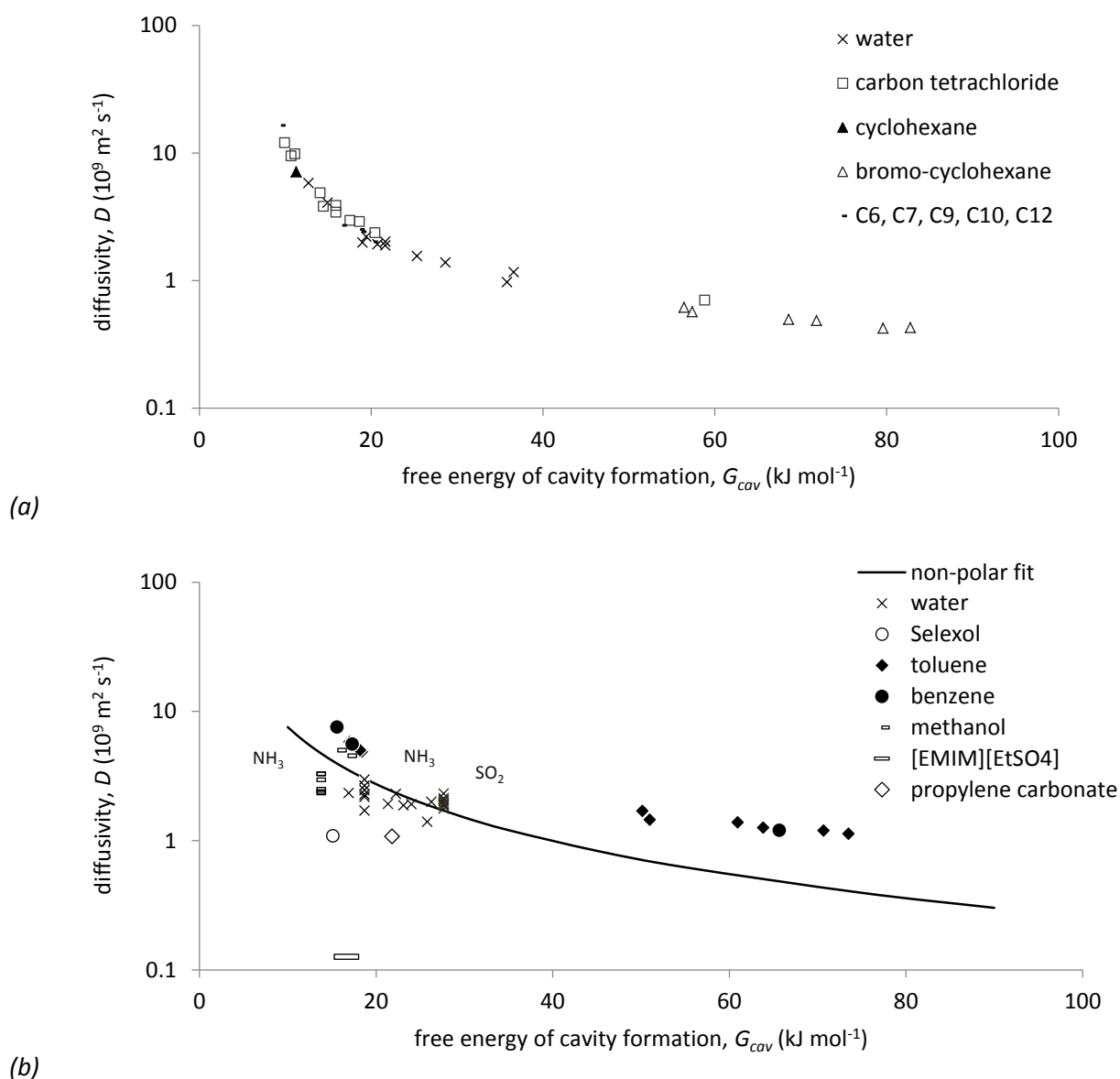


Figure 2.7 Gas diffusivity in solutions with only non-polar solute-solvent interactions (a) and comparison with solutions divergent to the non-polar trend (b).

2.5 Discussion

A key outcome of this study was the capability to predict gas solubility based upon a theoretical physical structure of the solvent (G_{cav}) and solvent-solute interactions (G_{int}), which accurately represent empirical Henry's constants and enable solvents to be targeted for specific gas separation tasks based upon few easily obtainable physical solvent/solute parameters. Expansion of mass transfer relationships reveal the importance of diffusivity in addition to solubility during physical

absorption, where selective absorption can be imparted between gases with differing diffusivities by disparate rates of solute penetration from the solvent boundary layer in to the greater solvent bulk. It was found that diffusivity and solubility both possess a dependency upon calculated G_{cav} , which enables each solvent-specific mass transfer contribution to be evaluated within the same theoretical framework. However, whilst solubility increased with increasing G_{cav} (indirectly due to the relationship between solute size and dispersion forces) diffusivity decreased as G_{cav} increased due to the reduced likelihood of solute-neighbouring cavities forming to facilitate transport through the condensed solvent. Each gas separation process may have different requirements, depending upon the substrate input gas and the desired outcome. Three generic process types have therefore been identified and are explained through key specific separation examples:

1. Bulk separation – a binary gas is separated in to two pure components that are both retained, e.g. H_2 from CH_4 in natural gas

For the bulk separation of two gases selectivity is important in order to effectively achieve separation, although neither gas stream exiting the absorber is emitted and therefore dissolved gases can be flashed and recycled to aid selectivity. Bulk separations commonly comprise the treatment of fuel gases, since both components have inherent value. Therefore commonly both gas components are non-polar. The close correlation of non-polar gas solubility with G_{cav} allows the selection of an appropriate physical solvent for separation of a binary gas using arguments based purely on the molecular size of the respective gases and of the solvent. For example the separation of non-polar H_2 ($\sigma_2 = 2.94 \times 10^{-8}$ cm) and CH_4 ($\sigma_2 = 3.70 \times 10^{-8}$ cm) is commonly researched for the generation of syngas. Selective absorption of CH_4 can therefore be achieved due to a larger polarizability than H_2 (2.70×10^{-24} cm³ and 0.80×10^{-24} cm³ respectively), which liberates more free energy via dispersion interaction with the solvent. Therefore solvent suitability must be judged upon its ability to provide low G_{cav} and reciprocate dispersion interactions, irrespective of solvent polarity. The steepness of the non-polar solubility gradient for each solvent is dependent upon the

compensation for G_{cav} by G_{int} and affects the selectivity imparted by the solvent, based purely upon the difference in solute size, where larger gases are preferentially absorbed. For example, whilst water produces the shallowest non-polar solubility gradient of any solvent examined and offers a maximum selectivity for CH_4 over H_2 ($x_{\text{CH}_4}/x_{\text{H}_2}$) of just 1.78, the selectivity for CH_4 over H_2 ($x_{\text{CH}_4}/x_{\text{H}_2}$) in *n*-heptane is 5.05 (284 % that of water) (Figure 2.4a). Therefore the use of a similar chilled hydrocarbon solvent (specifying 37 mole % *n*-pentane) has been described for the absorptive separation of CH_4 from H_2 for the purification of off-gas from a petroleum refinery, where excellent H_2 separation (99.8 mole %) was reported (Wood and Mehra, 1995). Importantly, this contrast in solubility is not related to the solvent polarity, but is the result of large G_{cav} exhibited by water, which are poorly compensated for by very weak dispersion interactions. For example, the strength of an individual dispersion interaction between water and CH_4 is 43 % less than that calculated between two CH_4 molecules (Israelachvili, 2011). This is due to the uniquely small solvent size of water ($\sigma_1 = 2.75 \times 10^{-8}$ cm). To illustrate, the non-polar solvent *n*-heptane ($\sigma_1 = 6.25 \times 10^{-8}$ cm) demonstrated mole fraction solubilities between 2.5×10^{-4} and 1.2×10^{-2} across a G_{cav} range of approximately 10-20 kJ mol^{-1} , compared to mole fractions of 6.9×10^{-6} to 8.6×10^{-5} for the same range of gases in water (G_{cav} of 12.7-25.3 kJ mol^{-1}). This is because a cavity of fixed absolute size perturbs a greater number of small water molecules during its formation than for *n*-heptane, where fewer large molecules occupy the volume and therefore fewer require exclusion upon cavity formation. As a result water uniquely exhibits exceptional negative entropy in opposition to cavity formation (Graziano, 2002). Therefore solvents of a greater size are necessary for absorption of non-polar gas solutes. For example the commercial solvent Selexol® is polar (2.82 D) but has a very large size parameter ($\sigma_1 = 8.55 \times 10^{-8}$ cm) and consequently has been demonstrated as a physical solvent for the selective separation of non-polar CH_4 and ethane (C_2H_6) (Mehra, 1983).

2. Contaminant removal from a product gas – undesirable component is separated from a single retentate gas, e.g. siloxanes from CH₄ in biogas

For contaminant removal from product gas a large selectivity for the contaminant is critical since the absorbed components are not retained upon desorption and valuable product may be lost. Additionally, the contaminant is likely to be present at considerably lower partial pressure than the other gaseous components and thus will exhibit low solubility due to Henry's law. For example volatile siloxane polymers are present in biogas ca.10-100 ppmv. Siloxanes are known to be completely miscible in *n*-alkanes (Dickinson and McLure, 1974) and are likely to be highly soluble in other organic solvents due to a large σ_2 and correspondingly large dispersion interaction as demonstrated by the use of Selexol to achieve 99 % removal landfill gas at full scale (Table 2.2a) (Wheless and Pierce, 2004). However, even assuming miscibility, the selectivity over CH₄ must be poor and therefore CH₄ losses in this case must be very large. It is in these circumstances that chemical absorption is most likely to be considered if applicable, depending upon the partial pressure and chemical reactivity of the contaminant gas. In cases of a polar contaminant gas in a non-polar substrate better selectivity may be imparted by use of a polar solvent. For example, the protic polar solvent methanol can selectively remove greater than 99 % of the acid gas H₂S despite only a 0.5 % partial pressure due to additional polar and H-bonding interactions that are absent between methanol and the H₂ component (Table 2.2a) (Ranke, 1973). Similarly water is particularly effective for absorption of H-bonding gases, i.e. ammonia (NH₃), displaying a NH₃ solubility comparative to Selexol (Figure 2.4c). Consequently water was used to remove up to 95 % of NH₃ from air despite only a 1 % initial partial pressure (Table 2.2a) (Javed *et al.*, 2006). For non-H-bonding polar gases, solvents possessing an exceptional dipole moment can allow significant selectivity over a non-polar substrate gas. For example, propylene carbonate is highly polar ($\mu_1 = 4.98$) and therefore polar SO₂ ($\mu_2 = 1.63$) is 386 times more soluble in propylene carbonate than a non-polar solute of identical G_{cav} . Therefore propylene carbonate, known commercially as Fluor solvent[®], has been

recommended over Selexol® for selective absorption of polar components despite exhibiting lower absolute gas solubilities (Bucklin and Schendel, 1984).

3. Contaminant removal from a waste gas – a specific contaminant is removed from a waste gas mixture before emission, e.g. CO₂ from N₂ in flue gas

Absorption of CO₂ from mixtures with N₂ is a common example of removal of contaminants from waste gases, where selectivity is not critical due to the zero value of nitrogen. Many organic solvents offer high CO₂ solubility with polar aprotic Selexol® affording the greatest ($x_{\text{CO}_2} = 0.049$) by combination of steep non-polar solubility gradient and additional polar interactions with CO₂. However non-polar perfluoro-*n*-heptane yields the next greatest CO₂ absorption capacity as a result of its uniquely low respective values of G_{cav} without additional polar interactions. Even polar solvents (excluding Selexol®) cannot surpass the CO₂ solubility in perfluoro-*n*-heptane via polar solute-solvent interactions. Although the polymeric nature of Selexol® yields an exceptionally low vapour pressure, which is important to prevent solvent loss, the vapour pressure of perfluoro-*n*-heptane is less than that of methanol, which is a successful commercial physical solvent and therefore perfluoro-*n*-heptane may be a practical solvent candidate.

The significance of the role of diffusivity in solvent selection is dependent upon the hydrodynamics of the absorption system, which determines whether flow is laminar, where diffusion can dominate transport or turbulent, where convective mixing. Under laminar flow, the diffusivity of solutes can determine respective values of effective solubility by determining the rate that the equilibrium between solvent boundary and solvent bulk is reached (Figure 2.2). As a result selectivity can be diminished below that indicated by the ideal Henry's constants of two gases since higher solubility gases, typically possessing greater G_{cav} , will diffuse more slowly than lower solubility gases possessing lower G_{cav} . This impact of diffusivity upon selectivity was demonstrated by the mass transfer of O₂ and N₂ in cyclohexane during aeration, required for the subsequent production of cyclohexanol and cyclohexanone (Tekie *et al.*, 1997). Here, a turbulent mixing gas inducing reactor

(GIR) displayed approximately equivalent $k_L a$ of 1.0 s^{-1} for O_2 and N_2 , whilst a laminar flow surface aeration reactor (SAR) exhibited a selectivity for O_2 over N_2 (approximate $k_L a$ of 0.1 s^{-1} and 0.05 s^{-1} respectively). This was attributed to the greater diffusivity of O_2 in cyclohexane compared to N_2 . An analogous trade-off is documented for gas separations using selective gas-permeable membrane technology, despite the absence of a liquid solvent, where selectivity is gauged by comparison of gas permeability (P , Barrers), which comprises the multiple of a solubility factor (S , $\text{cm}^3 \text{ cm}^{-3} \text{ atm}^{-1}$) and diffusivity ($\text{m}^2 \text{ s}^{-1}$) (Tremblay *et al.*, 2006). Interestingly, permeability data for gas pairs in various membrane materials (analogous to various solvents) demonstrate that gas diffusivity is the primary influence upon selectivity through the solid phase, with only a moderate impact due to solubility (Robeson *et al.*, 2014). The collation of numerous empirical diffusivities for CH_4 demonstrates that D_{CH_4} within dense polymer solids (ca. 10^{-10} - $10^{-14} \text{ m}^2 \text{ s}^{-1}$) typically extend many orders of magnitude below those observed within the solvent phase (ca. $10^{-9} \text{ m}^2 \text{ s}^{-1}$) (Figure 2.7a). However, conversion of the average solubility coefficient for CH_4 within the polymers (S_{CH_4} , $0.0221 \text{ cm}^3 \text{ (STP) cm}^{-3} \text{ cmHg}^{-1}$) in to units familiar to Henry's law (H_{CH_4} , $0.0752 \text{ mol L}^{-1} \text{ atm}^{-1}$) reveals that solubility remains competitive within the solid and liquid phases ($k_{\text{H,CH}_4}$ in water is $0.0015 \text{ mol L}^{-1} \text{ atm}^{-1}$ at 25°C and 1 bar, Wilhelm *et al.*, 1977). Although the validity of direct comparison between the solid and liquid phase systems is uncertain, this highlights the importance of the solubility/diffusivity trade-off when evaluating real selectivity. In circumstances where selectivity is un-important, such as the removal of a contaminant from a waste gas, diffusivity may be critical to reducing process scale by forming a higher rate system. For example, CO_2 solubility is greatest in Selexol® and perfluoro-*n*-heptane, with Selexol exhibiting approximately 2.5 times greater solubility. However, CO_2 diffusivity is estimated to be an order of magnitude greater in perfluoro-*n*-heptane (approximately $1 \times 10^{-8} \text{ m}^2 \text{ s}^{-1}$) based upon G_{cav} , whereas larger G_{cav} and polar interactions in Selexol® yields a lower diffusivity ($1.09 \times 10^{-9} \text{ m}^2 \text{ s}^{-1}$) (Lefortier *et al.*, 2012).

2.6 Conclusions

- First principle modelling enables an accurate description of the physical solubility of gases across a broad range of polar and non-polar gases within polar and non-polar solvents, where macroscopic models proposed in previous literature are too specific to be similarly widely applicable.
- As a result, many gas solubilities and diffusivities can be predicted and rationalised on the basis of the physical molecular attributes of gas solute and liquid solvent, which contribute to the calculation G_{cav} and G_{int} and allow prediction of respective Henry's constants.
- This approach can be used to retrospectively evaluate the selection of physical and mass transfer observed within the gas absorption literature and for full-scale operations.
- The theoretical framework established can be used as a tool by future research projects for the justification of physical solvent selection to avoid dependency upon empirical data, which may not be readily available in many circumstances.

Acknowledgments

The authors would like to thank the Engineering and Physical Sciences Research Council (EPSRC, V/N: 08001923), Anglian Water, Northumbrian Water, Severn Trent Water and Yorkshire Water for their financial support.

Appendix A

Scaled particle theory (SPT) is a first principles model capable of estimating Henry's constants (K_{H} , atm) for gas solute-solvent systems by appreciating the free energy contributions from cavity formation within the solvent (G_{cav} , cal mol⁻¹) and solute-solvent interactions (G_{int} , cal mol⁻¹) (equation A1):

$$\ln K_H = G_{cav} + G_{int} + RT \ln \left(\frac{RT}{V_m} \right) \quad A1$$

where R is the molar gas constant ($1.987 \text{ cal K}^{-1} \text{ mol}^{-1}$) and T is the system temperature (K) (Pierotti 1963; Pierotti 1965; Pierotti 1975). Values of G_{cav} for specific gas solute-solvent systems can be calculated using only solvent and solute size parameters (σ_1 and σ_2 respectively) and the molar volume for the solvent (A2 – A5):

$$\frac{G_{cav}}{RT} = -\ln(1 - y) + (3y/1 - y)R + [(3y/1 - y) + \frac{9}{2}(y/1 - y)^2]R^2 \quad A2$$

$$R = \frac{\sigma_2}{\sigma_1} \quad A3$$

$$y = \frac{\pi \rho \sigma_1^3}{6} \quad A4$$

$$\rho = \frac{N}{V_m} \quad A5$$

where N is Avogadro's number. Since G_{cav} reflects the work required to form a cavity within the condensed solvent phase, this is always a positive value. The initiation of solute-solvent interactions upon insertion of the solute in to the cavity liberates free energy. Therefore G_{int} is always negative and may be calculated by consideration of the dispersion, induction and dipolar interactive contributions, using the polarizability (α_i , cm^3) and dipole moment (μ_i , e.s.u. cm) for both solvent and solute (A6 – A10):

$$\frac{G_i}{RT} = -\left(\frac{16}{3}\right) \left(\frac{e_{dis}^*}{kT}\right) - 8 \frac{e_{ind}^* + e_{dip}^*}{kT} \quad A6$$

$$e_i^* = \frac{\pi \rho C_i}{6\sigma_{12}^3} \quad A7$$

$$C_{dis} = 4\epsilon_{12}\sigma_{12}^6 = 4(\epsilon_1\epsilon_2)^{\frac{1}{2}}[(\sigma_1 + \sigma_2)/2]^6 \quad A8$$

$$C_{ind} = \mu_1^2\alpha_2 + \mu_2^2\alpha_1 \quad A9$$

$$C_{dip} = \frac{2\mu_1^2\mu_2^2}{3kT} \quad A10$$

where k is the Boltzmann constant ($1.38 \times 10^{-16} \text{ erg K}^{-1}$). Parameters for a range of different gas solutes (Table A1a) and physical solvents (Table A1b) have been sourced from the literature (Hirschfelder *et al.*, 1954; Pierotti *et al.*, 1963; Pierotti *et al.*, 1965; Wilhelm and Battino, 1971; De

Ligny and Van Der Veen, 1972; Pierotti *et al.*, 1975; Wilcock *et al.*, 1978; Brückl and Kim, 1981). Values of σ_2 for the volatile siloxane polymers were unavailable in the literature, with the exception of D4 (Wilcock *et al.*, 1978), and were estimated using respective density data of the respective solvents at room temperature (equations A11 – A12):

$$\sigma_1 = (0.9275 \pm 0.0126)\sigma_0 - (0.8465 \pm 0.0084) \times 10^{-8} \quad \text{A11}$$

$$\sigma_0 = \left(\frac{6V_m}{N\pi} \right)^{\frac{1}{3}} \quad \text{A12}$$

where σ_1 determined for each siloxane in the solvent phase was considered directly analogous to respective values of σ_2 in the vapour phase (Brückl *et al.*, 1981). Similarly, values for solvent polarizability were calculable from refractive index data if not available from the literature (equation A13):

$$\alpha_1 = \frac{(n_D^2 - 1)3M_r}{(n_D^2 + 2)\rho 4\pi N} \quad \text{A13}$$

where n_D is the solvent refractive index and ρ here is the solvent density (Brückl and Kim, 1981).

Table 2.A1a Scaled particle theory gas solute parameters

Gas	Chemical formula	Molecular mass M_r g mol^{-1}	Size parameter σ_2 10^8 cm	Energy parameter ϵ_2/k K	Dipole moment μ_2 Debyes	Polarizability α_2 10^{24} cm^3
Environmentally significant non-polar gases						
Hydrogen	H ₂	2.00	2.94	42	0	0.802
Methane	CH ₄	16.04	3.70	157	0	2.70
Nitrogen	N ₂	28.01	3.70	95	0	1.73
Ethane	C ₂ H ₆	30.07	4.38	236	0	4.33
Oxygen	O ₂	32.00	3.46	118	0	1.56
Propane	C ₃ H ₈	44.10	5.06	230	0	6.16
<i>n</i> -Butane	C ₄ H ₁₀	58.12	4.997	410	0	8.20
Environmentally significant polar gases						
Ammonia	NH ₃	17.03	3.38	183	1.471	2.26
Acetylene	C ₂ H ₂	26.04	4.16	199	0	3.19
Carbon monoxide	CO	28.01	3.76	100	-	1.93
Ethylene	C ₂ H ₄	28.05	4.07	230	0	3.19
Nitric oxide	NO	30.01	3.17	131	0.159	1.70
Hydrogen sulfide	H ₂ S	34.08	3.67	250	0.97	3.782
Carbon dioxide	CO ₂	44.01	3.94	195	0	2.59
Nitrous oxide	N ₂ O	44.01	3.85	228	0.161	2.92
Sulfur dioxide	SO ₂	64.06	4.29	252	1.633	4.28
Chlorine	Cl ₂	70.91	4.12	357	0	4.50
Other gases and vapours						
Helium	He	4.00	2.63	6.03	0	0.204
Neon	Ne	20.18	2.78	34.9	0	0.393
Argon	Ar	39.95	3.40	122	0	1.63
Krypton	Kr	83.80	3.60	158	0	2.46
Xenon	Xe	131.29	4.06	229	0	4.00
Radon	Rn	222	4.36	290	0	5.86
Hexamethyldisiloxane	L2	162.38	7.29	-	0.74	19.38
Octamethyltrisiloxane	L3	236.53	8.16	-	0.99	26.73
Decamethyltetrasiloxane	L4	310.69	8.88	-	1.21	34.10
Hexamethylcyclotrisiloxane	D3	222.46	7.35	-	-	20.50
Octamethylcyclotetrasiloxane	D4	296.62	8.32	696	1.09	29.56
Decamethylcyclopentasiloxane	D5	370.77	9.09	-	1.35	36.87

Table 2.A1b Scaled particle theory solvent parameters

Physical solvent	Molar volume V_m $\text{cm}^3 \text{mol}^{-1}$	Size parameter σ_2 10^8cm	Energy parameter ϵ_2/k K	Dipole moment μ_2 Debyes	Polarizability α_2 10^{24}cm^3
Non-polar solvents					
Benzene	89.4	5.26	531	0	10.39
Cyclohexane	108.7	5.63	573	0	11.00
<i>n</i> -Hexane	131.6	5.92	517	0	11.83
Toluene	106.9	5.64	575	0	12.32
Methyl-cyclohexane	128.4	5.99	599	0	12.75
<i>n</i> -Heptane	147.4	6.25	573	0	13.70
<i>n</i> -Octane	163.4	6.54	611	0	15.50
<i>n</i> -Nonane	179.6	6.83	650	0	17.34
<i>n</i> -Decane	196.0	7.08	601	0	19.17
Carbon tetrachloride	97.1	5.37	536	0	10.52
Bromo-cyclohexane	122.7	6.06	707	-	-
<i>n</i> -Dodecane	228.3	7.58	715	0	21.90
<i>n</i> -Tetradecane	260.7	8.00	716	0	26.60
Perfluoro- <i>n</i> -heptane	227.3	7.04	455	0	12.97
Polar aprotic solvents					
Acetonitrile	52.8	4.20	275	3.38	4.42
Acetone	74.0	4.76	362	2.78	6.43
Dimethylsulfoxide	71.4	4.91	333	3.90	7.97
Propylene carbonate	85.2	5.26	400	4.98	8.52
[EMIM][EtSO ₄]	190.82	7.00	-	-	-
Genosorb 1753 (Selexol)	328.3	8.55	498	2.82	34.36
Polar protic solvents					
Water	18.1	2.75	78	1.86	1.47
Methanol	40.7	3.69	234	1.72	3.26
Ethanol	58.7	4.34	324	1.70	5.12
Ethylene glycol	56.0	4.37	658	2.34	5.72

Table 2.A2 Solubility and diffusivity references for figures not included within the text.

Barrie, J. A. <i>et al.</i> , 1978
Battino and Clever, 1966
Bermejo, M. D. <i>et al.</i> , 2013
Edwards, C. J. C. <i>et al.</i> , 1980
Hayduk and Pahlevanzadeh, 1987
Hesse, P. J. <i>et al.</i> , 1996
Hildebrand and Lamoreaux, 1974a
Hildebrand and Lamoreaux, 1974b
Himmelblau, D. M., 1964
Jalili, A. H., 2010
Jou, F. <i>et al.</i> , 2006
Kuthan, K. <i>et al.</i> , 1989
Littel, R. J. <i>et al.</i> , 1991
Littel, R. J. <i>et al.</i> , 1992a
Littel, R. J. <i>et al.</i> , 1992b
Liu, Q. <i>et al.</i> , 1996
Lühring and Schumpe, 1989
Miyano and Hayduk, 1986
Murrieta-Guevara, F. <i>et al.</i> , 1988
Sahgal, A., <i>et al.</i> , 1978
Tominaga, T. <i>et al.</i> , 1986
Versteeg and van Swaaij, 1988
Witherspoon and Saraf, 1965

References

Abraham, M. H. (1993), "Scales of solute hydrogen-bonding: Their construction and application to physicochemical and biochemical processes", *Chemical Society Reviews*, vol. 22, no. 2, pp. 73-83.

Abraham, M. H., Andonian-Haftvan, J., Whiting, G. S., Leo, A. and Taft, R. S. (1994), "Hydrogen bonding. Part 34. The factors that influence the solubility of gases and vapours in water at 298 K, and a new method for its determination", *Journal of the Chemical Society, Perkin Transactions 2*, no. 8, pp. 1777-1791.

Abraham, M. H., Whiting, G. S., Carr, P. W. and Ouyang, H. (1998), "Hydrogen bonding. Part 45. The solubility of gases and vapours in methanol at 298 K: An LFER analysis", *Journal of the Chemical Society, Perkin Transactions 2*, no. 6, pp. 1385-1390.

Ahmed, H., Poole, C. F. and Kozerski, G. E. (2007), "Determination of descriptors for organosilicon compounds by gas chromatography and non-aqueous liquid-liquid partitioning", *Journal of Chromatography A*, vol. 1169, no. 1-2, pp. 179-192.

Ajhar, M., Travesset, M., Yüce, S. and Melin, T. (2010), "Siloxane removal from landfill and digester gas - A technology overview", *Bioresource technology*, vol. 101, no. 9, pp. 2913-2923.

Albo, J., Luis, P. and Irabien, A. (2011), "Absorption of coal combustion flue gases in ionic liquids using different membrane contactors", *Desalination and Water Treatment*, vol. 27, no. 1-3, pp. 54-59.

Aschenbrenner, O. and Styring, P. (2010), "Comparative study of solvent properties for carbon dioxide absorption", *Energy and Environmental Science*, vol. 3, no. 8, pp. 1106-1113.

Atchariyawut, S., Jiraratananon, R. and Wang, R. (2007), "Separation of CO₂ from CH₄ by using gas-liquid membrane contacting process", *Journal of Membrane Science*, vol. 304, no. 1-2, pp. 163-172.

Barrie, J. A., Dawson, R. B. and Sheppard, R. N. (1978), "Diffusion in binary liquid mixtures of non electrolytes", *Journal of the Chemical Society, Faraday Transactions 1: Physical Chemistry in Condensed Phases*, vol. 74, pp. 490-497.

Battino, R. and Clever, H. L. (1966), "The solubility of gases in liquids", *Chemical Reviews*, vol. 66, no. 4, pp. 395-463.

Bermejo, M. D., Fieback, T. M. and Martín, Á. (2013), "Solubility of gases in 1-alkyl-3-methylimidazolium alkyl sulfate ionic liquids: Experimental determination and modeling", *Journal of Chemical Thermodynamics*, vol. 58, pp. 237-244.

Brückl, N. and Kim, J. I. (1981), "Gibbs Free Energies of Solute and Solvent Interactions for He, Ar, Kr, Xe, H₂, O₂, N₂, CH₄, SF₆, C₂H₄, CO₂, and C₂H₂ in Various Solvents: Comparison of Theoretical Prediction with Experiment", *Zeitschrift für Physikalische Chemie Neue Folge*, vol. 126, pp. 133-150.

Bucklin, R. W. and Schendel, R. L. (1984), "Comparison of Fluor Solvent and Selexol Processes", *Energy Process*, vol. 4, no. 3, pp. 137-142.

Burr, B. and Lyddon, L. (2008), "A comparison of physical solvents for acid gas removal", *GPA Annual Convention Proceedings*, vol. 1, pp. 100-113.

Campanell, F. C., Battino, R. and Seybold, P. G. (2010), "On the role of solute polarizability in determining the solubilities of gases in liquids", *Journal of Chemical and Engineering Data*, vol. 55, no. 1, pp. 37-40.

Cohan, D. S. and Douglass, C. (2011), "Potential emissions reductions from grandfathered coal power plants in the United States", *Energy Policy*, vol. 39, no. 9, pp. 4816-4822.

Côte, P., Bersillon, J. - and Huyard, A. (1989), "Bubble-free aeration using membranes: Mass transfer analysis", *Journal of Membrane Science*, vol. 47, no. 1-2, pp. 91-106.

Deed, C., Gronow, J., Rosevear, J., Braithwaite, P., Smith, R. and Stanley, P. (2004), "Guidance on Gas Treatment Technologies for Landfill Gas Engines", *Environment Agency Landfill Directive*.

De Ligny, C. L. and Van Der Veen, N. G. (1972), "A test of Pierotti's theory for the solubility of gases in liquids, by means of literature data of solubility and entropy of solution", *Chemical Engineering Science*, vol. 27, no. 2, pp. 391-401.

Demontigny, D., Tontiwachwuthikul, P. and Chakma, A. (2005), "Comparing the absorption performance of packed columns and membrane contactors", *Industrial and Engineering Chemistry Research*, vol. 44, no. 15, pp. 5726-5732.

Dickinson, E. and McLure, I. A. (1974), "Thermodynamics of n-alkane + dimethylsiloxane mixtures. Part 3.-Excess volumes", *Journal of the Chemical Society, Faraday Transactions 1: Physical Chemistry in Condensed Phases*, vol. 70, pp. 2328-2337.

Dindore, V. Y., Brilman, D. W. F., Geuzebroek, R. H. and Versteeg, G. F. (2004), "Membrane-solvent selection for CO₂ removal using membrane gas-liquid contactors", *Separation and Purification Technology*, vol. 40, no. 2, pp. 133-145.

Edwards, C. J. C., Stepto, R. F. T. and Semlyen, J. A. (1980), "Studies of cyclic and linear poly(dimethyl siloxanes): 5. Diffusion behaviour in dilute solution", *Polymer*, vol. 21, no. 7, pp. 781-786.

Edwards, C. J. C., Stepto, R. F. T. and Semlyen, J. A. (1982), "Studies of cyclic and linear poly(dimethyl siloxanes):7. Diffusion behaviour in a poor solvent", *Polymer*, vol. 23, no. 6, pp. 865-868.

Eley, D. D. (1939), "On the solubility of gases. Part I. - The inert gases in water", *Transactions of the Faraday Society*, vol. 35, pp. 1281-1293.

Evren, V. and Özdural, A. R. (1995), "A new technique for the determination of mass transfer coefficients in packed columns for physical gas absorption systems", *The Chemical Engineering Journal and The Biochemical Engineering Journal*, vol. 57, no. 1, pp. 67-71.

Frank, H. S. and Evans, M. W. (1945), "Free volume and entropy in condensed systems III. Entropy in binary liquid mixtures; Partial molal entropy in dilute solutions; Structure and

thermodynamics in aqueous electrolytes", *The Journal of chemical physics*, vol. 13, no. 11, pp. 507-532.

Frank, M. J. W., Kuipers, J. A. M. and Van Swaaij, W. P. M. (1996), "Diffusion coefficients and viscosities of CO₂ + H₂O, CO₂ + CH₃OH, NH₃ + H₂O, and NH₃ + CH₃OH liquid mixtures", *Journal of Chemical and Engineering Data*, vol. 41, no. 2, pp. 297-302.

Graziano, G. (2002), "Size dependence of the solubility of nonpolar compounds in different solvents", *Canadian Journal of Chemistry*, vol. 80, no. 4, pp. 401-412.

Groves, M., Schwefer, M. and Siefert, R. (2006), "Nitric acid – Without the Emissions", *Chemical Engineer*, July, pp. 66-71.

Groves, M. and Frank, C. (2009), "EnviNOx®: Process for N₂O and NO_x Abatement in Nitric Acid Plants", *Nitrogen and Syngas Conference, February 22-25 2009, Rome, Italy*.

Grund, G., Schumpe, A. and Deckwer, W. -. (1992), "Gas-Liquid mass transfer in a bubble column with organic liquids", *Chemical Engineering Science*, vol. 47, no. 13-14, pp. 3509-3516.

Gwinner, B., Roizard, D., Lapicque, F., Favre, E., Cadours, R., Boucot, P. and Carrette, P. -. (2006), "CO₂ capture in flue gas: Semiempirical approach to select a potential physical solvent", *Industrial and Engineering Chemistry Research*, vol. 45, no. 14, pp. 5044-5049.

Hayduk, W. and Pahlevanzadeh, H. (1987), "SOLUBILITY OF SULFUR DIOXIDE AND HYDROGEN SULFIDE IN ASSOCIATING SOLVENTS", *Canadian Journal of Chemical Engineering*, vol. 65, no. 2, pp. 299-307.

Heintz, Y. J., Sehabiague, L., Morsi, B. I., Jones, K. L. and Pennline, H. W. (2008), "Novel physical solvents for selective CO₂ capture from fuel gas streams at elevated pressures and temperatures", *Energy and Fuels*, vol. 22, no. 6, pp. 3824-3837.

Hesse, P. J., Battino, R., Scharlin, P. and Wilhelm, E. (1996), "Solubility of gases in liquids. 20. Solubility of He, Ne, Ar, Kr, N₂, O₂, CH₄, CF₄, and SF₆ in n-Alkanes n-C₁H₂I+2 (6 = I = 16) at 298.15 K", *Journal of Chemical and Engineering Data*, vol. 41, no. 2, pp. 195-201.

Hildebrand, J. H. and Scott, R. L. (1950), "The Solubility of Nonelectrolytes New 3rd Edition", *American Chemical Society Monograph No. 17, Reinhold Publishing Corporation.*

Hildebrand, J. H., Prausnitz, J. M. and Scott, R. L. (1970), "Regular and Related Solutions – The Solubility of Gases, Liquid, and Solids", *Van Nostrand Reinhold Company, New York, USA.*

Hildebrand, J. H. and Lamoreaux, R. H. (1974a), "Solubility of gases in liquids: Fact and theory", *Industrial and Engineering Chemistry*, vol. 13, no. 2, pp. 110-115.

Hildebrand, J. H. and Lamoreaux, R. H. (1974b), "Diffusivity of Gases in Liquids", *Proceedings of the National Academy of Sciences USA*, vol. 71, no. 9, pp. 3321-3324.

Himmelblau, D. M. (1964), "Diffusion of dissolved gases in liquids", *Chemical Reviews*, vol. 64, no. 5, pp. 527-550.

Hirschfelder, J. O., Curtiss, C. F., and Bird, R. B. (1954), "Molecular theory of gases and liquids", *Wiley, New York.*

Huppmann, R., Lohoff, H. W. and Schröder, H. F. (1996), "Cyclic siloxanes in the biological waste water treatment process - Determination, quantification and possibilities of elimination", *Fresenius' journal of analytical chemistry*, vol. 354, no. 1, pp. 66-71.

Israelachvili, J. N. (2011), "Intermolecular and Surface Forces, Third Edition", *Elsevier.*

Jalili, A. H., Mehdizadeh, A., Shokouhi, M., Ahmadi, A. N., Hosseini-Jenab, M. and Fateminassab, F. (2010), "Solubility and diffusion of CO₂ and H₂S in the ionic liquid 1-ethyl-3-methylimidazolium ethylsulfate", *Journal of Chemical Thermodynamics*, vol. 42, no. 10, pp. 1298-1303.

Javed, K. H., Mahmud, T. and Purba, E. (2006), "Enhancement of mass transfer in a spray tower using swirling gas flow", *Chemical Engineering Research and Design*, vol. 84, no. 6 A, pp. 465-477.

Jefferson, B., Nazareno, C., Georgaki, S., Gostelow, P., Stuetz, R. M., Longhurst, P. and Robinson, T. (2005), "Membrane gas absorbers for H₂S removal - Design, operation and technology

integration into existing odour treatment strategies", *Environmental technology*, vol. 26, no. 7, pp. 793-804.

Jou, F. -, Schmidt, K. A. G. and Mather, A. E. (2006), "Vapor-liquid equilibrium in the system ethane + ethylene glycol", *Fluid Phase Equilibria*, vol. 240, no. 2, pp. 220-223.

Karoor, S. and Sirkar, K. K. (1993), "Gas absorption studies in microporous hollow fiber membrane modules", *Industrial and Engineering Chemistry Research*, vol. 32, no. 4, pp. 674-684.

Kierzkowska-Pawlak, H. and Chacuk, A. (2010), "Carbon dioxide desorption from saturated organic solvents", *Chemical Engineering and Technology*, vol. 33, no. 1, pp. 74-81.

Kies, F. K., Benadda, B. and Otterbein, M. (2006), "Hydrodynamics, mass transfer and gas scrubbing in a co-current droplet column operating at high gas velocities", *Chemical Engineering and Technology*, vol. 29, no. 10, pp. 1205-1215.

Kohl, A. and Nielsen, R. (1997), "Gas Purification, Fifth Edition", *Gulf Publishing Company*.

Kuthan, K., Endršt, M. and Brož, Z. (1989), "Mass transfer in liquid films during absorption Part II. Solubilities and diffusivities of He, N₂ and C₃H₈ in aqueous ethylene glycol solutions at 25°C", *Chemical Engineering and Processing*, vol. 25, no. 2, pp. 65-74.

Lazaridis, T. (2001), "Solvent size vs cohesive energy as the origin of hydrophobicity", *Accounts of Chemical Research*, vol. 34, no. 12, pp. 931-937.

Leaist, D. G. (1984), "Diffusion coefficient of aqueous sulfur dioxide at 25 °C", *Journal of Chemical and Engineering Data*, vol. 29, no. 3, pp. 281-282.

Lebrero, R., Bouchy, L., Stuetz, R. and Muñoz, R. (2011), "Odor assessment and management in wastewater treatment plants: A review", *Critical Reviews in Environmental Science and Technology*, vol. 41, no. 10, pp. 915-950.

Lee, B. (1985), "The physical origin of the low solubility of nonpolar solutes in water", *Biopolymers - Peptide Science Section*, vol. 24, no. 5, pp. 813-823.

Lefortier, S. G. R., Hamersma, P. J., Bardow, A. and Kreutzer, M. T. (2012), "Rapid microfluidic screening of CO₂ solubility and diffusion in pure and mixed solvents", *Lab on a Chip - Miniaturisation for Chemistry and Biology*, vol. 12, no. 18, pp. 3387-3391.

Li, D., Shi, P., Wang, J., Li, J. and Su, R. (2014), "High-efficiency absorption of high NO_x concentration in water or PEG using capillary pneumatic nebulizer packed with an expanded graphite filter", *Chemical Engineering Journal*, vol. 237, pp. 8-15.

Littel, R. J., Versteeg, G. F. and Van Swaaij, W. P. M. (1991), "Physical absorption into non-aqueous solutions in a stirred cell reactor", *Chemical Engineering Science*, vol. 46, no. 12, pp. 3308-3313.

Littel, R. J., Versteeg, G. F. and Van Swaaij, W. P. M. (1992a), "Diffusivity measurements in some organic solvents by a gas-liquid diaphragm cell", *Journal of Chemical and Engineering Data*, vol. 37, no. 1, pp. 42-45.

Littel, R. J., Versteeg, G. F. and van Swaal, W. P. M. (1992b), "Solubility and diffusivity data for the absorption of COS, CO₂, and N₂O in amine solutions", *Journal of Chemical and Engineering Data*, vol. 37, no. 1, pp. 49-54.

Liu, Q., Takemura, F. and Yabe, A. (1996), "Solubility and diffusivity of carbon monoxide in liquid methanol", *Journal of Chemical and Engineering Data*, vol. 41, no. 3, pp. 589-592.

Loerting, T., Tautermann, C., Kroemer, R. T., Kohl, I., Hallbrucker, A., Mayer, E. and Liedl, K. R. (2000), "On the surprising kinetic stability of carbonic acid (H₂CO₃)", *Angewandte Chemie - International Edition*, vol. 39, no. 5, pp. 892-894.

Lühning, P. and Schumpe, A. (1989), "Gas solubilities (H₂, He, N₂, CO, O₂, Ar, CO₂) in organic liquids at 293.2 K", *Journal of Chemical and Engineering Data*, vol. 34, no. 2, pp. 250-252.

Luis, P., Ortiz, I., Aldaco, R., Garea, A. and Irabien, Á. (2007), "Recovery of sulfur dioxide using non-dispersive absorption", *International Journal of Chemical Reactor Engineering*, vol. 5. Article number A52.

Luis, P., Garea, A. and Irabien, A. (2009), "Zero solvent emission process for sulfur dioxide recovery using a membrane contactor and ionic liquids", *Journal of Membrane Science*, vol. 330, no. 1-2, pp. 80-89.

Mansourizadeh, A., Ismail, A. F. and Matsuura, T. (2010), "Effect of operating conditions on the physical and chemical CO₂ absorption through the PVDF hollow fiber membrane contactor", *Journal of Membrane Science*, vol. 353, no. 1-2, pp. 192-200.

McLeod, A., Jefferson, B. and McAdam, E. J. (2013), "Quantifying the loss of methane through secondary gas mass transport (or 'slip') from a micro-porous membrane contactor applied to biogas upgrading", *Water research*, vol. 47, no. 11, pp. 3688-3695.

Mehra Y. R. (1983), "Process for Recovery of Natural Gas Liquids from a Sweetened Natural gas stream", *United States Patent 4421535*.

Miller, M. B., Luebke, D. R. and Enick, R. M. (2010), "CO₂-philic oligomers as novel solvents for CO₂ absorption", *Energy and Fuels*, vol. 24, no. 11, pp. 6214-6219.

Miyano, Y. and Hayduk, W. (1986), "Solubility of butane in several polar and nonpolar solvents and in an acetone-butanol solvent solution", *Journal of Chemical and Engineering Data*, vol. 31, no. 1, pp. 77-80.

Murrieta-Guevara, F., Romero-Martinez, A. and Trejo, A. (1988), "Solubilities of carbon dioxide and hydrogen sulfide in propylene carbonate, N-methylpyrrolidone and sulfolane", *Fluid Phase Equilibria*, vol. 44, no. 1, pp. 105-115.

Nii, S., Takeuchi, H. and Takahashi, K. (1992), "Removal of CO₂ by gas absorption across a polymeric membrane", *Journal of Chemical Engineering of Japan*, vol. 25, no. 1, pp. 67-72.

Padurean, A., Cormos, C. -. and Agachi, P. -. (2012), "Pre-combustion carbon dioxide capture by gas-liquid absorption for Integrated Gasification Combined Cycle power plants", *International Journal of Greenhouse Gas Control*, vol. 7, pp. 1-11.

Pierotti, R. A. (1963), "The solubility of gases in liquids", *Journal of Physical Chemistry*, vol. 67, no. 9, pp. 1840-1845.

Pierotti, R. A. (1965), "Aqueous solutions of nonpolar gases", *Journal of Physical Chemistry*, vol. 69, no. 1, pp. 281-288.

Pierotti, R. A. (1976), "A scaled particle theory of aqueous and nonaqueous solutions", *Chemical reviews*, vol. 76, no. 6, pp. 717-726.

Ranke, G. (1973), "Advantages of the Rectisol-wash Process in the Selective H₂S Removal from Gas Mixtures", *Linde Reports on Science and Technology*, vol. 18, pp. 7-13.

Rasi, S., Lantelä, J., Veijanen, A. and Rintala, J. (2008), "Landfill gas upgrading with countercurrent water wash", *Waste Management*, vol. 28, no. 9, pp. 1528-1534.

Reed, W. B., Semmens, M. J. and Cussler, E. L. (1995), "Membrane contactors", in *Membrane Separations Technology Principles and Applications*, Elsevier.

Robeson, L. M., Smith, Z. P., Freeman, B. D. and Paul, D. R. (2014), "Contributions of diffusion and solubility selectivity to the upper bound analysis for glassy gas separation membranes", *Journal of Membrane Science*, vol. 453, pp. 71-83.

Ross, M. and Hildebrand, J. H. (1964), "Diffusion of hydrogen, deuterium, nitrogen, argon, methane, and carbon tetrafluoride in carbon tetrachloride", *The Journal of Chemical Physics*, vol. 40, no. 8, pp. 2397-2399.

Sahgal, A., La, H. M. and Hayduk, W. (1978), "SOLUBILITY OF ETHYLENE IN SEVERAL POLAR AND NON-POLAR SOLVENTS.", *Canadian Journal of Chemical Engineering*, vol. 56, no. 3, pp. 354-357.

Schwartz, S. E. (1986), "Mass-transport considerations pertinent to aqueous phase reactions of gases in liquid-water clouds", *NATO ASI Series*, vol. G6, pp. 415-471.

Sherwood, T. K. and Holloway, F. A. L. (1940), "Performance of Packed Tower – Experimental Studies of Absorption and Desorption", *Transactions of the American Institute of Chemical Engineers*, vol. 36, pp. 21-37.

Sweny, J. W. (1973). "Synthetic Fuel Gas Purification by the Selexol Process", *165th National Meeting of the American Chemical Society Division of Fuel and Chemistry, Dallas, Texas, USA, April 8-12*.

Tan, X., Tan, S. P., Teo, W. K. and Li, K. (2006), "Polyvinylidene fluoride (PVDF) hollow fibre membranes for ammonia removal from water", *Journal of Membrane Science*, vol. 271, no. 1-2, pp. 59-68.

Tanda, T., Shirai, K., Matsumura, Y. and Kitahara, H. (2011), "New correlation for mass transfer characteristics of spray column", *Industrial and Engineering Chemistry Research*, vol. 50, no. 23, pp. 13554-13560.

Tekie, Z., Li, J. and Morsi, B. I. (1997), "Mass Transfer Parameters of O₂ and N₂ in Cyclohexane under Elevated Pressures and Temperatures: A Statistical Approach", *Industrial and Engineering Chemistry Research*, vol. 36, no. 9, pp. 3879-3888.

Tominaga, T., Battino, R., Gorowara, H. K., Dixon, R. D. and Wilhelm, E. (1986), "SOLUBILITY OF GASES IN LIQUIDS. 17. THE SOLUBILITY OF He, Ne, Ar, Kr, H₂, N₂, O₂, CO, CH₄, CF₄, AND SF₆ IN TETRACHLOROMETHANE AT 283-318 K.", *Journal of Chemical and Engineering Data*, vol. 31, no. 2, pp. 175-180.

Tremblay, P., Savard, M. M., Vermette, J. and Paquin, R. (2006), "Gas permeability, diffusivity and solubility of nitrogen, helium, methane, carbon dioxide and formaldehyde in dense polymeric membranes using a new on-line permeation apparatus", *Journal of Membrane Science*, vol. 282, no. 1-2, pp. 245-256.

Van Dam, M. H. H., Lamine, A. S., Roizard, D., Lochon, P. and Roizard, C. (1997), "Selective Sulfur Dioxide Removal Using Organic Solvents", *Industrial and Engineering Chemistry Research*, vol. 36, no. 11, pp. 4628-4637.

Versteeg, G. F. and van Swaaij, W. P. M. (1988), "SOLUBILITY AND DIFFUSIVITY OF ACID GASES (CO₂, N₂O) IN AQUEOUS ALKANOLAMINE SOLUTIONS.", *Journal of Chemical and Engineering Data*, vol. 33, no. 1, pp. 29-34.

Wheless, E. and Pierce, J. (2004), "Siloxanes in Landfill and Digester Gas Update", *SWANA 27th Landfill Gas Conference*, March 22-25.

Whitney, R. P and Vivian, J. E. (1941), "Solubility of chlorine in water", *Industrial and Engineering Chemistry*, vol. 33, no. 6, pp. 741-744.

Whitney, R. P and Vivian, J. E. (1949), "Absorption of Sulfur Dioxide in Water", *Chemical Engineering Progress*, vol. 45, no. 5, pp. 323-337.

Wilcock, R. J., McHale, J. L., Battino, R. and Wilhelm, E. (1978), "Solubility of gases in liquids. 12 Solubility of He, Ne, Ar, Kr, O₂, N₂, CO, CO₂, CH₄, CF₄, and SF₆ in octamethylcyclotetrasiloxane at 292 to 313 K", *Fluid Phase Equilibria*, vol. 2, no. 3, pp. 225-230.

Wilhelm, E. and Battino, R. (1971), "Estimation of Lennard-Jones (6,12) pair potential parameters from gas solubility data", *The Journal of Chemical Physics*, vol. 55, no. 8, pp. 4012-4017.

Wilhelm, E., Battino, R. and Wilcock, R. J. (1977), "Low-pressure solubility of gases in liquid water", *Chemical reviews*, vol. 77, no. 2, pp. 219-262.

Witherspoon, P. A. and Saraf, D. N. (1965), "Diffusion of methane, ethane, propane, and n-butane in water from 25 to 43°", *Journal of Physical Chemistry*, vol. 69, no. 11, pp. 3752-3755.

Wood, G. C. and Mehra, Y. R. (1995), "Absorption process without external solvent", *United States Patent*, 5462583.

Zhang, L. -, Wang, J. -, Xiang, Y., Zeng, X. -. and Chen, J. -. (2011), "Absorption of carbon dioxide with ionic liquid in a rotating packed bed contactor: Mass transfer study", *Industrial and Engineering Chemistry Research*, vol. 50, no. 11, pp. 6957-6964.

Chapter 3

Quantifying the loss of methane through secondary gas mass transport (or 'slip') from a micro-porous membrane contactor applied to biogas upgrading

Published in: Water Research (2013), vol. 47, no. 11, pp. 3688-3695.

Quantifying the loss of methane through secondary gas mass transport (or 'slip') from a micro-porous membrane contactor applied to biogas upgrading

Andrew McLeod, Bruce Jefferson and Ewan J. McAdam*

Cranfield Water Science Institute, Building 39, Cranfield University, Bedfordshire, MK43 0AL, UK

*Corresponding author e-mail: e.mcadam@cranfield.ac.uk

Abstract

Secondary gas transport during the separation of a binary gas with a micro-porous hollow fibre membrane contactor (HFMC) has been studied for biogas upgrading. In this application, the loss or 'slip' of the secondary gas (methane) during separation is a known concern, specifically since methane possesses the intrinsic calorific value. De-ionised (DI) water was initially used as the physical solvent. Under these conditions, carbon dioxide (CO_2) and methane (CH_4) absorption were dependent upon liquid velocity (V_L). Whilst the highest CO_2 flux was recorded at high V_L , selectivity toward CO_2 declined due to low residence times and a diminished gas-side partial pressure, and resulted in slip of approximately 5.2 % of the inlet methane. Sodium hydroxide was subsequently used as a comparative chemical absorption solvent. Under these conditions, CO_2 mass transfer increased by increasing gas velocity (V_G) which is attributed to the excess of reactive hydroxide ions present in the solvent, and the fast conversion of dissolved CO_2 to carbonate species reinitiating the concentration gradient at the gas-liquid interface. At high gas velocities, CH_4 slip was reduced to 0.1 % under chemical conditions. Methane slip is therefore dependent upon whether the process is gas phase or liquid phase controlled, since methane mass transport can be adequately described by Henry's law within both physical and chemical solvents. The addition of an electrolyte was found to further retard CH_4 absorption via the salting out effect. However, their applicability to physical solvents is limited since electrolytic concentration similarly impinges upon the solvents capacity for CO_2 . This study illustrates the significance of secondary gas mass transport, and furthermore shows that gas-phase controlled systems are recommended where greater selectivity is required.

Keywords: binary gas; slipping; slippage; fugitive; solvent recirculation; gas/liquid

3.1 Introduction

Biogas is a renewable source of methane (CH_4) produced on a large scale at wastewater treatment works during anaerobic digestion. Typically the biogas has a CH_4 content of 55-60 % by volume, compared to >90 % CH_4 for natural gas. Carbon dioxide (CO_2) is the key balancing gas contributing 35-50 % of the total gas volume. As an inert gas, CO_2 lowers the calorific value (CV) of the biogas from 36 MJ m^{-3} for natural gas to 21 MJ m^{-3} (Ryckebosch *et al*, 2011). Whilst the lower CV of biogas is appropriate for direct utilisation in combined heat and power (CHP) applications, the CV must be upgraded for use as biomethane, or natural gas alternative, principally through the selective separation of the CO_2 . As a result of incentivisation schemes, it is increasingly preferable to upgrade biogas for 'gas to grid' instead of electricity generation via CHP because of the disparity in value of the gas for these applications. For example, as a consequence of the renewable heat incentive (RHI) in the UK, a cubic meter of biogas is worth approximately £0.49 if used as a natural gas alternative but only £0.14 when applied to CHP (Ofgem, 2014).

Several technologies exist for selective CO_2 removal, including pressure swing adsorption (PSA), dense membrane separation and absorption columns using either water or a chemical as the absorption solvent. Whilst the specific mechanism for gas separation differs between technologies, these current process options are not able to offer definitive selectivity during separation, thus some loss of the secondary gas can be expected. The term slip corresponds to the loss of this secondary gas, in this case methane, from the product side due to either co-permeation, in the case of dense permeation membranes, or co-dissolution during absorption. The significance of slip to process operation is application specific. For example, in the case of dilute hydrogen sulfide (H_2S) absorption from air for odour treatment (Jefferson *et al.*, 2005; Esquiroz-Molina *et al.*, 2013), the co-solubilisation of the ternary gases nitrogen and oxygen (and low concentration CO_2) are not quantified, or considered. However, for biogas upgrading the significance of methane slip is considerable since methane possesses the intrinsic value as the product gas. Few published studies have sought to quantify slip. Early studies of full-scale dense gas membranes for CH_4 recovery from

landfill gas reported up to 18 % methane slip (Ho and Sirkar, 1992) though this has since been reduced using multiple membrane arrays to enable subsequent treatment of the retentate gas stream which comprises low concentration methane. By comparison, 8 % and 13.1 % CH₄ slip have been reported for PSA and absorption respectively, the latter using water as the solvent and a pressurised gas phase of between 20-25 bar (Baldwin, 2011; Lantela *et al.*, 2011).

For biogas upgrading at sewage works, packed tower absorption is the predominant technology employed with water used as the absorption solvent, for process simplicity, and due to the wide availability of treated final effluent on-site. Water demonstrates a reasonable selectivity for CO₂ since methane is only a partially soluble gas. Consequently, analysis of methane transport during process evaluation is often neglected. However, high liquid flow rates are demanded in absorption technologies that result in high methane slip over long operational periods. Several authors have considered the application of hollow fibre membrane contactors (HFMCs) as an alternative absorption technology to conventional packed towers for biogas upgrading (Atchariyawut *et al.*, 2007; Simons *et al.*, 2009). The hydrophobic membrane enables separation of the gas and liquid phases, with gaseous diffusion facilitated through the micro-porous membrane which enhances mass transfer and increases specific surface area availability compared to conventional absorbers. Consequently, Nii *et al.* (1992) noted an order of magnitude reduction in liquid flow rate when comparing a polydimethylsiloxane HFMC with a conventional packed absorption column to achieve comparable removal of CO₂ from flue gas. Whilst enhanced mass transfer has been ascertained, the fate of the secondary gas, or the slip, during absorption has not been examined and is central to understanding process efficacy. This study therefore seeks to quantify: (i) the mass transfer of the two principal biogas components methane and carbon dioxide to determine the significance of methane slip from HFMC applied to upgrading; (ii) the capacity to mitigate methane slip through manipulating solvent chemistry; and (iii) evaluating the impact of multiple solvent cycles on methane slip compared to single pass operation.

3.2 Materials and methods

3.2.1 Equipment setup and operation

Methane (99.995 %) and carbon dioxide (99.7 %) (BOC gases, Ipswich, UK) gases were controlled using mass flow controllers (0.01-1.0 L min⁻¹, Roxspur Measurement and Control Ltd., Sheffield, UK) and were mixed in-line to provide an initial 60/40 CH₄/CO₂ gas composition to the shell-side of the HFMC (Liqui-Cel® 1.7x5.5 MiniModule®, Membrana GmbH, Wuppertal, Germany) (Figure 3.1).

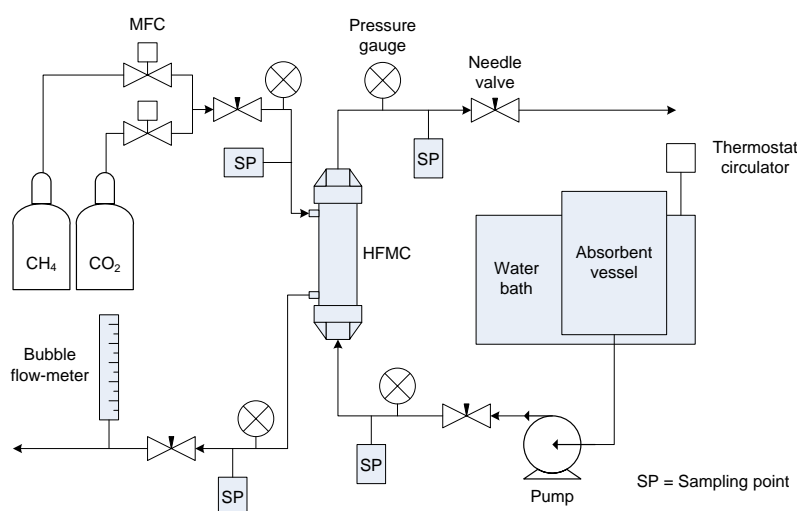


Figure 3.1 Schematic of the experimental set-up used for determining 'slip' from a polypropylene micro-porous hollow fibre membrane contactor.

The outlet gas flow rate was measured using a bubble flow meter (50 mL, Restek, Bellefonte, USA). Absorbent was stored in a 50 L PVC tank and maintained at 24-26 °C by a thermostat circulator (GD120, Grant Instruments Cambridge Ltd., Shepreth, UK) sited in the water bath. The absorbent was passed through the fibre lumen in counter-current mode using a centrifugal pump (max. 6 L min⁻¹, 50010 series, Jabsco GmbH, Norderstedt, Germany). The HFMC comprised 7400 polypropylene (PP) fibres, with a nominal outer diameter (OD) and length of 300 µm and 0.113 m respectively, yielding a surface area of 0.58 m² (based on inner fibre diameter, ID of 220 µm). The fibres were characterised with a nominal pore size of 0.03 µm and porosity of 40 %. The fibres were potted in

polyurethane fixed in a polycarbonate shell with an ID of 0.0425 m resulting in a packing density of 0.369.

Solvent recirculation was investigated to compare multiple passes (or cycles) of solvent use to single pass solvent use. For these experiments, a 10 L absorbent reservoir was incorporated into the liquid side of the experimental design to minimise the impact of sampling from the liquid phase on the resultant mass transfer data. The vessel was magnetically stirred to ensure complete mixing of the bulk solvent. During multiple-pass (MP) experiments, a smaller HFMC was employed to ensure that the MP tests could be conducted with a reasonably short timeframe. This smaller module (Liqui-Cel® 1x5.5 MiniModule®, Membrana GmbH, Wuppertal, Germany) comprised of 2300 identical hollow fibres (OD 300 µm/ ID of 220 µm/pore size 0.03 µm) but 0.10 m in length, yielding a surface area of 0.18 m².

3.2.2 Preparation and sampling

All absorbents were based on de-ionised (DI) water with a resistivity of 15.0 MΩ cm⁻¹. For experiments using chemically based solvents, either sodium chloride (NaCl) or sodium hydroxide (NaOH) was used (NaCl 99 % and NaOH 98 % pellets, Fisher Chemicals, Loughborough, UK). Chemical solutions were initially prepared as concentrates by adding 1755 g NaCl and/or 1320 g NaOH to 10 L of DI water with thorough mixing to ensure complete dissolution. Concentrates were then diluted in the absorbent tank to provide 1.0 M solutions. To determine liquid phase concentrations, the method adapted from Alberto *et al.*, (2000) was used in which evacuated vials were employed to ensure no exposure of aqueous solvent samples to the environment. Prior to use, the 22.7 mL GC-MS glass vials were capped and sealed with gas-tight PTFE/aluminium crimp caps (Fisherbrand, Fisher Scientific, Loughborough, UK). Vials were then evacuated for 20 seconds using a vacuum pump (CAPEX L2C, Charles Austen Pumps, Byfleet, Surrey, UK) at fixed pressure to ensure consistent vacuum pressures in each vial (0.3 atm). Aqueous solvent samples were collected from a luer lock needle fitted on the liquid outlet. The reduced vial pressure imposed a vacuum on the

liquid side enabling collection of a liquid sample, which when complete, had equilibrated to atmospheric pressure. Liquid samples were agitated for 7 minutes (maximum speed, Multi Reax, Heidolph, Schwabach, Germany), and were subsequently left to equilibrate overnight. The resultant dissolved phase concentrations were calculated based on a mass balance (Alberto *et al.*, 2000). Methane flux was calculated using:

$$J_{CH_4} = \frac{(Q_{L,i} \times c_f) - (Q_{L,o} \times c_r)}{M_{r,CH_4} \times A_m} \quad 1$$

Where J_{CH_4} is methane flux ($\text{mol m}^{-2} \text{s}^{-1}$), $Q_{L,i}$ and $Q_{L,o}$ are the inlet and outlet liquid flow rates respectively ($\text{m}^3 \text{s}^{-1}$), c_f and c_r are CH_4 concentrations found in the liquid feed and retentate respectively (g m^{-3}), M_{r,CH_4} is the relative molecular mass of methane and A_m is the active surface area of the HFMC (m^2). Gas samples were taken from GC septa fitted on the gas-side upstream and downstream of the contactor and injected onto a gas chromatograph. The CO_2 flux was calculated according to Atchariyawut *et al.* (2007):

$$J_{CO_2} = \frac{[(Q_{L,i} \times c_f) - (Q_{L,o} \times c_r) \times 273.15 \times 1000]}{22.4 \times T_g \times A_m} \quad 2$$

Where J_{CO_2} is the CO_2 flux ($\text{mol m}^{-2} \text{s}^{-1}$), $Q_{g,i}$ and $Q_{g,o}$ are the inlet and outlet gas flow rates respectively ($\text{m}^3 \text{s}^{-1}$), c_f and c_r are the CO_2 mole fraction in the gas feed and gas retentate respectively, T_g is the gas temperature (K) and A_m is the active surface area (m^2). Selectivity was calculated using (Rongwong *et al.*, 2012; Lu *et al.*, 2006):

$$\text{Selectivity} = \frac{R_{CO_2} / R_{CH_4}}{F_{CO_2} / F_{CH_4}} \quad 3$$

Where R_{CO_2} and R_{CH_4} are the CO_2 and CH_4 concentrations in the retentate liquid (g L^{-1}), and F_{CO_2} and F_{CH_4} are the CO_2 and CH_4 concentrations in the gas feed (g L^{-1}). All samples were analysed in triplicate.

3.2.3 Analysis

A gas chromatograph (GC) fitted with a thermal conductivity detector (TCD) was used to analyse the gas and liquid samples (200 Series GC-TCD Cambridge Scientific Instruments Ltd., Witchford, UK). Gas solutes were separated on an Alltech® CTR I concentric packed column which has a concentric column with a 1/4" outer column surrounding an 1/8" inner column (Alltech Associates Inc., Deerfield, Illinois, USA). Samples were introduced onto the column in a 1 mL volume and eluted using helium as the carrier gas at an entry pressure of 4.2 bar(g). The isothermal method used an injector temperature of 150 °C, an oven temperature of 30 °C and a detector temperature of 180 °C. The instrument was calibrated using certificated CO₂ and CH₄ gas standards (Scientific Technical Gases Ltd., Staffordshire, UK) prior to each analysis. A sharp methane peak eluted from the inner column containing mixed porous polymer packing at a retention time of 30 seconds followed by the CO₂ peak at 90 seconds. Concentration of chemically absorbed CO₂ in NaOH containing solutions, existing as carbonate, was ascertained by titration of retentate absorbent with 1.0 M HCl using BaCl₂ to neutralise the carbonate ions (Benedetti-Pichler and Cefola, 1939).

3.3 Results

3.3.1 Impact of solvent chemistry on biogas component flux

A CO₂ flux of $7.6 \times 10^{-5} \text{ mol}_{\text{CO}_2} \text{ m}^{-2} \text{ s}^{-1}$ was recorded using DI water as the absorption solvent, at a V_G of 0.0047 m s^{-1} and V_L of 0.0054 m s^{-1} , which corresponded to an L/G of 1.15, with a Reynolds number (Re) of 1.32 (Figure 3.2a). The L/G was progressively increased by raising liquid velocity to a maximum of 0.024 m s^{-1} ($Re = 5.90$), upon which a CO₂ flux of $1.7 \times 10^{-4} \text{ mol}_{\text{CO}_2} \text{ m}^{-2} \text{ s}^{-1}$ was recorded, representing an increase in CO₂ flux of approximately 200 %. Analogous behaviour was observed for CO₂ flux when NaCl was added as a simple electrolyte, where V_L ranged from 0.0074 m s^{-1} ($Re = 1.71$) to 0.022 m s^{-1} ($Re = 5.12$). Re values for the gas on the shell side ranged between an initial $Re = 10.5$

(accounting for viscosity of initial gas mixture and V_G of 0.0047 m s^{-1} ; Jackson, 1956) to a minimum $Re = 4.2$ at the HFMC outlet for DI solvent. Substitution of the DI and NaCl physical solvents for a 1 M NaOH chemical solvent resulted in a CO_2 flux of $2.98 \times 10^{-4} \text{ mol}_{\text{CO}_2} \text{ m}^{-2} \text{ s}^{-1}$ and $>99\%$ CH_4 concentration in the outgas, which remained unchanged when V_L was varied from 0.0122 m s^{-1} ($Re = 2.47$) to 0.0242 m s^{-1} ($Re = 4.90$). This corresponded to a plateau in CO_2 flux with increasing V_L , indicating that the process was gas phase controlled (Li *et al.*, 2005; Esquiroz-Molina *et al.*, 2013). Gas velocity (V_G) was subsequently increased from 0.0047 m s^{-1} to a maximum of 0.031 m s^{-1} at a fixed V_L of 0.0089 m s^{-1} to reduce the L/G ratio and identify the impact upon CO_2 flux (Figure 3.2b).

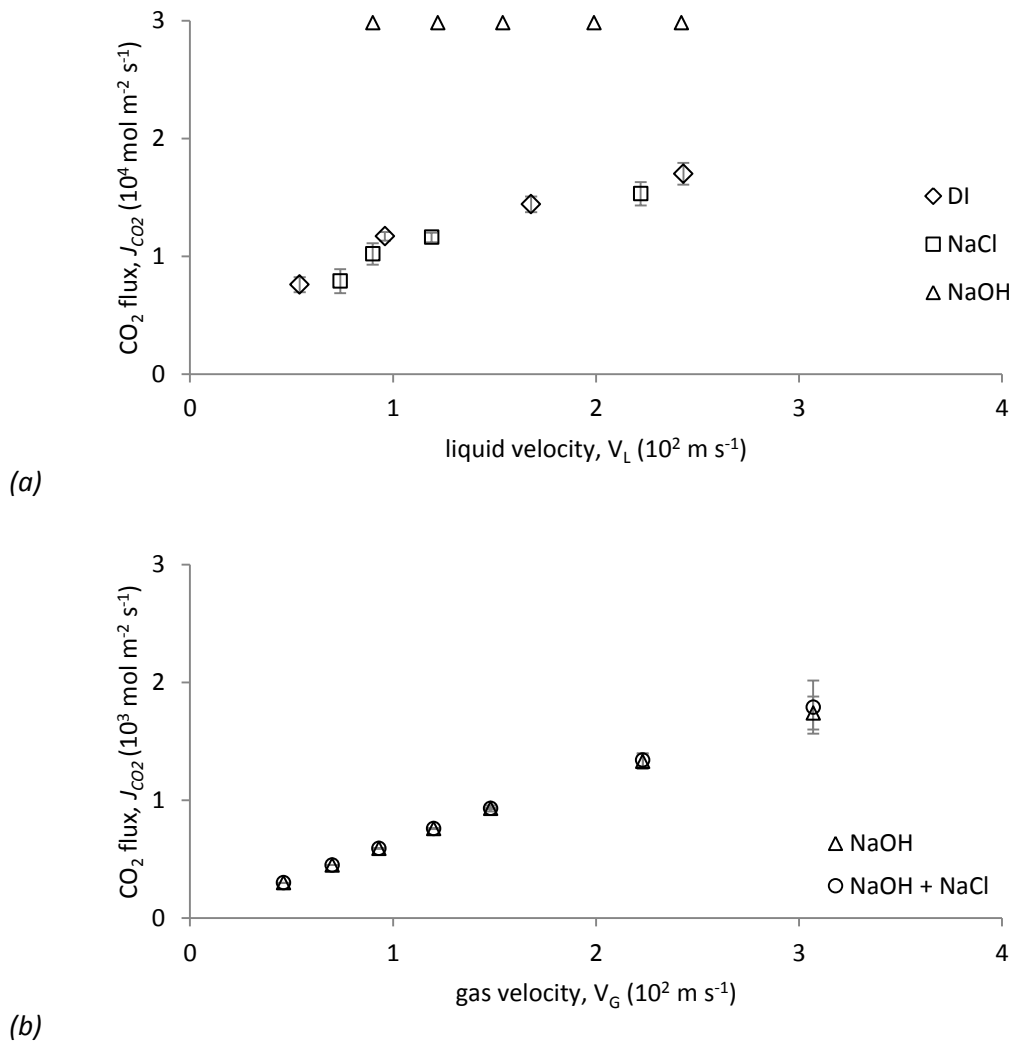


Figure 3.2 Impact of liquid velocity (V_L 0.0054 m s^{-1} to 0.024 m s^{-1}) with fixed initial gas velocity (V_G 0.0047 m s^{-1}) on CO_2 flux in DI, NaCl, and NaOH solvents ($24\text{--}26^\circ \text{C}$) (a) and impact of V_G (0.0017 m s^{-1} to 0.031 m s^{-1}) at fixed V_L (0.0089 m s^{-1}) on CO_2 flux in NaOH and NaOH + NaCl solvents ($24\text{--}26^\circ \text{C}$) (b).

CO₂ flux was found to be dependent upon V_G, with the highest CO₂ flux of $1.74 \times 10^{-3} \text{ mol}_{\text{CO}_2} \text{ m}^{-2} \text{ s}^{-1}$ recorded at a V_G of 0.031 m s^{-1} . Similarly to DI water, no quantifiable difference in CO₂ flux could be noted following the inclusion of NaCl to NaOH. Since both physical and chemical systems were ostensibly controlled by differing phases, direct comparison is difficult to ascertain. However, both V_L (0.009 m s^{-1}) and V_G (0.0047 m s^{-1}) were identical for DI and NaOH at an L/G of 1.92 which corresponded to the minimum CO₂ flux of $2.98 \times 10^{-4} \text{ mol}_{\text{CO}_2} \text{ m}^{-2} \text{ s}^{-1}$ recorded for the chemical solvent. The flow regime for gas in the shell side during variable V_G experiments using NaOH absorbents was relatively consistent with that observed for DI experiments where V_G was fixed. $Re = 70$ represents the greatest possible value, for an initial gas mixture and maximum V_G of 0.031 m s^{-1} , although this declines with loss of V_G and change in composition via rapid CO₂ absorption by NaOH.

The highest CH₄ flux was recorded using DI water. At an L/G of 1.15, methane flux was $2.03 \times 10^{-6} \text{ mol}_{\text{CH}_4} \text{ m}^{-2} \text{ s}^{-1}$ which increased to a maximum flux of $1.15 \times 10^{-5} \text{ mol}_{\text{CH}_4} \text{ m}^{-2} \text{ s}^{-1}$ at an L/G of 5.2 (Figure 3.3).

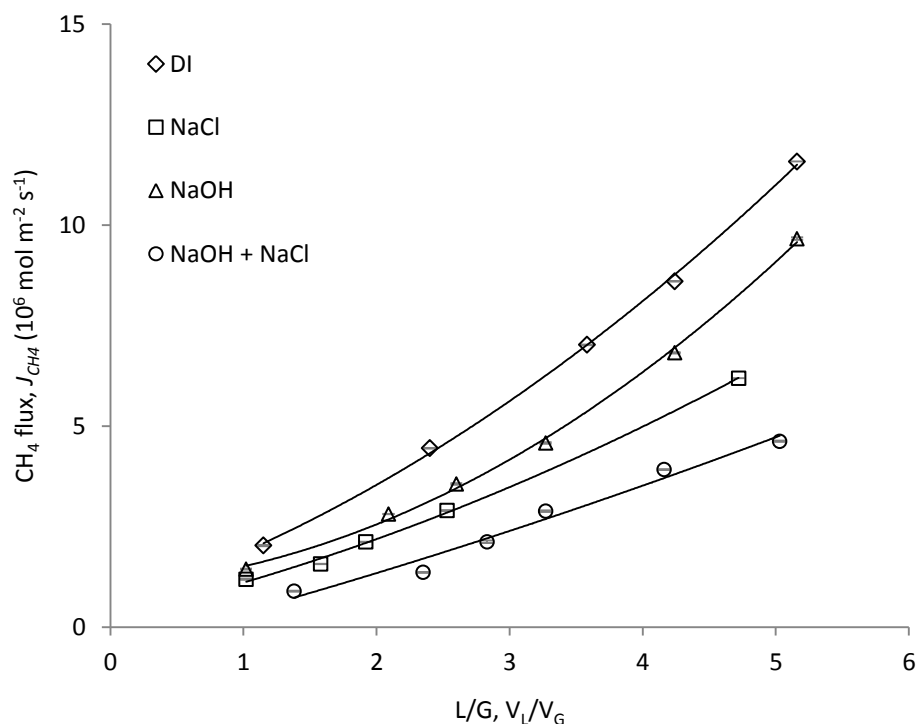


Figure 3.3 The impact of liquid velocity (V_L 0.0046 m s^{-1} to 0.024 m s^{-1}) on CH₄ flux in four solvents DI, NaCl, NaOH, and NaOH/NaCl (24-26 °C).

Methane flux diminished markedly with the inclusion of NaCl to DI water. To illustrate, a CH_4 flux of $6.2 \times 10^{-6} \text{ mol}_{\text{CH}_4} \text{ m}^{-2} \text{ s}^{-1}$ was recorded at L/G 4.7 compared to $8.6 \times 10^{-6} \text{ mol}_{\text{CH}_4} \text{ m}^{-2} \text{ s}^{-1}$ for DI water at the lower L/G of 4.2. For the NaOH solvent, CH_4 fluxes were comparable to those of NaCl below L/G 2.6. However, at L/G greater than 2.6, CH_4 flux recorded for the NaOH solvent apparently increased as an exponent of L/G, subsequently recording a CH_4 flux of $9.7 \times 10^{-6} \text{ mol}_{\text{CH}_4} \text{ m}^{-2} \text{ s}^{-1}$ at L/G 5.2, only 15 % below that observed for DI water. Addition of NaCl to NaOH introduced the greatest limitation to CH_4 flux, recording between 8.9×10^{-7} and $4.6 \times 10^{-6} \text{ mol}_{\text{CH}_4} \text{ m}^{-2} \text{ s}^{-1}$ for L/G ranging 1.4 to 5.

Following process optimisation using the rate limiting phase (V_G in the case of chemical based solvents NaOH and NaOH/NaCl; and V_L for the physical solvents DI water and aqueous NaCl), selectivity toward CO_2 was estimated for each solvent (Figure 3.4). For physical solvents, selectivity was greater when using NaCl. However, a linear decrease toward CO_2 selectivity was noted for both solvents when V_L was increased. For example, for DI water, selectivity decreased from 166 at L/G 2.4 to 106 at L/G 5.2. The NaCl/NaOH solvent increased selectivity for CO_2 at L/G 0.29 from 1030 for NaOH to 2250. At higher L/G, selectivity diminished to that observed for physical solvents.

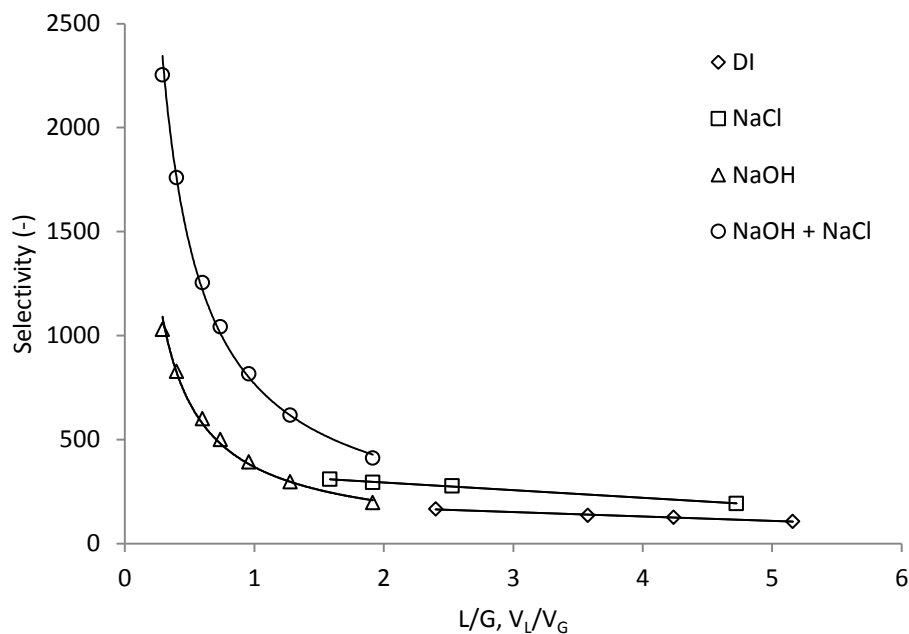


Figure 3.4 Influence of hydrodynamic conditions on CO_2 selectivity. Liquid velocity (V_L) varied from 0.0074 m s^{-1} to 0.024 m s^{-1} for DI and NaCl solvents and (gas velocity, V_G fixed to 0.0047 m s^{-1}). For NaOH and NaOH + NaCl, V_G varied between 0.0046 m s^{-1} and 0.031 m s^{-1} (V_L fixed at 0.0089 m s^{-1}).

Data was selected from the reported datasets to enable an approximate comparison of slip, from the solvents evaluated. To normalise the datasets, an outlet gas composition of 85 % methane, equivalent to North Sea natural gas (Persson *et al.*, 2007), was selected (Table 3.1). The highest slip was observed when using DI water at 5.2 %. In comparison, the chemical solvent reduced methane slip to 0.1 %. Adding the NaCl electrolyte reduced methane slip in both physical and chemical solvents to 4.0 % and 0.03 % respectively.

Table 3.1 Methane slip in DI, NaCl, NaOH, and NaOH + NaCl solvents (24-26 °C) under conditions affording an output gas composition of 85 % CH₄.

Absorbent	L/G	Liquid velocity	Gas velocity	CH ₄ slip	CH ₄ slip vol.	Q _{CH₄} out	CH ₄ slip
	V _L /V _G	V _L , m s ⁻¹	V _G , m s ⁻¹	g m ⁻³	10 ⁴ m ³ h ⁻¹	m ³ h ⁻¹	% CH ₄ out
DI	5.18	0.0241	0.0047	16.0	5.8	0.011	5.22
1 M NaCl	5.00	0.0233	0.0047	9.6	4.1	0.010	4.00
1 M NaOH	0.33	0.0089	0.0300	10.0	1.3	0.136	0.10
1 M NaOH + 1 M NaCl	0.55	0.0089	0.0173	4.6	0.6	0.179	0.03

3.3.2 Application of solvent recirculation to minimise slip

Single pass solvent use was compared to recirculating the solvent in multi-pass (MP) to enable greater utilisation of the available solvent (Figure 3.5). Cumulative losses were compared following subsequent solvent uses (without regeneration) based upon a parameter normalised to CO₂ removal (CH₄ lost per gram CO₂ absorbed, g_{CH₄} g_{CO₂}⁻¹). For both solvents, a pseudo-plateau was evidenced following one recirculation which can be explained by the saturation of the solvent with CH₄ after one circulation.

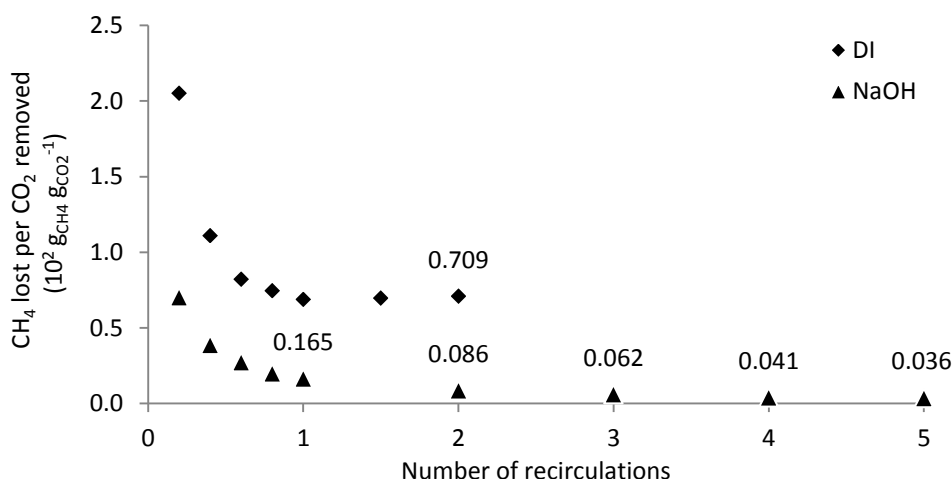


Figure 3.5 Methane losses over multiple solvent recirculations using DI or NaOH solvents. Methane losses normalised to CO₂ removed during gas separation. DI water V_L 0.024 m s⁻¹ and V_G 0.0031 m s⁻¹ (L/G 7.7); NaOH solvent V_L 0.032 m s⁻¹ and V_G 0.058 m s⁻¹ (L/G 0.42).

This is supported by the measured dissolved phase methane concentration which stabilised following approximately one recirculation. However, methane losses were lower using the NaOH solvent. For example, following two solvent recirculations, the losses were 0.086 g_{CH4} g_{CO2}⁻¹ and 0.709 g_{CH4} g_{CO2}⁻¹ for the NaOH and DI solvents respectively. Over five solvent recirculations, the chemical solvent supported an outlet gas phase concentration of >99 % CH₄ (Figure 3.6). In contrast, outlet gas quality rapidly diminished for the DI solvent following less than one use.

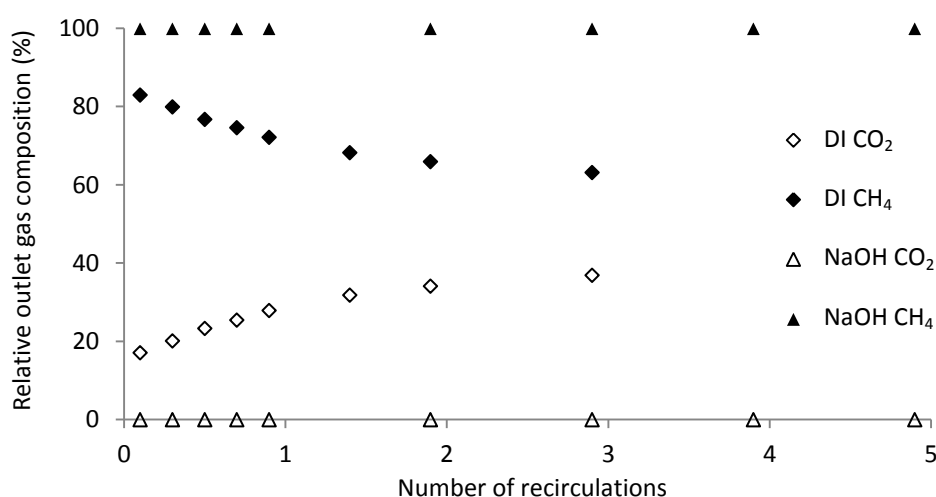


Figure 3.6 Outlet gas composition measured during sequential solvent recirculations using DI and NaOH absorption solvents (24-26 °C). V_L 0.024 m s⁻¹ and V_G 0.0031 m s⁻¹ for DI (L/G 7.7) and V_L 0.032 m s⁻¹ and V_G 0.058 m s⁻¹ for NaOH (L/G 0.42).

3.4 Discussion

A significant finding in this study was that methane slip was dependent upon whether the process was gas phase or liquid phase controlled. For physical solvents such as DI water, the liquid phase presented the rate limiting condition to CO₂ mass transfer. This manifested as an increase in CO₂ flux, and therefore an enhancement in gas-side methane purity, when V_L was increased. The DI solvent approached saturation for CH₄ at low V_L . This can be explained by the partial solubility of methane in water, yielding a predicted saturation concentration of 13.5 mg L⁻¹ at a partial pressure of 60 % (Wilhelm *et al.*, 1977). A proportionate increase in methane flux was subsequently observed with an increase in V_L and can be explained by the continual saturation of newly introduced solvent at the solvent-membrane boundary. In contrast, dissolved CO₂ concentration diminished at high V_L from a maximum of 500 mg_{CO2} L⁻¹ at V_L 0.011 m s⁻¹, to 387 mg_{CO2} L⁻¹ at V_L 0.024 m s⁻¹. This can be explained by a combination of the lower residence time available for absorption which limited radial gas transport from the solvent-membrane boundary due to under-developed laminar flow conditions ($Re \ll 2100$) observed throughout for DI water ($Re_{max} = 5.90$) (Dindore *et al.*, 2005), and a reduction in gas-side CO₂ partial pressure at higher V_L . This reduction in CO₂ solvent concentration subsequently reduced selectivity toward CO₂ with an increase in V_L (Figure 3.4). The hydrodynamic conditions were comparable for all solvents across the V_L ranges examined, with insufficient difference in viscosity and density of electrolytic solutions for any significant change in flow regime (Zhang and Han, 1996; Sipos *et al.*, 2000; Laliberté, 2007).

For the chemically reactive NaOH solvent, the process was gas phase controlled, which is illustrated by the negligible gradient recorded for CO₂ flux following an increase in V_L (Figure 3.2a). The chemical reaction rate to bicarbonate (HCO₃⁻, 11000 m³ kmol_{CO2}⁻¹ s⁻¹) may be considered ‘fast’ with respect to the hydraulic residence time within the HFMC (< 1 s) (Kucka *et al.*, 2002; Pohoricki and Moniuk, 1988). The rate limiting reaction pathway via carbonic acid (H₂CO₃) is implicit, with pH key to the stabilisation of hydrolysed CO₂ within the liquid phase due to ionisation to HCO₃⁻ and carbonate (CO₃²⁻) species. Consequently, whilst operated within the low Gz number range applied to

physical solvents, this conversion to carbonate species, in the presence of a high reactant concentration, was sufficient to re-establish the concentration gradient at the membrane-solvent boundary. The excess of reactive OH^- within the reaction zone further enabled a reduction in the operational L/G ratio. This limited CH_4 flux, as the physical dissolution of CH_4 in NaOH can be similarly described by Henry's law and is thus attributable to solvent flow rate. To illustrate, to achieve an equivalent outlet CH_4 purity of 85 %, the L/G required for DI and NaOH solvents were 5.2 and 0.33 yielding slip of 5.2 % and 0.1 % respectively. Interestingly, when using the chemical solvent at $\text{L/G} > 1$, the gas-side CO_2 concentration was reduced to below the limit of detection and was coincident with a non-linear increase in methane flux (Figure 3.3). It is posited that this CH_4 flux enhancement arises from the increase in gas-side CH_4 partial pressure suggesting that an optimum L/G should be identified to limit slip in addition to gas-side CO_2 .

Selectivity was enhanced in both chemical and physical absorption systems by the inclusion of NaCl (Figure 3.4). The NaCl behaved as an electrolyte, which induced salting out of the physically absorbed gas species resulting in a reduction in the attainable saturation constant. Setschenow (1889) supposed that 'salting out' was induced by a preference of water molecules to hydrate and dissolve ionic species rather than the uncharged gas candidates. Latterly Masterton and Lee (1970) used scaled particle theory (SPT) to suggest that salting out increased the work required to form a cavity (within the condensed liquid phase) of sufficient size to accommodate a gas solute. Consequently, electrolyte addition to the physical solvent (DI) reduced methane slip to 4 % compared to 5.2 % for DI water. The use of NaCl to improve outlet gas quality was also assessed by Atchariyawut *et al.* (2007). The authors based the improvement in outlet gas quality on the electrolytes capacity to reduce water vapour content. Whilst the author's hypothesis of reduced water activity is valid, clearly the contribution of reduced methane slip must also be considered.

Due to the inclusion of NaCl, the CO_2 saturation constant was reduced by 22 %. However, the measured dissolved CO_2 concentration was below this saturation concentration and hence the impact on CO_2 flux was seemingly negligible (Figure 3.2a). It is posited that further lowering of the

solubility constant will impede absorption performance. Interestingly, whilst the chemical solvent reduced slip through enabling lower L/G operation, NaOH similarly dissociates into ionic form, presenting a synergistic effect since slip is therefore also retarded through salting out of the Na^+ and OH^- ions (Weisenberger and Schumpe, 1996), and is supported by the diminished CH_4 flux recorded for NaOH when compared to DI (Figure 3.3). Consequently, the addition of NaCl to NaOH absorbent effectively doubled the electrolytic solvent concentration, further inhibiting CH_4 flux and subsequently enhanced selectivity for CO_2 by approximately 200 %. Since the chemical solvent's reactivity offsets the lower physical absorption constant for CO_2 , it is suggested that higher electrolytic concentrations can be implemented and methane slip further decreased.

Using multi-pass absorption enables further cessation of slip since both physical and chemical solvents are essentially saturated with CH_4 in a single pass, thus subsequent solvent recirculation should retard further CH_4 flux, tending measured CH_4 flux to zero. However, the capacity to utilise physical solvents in multi-pass absorption is limited as approximately 50 % of the maximum CO_2 load is also reached in single-pass. In comparison, the CO_2 flux and outlet gas quality recorded for the chemical solvent following five recirculations was analogous to single pass, demonstrating a sustained excess of highly reactive hydroxide OH^- ions. Based on an idealised stoichiometric conversion of 2:1, OH^- : CO_2 (Vas Bhat *et al.*, 2000) and an L/G of 5.2, approximately 37 chemical solvent recirculations are possible before reaching a OH^- concentration of 0.1 M. Interestingly, whilst an order of magnitude lower in chemical concentration, 0.1 M NaOH has been shown sufficient to maintain a >99 % CH_4 outlet gas concentration under analogous hydrodynamic conditions (Galan-Sanchez, 2011).

Physical absorption in HFMC demonstrated methane slip of 5.2 %. Although direct comparison to conventional water scrubbers cannot be made due to differences in gas-side preconditioning and scale, this is markedly lower than the 13.1 % slip recorded for a pilot scale unit applied to landfill gas (Läntelä *et al.*, 2011) and is ostensibly a function of lower solvent consumption; an observation which is supported by previous authors (Nii *et al.*, 1992; Falk-Pedersen

and Dannström, 1997). Lower slip values of 4 % to 5 % have been recorded for full-scale water scrubbers, though it is unclear whether the balance includes the use of abatement technologies such as thermal oxidisers which oxidise the slipped methane to CO₂ (Patterson *et al.*, 2011; Wolf and Nettelbreker, 2011). In addition, to the financial significance of enhancing the recovery of biomethane through minimising slip, financial incentivisation now also rewards installations which operate at slip below 0.5 % (Wolf and Nettelbreker, 2011). Based on this study, to reach this target without the use of abatement technologies, chemical solvents are required as this enables the shift to gas-phase control which minimises slip through minimum solvent consumption; though the energy penalty associated with solvent regeneration must also be considered. The characteristically low absorbent demand of HFMCs could conceivably limit the energy necessary for chemical regeneration through a reduction in liquid volume, which is also coupled to a significantly reduced pumping requirement. This is in addition to the revenue from the methane that would otherwise have been lost at higher slip. For example, assuming biogas production of 1000 m³ hour⁻¹ (a moderate full-scale flow rate) with 60 % initial CH₄ content, an upgrading plant operating at 5.2 % slip would lose approximately 87,500 £ y⁻¹ at 32 p m⁻³. In contrast, a NaOH solvent with 0.1 % slip would only lose 1,700 £ y⁻¹. Only 500 £ y⁻¹ would be lost at 0.03 % slip in a NaOH + NaCl absorbent.

In practice, there is a trade-off between CAPEX and OPEX, such that the application of highly reactive chemical solvents will be used to reduce asset scale by increasing throughput, consequently, the number of achievable solvent recirculations could be lower than presented in this study. However, both energy and carbon returns demonstrate that operation greater than one recirculation is sufficient to derive a net energy benefit through minimising methane slip (Figure 3.7).

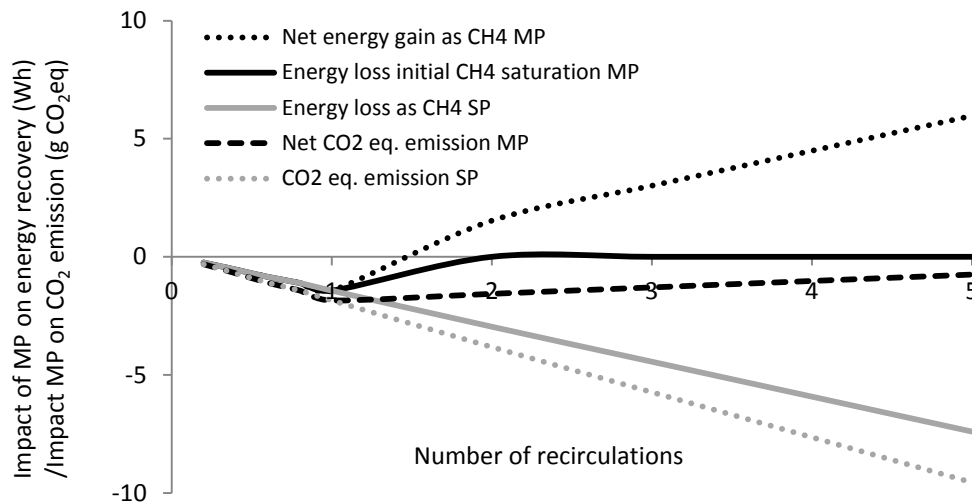


Figure 3.7 Energy and carbon balance based on methane slip during single pass (SP) and multi-pass (MP) solvent recirculation. A net energy gain is determined once solvent is recirculated more than once. Carbon neutrality requires greater than five solvent recirculations based on the modelled hydrodynamic conditions (assumptions $0.52 \text{ kg}_{\text{CO}_2} \text{ kWh}^{-1}$; 40 % electrical efficiency).

A criticality in L/G was also demonstrated where unnecessary operation at $L/G > 1$ could impinge upon methane losses. This underpins a tacit advantage of HFMCs versus conventional packed columns in that the latter are operationally limited to turn-up/turn-down during process perturbation such as inlet gas composition or flow variation. By comparison HFMCs can achieve more rapid transitions in V_L due to phase separation which enables HFMCs to operate at minimum V_L and thus limit further slip.

3.5 Conclusions

The significance of methane slip during biogas upgrading was dependent upon whether the process was gas phase or liquid phase controlled since methane transport was governed by Henry's law and hence independent of chemical reactivity.

- For physical solvents, absorption was dependent upon V_L . However, at high V_L , selectivity toward CO_2 declined due to low residence times and an underdeveloped regime

- For chemical solvents, CO₂ mass transfer was dependent upon V_G which was driven by an excess of OH⁻ ions available in the solvent for chemical reaction
- Electrolytes can retard CH₄ absorption via the salting out effect. In physical solvents, electrolytic concentration is limited by the effect upon CO₂ solubility. However, in chemical solvents, CO₂ absorption is decoupled from physical constants, thus an excess of electrolyte can enhance selectivity further
- Multi-pass chemical solvent recirculation enables further methane slip prevention. Initial saturation of the solvent for CH₄, ensures that CH₄ flux tends toward zero following subsequent uses for CO₂.

Acknowledgments

The authors would like to thank the Engineering and Physical Sciences Research Council (EPSRC, V/N: 08001923), Anglian Water, Northumbrian Water, Severn Trent Water and Yorkshire Water for their financial support.

References

- Alberto, M.C.R., Arah, J.R.M., Neue, H.U., Wassmann, R., Lantin, R.S., Aduna, J.B. and Bronson, K.F. (2000), "A sampling technique for the determination of dissolved methane in soil solution", *Chemosphere*, vol. 2, no. 1, pp. 57-63.
- Atchariyawut, S., Jiratananon, R. and Wang, R. (2007), "Separation of CO₂ from CH₄ by using gas-liquid membrane contacting process", *Journal of Membrane Science*, vol. 304, no. 1-2, pp. 163-172.
- Baldwin, J. (2011), "Biomethane market opportunities", *Rushlight Events: Commercial issues and technology developments in organic waste investments*, 22nd February, London, UK.

Benedetti-Pichler, A.A. and Cefola, M. (1939), "Warder's method for the titration of carbonates", *Industrial & Engineering Chemistry Analytical Edition*, vol. 11, no. 6, pp. 327-332.

Dindore, V.Y., Brilman, D.W.F. and Versteeg, G.F. (2005), "Hollow fiber membrane contactor as a gas-liquid model contactor", *Chemical Engineering Science*, vol. 60, no. 2, pp. 467-479.

Esquiroz-Molina, A., Georgaki, S., Stuetz, R., Jefferson, B. and McAdam, E. J. (2013), "Influence of pH on gas phase controlled mass transfer in a membrane contactor for hydrogen sulphide absorption", *Journal of Membrane Science*, vol. 427, pp. 276-282.

Falk-Pedersen, O. and Dannström, H. (1997), "Separation of carbon dioxide from offshore gas turbine exhaust", *Energy Conversion and Management*, vol. 38, no. 1, S81-S86.

Galan-Sanchez, I. (2011), "Enhancing Energy Production from Gas Engines used for Landfill Applications", *MSc Thesis, Cranfield Water Science Institute, Cranfield University*.

Ho, W. S. and Sirkar, K. K. (1992), "Membrane Handbook", *Kluwer Academic Publishers*, pp. 91-92.

Jackson, W. M. (1956), "Viscosities of the binary gas mixtures, methane-carbon dioxide and ethylene-argon", *Journal of Physical Chemistry*, vol. 60, no. 6, pp. 789-791.

Jefferson, B., Nazareno, C., Georgaki, S., Gostelow, P., Stuetz, R. M., Longhurst, P. and Robinson, T. (2005), "Membrane gas absorbers for H₂S removal - Design, operation and technology integration into existing odour treatment strategies", *Environmental technology*, vol. 26, no. 1, pp. 793-804.

Kucka, L., Kenig, E.Y. and Górak, A. (2002), "Kinetics of the gas-liquid reaction between carbon dioxide and hydroxide ions", *Industrial and Engineering Chemistry Research*, vol. 41, no. 24, pp. 5952-5957.

Laliberté, M. (2007), "Model for calculating the viscosity of aqueous solutions", *Journal of Chemical and Engineering Data*, vol. 52 no. 2, pp. 321-335.

Läntelä, J., Rasi, S., Lehtinen, J. and Rintala, J. (2011), "Landfill gas upgrading with pilot-scale water scrubber: Performance assessment with absorption water recycling", *Applied Energy*, vol. 92 no. 1, pp. 307-314.

Li, J.-L. and Chen, B.-H. (2005), "Review of CO₂ absorption using chemical solvents in hollow fiber membrane contactors", *Separation and Purification Technology*, vol. 41, no. 2, pp. 109-122.

Lu, J., Zheng, Y. and He, D. (2006), "Selective absorption of H₂S from gas mixtures into aqueous solutions of blended amines of methyldiethanolamine and 2-tertiarybutylamino-2-ethoxyethanol in a packed column", *Separation and Purification Technology*, vol. 52, no. 2, pp. 209-217.

Masterton, W.L. and Lee, T.P. (1970), "Salting coefficients from scaled particle theory", *Journal of Physical Chemistry*, vol. 7, no. 8, pp. 1776-1782.

Nii, S., Takeuchi, H. and Takahashi, K. (1992), "Removal of CO₂ by gas absorption across a polymeric membrane", *Journal of Chemical Engineering of Japan*, vol. 25, no. 1, pp. 67-72.

Ofgem (2014), <https://www.ofgem.gov.uk/publications-and-updates/full-tariff-tables> (accessed 1st September 2014).

Patterson, T., Esteves, S., Dinsdale, R. and Guwy, A. (2011) "An evaluation of the policy and techno-economic factors affecting the potential for biogas upgrading for transport fuel use in the UK", *Energy Policy*, vol. 39, no. 3, pp. 1806-1816.

Persson M., Jonsson, O. and Wellinger, A. (2007), "Task 37 – Biogas upgrading to vehicle fuel standards and grid injection", *IEA Bioenergy*, 20-21.

Pohorecki, R. and Moniuk, W. (1988) "Kinetics of reaction between carbon dioxide and hydroxyl ions in aqueous electrolyte solutions", *Chemical Engineering Science*, vol. 43, no. 7, pp. 1677-1684.

Rongwong, W., Boributh, S., Assabumrungrat, S., Laosiripojana, N. and Jiraratananon, R., (2012), "Simultaneous absorption of CO₂ and H₂S from biogas by capillary membrane contactor", *Journal of Membrane Science*, vol. 392–393, pp. 38-47.

Ryckebosch, E., Drouillon, M. and Vervaeren, H. (2011), "Techniques for transformation of biogas to biomethane", *Biomass and Bioenergy*, vol. 35, no. 5, pp. 1633-1645.

Setschenow, J. Z. (1889) "Über Die Konstitution Der Salzlosungen auf Grund Ihres Verhaltens Zu Kohlensäure", *Zeitschrift für Physikalische Chemie*, vol. 4, pp. 117–125.

Simons, K., Nijmeijer, K. and Wessling, M. (2009), "Gas–liquid membrane contactors for CO₂ removal", *Journal of Membrane Science*, vol. 340, no. 1-2, pp. 214-220.

Sipos, P. M., Hefter, G. and May, P. M. (2000), "Viscosities and densities of highly concentrated aqueous MOH solutions (M⁺ = Na⁺, K⁺, Li⁺, Cs⁺, (CH₃)₄N⁺) at 25.0 °C", *Journal of Chemical and Engineering Data*, vol. 45, no. 4, pp. 613-617.

Vas Bhat, R.D., Kuipers, J.A.M. and Versteeg, G.F. (2000), "Mass transfer with complex chemical reactions in gas-liquid systems: Two-step reversible reactions with unit stoichiometric and kinetic orders", *Chemical Engineering Journal*, vol. 76, no. 2, pp. 127-152.

Weisenberger, S. and Schumpe, A. (1996), "Estimation of Gas Solubilities in Salt Solutions at Temperatures from 273 K to 363 K", *AIChE Journal*, vol. 42, no. 1, pp. 298-300.

Wilhelm, E., Battino, R. and Wilcock, R.J. (1977), "Low-pressure solubility of gases in liquid water", *Chemical Reviews*, vol. 77, no. 2, pp. 219-262.

Wolf M. and Nettelbreker U. (2011), "Method for Biogas Treatment and Biogas Installation", *United States patent Application publication*, US20110245572.

Zhang, H. and Han, S. (1996), "Viscosity and density of water+sodium chloride+potassium chloride solutions at 298.15 K", *Journal of Chemical and Engineering Data*, vol. 41, no. 3, pp. 516-520.

Chapter 4

Removal of dissolved methane from aqueous solution using a micro-porous hollow fibre membrane contactor (HFMC)

For submission to: Journal of membrane science

Removal of dissolved methane from aqueous solution using a micro-porous hollow fibre membrane contactor (HFMC)

Andrew McLeod, Bruce Jefferson and Ewan J. McAdam*

Cranfield Water Science Institute, Building 39, Cranfield University, Bedfordshire, MK43 0AL, UK

*Corresponding author e-mail: e.mcadam@cranfield.ac.uk

Abstract

The removal of dissolved methane (CH_4) from wastewater has been investigated using a micro-porous hollow fibre membrane contactor (HFMC). This is of interest to the wastewater treatment industry because up to 50 % of CH_4 produced by anaerobic processes can be lost through fugitive emission, which undermines their potential for high biogas yield and low carbon footprint. Additionally, dissolved CH_4 found in landfill leachate readily escapes in to the headspace of drainage systems, forming hazardous combustible atmospheres. Over 97 % removal efficiency was achieved from water saturated by a 75:25/ CH_4 : CO_2 gas mixture, which enabled a reduction in greenhouse gas (GHG) emission of 1.1 $\text{kg}_{\text{CO}_2, \text{eq.}}$ for each m^3 of liquid degassed. 97 % was also sufficient to remove CH_4 below the dissolved concentration necessary for theoretical formation of combustible atmospheres. Mass transfer was liquid phase limited, which allowed relatively low sweep gas flow rate (Q_G) for recovery of a 41 % gas phase CH_4 purity. This could be directly applied to energy recovery, where electricity could be generated at 0.12 kWh per m^3 of degassed liquid using gas turbines operating with 21 % efficiency. However there was a trade-off between removal efficiency and recovered purity, where the high gas flow rates (Q_G) for optimal CH_4 removal heavily diluted the recovered CH_4 . This trade-off can be appeased through extension of the HFMC active length to increase the gas-liquid contact time or by re-designing the HFMC to prevent the premature emergence of gas phase mass transfer resistance sufficiently to allow a closer approach to the minimum G/L and reduce CH_4 dilution in the sweep gas.

Keywords: methane removal; methane recovery; degas; degassing; anaerobic; landfill leachate

4.1 Introduction

Methane (CH_4) is a combustible greenhouse gas (GHG) generated by water-borne anaerobic processes in landfill and at wastewater treatment works (WWTW). If collected this CH_4 can be used as an efficient fuel gas, due to a large heat of combustion (891 kJ mol^{-1}), however dissolved CH_4 readily escapes to the atmosphere at the interface of the liquid and gas phases, due to a large dimensionless Henry's constant (Table 4.1), where it is 25 times more potent than carbon dioxide (CO_2) as a GHG (Pittam and Pilcher, 1972; Daelman *et al.*, 2012).

Table 4.1 Water solubility (mole fraction), dimensionless Henry's constant and diffusivity for O_2 and CH_4 in water and respective molecular size.

Gas	Water solubility (1 atm, 25 °C) $x (10^4)$	Henry's constant (25 °C) $H (-)$	Diffusivity (25 °C) $D (10^9 \text{ m}^2 \text{ s}^{-1})$	Molecular size parameter $\sigma (10^8 \text{ cm})$
Oxygen (O_2)	0.2298	32.12	2.20	3.46
Nitrogen (N_2)	0.1173	62.93	1.83	3.70
Methane (CH_4)	0.2507	29.45	1.88	3.70

Resultant fugitive CH_4 emission from anaerobic wastewater treatments currently undermines their potential for high energy recovery (as biogas) and low carbon footprint, with up to 50 % of CH_4 produced lost due to high dissolved concentrations of $20.2 \text{ mg}_{\text{CH}_4} \text{ L}^{-1}$ within the effluent of an expanded granular sludge blanket (EGSB) reactor at 16 °C (McAdam *et al.*, 2011), whilst explosive atmospheres can form within the headspace of landfill leachate drainage networks. A minimum flammable concentration of gaseous CH_4 (4.4 %) can be reached from a $0.98 \text{ g}_{\text{CH}_4} \text{ m}^{-3}$ solution (at 25 °C) and therefore leachate concentrations, typically ranging from $2 \text{ g}_{\text{CH}_4} \text{ m}^{-3}$ to $15 \text{ g}_{\text{CH}_4} \text{ m}^{-3}$, are subject to a $0.14 \text{ g}_{\text{CH}_4} \text{ m}^{-3}$ limit of consent for discharge to sewers (Rooksby, 2007). At present this is achieved via displacement of dissolved CH_4 in to the atmosphere by aeration of the leachate, without provision for subsequent CH_4 recovery.

Gas-liquid micro-porous hollow fibre membrane contactors (HFMCs) present the unique potential to maximise the utilisation of valuable dissolved CH_4 by combining a high level of removal

with recovery of good purity CH₄. HFMCs achieve this, in contrast to conventional column-type aeration technologies, by the fine, independent control of sweep gas and liquid flow rates (Q_G and Q_L respectively) for precise optimisation of the G/L ratio (Q_G/Q_L) necessary for effective stripping. As a result, even HFMCs operating with an excess Q_G impose a fraction of the G/L ratio required by column contactors (He *et al.*, 2004), where stripped CH₄ is diluted below useful gas phase concentrations. However, whilst HFMCs using both dense permeable and micro-porous membranes have been studied for degassing of dissolved oxygen (O₂) and carbon dioxide (CO₂) (Dang *et al.*, 2003; Ito *et al.*, 1998; Koonaphapdeelert *et al.*, 2009; Sengupta *et al.*, 1998; Tai *et al.*, 1994; Tan *et al.*, 2005), subsequent recovery of the stripped gas in pure form is not routinely performed or discussed. Published investigations of CH₄ degassing using HFMCs are particularly limited, with no study using micro-porous membranes; however subsequent recovery is attempted due to the intrinsic value of CH₄. Semi-empirical modelling suggests that up to 97 % CH₄ purity is achievable in the recovered gas phase by removal from coal seams using urethane/polyethylene composite membranes at high pressure (10 atm), although only a 16.8 % removal efficiency of dissolved methane was determined in this instance (Cramer *et al.*, 2009). Conversely, whilst CH₄ degassing of anaerobic effluents using permeable PDMS membranes was capable of a superior 72 % removal efficiency, a G/L of 21.25 resulted in a respective gas phase CH₄ concentration of just 0.028 % by volume in sweep gas mode (Cookney *et al.*, 2012). An apparent trade-off between removal efficiency and recovered purity is indicated from these studies, however neither of these investigations included discussion of mass transfer characteristics sufficiently to indicate how this trade-off may be satisfied or how processes may be designed at scale.

The objective of the present study is to determine the capability of a micro-porous HFMC to facilitate simultaneous high removal efficiency and high CH₄ purity in the sweep gas, whilst characterising CH₄ mass transfer characteristics to enable effective process comparisons and envisage a reasonable route for scale-up.

4.2 Materials and methods

4.2.1 Equipment setup and operation

A 10 L volume of de-ionised (DI) water ($15 \text{ M}\Omega \text{ cm}^{-1}$), maintained at 25°C in a water bath with a thermostatic circulator (GD120, Grant Instruments Cambridge Ltd., Shepreth, UK), was saturated by a 75:25 / $\text{CH}_4:\text{CO}_2$ gas mixture diffused through the liquid at a flow rate of $1.67 \times 10^{-5} \text{ m}^3 \text{ s}^{-1}$ for one hour, which was determined to be sufficient time to achieve saturation (Figure 4.1).

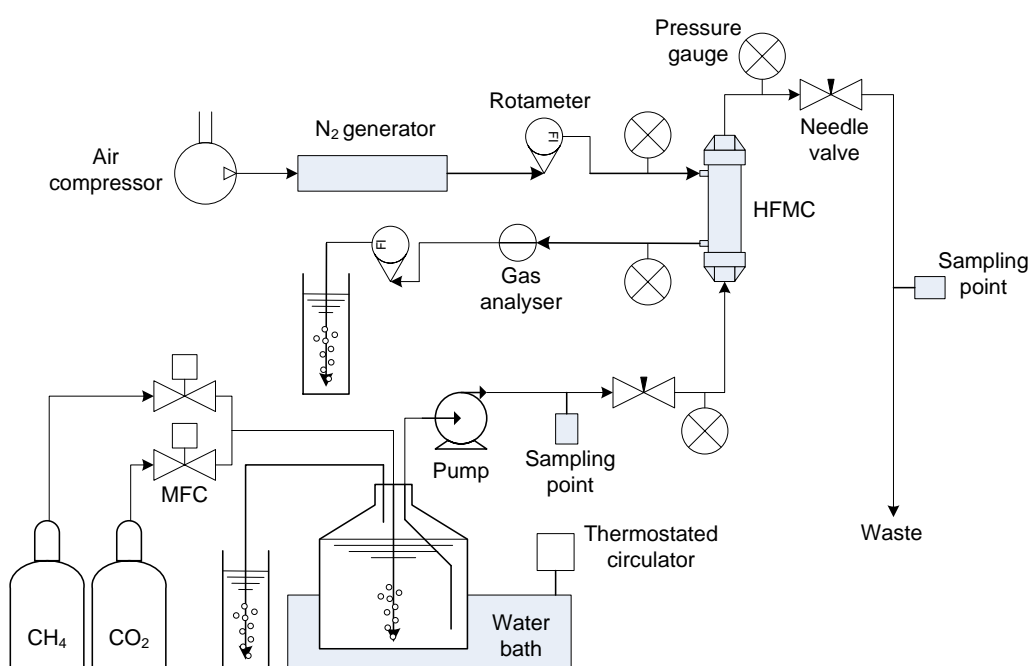


Figure 4.1 Schematic of the membrane degas apparatus, including liquid saturation aspirator, sweep gas generation equipment and degassing membrane module (HFMC).

Methane (CH_4 , 99.995 %) and carbon dioxide (CO_2 , 99.7 %) gas (BOC gases, Ipswich, UK) flows were controlled using two mass flow controllers ($0.20\text{--}20.0 \text{ L min}^{-1}$, Roxspur Measurement and Control Ltd., Sheffield, UK) and mixed in line. Once saturation was achieved the liquid was fed, by a peristaltic pump (520, Watson-Marlow Pumps, Falmouth, UK), to the lumen-side of the HFMC (Liqui-Cel® 1.7x5.5 MiniModule®, Membrana GmbH, Wuppertal, Germany) whilst maintaining gas dispersion throughout. The HFMC comprised 7400 polypropylene (PP) fibres possessing nominal

inner diameters (ID) of 220 μm , outer diameters (OD) of 300 μm , a mean pore size of 0.03 μm and 40 % porosity. An active length of 0.113 m was determined from the total surface area of 0.58 m^2 given by the manufacturer, based on the fibre ID. Fibres were potted in polyurethane and encased within a polycarbonate cylindrical shell, with a diameter of 0.0425 m, resulting in an average packing fraction (θ) of 0.369. N_2 sweep gas was produced from compressed air (4 bar) using a nitrogen generator, which was then regulated to below 1 bar(g) and fed through the HFMC shell counter-currently to the liquid (Cookney *et al.*, 2012). Sweep gas flow rate was controlled using variable area flow controllers (Key Instruments, Treviso, PA, USA), which were also used to monitor outlet gas flow rate by fully opening the aperture. Pressure on both the liquid and gas side was monitored by pressure gauges (DPG1000, Omega Engineering Ltd., Manchester, UK) and controlled by needle valves to maintain a greater pressure on the liquid side, to avoid gas bubbling, whilst operating below the membrane penetration pressure for water (4.1 bar) to avoid pore wetting.

4.2.2 Sampling and analysis

Liquid phase samples were collected in evacuated vials (Vacutainer®, Becton Dickinson and Company, Franklin Lakes, NJ, USA) before and after the HFMC from luer lock needles fitted on the liquid inlet and outlet. The reduced pressure in the sampling vials enabled collection of liquid samples, which when equilibrated to atmospheric pressure left a small headspace above the liquid. Previous research using the Vacutainer® brand has indicated a residual 400 ppmv of CH_4 present within the empty vials prior to sampling (Daelman *et al.*, 2012). Although a residual CH_4 concentration was not detected in the present study the results were re-assessed under this assumption, however only minimal under-estimation of CH_4 removal from the liquid would result from such a residual concentration. Liquid samples were agitated for 7 minutes (maximum speed, Multi Reax, Heidolph, Schwabach, Germany), and left to equilibrate overnight. The resultant dissolved phase concentrations were calculated from the headspace by gas chromatography (GC, 200 Series GC-TCD Cambridge Scientific Instruments Ltd., Witchford, UK) based on a mass balance

using Henry's law (Alberto *et al.*, 2000). Headspace samples were introduced through the injector (150 °C) to the instrument in 1 mL volumes and the gases separated on an Alltech® CTR I concentric packed column comprising a 1/4" outer column surrounding an 1/8" inner column (regulated to 30 °C) (Alltech Associates Inc., Deerfield, Illinois, USA), using a helium (He) carrier gas (4.2 barg) and quantified using a thermal conductivity detector (TCD, operating at 180 °C). This procedure was also conducted during calibration of the instrument using certified CH₄ gas standards (Scientific Technical Gases Ltd., Staffordshire, UK) prior to each analysis. Methane eluted from both the inner and outer concentric columns after 0.5 minutes and 6 minutes respectively, with the sharper peak of the inner column selected for analysis due to a greater reliability for integration. CH₄ exiting the HFMC in the sweep gas was recorded in-line using an infrared biogas analyser (Yieldmaster, Bluesens gas sensor GmbH, Herten, Germany), with a 0.2 % full scale accuracy from 0-100 % volume CH₄, using the associated software (BACVis, Bluesens gas sensor GmbH, Herten, Germany).

4.2.3 Mass transfer and minimum G/L calculations

Liquid-side mass transfer coefficients were determined using CH₄ concentrations in the liquid upon entering and exiting the HFMC and liquid and gas flow rates (1):

$$k_L = \frac{-Q_L}{(\pi d L n)} \left[\frac{1}{\left(1 - \frac{Q_L}{Q_G H}\right)} \right] \times \ln \left[\frac{c_{CH_4, in}}{\left(1 - \frac{Q_L}{Q_G H}\right) c_{CH_4, in} + \left(\frac{Q_L}{Q_G H}\right) c_{CH_4, out}} \right] \quad 1$$

where k_L is the mass transfer coefficient ($m\ s^{-1}$), d is the inner diameter of a single membrane fibre ($2.2 \times 10^{-4}\ m$), n is the number of fibres in the HFMC (7400), L is the active length of the HFMC (0.113 m), $c_{CH_4, in}$ and $c_{CH_4, out}$ are the methane liquid concentrations in and out of the HFMC respectively ($mg\ m^{-3}$), Q_L and Q_G are liquid and gas flow rates respectively ($m^3\ s^{-1}$) and H is the dimensionless Henry's constant (Table 4.1) (Tai *et al.*, 1994). Lumen-side liquid mass transfer is routinely approximated by the Graetz-L  v  que equation (2):

$$Sh = \frac{k_L d}{D} = 1.62 \left(\frac{d^2 V_L}{DL} \right)^{0.33} \quad 2$$

where Sh is the dimensionless Sherwood number, d is the 'characteristic length' (here equivalent to single fibre diameter), D is the gas diffusivity ($1.88 \times 10^{-9} \text{ m}^2 \text{ s}^{-1}$ for CH_4 in water at 25°C , Witherspoon and Saraf, 1965), V_L is the liquid velocity (m s^{-1}) determined from Q_L and the cross-sectional area for liquid flow (approximately $2.81 \times 10^{-4} \text{ m}^2$ in the HFMC lumen) (Yang and Cussler, 1986). The minimum ratio of sweep gas to liquid theoretically necessary to achieve a target removal efficiency can be determined on the basis of the dimensionless Henry's constant (3):

$$\left(\frac{Q_G}{Q_L} \right)_{\text{minimum}} = \frac{c_{\text{CH}_4, \text{in}} - c_{\text{CH}_4, \text{out}}}{H c_{\text{CH}_4, \text{in}}} \quad 3$$

where Q_G and Q_L are the gas and liquid flow rates respectively ($\text{m}^3 \text{ s}^{-1}$) and H is the dimensionless Henry's constant for CH_4 (Table 4.1) (Crittenden *et al.*, 2005). Gas-side mass transfer coefficients (k_G , m s^{-1}) were determined using data for gas phase CH_4 composition exiting the HFMC shell (4):

$$k_G = \frac{Q_G}{A_m} \times \ln \left(\frac{c_{\text{CH}_4, \text{out gas}}}{c_{\text{CH}_4, \text{in gas}}} \right) \quad 4$$

where A_m is the membrane surface area (0.79 m^2 based upon fibre OD for shell-side gas flow), and $c_{\text{CH}_4, \text{in gas}}$ and $c_{\text{CH}_4, \text{out gas}}$ are the methane concentrations in the gas inlet (assumed as 0.00018% volume in air) and outlet respectively (Kreulen *et al.*, 1993).

4.3 Results

4.3.1 Removal of dissolved CH_4

CH_4 removal efficiencies were determined for several fixed sweep gas flow rates (Q_G), increasing progressively from $1.67 \times 10^{-7} \text{ m}^3 \text{ s}^{-1}$ up to $1.67 \times 10^{-4} \text{ m}^3 \text{ s}^{-1}$, whilst varying Q_L between $1.7 \times 10^{-7} \text{ m}^3 \text{ s}^{-1}$ and $1.28 \times 10^{-5} \text{ m}^3 \text{ s}^{-1}$ (Figure 4.2).

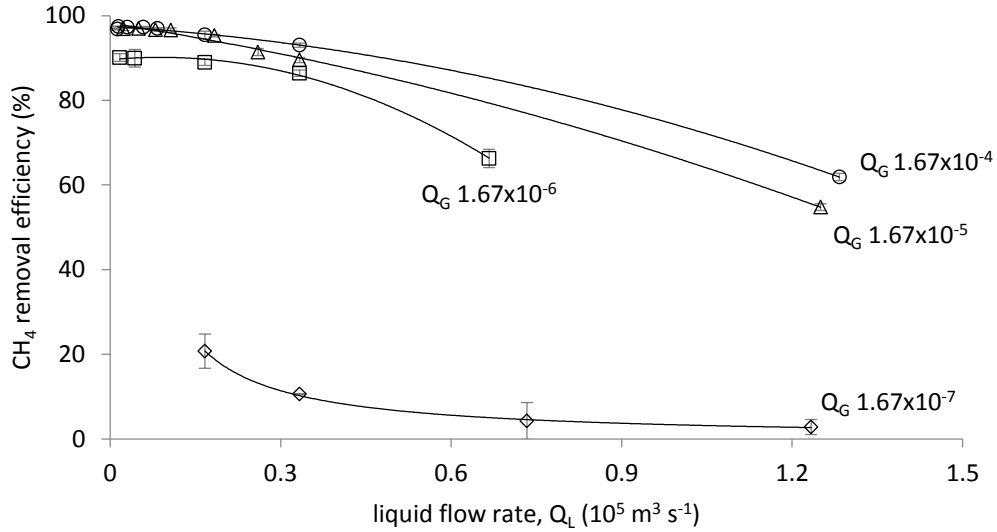


Figure 4.2 CH_4 removal efficiency from water saturated by a 75/25 CH_4/CO_2 gas mixture (1 atm, 25 °C) for sweep gas Q_G of increasing orders of magnitude ($1.67 \times 10^{-7} \text{ m}^3 \text{ s}^{-1}$ - $1.67 \times 10^{-4} \text{ m}^3 \text{ s}^{-1}$) with variable Q_L ($0.017 \times 10^{-5} \text{ m}^3 \text{ s}^{-1}$ - $1.28 \times 10^{-5} \text{ m}^3 \text{ s}^{-1}$) using a HFMC.

Removal efficiency was enhanced by reducing Q_L for each respective fixed value of Q_G , but was decreased by lowering the fixed value of Q_G . Consequently a maximum removal efficiency of approximately 97 % was observed at maximum Q_G and minimum Q_L , corresponding to $0.5 \text{ g}_{\text{CH}_4} \text{ m}^{-3}$ exiting the HFMC (from an initial $16.7 \text{ g}_{\text{CH}_4} \text{ m}^{-3}$). However this removal efficiency was maintained up to a Q_L of $2.3 \times 10^{-7} \text{ m}^3 \text{ s}^{-1}$ at $Q_G \geq 1.67 \times 10^{-5} \text{ m}^3 \text{ s}^{-1}$. Above a Q_L of $2.3 \times 10^{-7} \text{ m}^3 \text{ s}^{-1}$ removal efficiency fell below 97 %, declining to a greater extent for a Q_G of $1.67 \times 10^{-5} \text{ m}^3 \text{ s}^{-1}$ versus $1.67 \times 10^{-4} \text{ m}^3 \text{ s}^{-1}$, resulting in respective removal efficiencies of 51 % and 59 % at similar maximum Q_L . Removal efficiencies for a Q_G of $1.67 \times 10^{-6} \text{ m}^3 \text{ s}^{-1}$ were consistently below those of greater Q_G , however, a relatively high removal efficiency of 90.1 % was maintained at minimum Q_L , which fell to 66.3 % by increasing Q_L to $0.67 \times 10^{-5} \text{ m}^3 \text{ s}^{-1}$. Further decrease of Q_G to the minimum ($1.67 \times 10^{-7} \text{ m}^3 \text{ s}^{-1}$) had a much larger detrimental effect upon removal efficiency, which fell from a relatively low 20.7 % to just 2.8 % with increasing Q_L (from $1.67 \times 10^{-6} \text{ m}^3 \text{ s}^{-1}$ to $1.23 \times 10^{-5} \text{ m}^3 \text{ s}^{-1}$).

The theoretical minimum G/L ratio required for any given target removal efficiency can be determined based upon the Henry's constant for the dissolved gas (3). The ability of the HFMC to

approach this theoretical value can be assessed by comparison with experimental removal efficiencies plotted against respective G/L values (Figure 4.3).

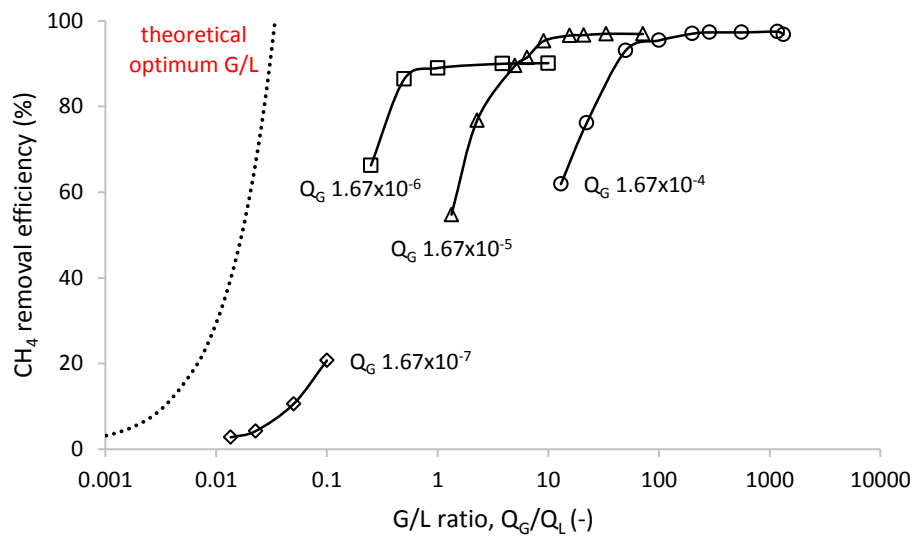


Figure 4.3 Comparison of experimental CH_4 removal efficiencies at respective values of G/L ratio with removal efficiencies at the theoretical optimum G/L, determined on the basis of equilibrium obeying Henry's law.

The greatest experimental removal efficiency (97 %) was achieved at a G/L of 15.6 ($Q_G = 1.67 \times 10^{-5} \text{ m}^3 \text{ s}^{-1}$), which was approximately 472 times the theoretical optimum G/L required (0.033). Whilst further reduction in G/L was detrimental to removal efficiency, approximately 90 % removal efficiency was maintained at a G/L of 1 ($Q_G = 1.67 \times 10^{-6} \text{ m}^3 \text{ s}^{-1}$), which was only 30 times in excess of the minimum G/L (0.031). The closest approximation of the theoretical optimum G/L to experimental removal efficiency was achieved at the lowest Q_G ($1.67 \times 10^{-7} \text{ m}^3 \text{ s}^{-1}$), where a 2.8 % removal efficiency was observed at a G/L of 13.5 times the theoretical optimum G/L.

4.3.2 Purity of recovered CH_4

The purity of stripped CH_4 was increased by lowering Q_G from $1.67 \times 10^{-4} \text{ m}^3 \text{ s}^{-1}$ to $1.67 \times 10^{-6} \text{ m}^3 \text{ s}^{-1}$ for fixed values of Q_L (Figure 4a). However, the absolute CH_4 concentration ranges in the gas phase were enhanced by increasing the fixed value of Q_L such that the greatest purity of 41 % was observed at minimum Q_G ($1.67 \times 10^{-6} \text{ m}^3 \text{ s}^{-1}$) and maximum Q_L ($1.23 \times 10^{-5} \text{ m}^3 \text{ s}^{-1}$). CH_4 purity was most significantly

reduced by initial increase of Q_G above the minimum to $8.3 \times 10^{-6} \text{ m}^3 \text{ s}^{-1}$, decreasing by up to 15 %, whilst subsequent increases in Q_G were progressively less detrimental to CH_4 purity. Assessment of CH_4 purity against respective G/L revealed a reasonable log-linear relationship across the entire dataset (Figure 4.4b).

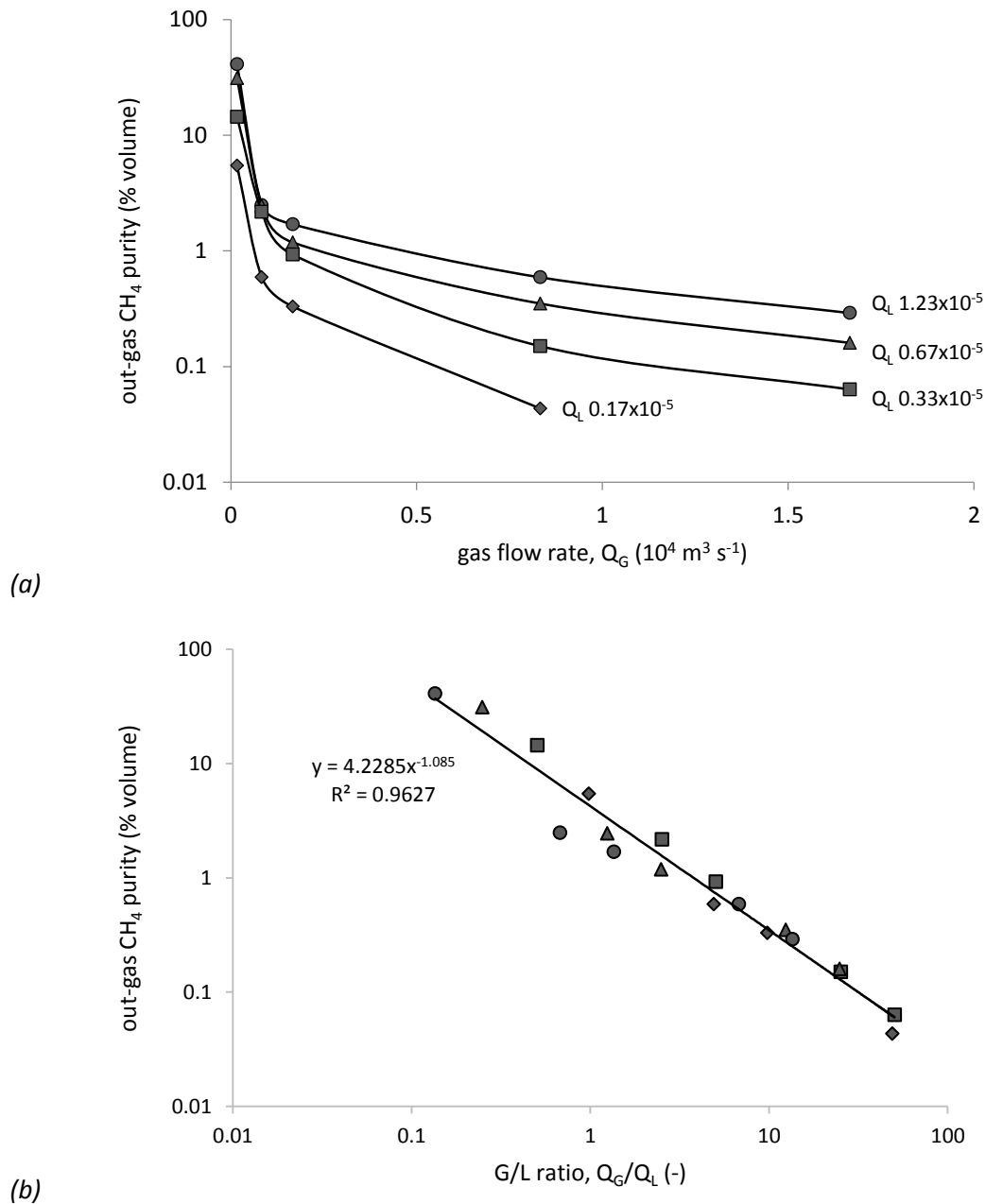


Figure 4.4 Impact of variable Q_G ($1.67 \times 10^{-7} \text{ m}^3 \text{ s}^{-1}$ to $1.67 \times 10^{-4} \text{ m}^3 \text{ s}^{-1}$) upon out-gas methane purity (% vol. CH_4) at fixed Q_L ($0.17 \times 10^{-5} \text{ m}^3 \text{ s}^{-1}$, $0.33 \times 10^{-5} \text{ m}^3 \text{ s}^{-1}$, $0.67 \times 10^{-5} \text{ m}^3 \text{ s}^{-1}$ and $1.23 \times 10^{-5} \text{ m}^3 \text{ s}^{-1}$) (a) and single correlation of out-gas methane purity the respective values of G/L (b).

4.3.3 CH_4 mass transfer

Mass transfer was highly dependent upon Q_L , represented by Reynolds number (Re), for Q_G of $1.67 \times 10^{-6} \text{ m}^3 \text{ s}^{-1}$ and above, indicating liquid phase control (Figure 4.5).

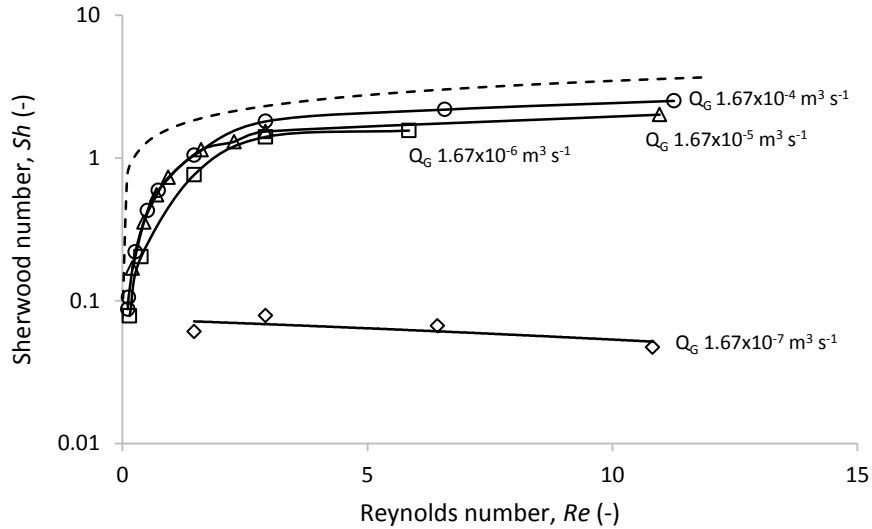


Figure 4.5 Effect of increasing the Reynolds number (Re) in the liquid upon mass transfer of CH_4 , represented by Sherwood number (Sh), for Q_G of increasing orders of magnitude ($1.67 \times 10^{-7} \text{ m}^3 \text{ s}^{-1}$ to $1.67 \times 10^{-4} \text{ m}^3 \text{ s}^{-1}$) and comparison with the Sh predicted by the Graetz-Lévêque equation (dashed line).

However, at the minimum Q_G ($1.67 \times 10^{-7} \text{ m}^3 \text{ s}^{-1}$) mass transfer was independent of Re (in the range of 1.5 to 10.8) and remained relatively constant within the limits of standard error. Experimental Sh approached within 20 % of values predicted by the Graetz-Lévêque equation at maximum Q_G ($1.67 \times 10^{-4} \text{ m}^3 \text{ s}^{-1}$). However, Sh was incrementally less well approximated as Q_G was diminished in magnitude to $1.67 \times 10^{-5} \text{ m}^3 \text{ s}^{-1}$ and then to $1.67 \times 10^{-6} \text{ m}^3 \text{ s}^{-1}$, until finally no correlation was observed at minimum Q_G ($1.67 \times 10^{-7} \text{ m}^3 \text{ s}^{-1}$).

4.4 Discussion

This study demonstrates the ability of HFMCs to achieve excellent removal efficiency and enable recovery of CH_4 of sufficient purity for direct application to energy generation, whilst operating within a liquid phase limited mass transfer regime. This strong dependency upon the liquid phase is

demonstrated by the positive relationship between Sh and Re for Q_G above $1.67 \times 10^{-6} \text{ m}^3 \text{ s}^{-1}$, which closely parallel values predicted by the Graetz-L  v  que equation (Figure 4.5). Despite inadequate study of CH_4 degassing in micro-porous systems for direct comparison, investigations of oxygen (O_2) degassing are reasonably analogous because the comparable solubility and diffusivity of these gases, due to similar molecular size and non-polarity, are key variables determining mass transfer (Table 4.1) (McLeod *et al.*, awaiting submission). Liquid phase controlled mass transfer data for degas of O_2 in a micro-porous HFMC displayed excellent correlation with the CH_4 data from the present study (at $Q_G \geq 1.67 \times 10^{-6} \text{ m}^3 \text{ s}^{-1}$) (Figure 4.6) (Tai *et al.*, 1998). Whilst corroborating the premise of liquid phase controlled CH_4 mass transfer, this comparison also clarifies the applicability of the Graetz-L  v  que equation to CH_4 mass transfer in the HFMC when Q_L is enhanced sufficiently to obtain $Gz \geq 20$ (for valid Graetz-L  v  que prediction of Sh ; Kreulen *et al.*, 1993). This is critical for confidently predicting mass transfer at greater scales. Dominance of mass transfer by the liquid phase can be expected when the gas phase and membrane coefficients (k_G and k_M respectively) are significantly greater than k_L , according to the resistance in series model (Kreulen *et al.*, 1993).

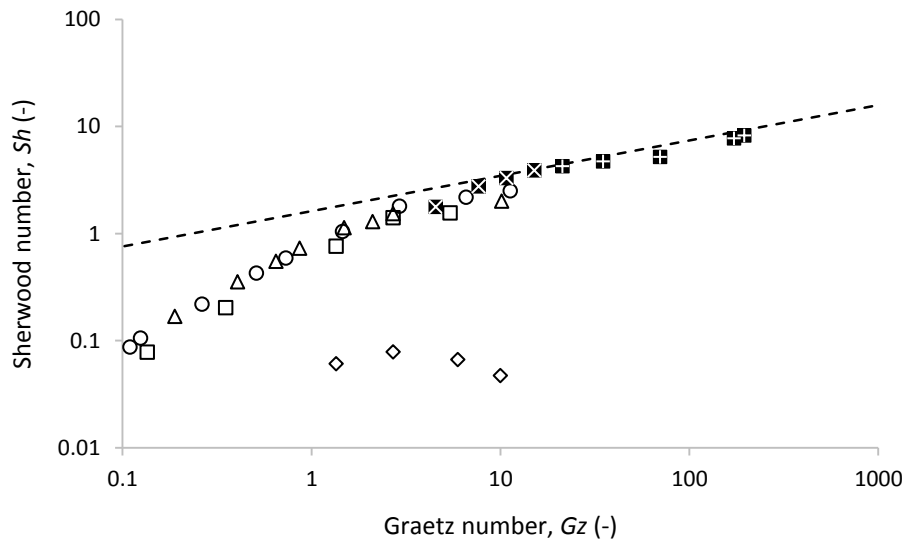


Figure 4.6 Comparison of CH_4 mass transfer (present study) with data adapted for O_2 degas in a micro-porous HFMC (black filled crossed shapes, adapted from Tai *et al.*, 1998) and the Graetz-L  v  que equation (dashed line).

The HFMC was consistently operated in large excess of the minimum G/L theoretically required for effective CH₄ stripping (Figure 4.3), which rapidly re-established the concentration gradient between liquid and gas, typically resulting in very large k_G (Table 4.2).

Table 4.2 Individual mass transfer coefficients for variable magnitudes of Q_G at fixed Q_L

Gas flow rate	Liquid flow rate	Liquid mass trans. coeff.	Gas mass trans. coeff.	Membrane mass trans. coeff.
$Q_G, 10^5 \text{ m}^3 \text{ s}^{-1}$	$Q_L, 10^5 \text{ m}^3 \text{ s}^{-1}$	$k_L, 10^5 \text{ m s}^{-1}$	$k_G, 10^5 \text{ m s}^{-1}$	$k_M, 10^5 \text{ m s}^{-1}$
16.7	3.33	1.54	123.81	5.30
1.67	3.33	1.31	18.04	5.30
0.167	3.33	1.20	2.38	5.30

A relatively large k_M ($5.3 \times 10^{-5} \text{ m s}^{-1}$, Table 4.2) was maintained by ensuring gas-filled pores via careful balance of the trans-membrane pressure and determined from the y-intercept of a Wilson plot (Figure 4.7).

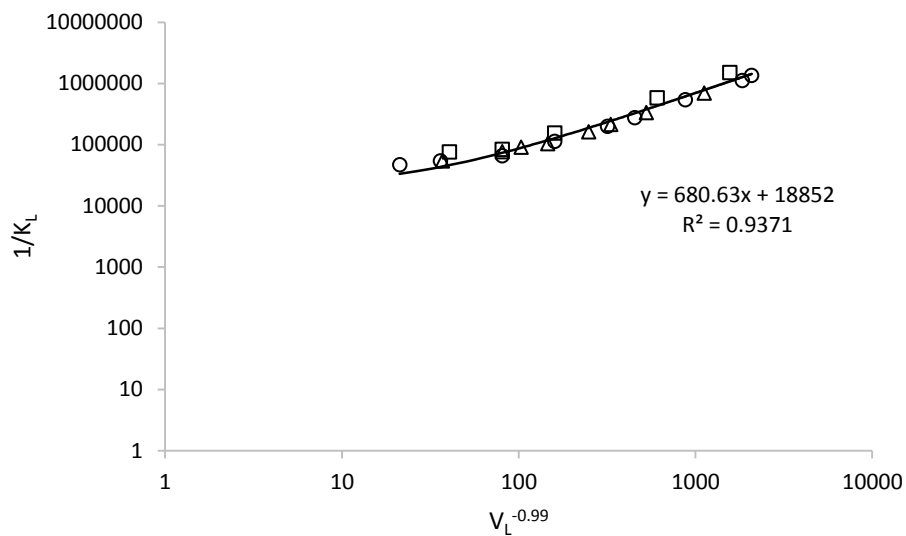


Figure 4.7 Wilson plot used to estimate the mass transfer coefficient of the membrane.

An exception occurred at minimum Q_G ($1.67 \times 10^{-7} \text{ m}^3 \text{ s}^{-1}$), where a zero response in Sh with variable Re indicated a switch to gas phase control of mass transfer (Figure 4.5). The emergence of this large gas phase resistance may be considered premature since operational G/L were significantly above

the minimum G/L even when an excess G/L of 3.5 times the minimum cited for air strippers was taken in to account (Figure 4.3) (Hand *et al.*, 1986). This was posited to be an artefact of gas channelling within the HFMC shell as Q_G was lowered significantly below the minimum value recommended within the operational specifications for the HFMC module ($4.72 \times 10^{-5} \text{ m}^3 \text{ s}^{-1}$) (MiniModule Start-up Guide, Liqui-Cel). The lab-scale module has a large packing fraction (0.369) for an optimised specific surface area ($3618 \text{ m}^2 \text{ m}^{-3}$) with the intention of degassing without anticipated recovery from the sweep gas. Shell-side laminar flows are typically inhibited by large packing fractions in HFMCs due to non-uniform spacing between fibres, which has resulted in the inclusion of packing fraction as a key parameter within several shell-side empirical mass transfer correlations (Prasad and Sirkar, 1988; Costello *et al.*, 1993; Gawroński and Wrzesinska, 2000; Lipnizki and Field, 2001). Shell-side modelling demonstrates a mal-distribution of fluid flow relative to the distribution of the spatial area between fibres at packing fractions above 0.3, such that approximately 40 % of fluid flowed through the largest 20 % void areas, whereas only 6 % of flow occurred through the smallest 20 % of void spaces (Zheng *et al.*, 2003). For the present HFMC design it is posited that variable local gas velocities and channelling of gas away from available membrane surface area become significant when the absolute value of Q_G is very low, forming areas of stagnation and resulting in the greater mass transfer resistance of the gas phase.

The maximum removal efficiency of 97 % required a Q_G of at least $1.67 \times 10^{-5} \text{ m}^3 \text{ s}^{-1}$ (corresponding to G/L of 15.3 and above), however a 90 % removal efficiency was still maintained at a Q_G of $1.67 \times 10^{-6} \text{ m}^3 \text{ s}^{-1}$ (above a G/L of 1) (Figure 4.2). This is critical for low GHG emission anaerobic wastewater treatment, where a 25 times greater GHG potency of CH_4 corresponds to a carbon saving of $1.03\text{-}1.11 \text{ kg}_{\text{CO}_2, \text{ eq.}} \text{ m}^{-3}$ for 90 % and 97 % methane removal efficiencies respectively, or $10.3\text{-}11.1 \text{ T}_{\text{CO}_2, \text{ eq.}} \text{ d}^{-1}$, assuming a $\text{ca.} 10000 \text{ m}^3 \text{ d}^{-1}$ of liquid flow (McAdam *et al.*, 2011). A 97 % removal efficiency was also sufficient to reduce an initial $16.7 \text{ g}_{\text{CH}_4} \text{ m}^{-3}$ saturated liquid concentration to $0.5 \text{ g}_{\text{CH}_4} \text{ m}^{-3}$ upon exit of the HFMC, which is approximately 50 % below the necessary concentration to form combustible atmospheres within leachate drainage systems ($0.98 \text{ g}_{\text{CH}_4} \text{ m}^{-3}$)

(Rooksby, 2007). Although the cited limit of consent ($0.14 \text{ g}_{\text{CH}_4} \text{ m}^{-3}$) was not achieved in this case (a removal efficiency above 99 % would be required) the removal of $16.2 \text{ g}_{\text{CH}_4} \text{ m}^{-3}$ indicates that consent would be met in the majority of cases, where lower initial concentrations between $2.0 \text{ g}_{\text{CH}_4} \text{ m}^{-3}$ and $15.0 \text{ g}_{\text{CH}_4} \text{ m}^{-3}$ are more common for landfill leachate (Rooksby, 2007). Removal efficiency in the micro-porous HFMC was superior to the 72 % maximum achieved previously using dense permeable PDMS membranes (at a G/L of 21.3) (Cookney *et al.*, 2012). In this instance the permeable membrane was mass transfer limiting and purportedly inhibited removal efficiency due to competitive permeation between CH_4 and CO_2 , suggesting that liquid phase limited mass transfer in a micro-porous HFMC is better suited to the degassing of binary gas solutions. At maximum Q_G ($1.67 \times 10^{-4} \text{ m}^3 \text{ s}^{-1}$) the HFMC operated within the designed specifications for sweep gas mode, however removal efficiency declined with increasing Q_L despite an enhancement of k_L (Figure 4.2; Figure 4.5). This is the result of increased Gz , which is defined as the time taken for transport of dissolved gas from the liquid bulk to the liquid-gas interface versus the mean liquid residence time within the HFMC (Dindore *et al.*, 2005). In the present study this effect competed with the simultaneous enhancement of mass transfer sufficiently to reduce removal efficiency; a result analogous to the reduced loading capacity of CO_2 in water observed at increased Q_L during absorption from biogas using an identical HFMC (McLeod *et al.*, 2013). A separate effect is postulated for the reduction of removal efficiency as Q_G was lowered below the recommended minimum for the HFMC due to shell-side flow mal-distribution, which increased the significance of k_G to overall mass transfer (Table 4.2). Although k_G was reduced by 85 % at a Q_G of $1.67 \times 10^{-5} \text{ m}^3 \text{ s}^{-1}$ versus the maximum Q_G , k_G was still over an order of magnitude in excess of k_L (at a Q_L of $3.33 \times 10^{-5} \text{ m}^3 \text{ s}^{-1}$) and removal efficiency was inhibited mostly at high Q_L (Figure 4.2). However, further reduction of Q_G to $1.67 \times 10^{-6} \text{ m}^3 \text{ s}^{-1}$ reduced k_G below the k_M to the same order of magnitude as k_L , resulting in inhibited removal efficiency across the entire Q_L range (Figure 4.2).

The efficiency with which electricity can be generated using a CH_4 fuel gas is dependent upon gas phase CH_4 concentration. Therefore, whilst ignition is possible from just 4.4 % CH_4 in air,

concentrations above 35% (13 MJ m^{-3}) are reported for modern micro-turbines (with a minimum 21 % efficiency) (Capstone, 2010). As a result the 41 % maximum purity achieved from the HFMC (at a G/L of 0.14) is sufficient for direct application to the generation of electricity above minimum efficiency. By comparison the CH_4 purity recovered using permeable PDMS membranes in sweep gas mode was very low (0.028 % for a 72 % removal efficiency), such that vacuum operation below 30 mbar was required to prevent dilution of the permeate by the sweep gas (Cookney *et al.*, 2012). Experiments for O_2 degassing in permeable membranes demonstrated near parity for removal efficiency in sweep gas (Q_G fixed at $1.67 \times 10^{-5} \text{ m}^3 \text{ s}^{-1}$) and vacuum (40 mbar) modes, whilst modelling of permeable membranes has indicated that vacuum mode is energetically favourable versus sweep gas mode for recovery of permeates with maximum purity (Tan *et al.*, 2005; Vallieres and Favre, 2004). However it was also stated that sweep gas mode was advantageous from the perspective of raw energy consumption for removal (without considering recovered purity), particularly when sufficiently low vacuum was unobtainable. Consequently the benefit of vacuum operation in the micro-porous HFMC is unclear, since the potential for pore wetting limits the applicable reduced pressure to 40 mbar (MiniModule start-up guide, Liquid-Cel). Despite the greater efficiency for power generation using the 75 % CH_4 purity from the PDMS module under vacuum, the micro-porous HFMC enabled a greater absolute energy recovery by virtue of the high liquid phase controlled mass transfer. To demonstrate; a wastewater treatment flowsheet with integrated anaerobic processes and $\text{ca.} 10000 \text{ m}^3 \text{ d}^{-1}$ influent to a EGSB reactor (in addition to conventional anaerobic digestion) was calculated to transform a conventional flowsheet (without an EGSB) from a net electricity consumer (normalised to $-0.039 \text{ kWh m}^{-3}$ of treated sewage) to a net electricity exporter ($+0.037 \text{ kWh m}^{-3}$) by combustion of a $\text{ca.} 75 \text{ \% CH}_4$ gas recovered using the PDMS module in vacuum mode, which resulted in a $+369.2 \text{ kWh d}^{-1}$ benefit (McAdam *et al.*, 2011). However the production of a 41 % CH_4 gas, possessing 15 MJ m^{-3} calorific value (assuming a 891 kJ mol^{-1} heat of combustion for CH_4), at a G/L of 0.14 is equivalent to 0.12 kWh m^{-3} of degassed liquid (assuming a 21 % efficiency for the gas turbine), corresponding to a $+827.2 \text{ kWh d}^{-1}$ benefit for the same anaerobic

flow-sheet; a 125 % approximate increase versus the PDMS module in vacuum mode. In sweep gas mode gas phase composition may also be changed by ‘back-flux’ of the 1 atm N₂ sweep gas to the N₂-free liquid, in a manner similarly observed during oxygenation of water using sealed-end fibres (Ahmed *et al.*, 1992). At the minimum G/L of 0.033 for 97 % removal efficiency 16.2 g_{CH₄} m⁻³ was transferred in to the gas phase, where a 43 % CH₄ purity may be obtained in the limit of zero N₂ back flux by addition of the molar contributions on the basis of a mass balance. However, if a 1:1 molar substitution of N₂ for CH₄ is assumed then up to 75 % CH₄ purity could be achievable.

The recovery of high CH₄ purity required conditions of high Q_L and low Q_G that were not optimised for removal efficiency due to increased Gz and lower k_G respectively, resulting in a trade-off between CH₄ purity and removal efficiency (Figure 4.8). This trade-off may be appeased by extension of HFMC active length to enable sufficient liquid-gas contact time to reach a targeted removal efficiency (5):

$$\ln\left(\frac{c_{CH_4,out}}{c_{CH_4,in}}\right) = \frac{k_L a L}{V_L} \quad 5$$

where $c_{CH_4, in}$ and $c_{CH_4,out}$ are the liquid phase concentrations before and after the HFMC respectively, V_L is liquid velocity (m s⁻¹), ‘ a ’ is the specific surface area (m² m³) and L is the required membrane length (m) (Reed *et al.*, 1995).

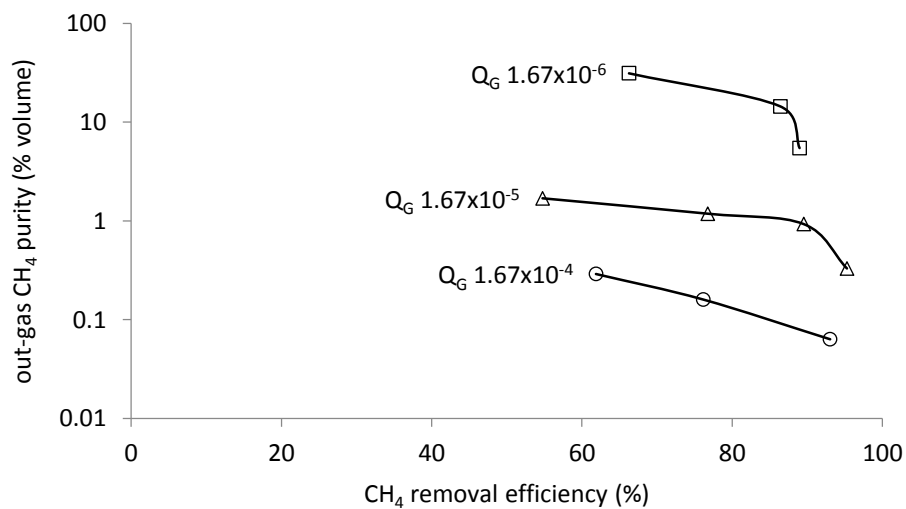


Figure 4.8 Trade-off between removal efficiency and purity of recovered CH₄.

At maximum Q_L for the HFMC module ($4.17 \times 10^{-5} \text{ m}^3 \text{ s}^{-1}$) a Gz of 33.7 is achieved and CH_4 mass transfer can be accurately predicted by the Graetz-L  v  que equation (Figure 4.6), resulting in an estimated k_L of $4.42 \times 10^{-5} \text{ m s}^{-1}$ ($Sh = 5.2$). At a G/L of 0.14 (for 41 % CH_4 recovery) Q_G would be sufficiently high ($5.83 \times 10^{-6} \text{ m}^3 \text{ s}^{-1}$) for avoid gas phase mass transfer resistance and allow a removal efficiency of at least 90.1 % (Figure 4.2). Under these conditions it is estimated that an extension of the HFMC active length to 0.63 m (or 6 HFMCs in series) would satisfy the trade-off and allow for concurrent 41 % CH_4 purity and 90.1 % removal efficiency. Whilst counter-current liquid and gas flow aids the limitation of back-transfer of stripped CH_4 along the length of the fibres, excessive module extension was found to be detrimental to removal efficiency during O_2 degassing due to the increased gas-side pressure drop within the HFMC (He *et al.*, 2004; Tan *et al.*, 2005). The trade-off may be alternatively appeased by re-designing the module to assuage the reduction of k_G at lower Q_G and enable a closer approach to the minimum G/L . Full scale HFMC designs differ significantly from the lab-scale module of the present study because gas is fed through the fibre lumen with shell-side liquid flow in order to minimise liquid-side pressure drop, reducing pumping costs, and enhance the resilience of the fibres to particulate matter in the liquid (Sengupta *et al.*, 1998). Whilst the gas experiences laminar flow through the fibre lumen, maximum contact of the liquid with the available membrane surface area is ensured by the inclusion of a centre baffle in the shell, which forces radial flow across the complete fibre bundle and prevents stagnation in the liquid phase. This is critical from the perspective of recovering high purity CH_4 because k_G will not be diminished by the formation of ‘dead-zones’ at very low Q_G , potentially allowing transition towards the minimum G/L without inhibiting removal efficiency. This advantage is indicated by the lowest recommended G/L attainable for a 1.7x5.5 ‘MiniModule’ (this study) and a 14x40 ‘Extra-Flow’ full-scale module of 1.13 and 0.12 respectively (when Q_L is maximised for optimal k_L) (MiniModule start-up guide; Extra-Flow start-up guide, Liqui-Cel).

4.5 Conclusions

Micro-porous HFMCs are capable of almost complete removal of dissolved CH_4 when operating with a N_2 sweep gas at a G/L of 15.3, where a 97 % removal efficiency from water saturated by 0.75 atm of CH_4 corresponded the abstraction of approximately $16.2 \text{ g}_{\text{CH}_4} \text{ m}^{-3}$ (or $1.1 \text{ kg}_{\text{CO}_2, \text{eq.}} \text{ m}^{-3}$) from solution. Mass transfer was largely liquid phase limited, which enabled operation at low Q_G sufficiently to recover 41 % CH_4 gaseous purity. Although permeable PDMS membranes have been demonstrated to recover ca.75 % purity, the lower purity gas was produced by the liquid phase controlled micro-porous HFMC in comparatively greater quantity, sufficiently to yield a greater energy recovery per unit of liquid degassed. The gas phase became influential to mass transfer as Q_G was lowered such that further enhancement of CH_4 purity by lowering Q_G was significantly detrimental to removal efficiency. However the emergence of gas phase mass transfer resistance was considered premature relative to the operational G/L, which was considerably above the minimum G/L even when a stripping factor of 3.5 was taken into account. It is postulated that operation using full-scale HFMC designs, where the sweep gas is fed through the fibre lumen, will prevent the formation of stagnant regions supposed to occur at very low Q_G in the present HFMC and ensure uniform contact with the entire available membrane surface area.

Acknowledgments

The authors would like to thank the Engineering and Physical Sciences Research Council (EPSRC, V/N: 08001923), Anglian Water, Northumbrian Water, Severn Trent Water and Yorkshire Water for their financial support.

References

Alberto, M. C. R., Arah, J. R. M., Neue, H. U., Wassmann, R., Lantin, R. S., Aduna, J. B. and Bronson, K. F. (2000), "A sampling technique for the determination of dissolved methane in soil solution", *Chemosphere – Global Change Science*, vol. 2, no. 1, pp. 57-63.

Ahmed, T. and Semmens, M. J. (1992), "The use of independently sealed microporous hollow fiber membranes for oxygenation of water: Model development", *Journal of Membrane Science*, vol. 69, no. 1-2, pp. 11-20.

Capstone CR65 and CR65 ICHP MicroTurbine, 2010, "http://www.capstoneturbine.com/_docs/datasheets/CR65%20&%20CR65%20ICHP%20Renewable_331039F_lowres.pdf" (accessed 4th August 2014).

Cookney, J., Cartmell, E., Jefferson, B. and McAdam, E. J. (2012), "Recovery of methane from anaerobic process effluent using poly-di-methyl-siloxane membrane contactors", *Water Science and Technology*, vol. 65, no. 4, pp. 604-610.

Costello, M. J., Fane, A. G., Hogan, P. A. and Schofield, R. W. (1993), "The effect of shell-side hydrodynamics on the performance of axial flow hollow fibre modules", *Journal of Membrane Science*, vol. 80, pp. 1-12.

Cramer, T. A., Johnson, D. W. and Urynowicz, M. A. (2009), "Membrane gas transfer of methane and carbon dioxide in submerged coal deposits", *Environmental technology*, vol. 30, no. 1, pp. 11-20.

Crittenden J. C., Rhodes Trussell R., Hand, D. W., Howe, K. J. and Tchobanoglous, G. (2005), "Water Treatment: Principles and Design 2nd edition", *John Wiley and Sons Inc.*, pp. 1192.

Daelman, M. R. J., van Voorthuizen, E. M., van Dongen, U. G. J. M., Volcke, E. I. P. and van Loosdrecht, M. C. M. (2012), "Methane emission during municipal wastewater treatment", *Water research*, vol. 46, no. 11, pp. 3657-3670.

Dang, T., Huntsberger, D. S. and Kitteringham, B. A. (2003), "Using membrane contactors for CO₂ removal to extend resin bed life", *Ultrapure Water*, vol. 20, no. 6, pp. 20-25.

Dindore, V. Y., Brillman, D. W. F. and Versteeg, G. F. (2005), "Hollow fiber membrane contactor as a gas-liquid model contactor", *Chemical Engineering Science*, vol. 60, no. 2, pp. 467-479.

Gawroński, R. and Wrzesinska, B. (2000), "Kinetics of solvent extraction in hollow-fiber contactors", *Journal of Membrane Science*, vol. 168, no. 1-2, pp. 213-222.

Hand, D. W., Crittenden, J. C., Gehin, J. L. and Lykins Jr., B. W. (1986), "DESIGN AND EVALUATION OF AN AIR-STRIPPING TOWER FOR REMOVING VOCs FROM GROUNDWATER.", *Journal / American Water Works Association*, vol. 78, no. 9, pp. 87-97.

He, J., Arnold, R. G., Sáez, A. E., Betterton, E. A. and Ela, W. P. (2004), "Removal of aqueous phase trichloroethylene using membrane air stripping contactors", *Journal of Environmental Engineering*, vol. 130, no. 11, pp. 1232-1241.

Ito, A., Yamagiwa, K., Tamura, M. and Furusawa, M. (1998), "Removal of dissolved oxygen using non-porous hollow-fiber membranes", *Journal of Membrane Science*, vol. 145, no. 1, pp. 111-117.

Keshavarz, P., Ayatollahi, S. and Fathikalajahi, J. (2008), "Mathematical modeling of gas-liquid membrane contactors using random distribution of fibers", *Journal of Membrane Science*, vol. 325, no. 1, pp. 98-108.

Koonaphapdeelert, S., Wu, Z. and Li, K. (2009), "Carbon dioxide stripping in ceramic hollow fibre membrane contactors", *Chemical Engineering Science*, vol. 64, no. 1, pp. 1-8.

Kreulen, H., Smolders, C. A., Versteeg, G. F. and Van Swaaij, W. P. M. (1993), "Microporous hollow fibre membrane modules as gas-liquid contractors. Part 2. Mass transfer with chemical reaction", *Journal of Membrane Science*, vol. 78, no. 3, pp. 217-238.

Lipnizki, F. and Field, R. W. (2001), "Mass transfer performance for hollow fibre modules with shell-side axial feed flow: using an engineering approach to develop a framework", *Journal of Membrane Science*, vol. 193, no. 2, pp. 195-208.

Liqui-Cel® Extra-Flow and SuperPhobic Start-up Guide, "<http://www.liqui-cel.com/technical-resources/startup-operating-guides.cfm>", (accessed 18th October 2013).

McAdam, E. J., Lüffler, D., Martin-Garcia, N., Eusebi, A. L., Lester, J. N., Jefferson, B. and Cartmell, E. (2011), "Integrating anaerobic processes into wastewater treatment", *Water Science and Technology*, vol. 63, no. 7, pp. 1459-1466.

McLeod, A., Jefferson, B. and McAdam, E. J. (2013), "Quantifying the loss of methane through secondary gas mass transport (or 'slip') from a micro-porous membrane contactor applied to biogas upgrading", *Water research*, vol. 47, no. 11, pp. 3688-3695.

McLeod, A., Jefferson, B. and McAdam, E. J. (awaiting submission), "A Framework to Identify Physical Solvents for Gas separations in Environmental gas-liquid absorption applications", *Environmental Science and Technology*.

MiniModule® Start-up Guide, "www.liqui-cel.com/uploads/documents/SU3_Rev%209_8-12_STARTUP%20MiniModule.pdf" (accessed 18th October 2013).

Pittam, D. A. and Pilcher, G. (1972), "Measurements of heats of combustion by flame calorimetry: Part 8. - Methane, ethane, propane, n-butane and 2-methylpropane", *Journal of the Chemical Society, Faraday Transactions 1: Physical Chemistry in Condensed Phases*, vol. 68, pp. 2224-2229.

Prasad, R. and Sirkar, K. K. (1988), "DISPERSION-FREE SOLVENT EXTRACTION WITH MICROPOROUS HOLLOW-FIBER MODULES", *AIChE Journal*, vol. 34, no. 2, pp. 177-188.

Reed, B. W., Semmens, M. J. and Cussler, E. L. (1995), "Membrane separations technology: Principles and applications – Chapter 10", *Elsevier science*,

Rooksby J. (2007), "Guidance for the Treatment of Landfill Leachate", *Environment Agency*, Chapter 2, pp. 39.

Sengupta, A., Peterson, P. A., Miller, B. D., Schneider, J. and Fulk Jr., C. W. (1998), "Large-scale application of membrane contactors for gas transfer from or to ultrapure water", *Separation and Purification Technology*, vol. 14, no. 1-3, pp. 189-200.

Tai, M. S. L., Chua, I., Li, K., Ng, W. J. and Teo, W. K. (1994), "Removal of dissolved oxygen in ultrapure water production using microporous membrane modules", *Journal of Membrane Science*, vol. 87, no. 1-2, pp. 99-105.

Tan, X., Capar, G. and Li, K. (2005), "Analysis of dissolved oxygen removal in hollow fibre membrane modules: Effect of water vapour", *Journal of Membrane Science*, vol. 251, no. 1-2, pp. 111-119.

Vallieres, C. and Favre, E. (2004), "Vacuum versus sweeping gas operation for binary mixtures separation by dense membrane processes", *Journal of Membrane Science*, vol. 244, no. 1-2, pp. 17-23.

Wilhelm, E., Battino, R. and Wilcock, R. J. (1977), "Low-pressure solubility of gases in liquid water", *Chemical reviews*, vol. 77, no. 2, pp. 219-262.

Witherspoon, P. A. and Saraf, D. N. (1965), "Diffusion of methane, ethane, propane, and n-butane in water from 25 to 43°", *Journal of Physical Chemistry*, vol. 69, no. 11, pp. 3752-3755.

Yang, M. and Cussler, E. L. (1986), "DESIGNING HOLLOW-FIBER CONTACTORS.", *AIChE Journal*, vol. 32, no. 11, pp. 1910-1916.

Zheng, J., Xu, Y. and Xu, Z. (2003), "Flow distribution in a randomly packed hollow fiber membrane module", *Journal of Membrane Science*, vol. 211, no. 2, pp. 263-269.

Chapter 5

**Biogas upgrading by chemical absorption using ammonia rich absorbents
derived from wastewater**

For submission to: Water Research

Biogas upgrading by chemical absorption using ammonia rich absorbents derived from wastewater

Andrew McLeod, Bruce Jefferson and Ewan J. McAdam*

Cranfield Water Science Institute, Building 39, Cranfield University, Bedfordshire, MK43 0AL, UK

*Corresponding author e-mail: e.mcadam@cranfield.ac.uk

Abstract

The use of ammonia (NH_3) rich wastewaters as a sustainable chemical absorption solvent for the selective extraction of carbon dioxide (CO_2) during biogas upgrading to 'biomethane' has been studied. Analogue ammonia absorption solvents comprising 100 to 10000 $\text{g}_{\text{NH}_4\text{-N}} \text{m}^{-3}$ demonstrated that ammonia enhanced CO_2 flux from the gas phase into the solvent by up to 25 times that of water, the conventionally applied absorption solvent. Importantly, this suggests that ammonia rich wastewaters can be used to facilitate a chemical reaction without demanding costly exogenic chemicals, complex chemical handling or solvent regeneration, which are critical barriers to implementation of chemical absorption. Centrifuge return liquors obtained from an anaerobic digester (2325 $\text{g}_{\text{NH}_4\text{-N}} \text{m}^{-3}$) and ion exchange regenerant (477 $\text{g}_{\text{NH}_4\text{-N}} \text{m}^{-3}$) from a cationic ion exchanger used to harvest ammonium from crude wastewater, were subsequently tested. The CO_2 fluxes measured for both endogenic solvents compared satisfactorily with analogue ammonia absorption solvents of equivalent ammonia concentration, indicating that the residual matrix did not influence enhancement deleteriously. During analogue trials, precipitated ammonium bicarbonate (NH_4HCO_3) was also recovered from the solvent due to the reaction between CO_2 and NH_3 . This suggests a new process pathway for ammonia, which avoids biological nitrification and produces a commercially attractive fertiliser. However, in real wastewater solvents, sodium bicarbonate and calcium carbonate were preferentially formed. This can be attributed to enhanced cationic competition and the salts' higher solubility product, although it is proposed that NH_4HCO_3 can be preferentially formed by manipulating ion exchange chemistry and operation to diminish cationic competition.

Keywords: ammonia; wastewater; biogas upgrading; sustainable; chemical absorption

5.1 Introduction

Biogas is a renewable source of methane (CH₄) produced by anaerobic digestion (AD) at wastewater treatment works (WWTW). Raw biogas typically comprises 50-60 % CH₄, compared to >90 % found in treated natural gas. Inert carbon dioxide (CO₂) is the major balancing component of raw biogas (40-50 %) and is responsible for its considerably lower calorific value (~21 MJ m⁻³) versus natural gas (~36 MJ m⁻³) (Ryckebosch *et al.*, 2011). Therefore, for biogas to be used as 'biomethane' or natural gas substitute, biogas must be upgraded, principally through CO₂ removal. To remove CO₂, physical absorption using water as the absorption solvent is most commonly applied principally due to preference for process simplicity (Petersson and Wellinger, 2009). However, high water flow rates demanded to maximise CO₂ mass transfer, process scale, pumping energy and the loss of methane through 'slip' (co-dissolution into the receiving solvent) present significant practical constraints (McLeod *et al.*, 2013). Chemical absorption enables higher selectivity toward CO₂ by mediating separation via a chemical reaction, which reduces solvent flow rate and therefore pumping costs and methane slip (Patterson *et al.*, 2011). Amines are typically used as a chemical reactant for upgrading. However, water utilities are generally reluctant to introduce chemicals due to the requirement for specialised expertise, health and safety concerns regarding chemical storage and handling, high maintenance cost and the requirement for a complex and energy intensive solvent regeneration step (Patterson *et al.*, 2011).

Ammonia (NH₃) has been investigated as a substitute for conventional amines because of its superior loading capacity, reduced energy for regeneration and significantly lower corrosive properties (Yeh *et al.*, 2005; Budzianowski, 2011). The efficacy of ammonium is dependent upon the equilibrium between ionised ammonium (NH₄⁺) and un-ionised or 'free' ammonia (NH₃) (1):



since only free ammonia is chemically reactive with CO₂ (2):



Equilibrium is dependent upon pH and temperature, where increasing pH or temperature drives the equilibrium position towards free ammonia (Thurston *et al.*, 1979) (Figure 5.1).

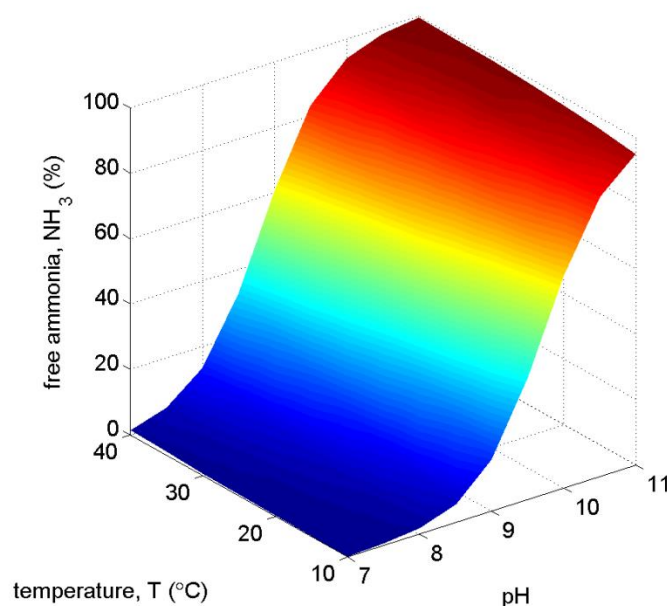


Figure 5.1 Effect of pH and temperature upon the empirically determined percentage free NH_3 , via influence of the $\text{NH}_4^+/\text{NH}_3$ equilibrium, in pure solution.

However, the exceptional volatility of NH_3 often demands chilling of the absorbent liquid to prevent NH_3 loss (or ‘slip’) in to the gas phase; imposing an additional cost and reducing reaction rate versus less volatile amine solutions operating at higher temperatures (Darde *et al.*, 2011). Limiting solution pH and ammonia concentration has been demonstrated to reduce NH_3 slip during CO_2 absorption (Budzianowski, 2011). It has also been proposed that NH_3 slip may also be reduced if hollow fibre membrane contactors (HFMCs) are used as an alternative to conventional packed column type liquid-gas contactors (Budzianowski, 2011).

In WWTW, there are several sources of ammonia-rich wastewaters. For example, return (or sludge) liquors often contain $\text{ca. } 1000 \text{ g}_{\text{NH}_4\text{-N}} \text{ m}^{-3}$ (Thornton *et al.*, 2007). Cation ion exchange media has also been used to harvest ammoniacal nitrogen ($\text{NH}_4\text{-N}$) from crude wastewater, secondary effluents and return liquors with the subsequent regenerant comprising an ammonia-rich phase of up to $10000 \text{ g}_{\text{NH}_4\text{-N}} \text{ m}^{-3}$ (Mackinnon *et al.*, 2003). Consequently, ammonia rich liquid streams offer

potential as a cost effective chemical for separating CO₂ during biogas upgrading at a WWTW, whilst also avoiding many of the disadvantages of exogenic chemicals such as bulk chemical storage or regeneration. The following investigation therefore aims to establish the applicability of ammonia rich wastewater as an alternative chemical solvent for biogas upgrading in combination with hollow fibre membrane contactors to limit the potential for ammonia volatility. Specifically, this study seeks to: (i) quantify CO₂ absorption behaviour within environmentally relevant range of NH₃ concentrations; (ii) establish pH and temperature boundaries for maximum CO₂ absorption behaviour; (iii) compare efficacy of real wastewater sources to synthetic absorbents of equal ammonia concentration; (iv) measure the volatility of NH₃ within process boundary conditions; and (v) establish the feasibility of recovering the reactant product (NH₄HCO₃).

5.2 Materials and methods

5.2.1 Equipment setup and operation

Methane (99.995 %) and carbon dioxide (99.7 %) (BOC gases, Ipswich, UK) gases were controlled using mass flow controllers (0.01-1.0 L min⁻¹, Roxspur Measurement and Control Ltd., Sheffield, UK) and were mixed in-line at a typical flow rate of 450 mL min⁻¹ for CH₄ and 300 mL min⁻¹ for CO₂ (total 750 mL min⁻¹) to provide a 60:40 / CH₄:CO₂ gas composition through the fibre lumen (polypropylene, PP) of the HFMC (Liqui-Cel® 1.7x5.5 MiniModule®, Membrana GmbH, Wuppertal, Germany) (Figure 5.2a). Absorbent was stored in a 10 L PVC tank, maintained at 24-26 °C by a thermostatic water bath (GD120, Grant Instruments Cambridge Ltd., Shepreth, UK). Absorbent was passed through the HFMC shell, in counter-current mode using a centrifugal pump (max. 6 L min⁻¹, 50010 series, Jabsco GmbH, Norderstedt, Germany). The HFMC comprised 7400 PP fibres, with a nominal outer diameter (OD) and length of 300 µm and 0.113 m respectively, yielding a surface area of 0.79 m². The fibres possessed a nominal pore size of 0.03 µm and porosity of 40 %, and presented a packing density of 0.369. Ammonia slip in to the gas phase was determined by the method described by Kuntke *et al.*

(2012). The out-gas was bubbled through diffusers in two 1 L capacity gas tight aspirator bottles (Schott Duran, VWR, The Netherlands) in series, containing 500 mL of 0.4 mol L⁻¹ sulfuric acid solution, where the second bottle enabled verification of complete NH₃ retention within the liquid in the first bottle.

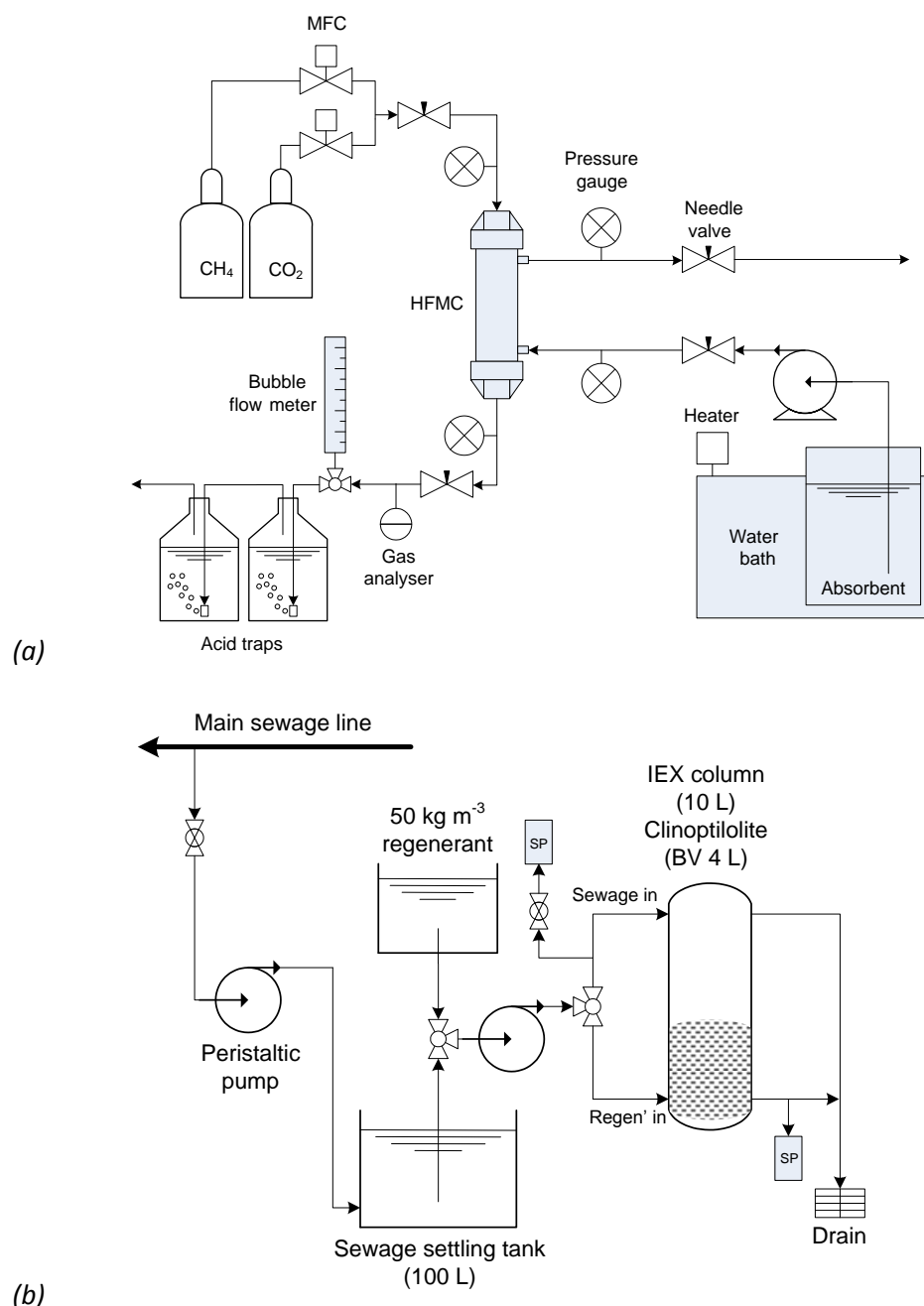


Figure 5.2 Set-up used for gas absorption in a polypropylene micro-porous hollow fibre membrane contactor (a); ion exchange column for removal of ammoniacal nitrogen from raw sewage by clinoptilolite and subsequent production ion exchange regenerant. SP indicates sampling point (b).

The ion exchanger comprised a 10 L column containing 4 L of clinoptilolite resin (RS Minerals, Guisborough, UK). The virgin bed was prepared by passing a 50 g_{NaCl} L⁻¹ (99 %, Fisher Chemicals, Loughborough, UK) regenerant through the column at 5 bed volumes per hour (BV h⁻¹) for 30 minutes followed by a DI rinse at 5 BV h⁻¹ for 60 minutes (McAdam *et al.*, 2010) (Figure 5.2b). The column was operated in down-flow using crude sewage (10-20 g_{NH4-N} m⁻³) at a flow rate of 4.2 BV h⁻¹ (Aiyuk *et al.*, 2004) until breakthrough, which was noted at 166 BV. The column was regenerated in up-flow using 20 L of 50 g_{NaCl} L⁻¹ at 1 BV h⁻¹. The IEX regenerant was fractionated in an initial 2 L fraction and a secondary 10 L fraction, with the remaining volume retained within the column. The IEX regenerant was filtered through a 1.2 µm filter (GF/C 15 mm, Fisher Scientific, Loughborough, UK) prior to use. Return liquor was collected from a digestate dewatering centrifuge at a local WWTW. The return liquor was filtered through a 6-12 µm filter before centrifugation (Sorvall Legend RT+, Thermo Fisher Scientific, Hemel Hempstead, UK) at 5000 rpm for 10 minutes, with the decant filtered through a 1.2 µm filter.

5.2.2 Chemical preparation, sampling and analysis

Synthetic absorbent was freshly prepared each day by adding saturated aqueous ammonia solution (35 %, 2.5 L, Fisher Chemicals) to DI water (15 MΩ cm⁻¹) and its concentration confirmed by ammonium cell test. The pH of real and synthetic absorbents was fixed at pH 11 (excluding variable pH experiments) through adjustment with sodium hydroxide or 32 % hydrochloric acid (Fisher Chemicals, Loughborough, UK). Ammonia analysis was undertaken using cell tests (4-80 mg_{NH4-N} L⁻¹, VWR International Ltd., Poole, UK) with photometric determination using a Spectroquant Nova 60 (Merck-Millipore, Darnstadt, Germany). Gas composition after the HFMC was determined from an average of 5 consecutive measurements at 20 s intervals using an infrared biogas analyser (Yieldmaster, accuracy <0.2 % full-scale, Bluesens gas sensor GmbH, Herten, Germany) and monitored online using the accompanying software (BACVis, Bluesens gas sensor GmbH, Herten,

Germany). Gas flow rate was measured using a bubble flow meter (50 mL, Restek, Bellefonte, USA).

Flux (J_{CO_2} , mol_{CO₂} m⁻² s⁻¹) was calculated using (3):

$$J_{CO_2} = \frac{[(Q_{G,in} \times c_{G,in}) - (Q_{G,out} \times c_{G,out})] \times 273.15 \times 1000}{(22.4 \times A_m \times T_G)} \quad 3$$

where $Q_{G, in}$ and $Q_{G, out}$ are gas flow rate before and after HFMC respectively (m³ s⁻¹), $c_{G, in}$ and $c_{G, out}$ are the CO₂ content before and after HFMC respectively (mol mol⁻¹), A_m refers to the membrane surface area for absorption (m²) and T_G is the gas temperature (K) (Atchariyawut *et al.*, 2007). Microscopy of membrane fibres and crystals was performed by scanning electron microscope (SEM, XL30, FEI, Hillsboro, Oregon, USA) and further analysed by energy dispersive x-ray spectroscopy (EDX, Oxford Instruments NTS, Abingdon, UK) and x-ray diffraction (XRD, D5005, Siemens, Munich, Germany).

5.3 Results

5.3.1 Assessment of CO₂ absorption using analogue ammonia absorbents

The influence of ammoniacal nitrogen equilibrium on driving CO₂ mass transfer in a HFMC was examined through variation of pH and temperature using synthetic ammonia solutions at fixed values of liquid and gas flow rate (Q_L and Q_G respectively, m³ s⁻¹) (Figure 5.3). An increase in solvent pH notably increased J_{CO_2} . This effect was exacerbated at higher free ammonia concentrations. For example, J_{CO_2} at pH 11 and 20 °C ranged from approximately 0.7x10⁻⁴ mol_{CO₂} m⁻² s⁻¹ in a 10 g_{NH₄-N} m⁻³ solution up to approximately 3.8x10⁻⁴ mol_{CO₂} m⁻² s⁻¹ in the 10000 g_{NH₄-N} m⁻³ solution. An increase in solvent temperature from 20 °C to 40 °C did not increase J_{CO_2} markedly within the low pH range. However, for the most concentrated solvent tested (10000 g_{NH₄-N} m⁻³), the higher temperature was noted to increase flux. This was particularly evident in the higher pH range in which CO₂ flux increased from 0.38x10⁻⁴ mol_{CO₂} m⁻² s⁻¹ at 20 °C (pH 11) to 0.48x10⁻⁴ mol_{CO₂} m⁻² s⁻¹ at 40 °C (pH 11).

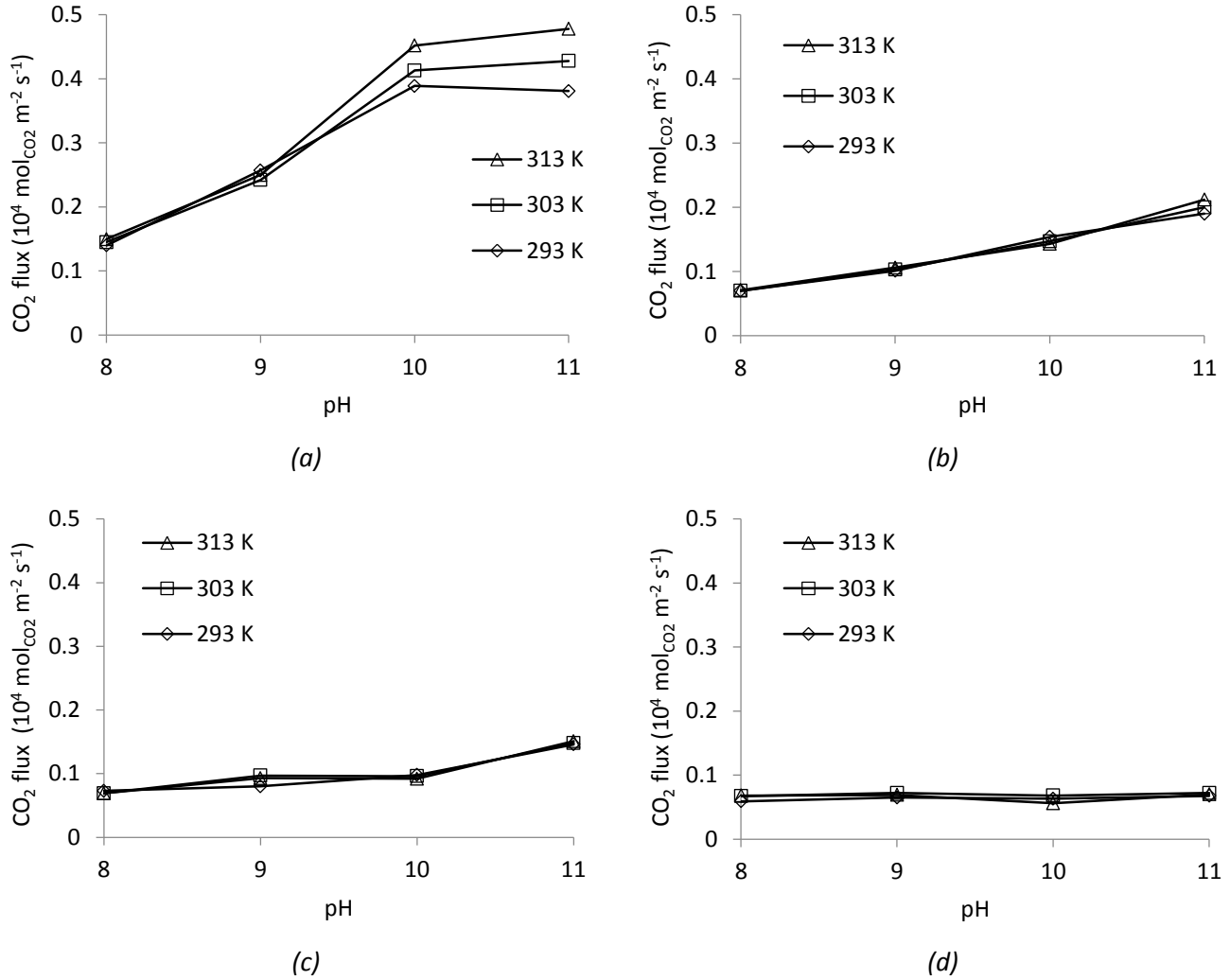


Figure 5.3 Effect of pH and temperature upon CO₂ flux (J_{CO_2}) in pure NH₃ solutions with concentrations of 10000 g_{NH4-N} m⁻³ (a), 1000 g_{NH4-N} m⁻³ (b), 100 g_{NH4-N} m⁻³ (c) and 10 g_{NH4-N} m⁻³ (d) under fixed Q_L and Q_G (1.67×10^{-6} m³ s⁻¹ and 1.25×10^{-5} m³ s⁻¹ respectively).

The influence of gas flow rate (Q_G) on CO₂ mass transfer was examined under a fixed solvent flow rate (Q_L , 6.7×10^{-6} m³ s⁻¹) and fixed solvent conditions of pH 11 and 20 °C (Figure 5.4a and 5.4b). For the boundary conditions tested, maximum biogas CH₄ compositions of between 98 % and 99 % were measured with the 5000 g_{NH4-N} m⁻³ and 10000 g_{NH4-N} m⁻³ solutions at a G/L of 0.075. An increase in Q_G decreased biogas methane composition in these ammonia-rich absorbents and was more noticeable for the 5000 g_{NH4-N} m⁻³ solution. In comparison, a negligible increase in biogas methane composition was noted when Q_G was decreased for the lower ammonia solution concentrations, representative of crude wastewater (10 g_{NH4-N} m⁻³ to 100 g_{NH4-N} m⁻³) (Figure 5.4a). Further data

analysis demonstrated a positive linear trend in J_{CO_2} as Q_G was increased for the lower ammonia solutions ($10 \text{ g}_{NH_4-N} \text{ m}^{-3}$ and $100 \text{ g}_{NH_4-N} \text{ m}^{-3}$) (Figure 5.4b).

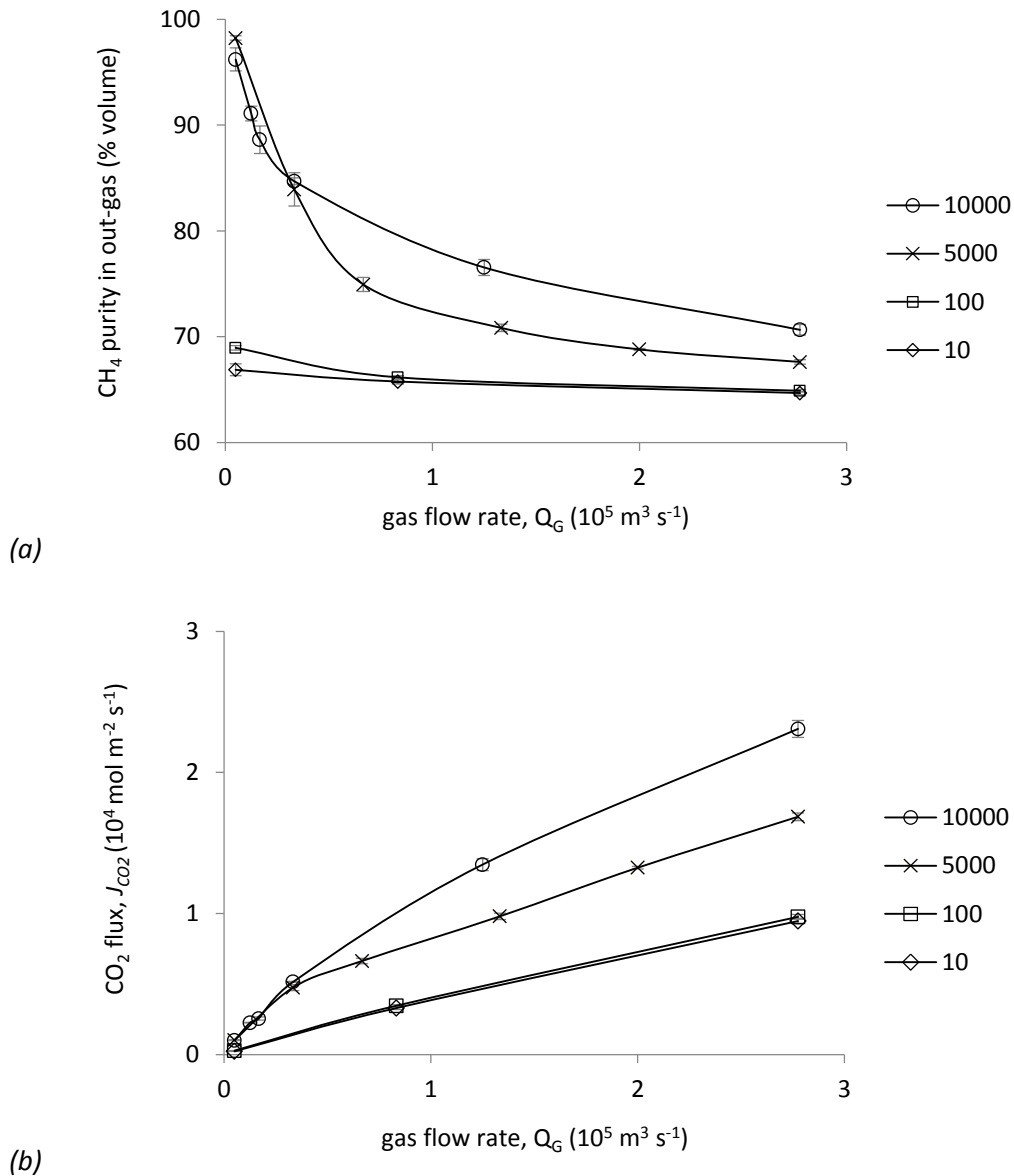


Figure 5.4 Effect of variable gas flow rate (Q_G , 0.05×10^{-5} – $2.8 \times 10^{-5} \text{ m}^3 \text{ s}^{-1}$) upon methane purity in the gas exiting the HFMC (a) and CO_2 flux at a fixed liquid flow rate (Q_L , $6.7 \times 10^{-6} \text{ m}^3 \text{ s}^{-1}$) in synthetic ammonia solutions at four distinct concentrations (10, 100, 5000, & 10000 $\text{g}_{NH_4-N} \text{ m}^{-3}$) (b).

Interestingly, at these concentrations, an increase in CO_2 flux was not recorded despite an order of magnitude increase in ammonia concentration. A positive non-linear increase in J_{CO_2} was measured for the higher ammonia concentrations as Q_G increased. At the maximum hydrodynamic conditions tested (G/L 4.2), J_{CO_2} increased from around $0.94 \times 10^{-4} \text{ mol}_{CO_2} \text{ m}^{-2} \text{ s}^{-1}$ for the 10 and 100 $\text{g}_{NH_4-N} \text{ m}^{-3}$

absorbents up to $1.7 \times 10^{-4} \text{ mol}_{\text{CO}_2} \text{ m}^{-2} \text{ s}^{-1}$ and $2.3 \times 10^{-4} \text{ mol}_{\text{CO}_2} \text{ m}^{-2} \text{ s}^{-1}$ through increasing ammonia absorbent concentration up to 5000 and 10000 $\text{g}_{\text{NH}_4\text{-N}} \text{ m}^{-3}$ respectively. The enhancement provided by the chemical reaction was described by the 'enhancement factor' (E) which can be applied providing an identical driving force for mass transfer is assumed (Figure 5.5) (Dindore *et al.*, 2005) (4):

$$E = \frac{\text{CO}_2 \text{ flux (chemical)}}{\text{CO}_2 \text{ flux (physical)}}$$

4

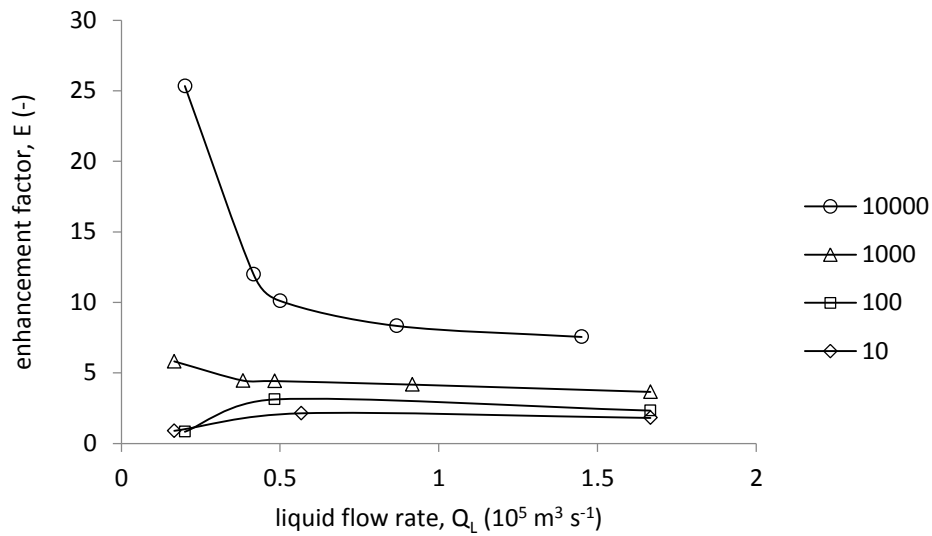


Figure 5.5 Effect of variable liquid flow rate (Q_L , 0.17×10^{-5} - $1.7 \times 10^{-5} \text{ m}^3 \text{ s}^{-1}$) upon enhancement factor (E, dimensionless), determined by ratio of CO_2 flux for each distinct NH_3 concentration (10, 100, 1000, & 10000 $\text{g}_{\text{NH}_4\text{-N}} \text{ m}^{-3}$) against CO_2 flux in DI water.

Under fixed gas-side conditions, the highest chemical enhancement was observed at the lowest Q_L which can also be characterised by an increase in G/L ratio. A maximum E of 25.3 was determined for the 10000 $\text{g}_{\text{NH}_4\text{-N}} \text{ m}^{-3}$ solution at $Q_L 0.2 \times 10^{-5} \text{ m}^3 \text{ s}^{-1}$. However, E reduced sharply following a decrease in ammonia concentration. To illustrate, whilst a similar trend in enhancement factor was noted following an order of magnitude reduction in ammonia concentration to 1000 $\text{g}_{\text{NH}_4\text{-N}} \text{ m}^{-3}$, a maximum E of only 5.8 was observed. Further reduction in ammonia concentration to 10 $\text{g}_{\text{NH}_4\text{-N}} \text{ m}^{-3}$ reduced E to nearly 1 which is comparable to the J_{CO_2} measured with DI water as the physical absorption solvent.

5.3.2 Measurement of ammonia volatility within process boundary conditions

The loss of ammonia into the gas phase through volatilisation was investigated by varying ammonia concentration (pH 11, 20 °C) in the upper threshold of that expected in environmental conditions (Figure 5.6).

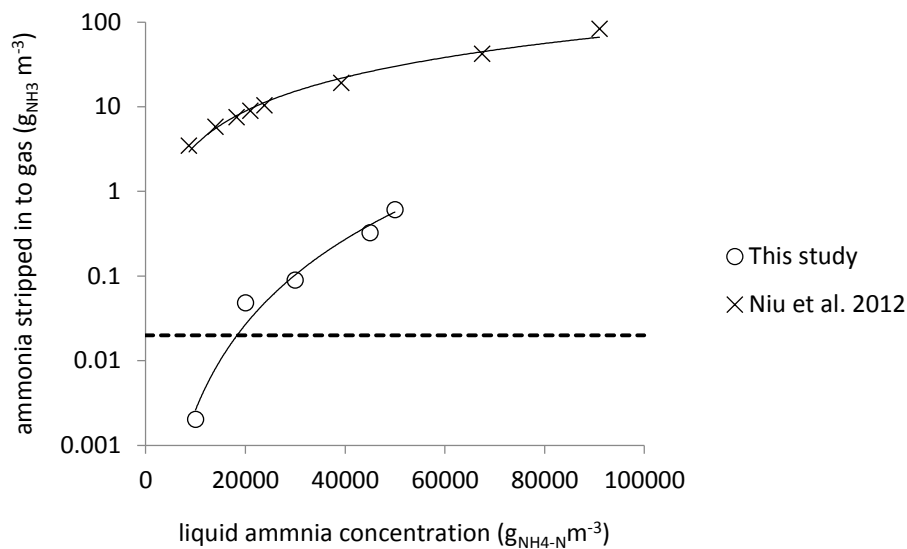


Figure 5.6 Effect of increasing NH_3 concentration upon stripping of NH_3 in to the with fixed liquid and initial gas flow rates (Q_L , $1.67 \times 10^{-6} \text{ m}^3 \text{ s}^{-1}$; Q_G , $1.25 \times 10^{-5} \text{ m}^3 \text{ s}^{-1}$), where the dotted line represents the concentration limit for ammonia in biogas for gas-to-grid and vehicular use ($0.020 \text{ g}_{\text{NH}_3} \text{m}^{-3}$).

At an ammonia concentration of $10000 \text{ g}_{\text{NH}_4\text{-N}} \text{m}^{-3}$ in solution, which is equivalent to a concentrated ion exchange regenerant (Mackinnon *et al.*, 2003), ammonia volatilised from solution equated to a $0.002 \text{ g}_{\text{NH}_3} \text{m}^{-3}$ concentration in the upgraded biogas phase. The ammonia concentration in the gas phase increased non-linearly with an increase in ammonia solvent concentration such that the UK acceptability standard for ammonia in the gas phase when injecting gas into the grid (dashed line) (Environmental Agency UK, 2013) was breached for ammonia absorbents tested with greater than $20000 \text{ g}_{\text{NH}_4\text{-N}} \text{m}^{-3}$. The ammonia slip was significantly lower in the HFMC versus a packed column operating across a comparable concentration range (Niu *et al.*, 2012).

5.3.3 Efficacy of real ammonia rich wastewaters to deliver enhanced CO₂ absorption

Enhancement factors were determined for ammonia solutions derived from return liquor and IEX regenerant (2325 g_{NH4-N} m⁻³ and 477 g_{NH4-N} m⁻³ respectively). The general trend of a higher E with a decrease in Q_L corresponded similarly with those observed for the analogue solutions (Figure 5.7a).

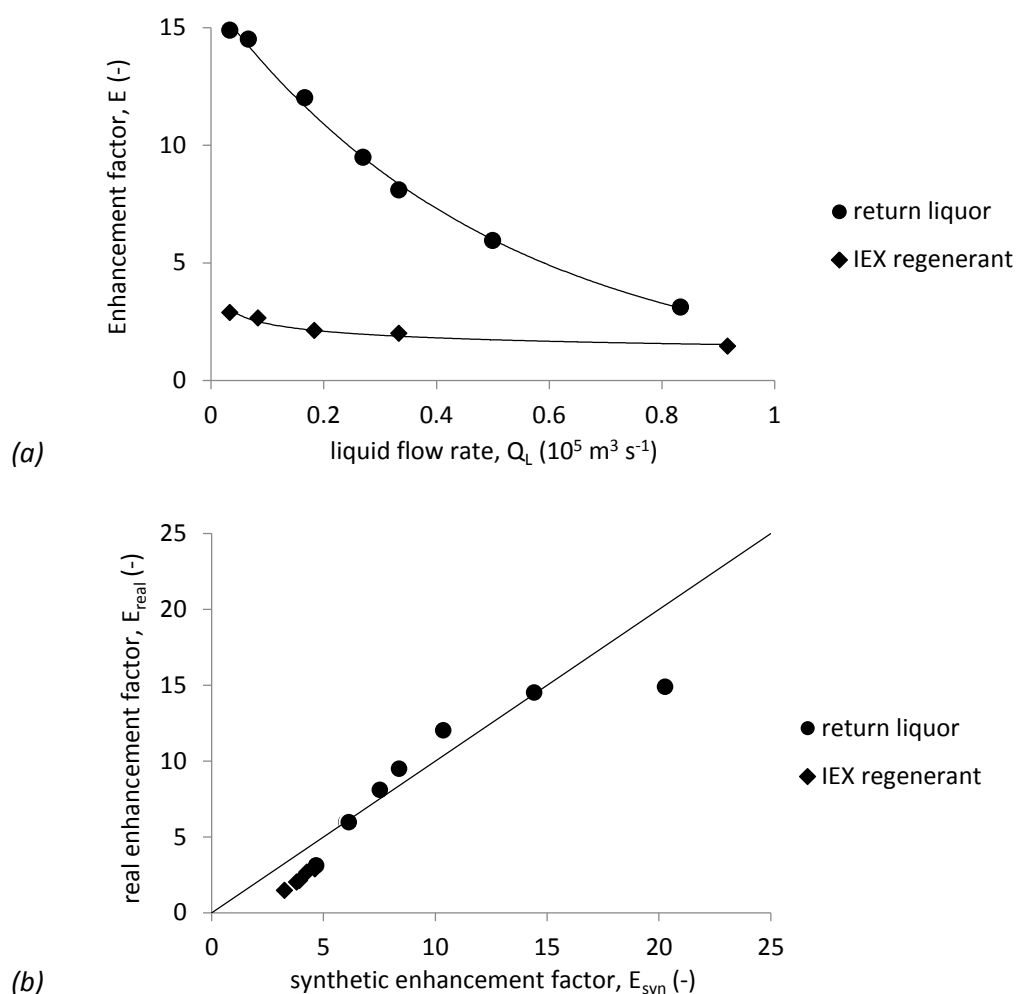


Figure 5.7 Effect of variable liquid flow rate (Q_L , 0.17×10^{-5} – 1.7×10^{-5} m³ s⁻¹) upon enhancement factor (E, dimensionless), determined by ratio of CO₂ flux for return liquor and IEX regenerant (2325 g_{NH4-N} m⁻³ & 477 g_{NH4-N} m⁻³ respectively) against J_{CO2} in DI water (a) and parity between enhancement determined for return liquor and IEX regenerant that expected for like synthetic NH₃ solutions (b).

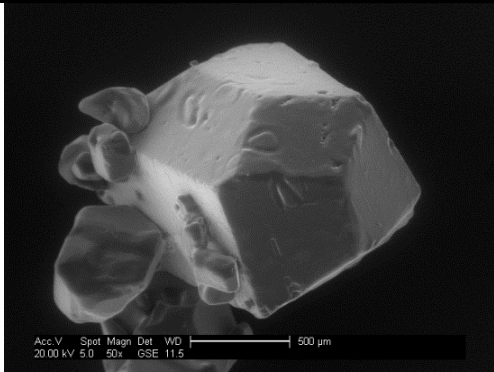
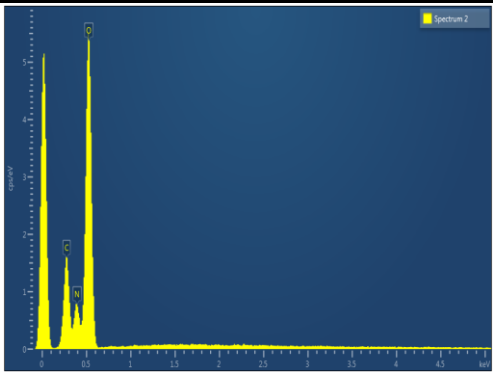
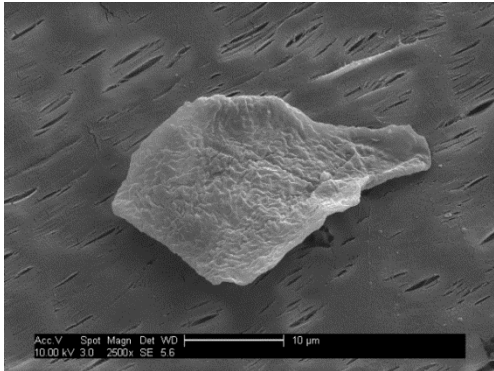
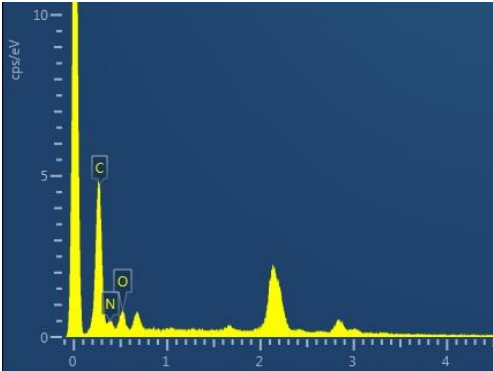
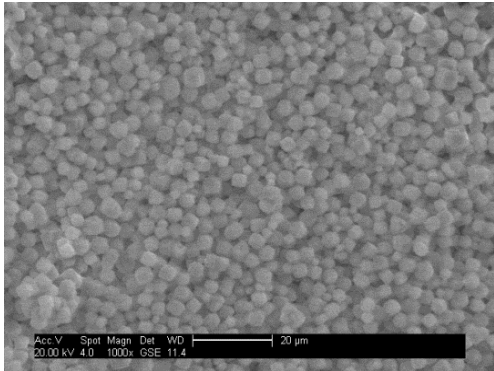
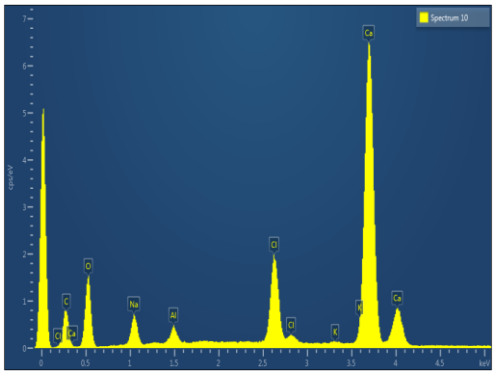
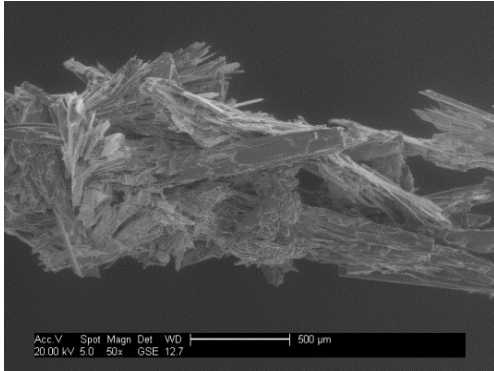
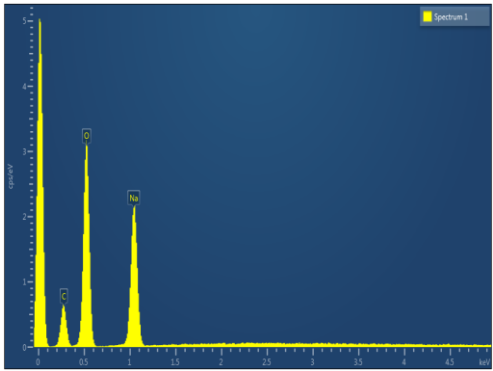
Maximum enhancement factors of 14.9 and 2.9 were determined for return liquor and IEX regenerant respectively at the lowest Q_L studied of 0.17×10^{-5} m³ s⁻¹ (G/L 7.35). Enhancement factors produced from the real wastewater were compared to those measured with analogue ammonia solutions using the same boundary conditions to ascertain how the real wastewater matrix

influences enhancement (Figure 5.7b). The enhancement factors for both wastewaters compared closely to those measured in ammonia analogues of equivalent ammonia concentration, though the IEX regenerant enhancement was marginally below the parity line (where $E_{\text{real}}/E_{\text{syn}} = 1$).

5.3.4 Identifying the products formed in real solutions

To establish the feasibility of producing a solid NH_4HCO_3 product (Equation 2) through the reactivity of NH_3 and CO_2 , synthetic biogas was bubbled through a $5000 \text{ mol}_{\text{NH}_4\text{-N}} \text{ m}^{-3}$ ($85000 \text{ g}_{\text{NH}_4\text{-N}} \text{ m}^{-3}$) analogue ammonia solution. Within a short time frame a crystalline solid was produced *in situ*, which displayed regularly shaped crystals when examined by SEM. (Table 5.1). The atomic composition of the crystal which comprised only carbon (C), oxygen (O) and nitrogen (N) was measured using EDX spectroscopy and an O:N ratio of 3:1 approximated, which suggests the crystalline identity as NH_4HCO_3 salt. This was confirmed by XRD. An identical NH_3 solution was then contacted with the gas using a single fibre membrane (PTFE was used for easy potting) for approximately 5 minutes. Although no solid was visible within the liquid reservoir, post-experimental examination of the fibre by SEM revealed that solid product had formed *in situ* upon the membrane surface, with a C, O and N composition determined by EDX. Substitution of the synthetic solvent for ion exchange regenerant within the PP HFMC, resulted in the *in situ* formation of precipitate within the liquid exiting the HFMC, which was collected in a coarse filter (6-12 μm retention) and imaged by SEM (Table 5.1). Although amorphous in appearance, the SEM image revealed a fine structure. EDX analysis revealed the absence of nitrogen, although calcium, carbon and oxygen peaks were present, suggesting the presence of calcium carbonate (CaCO_3) (Table 5.1). Impurities within the solid were also noted to include the cations sodium (Na), potassium (K) and aluminium (Al). During testing with return liquor under identical hydrodynamic conditions, *in situ* precipitation was not observed to occur. To enhance precipitation within the liquor, a fixed volume of return liquor (2 L) was recirculated in the HFMC to allow saturation by CO_2 . Whilst precipitation was not observed *in situ* following complete exhaustion of

Table 5.1 Scanning electron microscope (SEM) and energy dispersive X-ray (EDX) spectra of NH_4HCO_3 formed in situ by bubbling gas through bulk solvent and by nucleation on the membrane surface (a & b respectively), in situ CaCO_3 from IEX regenerant (c), and NaHCO_3 from dehydration of return liquor saturated by CO_2 (d).

	SEM	EDX
(a)		
(b)		
(c)		
(d)		

the solvent, a crystalline solid was obtained through mild evaporation of the saturated return liquor and imaged by SEM (Table 5.1). Whilst return liquor can be described as homogeneous in nature, EDX spectrum analysis suggested the crystal to be reasonably pure, comprising of only C, O and Na. The O:Na atomic ratio was approximately 3:1 indicative of sodium bicarbonate (NaHCO_3).

5.4 Discussion

This study has demonstrated that ammonia solutions at concentrations comparable to environmentally relevant wastewaters chemically enhance CO_2 absorption during biogas upgrading in a HFMC (Figure 5.5). Real wastewaters (IEX regenerant and return liquor) exhibited comparable CO_2 flux to the pure analogue solutions (Figure 5.7a and 5.7b); however NH_4HCO_3 was not isolated as a reaction product, with calcium carbonate (CaCO_3) forming *in situ* using IEX regenerant and sodium bicarbonate (NaHCO_3) produced by dehydration of saturated return liquor (Table 5.1). The biogas purity achieved during trials (>98 % methane purity) compares favourably to conventional chemical absorption. Consequently, ammonia rich wastewater presents the advantages of common chemicals without the demands for bulk chemical storage and handling. The flux of CO_2 into the prepared ammonia analogues demonstrated that pH was the principal driving force for the enhancement in CO_2 flux at fixed ammonia concentration, with maximum J_{CO_2} recorded at pH 11 (Figure 5.3). This can be explained by a shift in ammonium equilibrium toward free ammonia following an increase in pH, where nearly 100% of the ammoniacal nitrogen is present as free ammonia at pH 11 (Figure 5.1).

Flux was further enhanced under free ammonia conditions by an increase in initial ammonia absorbent concentration. However, using the low concentration analogues, an order of magnitude increase in ammonia from $10 \text{ g}_{\text{NH}_4\text{-N}} \text{ m}^{-3}$ to $100 \text{ g}_{\text{NH}_4\text{-N}} \text{ m}^{-3}$ did not increase CO_2 flux. Furthermore, following an increase in Q_G , no difference in flux was discernible between these two concentrations (Figure 5.4a). This is indicative of a physical absorption mechanism in which the rate of CO_2 separation is governed by the equilibrium constant and diffusivity of CO_2 in water, and subsequently the concentration boundary layer that develops at the membrane-liquid interface (Kreulen *et al.*,

1993a). The low enhancement factors provided by the low concentration analogues confirmed the low reactivity exhibited. However, at higher analogue ammonia concentrations (5000 and 10000 $\text{g}_{\text{NH}_4\text{-N}} \text{m}^{-3}$), an enhancement in CO_2 flux of up to E 25 was demonstrated (Figure 5.5) and within concentration boundaries practically achievable when using ion exchange to concentrate the ammonia phase (Mackinnon *et al.*, 2003). In HFMCs for gas separation, liquid phase resistance can be minimised by inclusion of a chemical reaction to the absorbent (Kreulen *et al.*, 1993b). The chemical conversion of CO_2 to NH_4HCO_3 is mediated within the concentration boundary layer which enables reestablishment of the concentration gradient at the liquid-membrane boundary, thereby enhancing CO_2 mass transfer (Dindore *et al.*, 2005). Consequently, for higher concentration ammonia absorbents, mass transfer was gas phase controlled and can be additionally evidenced by the enhancement in CO_2 flux provided by an increase in Q_G . Importantly, whilst the environmentally relevant ammonia concentration range tested in this study was substantially lower than has previously been employed for CO_2 separation using industry produced ammonia (>28 % wt.) (Han *et al.*, 2013), the chemical enhancement at higher concentrations enabled gas phase control which reduces process scale, requiring less absorbent which therefore diminishes both pumping costs and methane slip (McLeod *et al.*, 2013).

At the upper practical limit of ammonia concentration which can be established onsite ($\sim 10000 \text{ g}_{\text{NH}_4\text{-N}} \text{m}^{-3}$), an ammonia concentration of only $0.002 \text{ g}_{\text{NH}_4\text{-N}} \text{m}^{-3}$ was measured in the gas phase, which is an order of magnitude below the $0.02 \text{ g}_{\text{NH}_4\text{-N}} \text{m}^{-3}$ limit of consent for biomethane as a vehicle fuel or natural gas substitute (Persson *et al.*, 2007; Environmental Agency UK, 2013). Interestingly this is significantly below the ammonia slip previously observed when operating a packed column (Budzianowski, 2011). It is postulated that whilst the transport of NH_3 to the gas-liquid interface may be characterised by turbulent conditions in packed columns, due to the method of liquid delivery, the characteristic laminar liquid flow in HFMCs ($Re = 57 - 570$ in this study) limits the transport of NH_3 to relatively slow diffusion from the liquid bulk ($D_{\text{NH}_3} = 1.76 \times 10^{-9} \text{ m}^2 \text{ s}^{-1}$) (Tan *et al.*, 2006). Consequently the ammonia at the gas-liquid interface can be managed in HFMCs to allow

sufficient transfer of NH_3 from the liquid bulk to maintain reaction with CO_2 (forming non-volatile products) but restrict the exposure of excess NH_3 to the stripping effect of the contacting gas phase (Budzianowski, 2011). Therefore, HFMCs appear practically advantageous to limit ammonia slip, and when coupled with the relatively low NH_3 concentration range used, enable a sufficiently clean produced gas for use.

Both ammonia-rich wastewaters exhibited similar enhancement behaviour to analogue ammonia solutions of equivalent concentration (Figure 5.7) indicating that: (i) enhancement was ostensibly a function of initial ammonia concentration; (ii) the background organic and inorganic matrix of the real wastewaters did not impede chemical enhancement. High ionic strength is known to reduce the concentration of reactive free NH_3 (by influencing equation 1) in complex solutions at moderate pH (<8), i.e. anaerobic digestate (Hafner and Bisogni, 2009). However application of the model proposed by Hafner and Bisogni (2009) demonstrates that the impact of this salting out effect is comparatively marginal at high pH, particularly considering the additional ionic strength supplied by dissociated NaOH to provide the pH swing. To demonstrate; only a 1 % free ammonia difference determined for an ideal liquid and a $50 \text{ g}_{\text{NaCl}} \text{ L}^{-1}$ solution at pH 11 (Pitzer, 1973). However, a gradual decline in CO_2 flux was observed for the return liquor following longer term operation. It has been demonstrated that organic fouling of hydrophobic micro-porous membranes within a wastewater treatment membrane distillation reactor promoted pore wetting by altering the surface free energy of the membrane polymer (Goh *et al.*, 2013). Whilst not measured directly, the CO_2 flux decline in this study can be similarly ascribed to membrane fouling by the high residual organic fraction post filtration (Table 5.2).

Table 5.2 Characterisation of raw wastewater matrices and subsequently derived absorbents.

Wastewater matrix	pH	NH ₄ -N	Conductivity	COD	TSS
	-	g m ⁻³	mS cm ⁻¹	g m ⁻³	kg m ⁻³
Raw return liquor	8.3	2460	4.9	8400	5.6
Raw IEX regenerant	7.2	477	76.6	1060	
Filtered return liquor	11	2325	5.1	7900	4.6
Filtered IEX regenerant	11	477	76.6	1060	

Wetted pores impede CO₂ flux since diffusion through the penetrant absorbent is several orders of magnitude below that measured in a gas filled pore (Ho and Sirkar, 1992). Dedicated pre-conditioning treatments, such as upstream anion IEX resin beds, are able to remove the organic content of wastewaters sufficiently to reduce the associated fouling rate of polypropylene membrane materials (Theint Myat *et al.*, 2013). Although the introduction of further unit processes is not ideal, the additional cost may be compensated for by the economic potential from the biomethane and associated return liquor treatment by NH₄HCO₃ recovery. In comparison, no decline in CO₂ flux was observed during operation with the IEX regenerant. It is posited that lower organic composition and high ionic strength resist wetting (Table 5.2), due to an increase in fluid surface tension provided by the NaCl (Weissenborn and Pugh, 1995). However, the IEX regenerant produced in this study exhibited lower chemical enhancement than the return liquor due to the lower reactant concentration. The IEX ammonium regenerant concentration is dependent upon the zeolites cation exchange capacity (CEC), and ammonium loading (Mackinnon *et al.*, 2003). For example, the ammonium regenerant concentration in this study (477 g_{NH4-N} m⁻³) was comparable to other studies also using clinoptilolite (648 g_{NH4-N} m⁻³, Aiyuk *et al.* 2004). However, the study of a higher CEC zeolite (MesoLite) applied to AD supernatant has enabled a regenerant concentration of up to 10000 g_{NH4-N} m⁻³, where greater ionic strengths were applied to zeolite regeneration at reduced BV h⁻¹ (Mackinnon *et al.*, 2003). This suggests that application of high CEC zeolites to concentrated NH₄-N

substrates, in conjunction with management of process conditions, can optimise $\text{NH}_4\text{-N}$ concentration within the IEX regenerant for greater chemical enhancement during CO_2 absorption.

Ammonia was successfully precipitated to form NH_4HCO_3 as a reaction product in the ammonia analogue liquid via gas bubbling in batch, whilst recovery using a HFMC in a continuous system was shown to be possible by the formation of solid product on the liquid-side of a single membrane fibre (Table 5.1). Importantly, sequestration of both ammonia and CO_2 into precipitated NH_4HCO_3 eliminates the cost and complexity of solvent regeneration which represents a key barrier to uptake of chemical absorption in WWTW. However, in the IEX regenerant CaCO_3 was apparently preferentially formed over NH_4HCO_3 . The cations Na^+ , K^+ and Al^{3+} were also measured within the precipitate (Table 5.1). Consequently, cations within the IEX regenerant can inhibit NH_4HCO_3 precipitation through competitive scavenging of carbonate and since CaCO_3 is significantly less soluble than NH_4HCO_3 , the likelihood of early precipitation is enhanced and was observed in this short-term study (Table 5.3). Interestingly, zeolites typically favour NH_4^+ as the monovalent ion presents a small hydrated radius, which enhances diffusion into the zeolites macro-porous structure (Dyer and White, 1999). However, high concentrations of other cations e.g. Ca^{2+} will form competitive equilibria for occupation of the zeolite, reducing selectivity and capacity for NH_4^+ (Hankins *et al.*, 2004). High Ca^{2+} concentrations may be avoided during column loading by substituting sewage effluent for return liquor as the IEX substrate due to a more favourable $\text{NH}_4^+/\text{Ca}^{2+}$ concentration ratio (Neal *et al.*, 2005; Thornton *et al.*, 2007). Further, it has been demonstrated that Ca^{2+} is the first cation to be eluted from the column during regeneration because the zeolite in the vicinity of the column inlet is preferentially occupied by NH_4^+ during loading, only permitting significant occupation by Ca^{2+} further along the column once the majority of NH_4^+ has been removed from solution (Ciambelli *et al.*, 1985).

Table 5.3 Molecular masses and pure water solubilities of several binary carbonate and bicarbonate salts.

Name	Formula	Molecular mass g mol ⁻¹	Water solubility mol L ⁻¹ (20 °C)	Solubility product pK _{sp}	Ref.
Ammonium bicarbonate	NH ₄ HCO ₃	79.06	2.24	-0.70	Trypuć and Kiełkowska, (1998)
Sodium bicarbonate	NaHCO ₃	84.01	0.67	0.35	Trypuć and Kiełkowska, (1998)
Calcium carbonate	CaCO ₃	100.09	5.8x10 ⁻⁵	8.47	Haynes, (2012)

Therefore Ca²⁺ may be eliminated by eluent fractionation, without significant NH₄⁺ loss. Sodium bicarbonate (NaHCO₃) was preferentially precipitated in the return liquor, principally due to the large concentration of NaOH required to overcome the buffering capacity in the solvent during pH swing. Consequently, the increased Na⁺ gradient enhanced NaHCO₃ production over NH₄HCO₃ (Table 5.3). Simple CO₂ stripping has been demonstrated to reduce acidity (as CaCO₃) in mine water by up to 98 % by influencing the equilibrium between CO₂ and carbonate species in solution, and can also raise pH in digested sludge, suggesting that pre-aeration of the return liquor could rectify large hydroxide demands for pH swing (Geroni *et al.*, 2012; Bergmans *et al.*, 2013). Alternatively, it has been shown that the equilibrium between NH₃ and NH₄⁺ (1) can be successively re-established at low pH (i.e. 7.8), following progressive reaction of the minor NH₃ component, by recirculation of the solvent (Heckt *et al.*, 1990), thereby enabling reaction with the total ammoniacal nitrogen content without a pH swing, but likely restricting J_{CO₂}. Additionally, it is posited that a preference for NH₄HCO₃ over Na⁺ or Ca²⁺ analogues may also be imparted within the HFMC by manipulation of respective cation concentrations within the liquid boundary layer. NH₄⁺ due to reaction of NH₃ with CO₂ occurs exclusively at the liquid-membrane interface at sufficiently high Graetz number, as modelled for various amines during reaction with CO₂ (Wang *et al.*, 2004), whilst the majority of Ca²⁺ concentration exists within the liquid bulk. This principle is supported by the heterogeneous

nucleation and growth of NH_4HCO_3 solid upon the PTFE membrane surface using synthetic chemical solvent (Table 5.1), however the potential magnitude of this effect during competition with other cations is not yet clear.

The potential benefits of the concepts examined within this study can be judged on the basis of a comparison with a conventional WWTW, where biogas is applied to on-site electricity generation in combined heat and power (CHP) plants and $\text{NH}_4\text{-N}$ is treated by nitrification. Current UK tariffs for biogas utilisation are 0.49 £ m^{-3} for natural gas substitute versus 0.14 £ m^{-3} for electrical production with CHP (Ofgem, 2014). However, there is further economic utility in using ammonia for chemical absorption due to the reduced nitrogen load entering into biological nitrification, lowering aeration demand and in the production of ammonium bicarbonate as a fertiliser by-product, with an estimated wholesale value of 98 £ ton^{-1} based upon its nitrogen content (Hernandez and Torero, 2013). To illustrate, a full scale WWTW characterised by $500,000 \text{ m}^3 \text{ d}^{-1}$ total flow, $25000 \text{ kg}_{\text{NH}_4\text{-N}} \text{ d}^{-1}$ ($50 \text{ g}_{\text{NH}_4\text{-N}} \text{ m}^{-3}$) and $3400 \text{ m}^3 \text{ h}^{-1}$ raw biogas yield ($60:40 / \text{CH}_4:\text{CO}_2$) is assumed (Table 5.4) (for full calculations see Appendix).

Table 5.4 Operational costs and net benefit of several scenarios versus the current baseline case with 100 % $\text{NH}_4\text{-N}$ by nitrification and 100 % biogas to CHP.

	CHP	Upgrading	ABC	Aeration	Net gain	Total
CHP (current/baseline case)	+4.2	0	0	-1.0	-	3.2
CHP + upgrade (ret. liq.)	+3.6	+1.3 (100 %)	0	-0.8	+0.9	4.1
CHP + upgrade (ret. liq.)+ABC	+3.6	+1.3 (72 %)	+0.3 (17 %)	-0.8 (11 %)	+1.2	4.4
Upgrade (IEX regen.)	-4.2	+9.5 (90 %)	0	+1.0 (10 %)	+3.1	6.3
Upgrade (IEX regen.) +ABC	-4.2	+13.5 (74 %)	+2.3 (18 %)	+1.0 (8 %)	+7.2	9.4

An annual revenue of 3.2 M£ y^{-1} is taken as a baseline case, calculated by subtraction of the cost of aeration for total nitrification (1 M£ y^{-1}) from the CHP profit (4.2 M£ y^{-1}). Based upon a maximum G/L of 4.01 in this study, only 13 % of the biogas flow can be upgraded using return liquor, although

extrapolation of the data-set suggests that greater G/L could be used without detriment to J_{CO_2} (Figure 5.4b). However this still results in a net benefit of +0.9 M£ y^{-1} or +1.2 M£ y^{-1} versus conventional treatment with and without NH_4HCO_3 recovery respectively. Based upon the mass transfer observed using real return liquor in the present study ($1.53 \times 10^{-4} \text{ m s}^{-1}$), the total membrane length required can be calculated (Appendix). For the 13% biogas flow rate and a 95 % CH_4 purity in the subsequent biomethane, 6 full scale HFMCs (14x40 Liqui-cel Extra-flow, $L = 1.02 \text{ m}$, $A_m = 373 \text{ m}^2$) will be required. This is assumed to be the critical component of the system, where the cost of the polymeric material is known to account for the majority cost of the HFMC module (Ulbricht, 2014). Assuming a membrane polymer cost of 40 £ m^{-2} and a conservative membrane lifetime of 3 years (Prasad and Sirkar, 1989) a capital cost of 30000 £ y^{-1} and payback time of 9-16 days is estimated depending upon degree of NH_4HCO_3 recovery. If IEX is performed upon the secondary effluent then the total NH_4 -N capacity can be applied to upgrading as IEX regenerant and a net benefit of +3.1 M£ y^{-1} may be obtained even without recovery of NH_4HCO_3 due to the added value of biomethane. Importantly, this added value could not be realised if exogenic chemicals (i.e. MEA) were used for biogas upgrading to biomethane due to the high cost of chemical regeneration (-2.2 M£ y^{-1}) (Knudsen *et al.*, 2009). If total recovery of NH_4HCO_3 is assumed the IEX regenerant can be recycled, resulting in +6.2 M£ y^{-1} compared to the conventional flowsheet. Here the IEX media (clinoptilolite) represents a critical component in addition to the HFMC modules. Based on a required bed size of approximately 6000 t at 168 £ t^{-1} (Aiyuk *et al.*, 2004) and a feasible annual clinoptilolite media attrition of 10% (Svetich, 1993), a capital cost of 100000 £ y^{-1} is estimated for the IEX media. Based on the mass transfer observed in the IEX regenerant in the present study ($1.43 \times 10^{-4} \text{ m s}^{-1}$) a capital cost for the HFMC of 175000 £ y^{-1} is anticipated. Therefore a total payback time of 14 d is expected for the critical clinoptilolite and membrane module components. Interestingly, the revenue from sale of NH_4HCO_3 as a fertilizer product (+2.3 M£ y^{-1}) and cessation of aeration could eliminate the dependency of WWTW upon governmental incentivisation towards biogas application as a

biomethane natural gas substitute versus CHP, where uncertainty over the future value of biomethane currently impedes the implementation of for biogas upgrading facilities within the UK.

5.5 Conclusions

Ammonia solutions up to $10000 \text{ g}_{\text{NH}_4\text{-N}} \text{ m}^{-3}$ were successfully demonstrated as chemical absorbents for CO_2 , where >98 % methane purity was obtained. The chemical enhancement observed for return liquor and IEX regenerant was analogous to synthetic ammonium absorbents of equivalent concentration which verified their potential for chemical absorption. This challenges current perspectives on chemical absorption where concerns regarding chemical handling and chemical cost can be precluded. However, despite good chemical enhancement in return liquor, the fouling propensity observed necessitates pre-conditioning requirements. No observable fouling was noted with the IEX regenerant and through optimisation of IEX design and operation, higher NH_4^+ concentrations can be achieved which will inevitably enhance chemical reactivity. Importantly, the potential to recover the reaction product NH_4HCO_3 was demonstrated which indicates that the complex solvent regeneration process could be avoided and can significantly enhance the economic attractiveness of upgrading. Since alternate reaction products were produced from the ammonia rich wastewaters produced, further work on solution chemistry is demanded to fully establish the process complexity surrounding preferential production of NH_4HCO_3 . However, it is interesting to note that precipitation of CaCO_3 also provides value both as agricultural lime. Consequently, this process presents wider opportunities for an integrated approach to nutrient recovery.

Acknowledgments

The authors would like to thank the Engineering and Physical Sciences Research Council (EPSRC, V/N: 08001923), Anglian Water, Northumbrian Water, Severn Trent Water and Yorkshire Water for their financial support.

Appendix

The economic assessment of the wastewater flowsheet scenarios was performed on the basis of several key values and assumptions (Table 5.A1). The cost of nitrification was calculated on the basis of power consumption for aeration (P_w):

$$P_w = \frac{wRT}{29.7ne} \left[\left(\frac{P_2}{P_1} \right)^{0.283} - 1 \right] \quad \text{A1}$$

where w is the mass flow of air (kg s^{-1}), R is the molar gas constant (8.314 J mol^{-1}), T is the absolute inlet temperature (K), n is a constant (0.283 for air), e is electrical efficiency and P_1 and P_2 are the absolute inlet and outlet pressures respectively (atm) (Tchobanoglous *et al.*, 2003). The ion exchange characteristics of clinoptilolite, as used in the present study, were interpolated from the literature data to optimise the CEC with Q_L based upon the $500,000 \text{ m}^3 \text{ d}^{-1}$ full flow of secondary effluent (Aiyuk *et al.*, 2004). The most significant capital cost for IEX is that of the zeolite media, which was also given in the literature (Aiyuk *et al.*, 2004). Zeolites with greater CECs, i.e. MesoLite, allow for smaller bed sizes, although it is uncertain whether this will result in a lower capital cost since synthetic media is likely more expensive than naturally occurring zeolites. The chemical cost of IEX regenerant and tankering for disposal were calculated on the assumption that the regenerant is used twice. During regeneration of MesoLite it was demonstrated that the same volume of regenerant could be used at least twice without significant loss of efficacy (Mackinnon *et al.*, 2003). The value of NH_4HCO_3 was estimated on the basis of nitrogen content compared to that of urea, where market values were located in the literature (from 2002 until 2012) (Hernandez and Torero, 2013). This method of estimation is reasonable due to the strong correlation between both urea and anhydrous ammonia with the price of fossil fuel, used during synthesis of ammonia.

The capital cost of the membrane polymer can be determined by using the overall mass transfer coefficient (K_L , m s^{-1}) to calculate the membrane length needed to achieve a given CO_2 removal from the gas phase:

$$\ln\left(\frac{c_1}{c_0}\right) = \frac{-K_L a L}{V_L}$$

A2

where L is the active membrane length (m), a is the specific surface area for the HFMC ($\text{m}^2 \text{m}^{-3}$), V_L is the superficial liquid velocity (m s^{-1}), and c_0 and c_1 are the inlet and outlet dissolved CO_2 concentrations in the liquid respectively (Noble and Stern, 1995).

Table 5.A1. Values and assumptions used for cost calculations.

Parameter	Value	Reference
Flows and concentrations		
Q_L (Full flow), $\text{m}^3 \text{d}^{-1}$	500,000	Shurrock <i>et al.</i> , 2012
$Q_{\text{NH}_4\text{-N}}$ (Full flow), kg d^{-1}	25,000	Shurrock <i>et al.</i> , 2012
Q_G (raw biogas), $\text{m}^3 \text{d}^{-1}$	81,600	Farris, 2013
$\text{CH}_4:\text{CO}_2$	60:40	Farris, 2013
$Q_{\text{NH}_4\text{-N}}$ (Return flow), kg d^{-1}	6250	Thornton <i>et al.</i> , 2007
$C_{\text{NH}_4\text{-N}}$ (Return liquor), g m^{-3}	2325	This study
Q_L (Return flow), $\text{m}^3 \text{d}^{-1}$	2688	
C_{NaOH} (pH 11), kg m^{-3}	0.04	
C_{NaCl} (IEX regenerant), kg m^{-3}	25	Aiyuk <i>et al.</i> , 2004
Q_L (IEX regenerant), $\text{m}^3 \text{d}^{-1}$	19,947	
Aeration for nitrification		
$\text{O}_2:\text{NH}_4$ required	2	Tchobanoglos <i>et al.</i> , 2003
O_2 mass transfer efficiency	25	Tchobanoglos <i>et al.</i> , 2003
Electrical efficiency	70 %	Tchobanoglos <i>et al.</i> , 2003
Aeration tank depth, m	4.5	Tchobanoglos <i>et al.</i> , 2003
IEX operation		
Clinoptilolite CEC, $\text{kg}_{\text{NH}_4\text{-N}} \text{t}^{-1}$	7.53	Aiyuk <i>et al.</i> , 2004 (Interpolated)
BV, (m^3 or t)	5952	
Q_L capacity, $\text{m}^3 \text{d}^{-1}$	571,429	
N capacity, kg d^{-1}	44,859	
Time to exhaustion, d	1.8	
Bv per regeneration	6	Aiyuk <i>et al.</i> , 2004
Biogas		
Biogas to biomethane, £ m^{-3}	0.49	Ofgem, 2014
Biogas to CHP, £ m^{-3}	0.14	Ofgem, 2014

Table 5.A1. continued

Biogas to biomethane, £ y ⁻¹	9,537,408	
Biogas to CHP, £ y ⁻¹	5,662,836	
NH₄HCO₃		
Urea value, £ t ⁻¹	152.5	Hernandez and Torero, 2013
N _{NH₄HCO₃} :N _{Urea}	0.4	
NH ₄ HCO ₃ value, £ t ⁻¹	61	
NH ₄ HCO ₃ value, £ y ⁻¹	2,349,360	
Capital costs		
Clinoptilolite, £ t ⁻¹	168	Aiyuk <i>et al.</i> , 2004
Clinoptilolite, £ bed ⁻¹	1,000,000	
PP membrane, £ m ⁻²	675	Liqui-cel
Membrane (Return liquor), £ m ⁻²	10,838	This study (based on J _{CO₂} at G/L of 4.01)
Membrane (IEX regenerant), £ m ⁻²	103,245	This study (based on J _{CO₂} at G/L of 4.01)
Operational costs		
NaCl, £ t ⁻¹	30.5	
NaOH, £ t ⁻¹	21.35	Martin <i>et al.</i> , 2009
NaCl (IEX regenerant), £ y ⁻¹	5,543,261	
NaOH (pH swing), £ y ⁻¹	62,085	This study (pH 11)
IEX disposal (tanker), £ m ⁻³	11.76	Grefte <i>et al.</i> , 2013
IEX disposal (tanker), £ y ⁻¹	854,935	
Regeneration (MEA), MJ t _{CO₂} ⁻¹	3700	Knudsen <i>et al.</i> , 2009
Regeneration (MEA), £ y ⁻¹	2,204,675	
Electricity, £ kWh ⁻¹	0.1	
Exchange rates		
£ \$ ⁻¹	0.61	
£ € ⁻¹	0.84	

References

Aiyuk, S., Xu, H., van Haandel, A. and Verstraete, W. (2004), "Removal of ammonium nitrogen from pretreated domestic sewage using a natural ion exchanger", *Environmental Technology*, vol. 25, no. 11, pp. 1321-1330.

Atchariyawut, S., Jiraratananon, R. and Wang, R. (2007), "Separation of CO₂ from CH₄ by using gas-liquid membrane contacting process", *Journal of Membrane Science*, vol. 304, no. 1-2, pp. 163-172.

Bergmans, B. J. C., Veltman, A. M., van Loosdrecht, M. M., van Lier, J. B. and Rietveld, L. C. (2013), "Struvite formation for enhanced dewaterability of digested wastewater sludge", *Environmental Technology (United Kingdom)*, Article in press.

Budzianowski, W. M. (2011), "Mitigating NH₃ vaporization from an aqueous ammonia process for CO₂ capture", *International Journal of Chemical Reactor Engineering*, vol. 9, Article number A58.

Ciambelli, P., Corbo, P., Porcelli, C. and Rimoli, A. (1985), "Ammonia removal from wastewater by natural zeolites. I. Ammonium ion exchange properties of an Italian phillipsite tuff", *Zeolites*, vol. 5, no. 3, pp. 184-187.

Darde, V., Van Well, W. J. M., Stenby, E. H. and Thomsen, K. (2011), "CO₂ capture using aqueous ammonia: Kinetic study and process simulation", *Energy Procedia*, vol. 4, pp. 1443-1450.

Dindore, V. Y., Brilman, D. W. F. and Versteeg, G. F. (2005), "Hollow fiber membrane contactor as a gas-liquid model contactor", *Chemical Engineering Science*, vol. 60, no. 2, pp. 467-479.

Dyer, A. and White, K. J. (1999), "Cation diffusion in the natural zeolite clinoptilolite", *Thermochimica Acta*, vol. 340-341, pp. 341-348.

Environmental Agency (2013), "http://www.environment-agency.gov.uk/static/documents/Revised_Draft_Quality_Protocol_for_biomethane.pdf", pp 17-18. (accessed 2nd January 2014).

Farris, S. (2013), "Minworth Sewage Treatment Works a case study for biomethane to grid", *UK Biomethane Day 2013*, 21st May 2013, Birmingham, UK.

Geroni, J. N., Cravotta, C. A. and Sapsford, D. J. (2012), "Evolution of the chemistry of Fe bearing waters during CO₂ degassing", *Applied Geochemistry*, vol. 27, no. 12, pp. 2335-2347.

Goh, S., Zhang, J., Liu, Y. and Fane, A. G. (2013), "Fouling and wetting in membrane distillation (MD) and MD-bioreactor (MDBR) for wastewater reclamation", *Desalination*, vol. 323, pp. 39-47.

Grefte, A., Dignum, M., Cornelissen, E. R. and Rietveld, L. C. (2013), "Natural organic matter removal by ion exchange at different positions in the drinking water treatment lane", *Drinking Water Engineering and Science*, vol. 6, no. 1, pp. 1-10.

Hafner, S. D. and Bisogni Jr., J. J. (2009), "Modeling of ammonia speciation in anaerobic digesters", *Water research*, vol. 43, no. 17, pp. 4105-4114.

Han, K., Ahn, C. K., Lee, M. S., Rhee, C. H., Kim, J. Y. and Chun, H. D. (2013), "Current status and challenges of the ammonia-based CO₂ capture technologies toward commercialization", *International Journal of Greenhouse Gas Control*, vol. 14, pp. 270-281.

Hankins, N. P., Pliankarom, S. and Hilal, N. (2004), "An equilibrium ion-exchange study on the removal of NH₄⁺ ion from aqueous effluent using clinoptilolite", *Separation Science and Technology*, vol. 39, no. 15, pp. 3639-3663.

Haynes, W. M. (2012), "CRC Handbook of chemistry and physics 93rd edition", *CRC Press*.

Hecht, V., Bischoff, L. and Gerth, K. (1990), "Hollow fiber supported gas membrane for in situ removal of ammonium during an antibiotic fermentation", *Biotechnology and Bioengineering*, vol. 35, no. 10, pp. 1042-1050.

Hernandez, M. A. and Torero, M. (2013), "Market concentration and pricing behaviour in the fertilizer industry: a global approach", *Agricultural Economics*, vol. 44, no. 6, pp. 723-734.

Ho, W. S. and Sirkar, K. K. (1992), "Membrane Handbook", *Kluwer Academic Publishers*, pp. 888-889.

Knudsen, J. N., Jensen, J. N., Vilhelmsen, P. –J. and Biede, O. (2009), "Experience with CO₂ capture from coal flue gas in pilot scale: Testing of different amine solvents", *Energy Procedia*, vol. 1, no. 1, pp. 783-790.

Kreulen, H., Smolders, C. A., Versteeg, G. F. and Van Swaaij, W. P. M. (1993a), "Microporous hollow fibre membrane modules as gas-liquid contractors. Part 1. Physical mass transfer processes. A specific application: Mass transfer in highly viscous liquids", *Journal of Membrane Science*, vol. 78, no. 3, pp. 197-216.

Kreulen, H., Smolders, C. A., Versteeg, G. F. and Van Swaaij, W. P. M. (1993b), "Microporous hollow fibre membrane modules as gas-liquid contractors. Part 2. Mass transfer with chemical reaction", *Journal of Membrane Science*, vol. 78, no. 3, pp. 217-238.

Kuntke, P., Smiech, K. M., Bruning, H., Zeeman, G., Saakes, M., Sleutels, T. H. J. A., Hamelers, H. V. M. and Buisman, C. J. N. (2012), "Ammonium recovery and energy production from urine by a microbial fuel cell", *Water research*, vol. 46, no. 8, pp. 2627-2636.

Mackinnon, I.D.R., Barr, K., Miller, E., Hunter, S. and Pinel, T., (2003), "Nutrient removal from wastewaters using high performance materials", *Water Science and Technology*, vol. 47, no. 11, pp. 101-107.

Martin, B.D., Parsons, S.A. and Jefferson, B., (2009), "Removal and recovery of phosphate from municipal wastewaters using a polymeric anion exchanger bound with hydrated ferric oxide nanoparticles", *Water Science and Technology*, vol. 60, no. 10, pp. 2637-2645.

McAdam, E. J., Pawlett, M. and Judd, S. J. (2010), "Fate and impact of organics in an immersed membrane bioreactor applied to brine denitrification and ion exchange regeneration", *Water research*, vol. 44, no. 1, pp. 69-76.

McLeod, A., Jefferson, B. and McAdam, E. J. (2013), "Quantifying the loss of methane through secondary gas mass transport (or 'slip') from a micro-porous membrane contactor applied to biogas upgrading", *Water Research*, vol. 47, no. 11, pp. 3688-3695.

Neal, C., Jarvie, H. P., Neal, M., Love, A. J., Hill, L. and Wickham, H. (2005), "Water quality of treated sewage effluent in a rural area of the upper Thames Basin, southern England, and the impacts of such effluents on riverine phosphorus concentrations", *Journal of Hydrology*, vol. 304, no. 1-4, pp.103-117.

Niu, Z., Guo, Y., Zeng, Q. and Lin, W. (2012), "Experimental studies and rate-based process simulations of CO₂ absorption with aqueous ammonia solutions", *Industrial and Engineering Chemistry Research*, vol. 51, no. 14, pp. 5309-5319.

Ofgem (2014), <https://www.ofgem.gov.uk/publications-and-updates/full-tariff-tables> (accessed 1st September 2014).

Patterson, T., Esteves, S., Dinsdale, R. and Guwy, A. (2011), "An evaluation of the policy and techno-economic factors affecting the potential for biogas upgrading for transport fuel use in the UK", *Energy Policy*, vol. 39, no. 3, pp. 1806-1816.

Persson, M., Jonsson, O. and Wellinger, A. (2007), "Task 37 – Biogas upgrading to vehicle fuel standards and grid injection", *IEA Bioenergy*, pp. 8-9.

Petersson, A. and Wellinger, A. (2009), "Task 37 – Biogas upgrading technologies – developments and innovations", *IEA Bioenergy*, pp. 16-18.

Pitzer, K. S. (1973), "Thermodynamics of electrolytes. I. Theoretical basis and general equations", *Journal of Physical Chemistry*, vol. 77, no. 2, pp. 268-277.

Ryckebosch, E., Drouillon, M. and Vervaeren, H. (2011), "Techniques for transformation of biogas to biomethane", *Biomass and Bioenergy*, vol. 35, no. 5, pp. 1633-1645.

Shurrock, C., Driessen, W., Snelson, P. and Chadha, M. (2012), "Minworth STW the first Anammox[®] plant to yield an environmentally friendly and budget beating biological phosphorus solution", *Wastewater Treatment and Sewerage*, pp. 140.

Tan, X., Tan, S. P., Teo, W. K. and Li, K. (2006), "Polyvinylidene fluoride (PVDF) hollow fibre membranes for ammonia removal from water", *Journal of Membrane Science*, vol. 271, no. 1-2, pp. 59-68.

Tchobanoglous, G., Burton, F. L. and Stensel, D. H. (2003), "Wastewater engineering - treatment and reuse 4th edition", *Metcalf and Eddy*, pp. 437-441.

Thornton, A., Pearce, P. and Parsons, S. A. (2007), "Ammonium removal from digested sludge liquors using ion exchange", *Water Research*, vol. 41, no. 2, pp. 433-439.

Thurston, R. V., Russo, R. C. and Emerson, K. (1979), "Aqueous ammonia equilibrium – tabulation of percent un-ionised ammonia", *United States Environmental Protection Agency*, EPA-600/3-79-091.

Trypuć, M. and Kielkowska, U. (1998), "Solubility in the $\text{NH}_4\text{HCO}_3 + \text{NaHCO}_3 + \text{H}_2\text{O}$ System", *Journal of Chemical Engineering Data*, vol. 43, pp. 201-204.

Wang, R., Li, D. F. and Liang, D. T. (2004), "Modeling of CO_2 capture by three typical amine solutions in hollow fiber membrane contactors", *Chemical Engineering and Processing: Process Intensification*, vol. 43, no. 7, pp. 849-856.

Weissenborn, P. K. and Pugh, R. J. (1995), "Surface tension and bubble coalescence phenomena of aqueous solutions of electrolytes", *Langmuir*, vol. 11, no. 5, pp. 1422-1426.

Yeh, J. T., Resnik, K. P., Rygle, K. and Pennline, H. W. (2005), "Semi-batch absorption and regeneration studies for CO_2 capture by aqueous ammonia", *Fuel Processing Technology*, vol. 86, no. 14-15, pp. 1533-1546.

Chapter 6

**Controlling shell-side crystal nucleation in a gas-liquid membrane contactor
for simultaneous ammonium bicarbonate recovery and biogas upgrading**

Submitted to: Journal of membrane science

Controlling shell-side crystal nucleation in a gas-liquid membrane contactor for simultaneous ammonium bicarbonate recovery and biogas upgrading

Andrew McLeod, Pompilia Buzatu, Olivier Autin, Bruce Jefferson and Ewan J. McAdam*

Cranfield Water Science Institute, Building 39, Cranfield University, Bedfordshire, MK43 0AL, UK

*Corresponding author e-mail: e.mcadam@cranfield.ac.uk

Abstract

A gas-liquid hollow fibre membrane contactor process has been introduced for carbon dioxide (CO₂) separation from biogas using aqueous ammonia (NH₃) to chemically enhance CO₂ absorption and initiate heterogeneous nucleation of the reaction product, ammonium bicarbonate (ABC), at the membrane-solvent interface. Aqueous ammonia absorbents (2 to 7 M) were initially used in single pass for CO₂ separation from a synthetic biogas where nucleation of ABC crystals was observed at the perimeter of the micropores. Recirculation of the aqueous ammonia absorbent encouraged the growth of ABC crystals on the shell-side of the membrane that measured several microns in diameter. However, at high aqueous NH₃ concentrations (3-7 M), lumen-side crystallisation occurred and obstructed gas flow through the lumen of the HFMC. The suggested mechanism for lumen-side crystallisation was solvent breakthrough into the lumen due to pore wetting, which was promoted by low solvent surface tension at high NH₃ concentration. Preferential shell-side nucleation can therefore be promoted by: (1) raising surface tension of the absorbent; and, (2) selection of a membrane with a more regulated pore shape than the PTFE membrane used (d/L 0.065) as both actions can diminish solvent ingress into the pore. Raising surface tension through the inclusion of salt into the chemical absorbent also promoted greater CO₂ flux stability. Importantly, this study demonstrates that chemically enhanced HFMCs are an attractive prospect for gas-liquid separation applications where reaction product recovery offers further economic value.

Keywords: biomethane; membrane crystalliser; chemical absorption; crystallisation

6.1 Introduction

Many water utilities are now refining biogas into biomethane rather than using directly for electrical production due to the potential for higher revenue. To illustrate, in the UK, through support under the Renewable Heat Incentive (RHI), the revenue expected from biomethane is 0.49 £ m⁻³ versus just 0.14 £ m⁻³ for electrical production (Ofgem, 2014). The biomethane product must achieve methane quality that is equivalent or higher than natural gas, demanding separation of the carbon dioxide (CO₂) component from the biogas. This is generally facilitated using absorption in a packed column and is analogous to those currently trialled for carbon capture and storage (CCS). Process intensification is provided through the inclusion of a chemical solvent (e.g. monoethanolamine), which reacts with CO₂ to enhance its selective separation. However, the energy demanded for chemical solvent regeneration, coupled with solvent losses (due to volatility and degradation pathways) and the demand for specialist operators has limited uptake of chemical absorption for biogas upgrading by water utilities (Heile *et al.*, 2014).

Ammonia (NH₃) is now recognised as an emerging chemical reactant due to its higher absorption efficiency, greater chemical stability and lower energy demand for regeneration (Shuangchen *et al.*, 2013; Makhoulfi *et al.*, 2014). Absorption using aqueous NH₃ solutions therefore presents comparable advantages for water utilities undertaking biogas upgrading, but also offers the unique opportunity to utilise the ammonia-rich wastewater produced on-site as a low cost absorbent feedstock for enhanced CO₂ separation. The reaction between free NH₃ and CO₂ is known to proceed by (1) where ammonium bicarbonate (NH₄HCO₃), herein referred to as ABC, is the reaction product formed (1):



When recovered in crystalline form, ABC has applications as a nitrogen fertiliser as well as a feedstock in commercial manufacture. Consequently, controlled crystallisation of ABC reaction product from ammonia-rich wastewaters posits several advantages for biogas upgrading at sewage

works including: elimination of energy demand for absorbent regeneration, a reduction in load onto nitrification/de-nitrification processes, and production of ABC as a new revenue stream (bulk cost €111 tonne⁻¹) (Thornton, 2007).

To enable recovery of crystalline products within a controlled environment, Curcio *et al.* (2001) introduced the membrane crystallisation reactor (MCR). In their work, a micro-porous hydrophobic hollow fibre membrane contactor (HFMC) was used to facilitate non-dispersive contact between a heated crystallising solution (on the retentate side) and cooled pure water on the permeate side. The temperature differential provided the gradient for vapour transport from the crystallising solution through the membrane pores enabling an increased solute concentration (sodium chloride, NaCl) which upon exceeding its solubility limit, initiated nucleation and growth of NaCl crystals (Figure 6.1a). The underpinning mechanism by which the MCR operates therefore corresponds to evaporation-migration-condensation (Di Profio *et al.*, 2010) and has been used to recover NaCl and magnesium sulphate from nanofiltration retentate as crystalline products (Drioli *et al.*, 2004) and for the controlled production of Lysozyme crystals (Di Profio *et al.*, 2003).

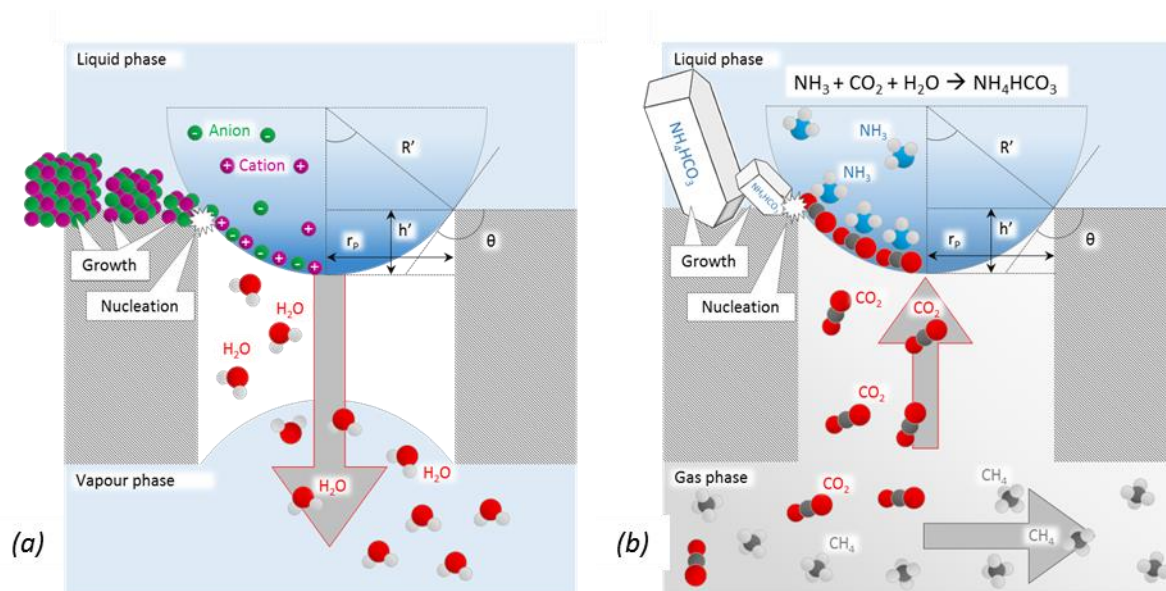


Figure 6.1 Operational mechanism of a membrane crystalliser through removal of solvent vapour to induce supersaturation (a) and proposed novel mechanism with supersaturation induced by rapid reaction of the solvent with absorbed gas (CO₂) (b).

The same microporous HFMC technology used to control crystallisation in MCr systems has now also been used to enable CO₂ separation from biogas through supporting an analogous absorption mechanism to conventional absorption columns (Heile *et al.*, 2014). In this case, the hydrophobic membrane facilitates non-dispersive contact between the chemical absorbent and gas phase with the gases free to diffuse through the open pore structure. Due to the increase in specific surface area afforded by the membrane contactor, the technology presents an inherent advantage in reducing both process scale and absorption solvent consumption, relative to conventional columns (Herzog and Falk-Pedersen, 2000). In this study, we therefore seek to introduce a gas-liquid membrane absorption crystallisation reactor that enables both the selective separation of CO₂ through reaction with ammonia and the subsequent nucleation and growth of the crystalline ammonium bicarbonate reaction product for recovery. The mechanism for nucleation and growth of ABC crystals in this study differs from classical MCr systems in that supersaturation is achieved by counter diffusion of solutes through the transport of CO₂ molecules from the gas phase into the crystallising fluid (an aqueous NH₃ solvent), where the driving force for CO₂ transport to the crystallising fluid is the enhancement in solubility provided by the chemical reaction with NH₃. Nucleation is then dependent upon CO₂ reaching sufficient concentration to initiate local supersaturation of the solvent (Figure 6.1b).

Makhloufi *et al.* (2014) recently screened a number of hollow-fibre membrane materials to determine compatibility for CO₂ absorption into aqueous ammonia for chemically enhanced post combustion CCS. The authors remit precluded an interest in recovering ABC as a by-product and determined that micro-porous fibres were inappropriate for application to CCS due to CO₂ flux instability caused by ABC precipitation on the gas-side, within the lumen of the membrane fibres. In this study, we therefore seek to introduce the mechanism underpinning controlled nucleation and growth of ABC on the shell-side (Solvent side) of a micro-porous HFMC to illustrate the potential of the gas-liquid membrane absorption crystallisation reactor for simultaneous gas separation with reaction product recovery. A micro-porous polytetrafluoroethylene (PTFE) HFMC is therefore used to

investigate: (i) the potential for chemical absorption in a microporous membrane to enable shell-side (absorbent side) crystal nucleation; (ii) investigation of absorbent conditions required to enable crystal growth; and (iii) the role of the microporous substrate in controlling nucleation. To our knowledge, this is the first study to describe the use of hydrophobic micro-porous membranes for the controlled nucleation and growth of a reaction product following chemical absorption from the gas phase.

6.2 Experimental

6.2.1 Fabrication, setup and operation of equipment

Table 6.1 Dimensions and surface characteristics of the single membrane fibres.

		PDMS ^b	PTFE ^b
<i>Fibre characteristics</i>			
Inner diameter	mm	0.18	1.51
Outer diameter	mm	0.31	1.91
Wall thickness	µm	65	200
Active length	m	0.1	0.1
Surface area ^a	m ²	0.97x10 ⁻⁴	6x10 ⁻⁴
Porosity	%	-	44
Mean pore radius	µm	-	0.16
Average surface roughness ^c	nm	76.6	82.2
Lumen cross sectional area	m ²	2.54x10 ⁻⁸	1.79x10 ⁻⁶
<i>Shell-side characteristics</i>			
Inner diameter	mm	6	6
Outer diameter	mm	4	4
Shell cross sectional area	m ²	2.82x10 ⁻⁵	2.54x10 ⁻⁵
Priming volume	mL	2.82	2.54
<i>Operational Characteristics</i>			
Flow regime		Co-current	Co-current
Shell-side		5 M NH ₃ (aq.)	2,3,5,7 M NH ₃ (aq.)
Lumen-side		50:50 CO ₂ :CH ₄	50:50 CO ₂ :CH ₄

^aBased on fibre outer diameter. ^bData provided by manufacturer. ^cMeasured using AFM.

Hydrophobic micro-porous PTFE fibres were obtained from Markel Corporation (Plymouth Meeting, Pennsylvania, USA) and comprised a 200 µm wall thickness and 44 % porosity (Table 6.1). To enable characterisation of crystal growth with minimal disturbance, single fibre modules were

manufactured. Modules comprised a transparent PVC shell with an inner diameter of 0.004 m and were completed with two acetal push-fit T-union-joints (1/4" Speedfit, John Guest Ltd., Middlesex, UK). Fibres were potted in epoxy resin (Bostik Ltd., Stafford, UK). For dense membrane experiments, polydimethylsiloxane (PDMS) fibres with a wall thickness of 65 μm were used in an identical module construction (Trelleborg sealing solutions, Stuttgart, Germany).

Methane (CH_4 , 99.995 %) and carbon dioxide (CO_2 , 99.7 %) (BOC gases, Ipswich, UK) were mixed in controlled proportions using mass flow controllers (0.2-20.0 L min^{-1} , Roxspur Measurement and Control Ltd., Sheffield, UK) to provide an initial 50:50 CH_4 : CO_2 gas composition and introduced through the fibre lumen (Figure 6.2). Liquid was pumped co-currently into the shell-side. Transmembrane pressure (TMP) was monitored by digital pressure gauges (DPG1000, Omega Engineering Ltd., Manchester, UK) and liquid and pressure flow controlled using needle valves.

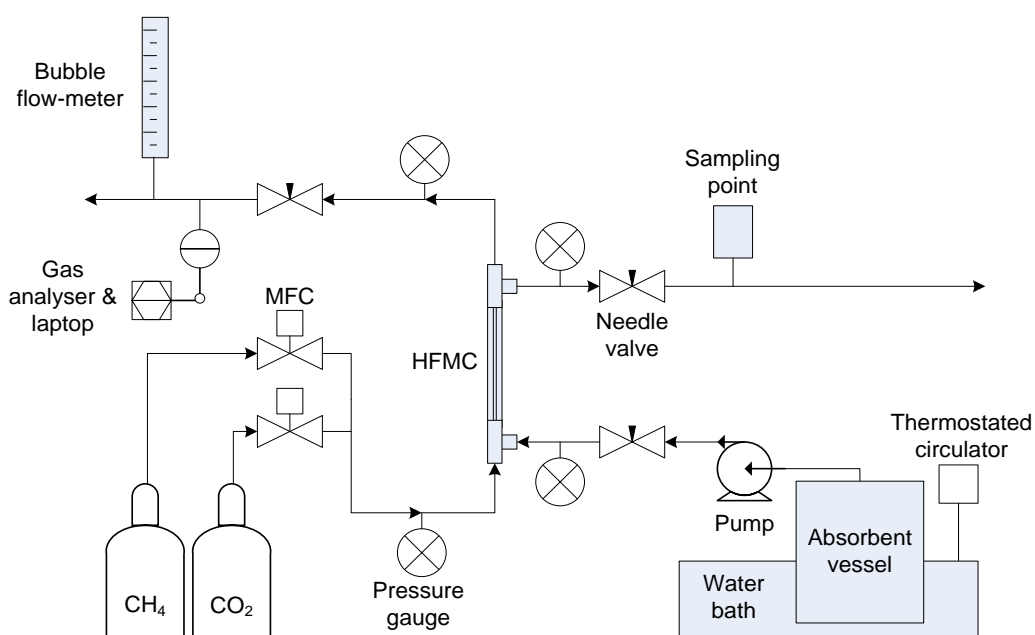


Figure 6.2 Schematic of experimental apparatus.

6.2.2 Sampling and analyses

Ammonia absorbents were prepared through dilution of an NH_3 concentrate (35 %, Fisher Chemicals, Loughborough, UK) using de-ionised (DI) water ($15.0 \text{ M}\Omega \text{ cm}^{-1}$). Absorbent pH was fixed to pH 11 to ensure 100 % of the ammoniacal nitrogen was available as un-ionised free NH_3 (Thurston *et al.*, 1979). Ammonia concentrations were confirmed by use of an ammonium cell test (4.-80. $\text{mg}_{\text{NH}_4\text{-N}} \text{ L}^{-1}$, VWR International Ltd., Poole, UK) with subsequent determination by spectrophotometry (Spectroquant Nova 60, Merck-Millipore, Darnstadt, Germany). Gas composition was determined using an infrared biogas analyser sited on the gas outlet (range 0-100 %, accuracy <0.2 % full-scale; Yieldmaster, Bluesens gas sensor GmbH, Herten, Germany). Gas flow rate was measured using a bubble flow meter (50 mL, Restek, Bellefonte, US). Carbon dioxide flux (J_{CO_2} , $\text{mol m}^{-2} \text{ s}^{-1}$) was calculated using gas flow rate, composition and temperature (2):

$$J_{\text{CO}_2} = \frac{[(Q_{G,\text{in}} \times c_{G,\text{in}}) - (Q_{G,\text{out}} \times c_{G,\text{out}})] \times 273.15 \times 1000}{(22.4 \times A_m \times T_G)} \quad 2$$

where $Q_{G,\text{in}}$ and $Q_{G,\text{out}}$ are gas flow rate before and after HFMC respectively ($\text{m}^3 \text{ s}^{-1}$), $c_{G,\text{in}}$ and $c_{G,\text{out}}$ are gas phase CO_2 concentrations before and after HFMC respectively (mol mol^{-1}), A_m is the membrane surface area for absorption (m^2) and T_G is the gas temperature (K) (Atchariyawut *et al.*, 2007).

Examination of the PTFE microporous membrane pore structure was determined using a scanning electron microscope (SEM) equipped with a field emission gun (sFEG) (XL30, FEI, Hillsboro, Oregon, USA). Pore size data was subsequently analysed to provide a size distribution using a log-normal distribution function (Li and Tan, 2000):

$$f_L(r) = \frac{1}{\sqrt{2\pi r}} [\ln(1 + \sigma^2)]^{-0.5} \times \exp \left[-\frac{(\ln(r/r_m)(1 + \sigma^2)^{0.5})^2}{2 \times \ln(1 + \sigma^2)} \right] \quad 3$$

Surface roughness of the virgin fibres was characterised using atomic force microscopy (AFM, Dimension 3100, Bruker, Massachusetts, US). Examination of sacrificial membrane samples to determine crystal nucleation and growth was conducted using SEM (up to x10000 magnification) for

the finer diameter PTFE fibres, and optical microscope for the wider diameter PDMS fibres. Fibre samples for SEM were first coated with gold-palladium (Au-Pd) using a cool sputtering SEM coating unit (E5100, Polaron Equipment/Quorum Technologies Ltd., Lewes, UK). Spectroscopic elemental analysis was performed in tandem with SEM by energy dispersive x-ray spectroscopy (EDX) using Aztec software (Oxford Instruments NTS, Abingdon, UK).

6.3 Results

6.3.1 Characterisation of the PTFE and PDMS membranes

Pore size analysis by SEM indicated that the average pore radius of the PTFE fibres was $0.157\ \mu\text{m}$ with radii distributed within a range between $0.13\ \mu\text{m}$ and $0.21\ \mu\text{m}$ (Figure 6.3).

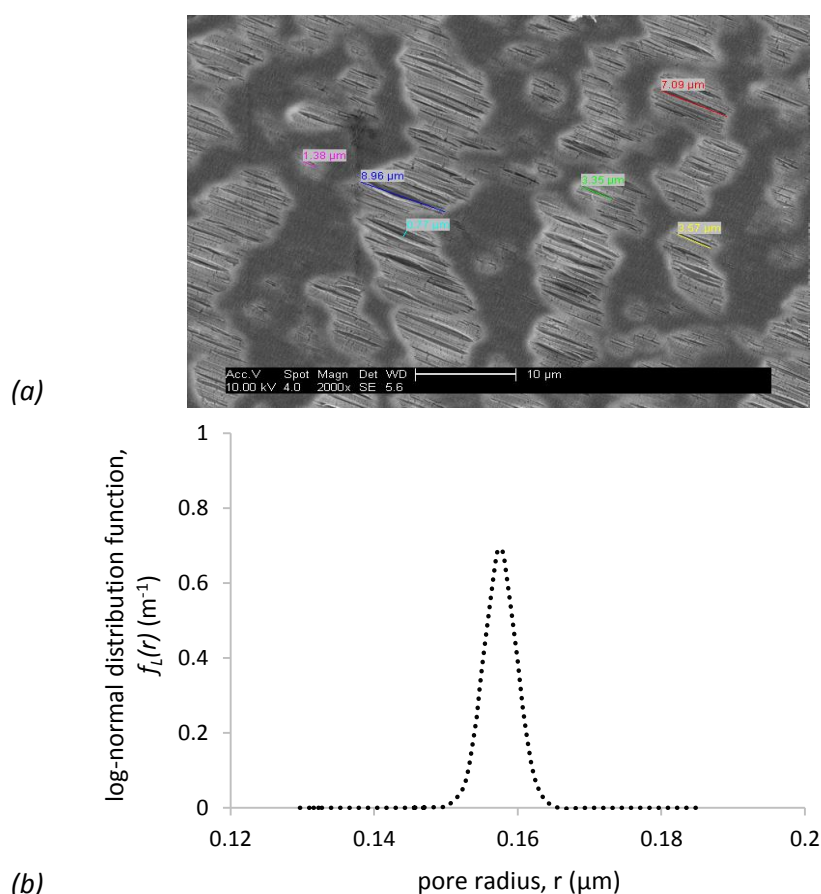


Figure 6.3 Pore structure analysis of the PTFE hollow fibre membrane used: Stretched pore geometry illustrated using SEM (2000x) (a) and statistical determination of pore radius using log-normal distribution (b).

This closely approximates to pore width data provided by the manufacturer (Table 6.1). The stretched length of the pores was approximately $4.9 \pm 3.1 \mu\text{m}$, yielding a pore diameter to length ratio (d/L) of 0.065. Average surface roughness of the PTFE fibres was 82 nm which is similar to that measured for the nonporous PDMS membrane (77 nm).

6.3.2 Removal of CO_2 using NH_3 as a chemical absorbent

The PTFE HFMC was initially tested in single pass mode (without absorbent recirculation). Gas velocity, V_G , was varied between 0.28 m s^{-1} and 18.62 m s^{-1} whilst both liquid velocity (V_L) and aqueous ammonia absorbent concentration were fixed at 0.02 m s^{-1} and $7 \text{ mol}_{\text{NH}_3} \text{ L}^{-1}$ respectively (Figure 6.4).

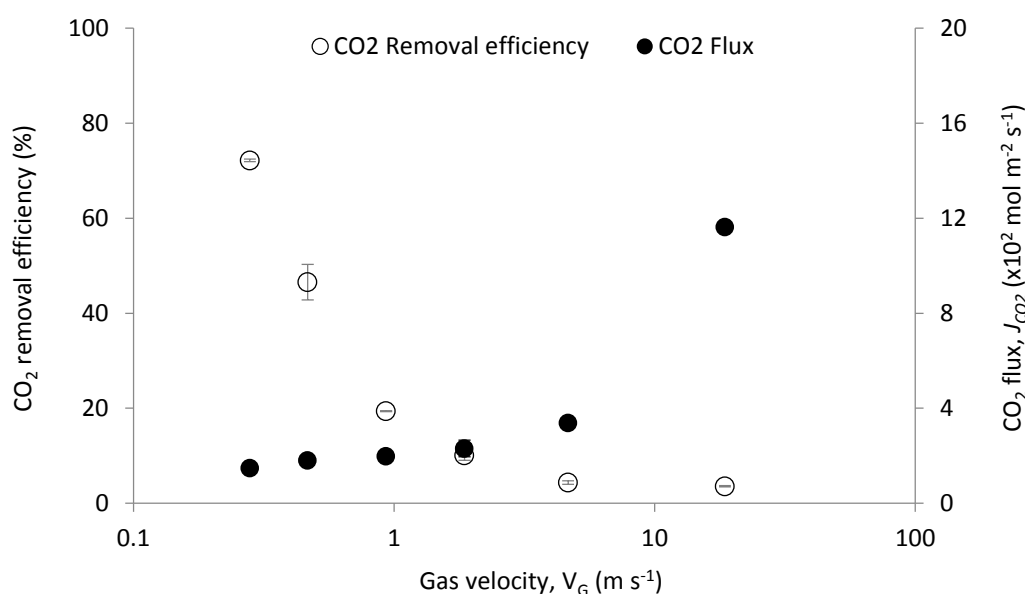


Figure 6.4 Effect of variable gas velocity (V_G) upon CO_2 removal efficiency and CO_2 flux, during absorption from a 50:50 CO_2 : CH_4 gas mixture using $7 \text{ mol}_{\text{NH}_3} \text{ L}^{-1}$ aqueous solution at fixed liquid velocity (V_L , 0.02 m s^{-1}) in a single fibre PTFE HFMC. Error bars indicate standard error.

A maximum CO_2 removal efficiency of 72 % was observed at the lowest V_G examined (0.28 m s^{-1}), which corresponded to a G/L ratio of 3. For these fixed conditions, methane content increased from 50 % at the inlet to 86 % CH_4 . As V_G was increased, CO_2 removal efficiency decreased to a minimum of 3.6 % which was recorded at the highest V_G tested (18.62 m s^{-1}). Whilst CO_2 removal efficiency

declined with an increase in V_G , CO_2 flux increased from 0.015 to $0.116 \text{ mol m}^{-2} \text{ s}^{-1}$ within the gas velocity range tested (Figure 6.4). Microscopic analysis of the shell-side of a PTFE fibre that had been used with $7 \text{ mol}_{\text{NH}_3} \text{ L}^{-1}$ aqueous ammonia solution and a G/L ratio of 10, showed white specks formed around the pore mouths indicating that crystal nucleation had been initiated (Figure 6.5).

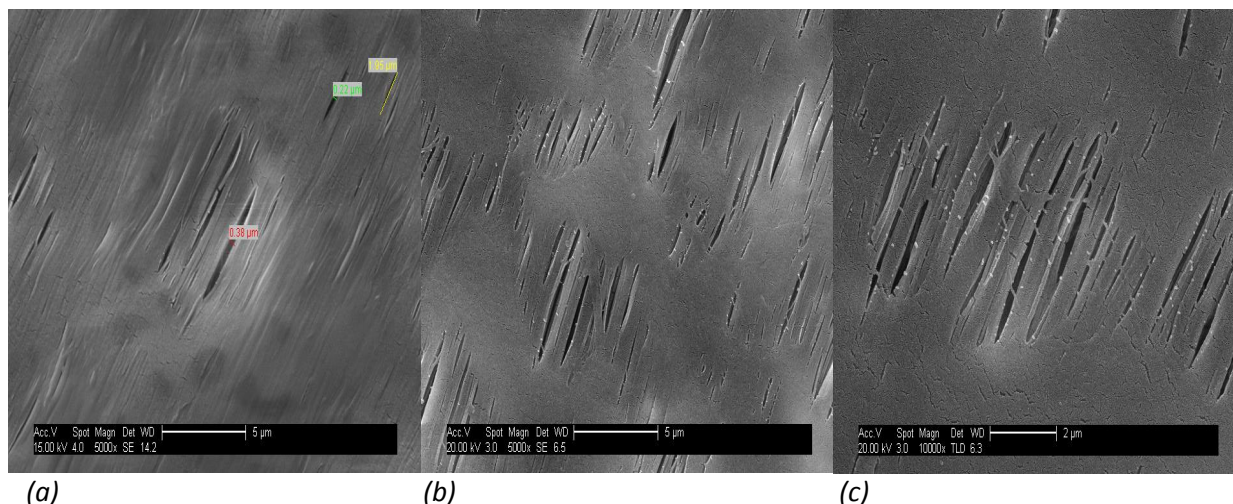


Figure 6.5 SEM surface analysis of: the virgin PTFE hollow fibre membrane surface (x5000) (a); and nucleation of ABC crystals is observed at the membrane-absorbent interface (shell-side) following CO_2 absorption using a $7 \text{ mol}_{\text{NH}_3} \text{ L}^{-1}$ ammonia solution in single pass operation (x5000) (b). Sample in image (b) observed at higher magnification (x10000) (c).

6.3.3 Identification of heterogeneous crystal growth

Crystal growth on the shell side of the module was identified within each of the 2 to 5 M NH_3 absorbents used ($V_G = 0.93 \text{ m s}^{-1}$, G/L 10) with carbon (C), oxygen (O) and nitrogen (N) peaks confirmed in the crystals formed by EDX (Table 6.2). Crystals that had grown in 3 to 5 $\text{mol}_{\text{NH}_3} \text{ L}^{-1}$ absorbents generally developed planar structures that were oriented roughly parallel to the membrane surface with multiple points of contact, whereas those formed in the 2 $\text{mol}_{\text{NH}_3} \text{ L}^{-1}$ absorbent developed perpendicular to the membrane surface with fewer crystal-membrane contact points. Following two to five absorbent recirculations, a progressive decline in CO_2 flux was observed at each free ammonia concentration tested (Figure 6.6). After 6 and 13 recirculations respectively, the 3 and 5 $\text{mol}_{\text{NH}_3} \text{ L}^{-1}$ absorbent experiments were stopped due to lumen-side crystallisation which

blocked the flow of gas (Figure 6.7). Lumen side crystals were tightly packed and propagated along the length of the hollow fibre. A similar decline in CO_2 flux was also observed using $2 \text{ mol}_{\text{NH}_3} \text{ L}^{-1}$ absorbent. However, whilst shell-side crystallisation was evidenced in the $2 \text{ mol}_{\text{NH}_3} \text{ L}^{-1}$ absorbent (Table 6.2), lumen-side crystallisation was not observed following 34 absorbent recirculations.

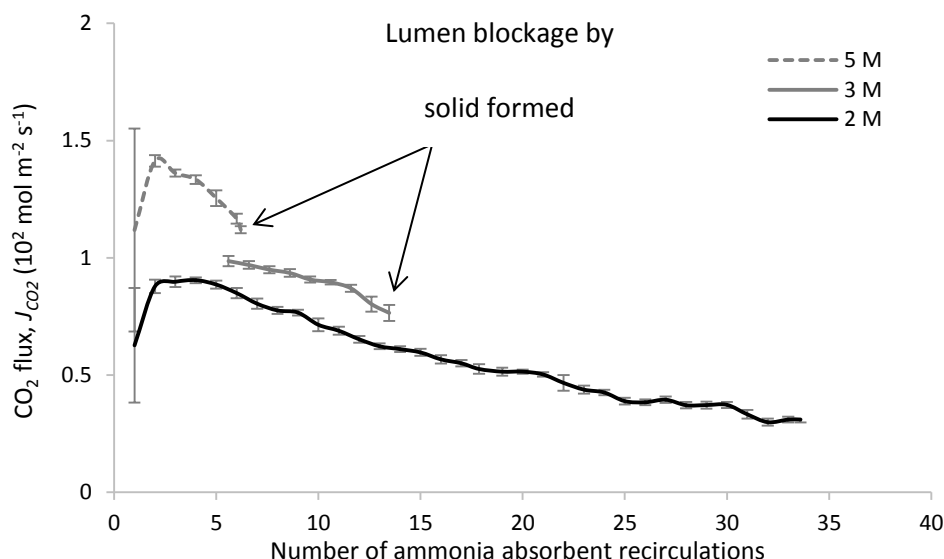


Figure 6.6 CO_2 flux observed with the PTFE membrane following NH_3 solvent recirculation (2 M, 3 M and 5 M) through the shell-side. Hydrodynamic conditions: G/L 10; V_G 0.93 m s^{-1} ; V_L 0.02 m s^{-1} . Lumen-side blockage observed for 3 M and 5 M solutions. Error bars indicate standard error.

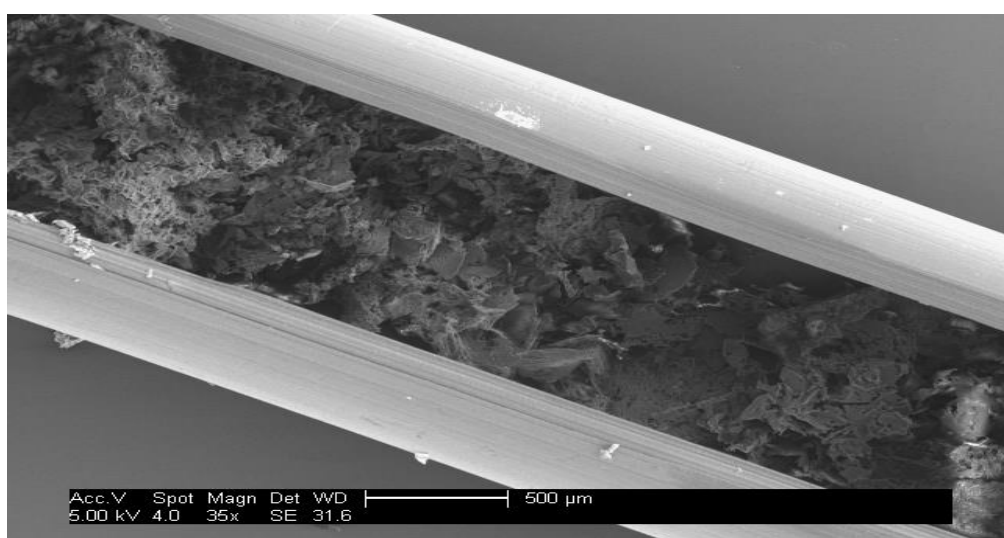
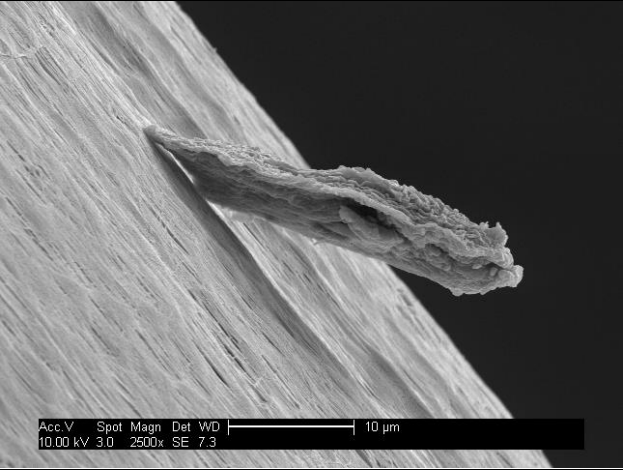
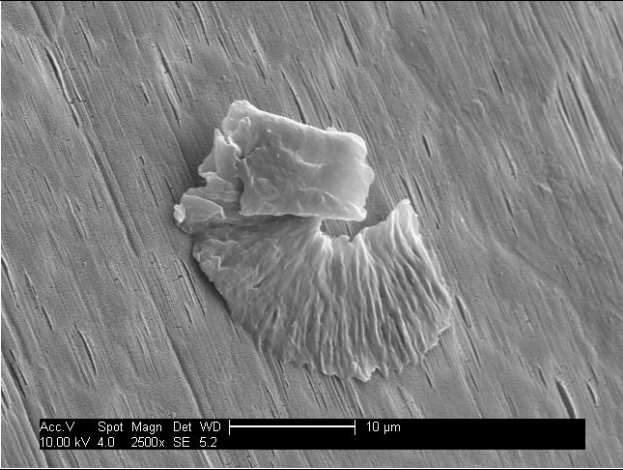
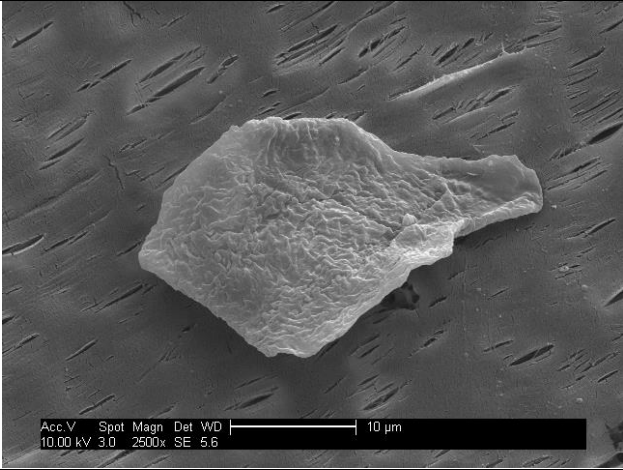
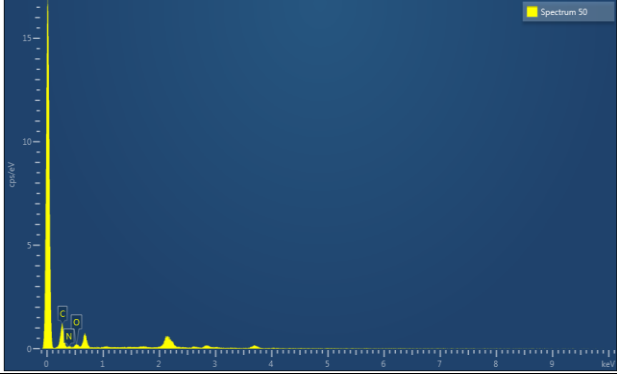
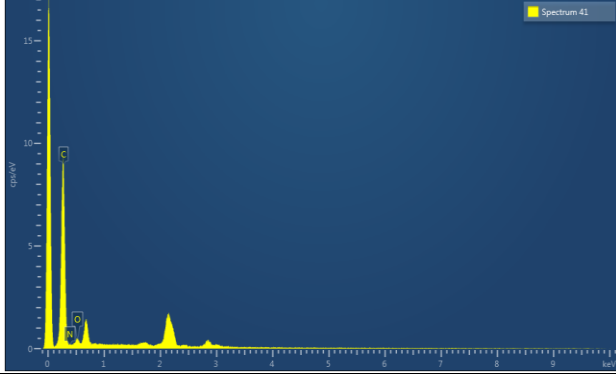
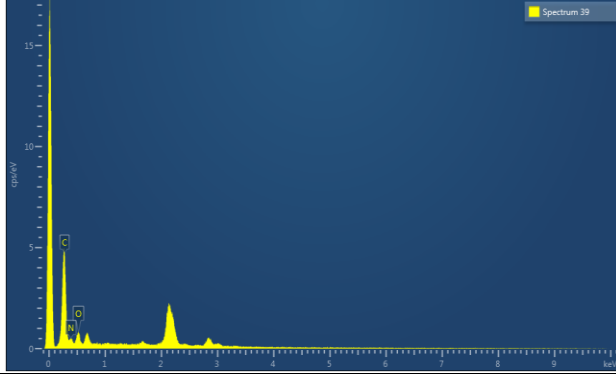


Figure 6.7 Dissected section of the PTFE hollow fibre membrane used for 5 M NH_3 absorbent recirculation. The experiment was stopped after 6 recirculations due to gas-side blockage. SEM analysis shows formation of ABC. Hydrodynamic conditions: G/L 10; V_G 0.93 m s^{-1} ; V_L 0.02 m s^{-1} .

Table 6.2 SEM images and EDX analyses of ammonium bicarbonate crystals grown on the PTFE membrane at the membrane-absorbent interface (shell-side) during recirculation of aqueous ammonia absorbents ranging 2 to 5 mol_{NH3} L⁻¹ in concentration.

	2 mol L ⁻¹	3 mol L ⁻¹	5 mol L ⁻¹
SEM/ SFEG			
EDX			

6.3.4 Using membrane type to control lumen-side crystallisation

Performance of a nonporous PDMS membrane was compared to the microporous membrane performance by recirculating $5 \text{ mol}_{\text{NH}_3} \text{ L}^{-1}$ absorbent and fixing hydrodynamic conditions sufficient to yield equivalent CO_2 fluxes to the PTFE membrane (G/L 0.39, Figure 6.8).

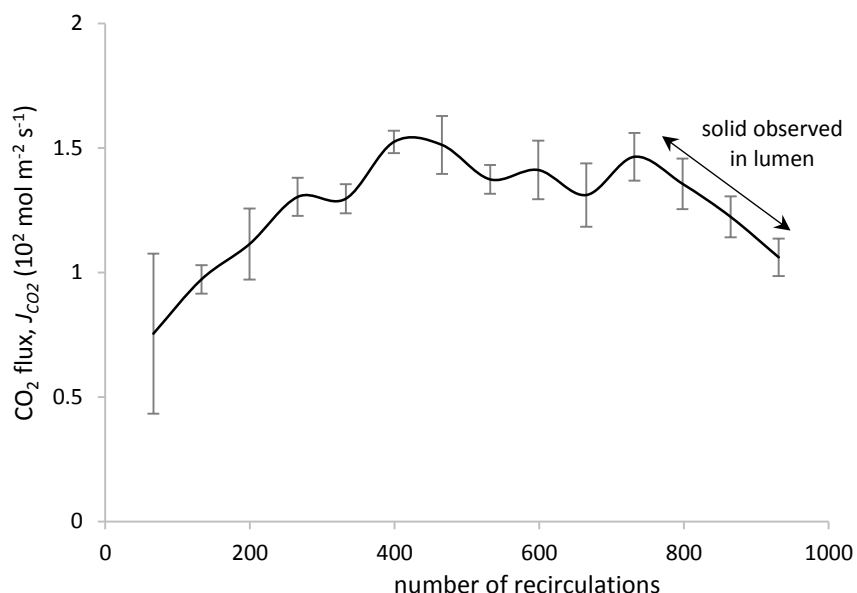
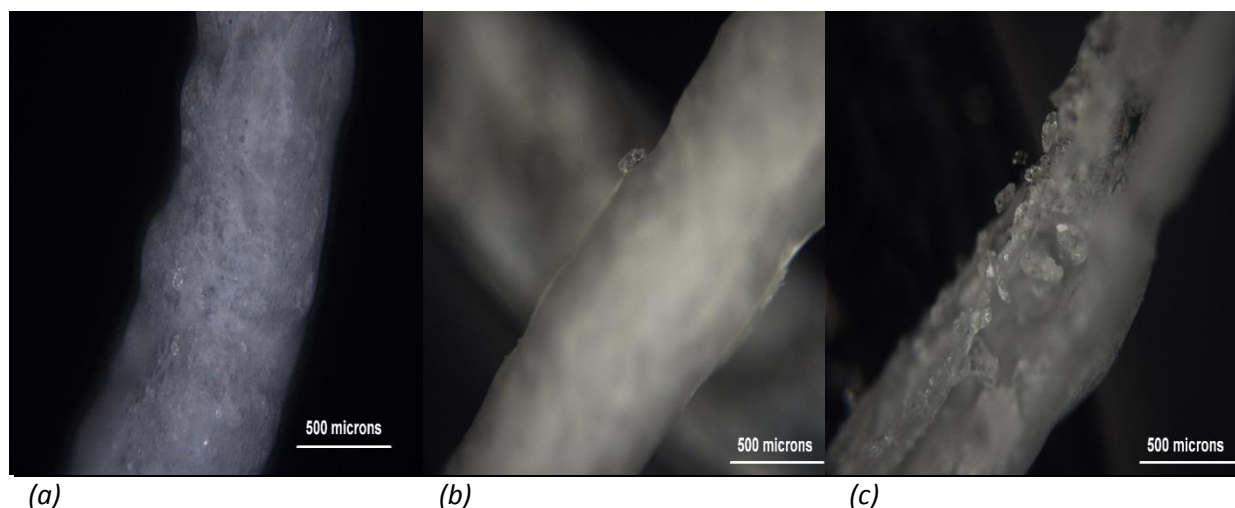


Figure 6.8 CO_2 flux observed with the nonporous PDMS hollow fibre membrane using 5 M NH_3 solvent recirculated through the module shell-side. Gas-side (lumen side) blockage noted following 800 solvent recirculations. Hydrodynamic conditions: G/L 0.4; V_L 0.1 m s^{-1} . Error bars indicate standard error.

A steady state period was observed between 400 and 800 solvent recirculations which corresponded to CO_2 fluxes of around $0.014 \text{ mol m}^{-2} \text{ s}^{-1}$. However, after around 800 recirculations a progressive decline in CO_2 flux was noted and the experiment was terminated after 931 recirculations. Whilst crystals were observed to have grown on the shell-side of the PDMS fibre (Figure 6.9), the reduction in CO_2 flux after 800 recirculations coincided with the formation of crystalline solid within the fibre lumen inducing deformation of the cylindrical fibre structure.



(a) (b) (c)
 Figure 6.9 Nonporous PDMS hollow fibre membrane following >800 recirculations of 5 M NH_3 absorbent: crystals formed inside the fibre lumen (a); an example crystal formed on the outside of the fibre (b) and the PDMS fibre dissected reveals crystals formed within the fibre lumen (c).

6.3.5 Manipulating solvent chemistry to promote shell-side nucleation on PTFE fibres

Carbon dioxide flux provided by the PTFE membrane using $3 \text{ mol}_{\text{NH}_3} \text{ L}^{-1}$ absorbent during recirculation were compared when using 1 % wt. glycerol as an additive to the $3 \text{ mol}_{\text{NH}_3} \text{ L}^{-1}$ absorbent as the addition of glycerol has been shown to diminish the volatility of ammonia (Shuangchen *et al.*, 2013) (Figure 6.10). With the glycerol added, initial mean CO_2 flux was 3.5 % lower than without glycerol addition and after 12 recirculations, CO_2 flux was 23 % lower than with the pure $3 \text{ mol}_{\text{NH}_3} \text{ L}^{-1}$ absorbent. Conversely, the addition of 5 % wt. NaCl to the $3 \text{ mol}_{\text{NH}_3} \text{ L}^{-1}$ absorbent increased CO_2 flux stability. To illustrate, after 13 recirculations of the $3 \text{ mol}_{\text{NH}_3} \text{ L}^{-1}$ absorbent with 5 % wt. NaCl added, CO_2 flux was 91 % of initial flux in comparison to only 81 % for the $3 \text{ mol}_{\text{NH}_3} \text{ L}^{-1}$ absorbent.

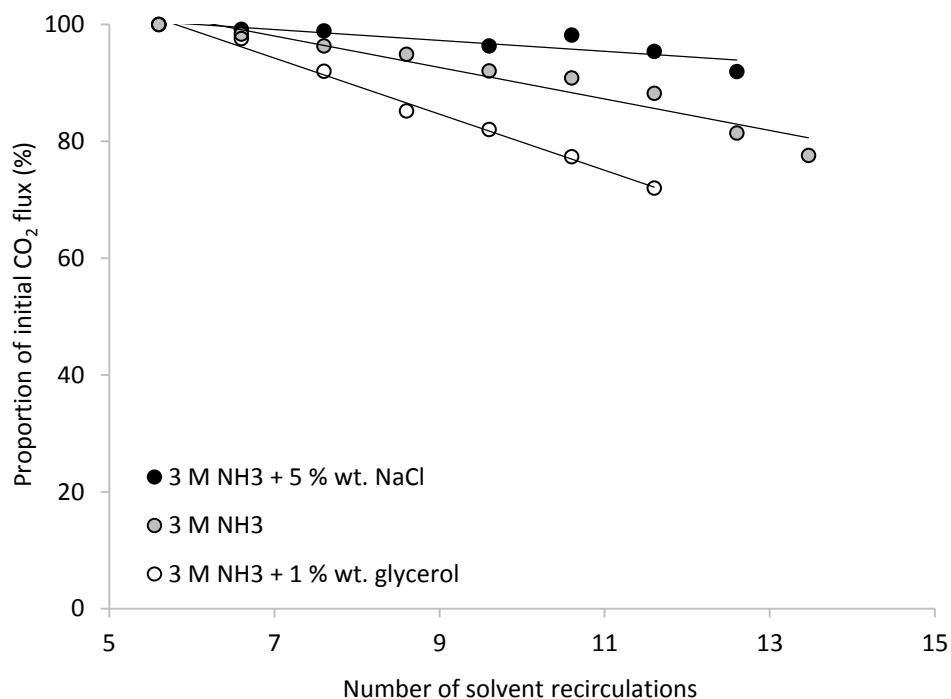


Figure 6.10 Impact of sodium chloride (5 % wt.) and glycerol (1 % wt.) on CO_2 flux when used as additives to 3 M NH_3 absorbent recirculated through the module shell-side. Hydrodynamic conditions: G/L 10; V_G 0.93 m s^{-1} ; V_L 0.02 m s^{-1} .

The change in surface tension following an increase in NaCl or aqueous ammonia concentration to deionised water was studied (Figure 6.11). With the inclusion of between 0.1 and 1 M NaCl (5.85 % wt.), surface tension increased by up to 2.2 mN m^{-1} . However, a reduction in surface tension of between -0.8 and -8.7 mN m^{-1} was measured for concentrations between 0.3 and $7 \text{ mol}_{\text{NH}_3} \text{ L}^{-1}$ which is within the range of aqueous ammonia absorbents studied and is consistent with the literature (Weissenborn and Pugh, 1995). The addition of 5 % wt. NaCl to aqueous ammonia reduced the change in surface tension. For example, at a concentration of $3 \text{ mol}_{\text{NH}_3} \text{ L}^{-1}$ a reduction in surface tension of -6.7 mN m^{-1} was recorded whereas with the inclusion of 5 % wt. NaCl, the change in surface tension reduced to only -3.9 mN m^{-1} .

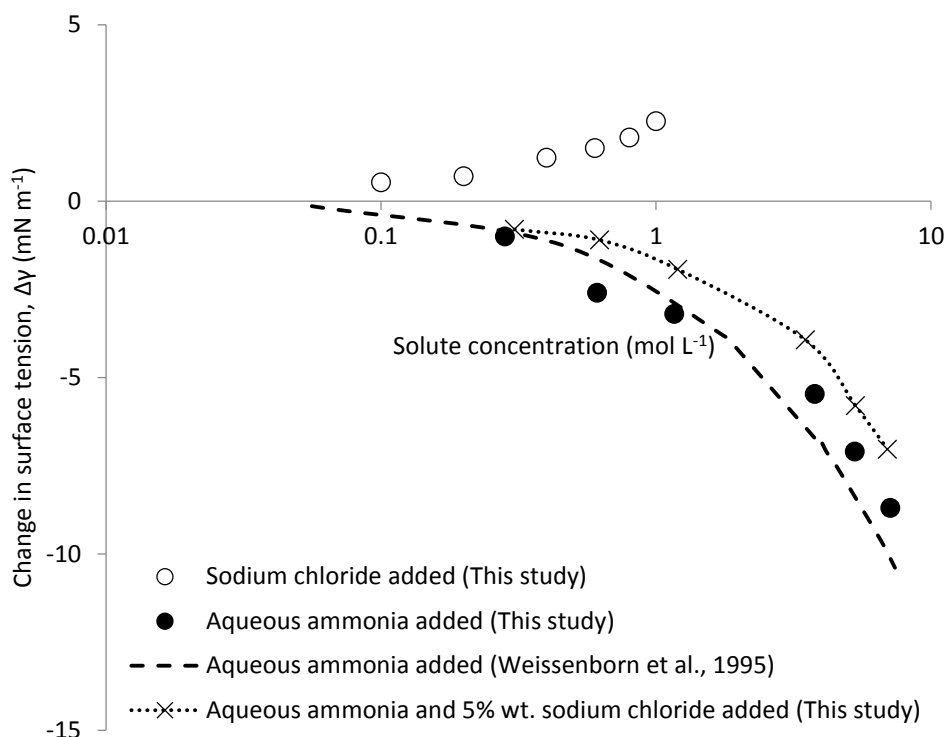


Figure 6.11 Changes in surface tension relative to deionised water driven by aqueous ammonia and sodium chloride solute concentration within the concentration range examined (NH_3 , 2-7 M; NaCl 5 % wt. or 0.85 M) (Weissenborn and Pugh, 1995).

6.4 Discussion

In this study, the use of a liquid phase chemical reaction to enhance CO_2 absorption and produce a crystalline reaction product has been demonstrated using a PTFE microporous hydrophobic hollow fibre membrane to promote the nucleation and growth of ammonium bicarbonate. During single pass experiments using a $7 \text{ mol}_{\text{NH}_3} \text{ L}^{-1}$ ammonia absorbent, an increase in V_G increased CO_2 flux into the receiving ammonia absorbent. In chemically reactive absorption systems, an increased gas phase flow rate is often observed to mediate solute flux (Esquiroz-Molina *et al.*, 2013) as this enables replenishment of CO_2 at the solvent-membrane interface and maintenance of a high bulk gas CO_2 partial pressure (Zeng *et al.*, 2013). When operating at high V_G (G/L 10) using 7 mol L^{-1} ammonia absorbent, an absorption rate of $44.2 \text{ kmol m}^{-3} \text{ h}^{-1}$ was recorded (Figure 6.4). For comparison, Zeng *et al.* (2013) recorded a CO_2 absorption rate of $3.3 \text{ kmol m}^{-3} \text{ h}^{-1}$ in a packed column using aqueous

ammonia ($4.5 \text{ mol}_{\text{NH}_3} \text{ L}^{-1}$) which illustrates the high CO_2 flux achieved with micro-porous HFMC. For this high flux condition, activation of a substantial number of nucleation sites around the micro-pores on the shell-side of the PTFE was demonstrated (Figure 6.4 b,c). This is supported by the work of Di Profio *et al.* (2003) where increased solute concentration enhanced supersaturation leading to an excess of nucleation. Interestingly, crystallisation is generally not observed in CO_2 /aqueous ammonia packed columns unless the ammonia concentration exceeds around $6 \text{ mol}_{\text{NH}_3} \text{ L}^{-1}$ (Budzianowski *et al.*, 2011). In this study, nucleation and crystal growth was observed at $2 \text{ mol}_{\text{NH}_3} \text{ L}^{-1}$ (Table 6.2). The enhanced nucleation potential of the hydrophobic PTFE membrane can be explained by the high contact angle (θ) exhibited (around 129° for PTFE-water), which favours heterogeneous nucleation over homogeneous nucleation (Figure 6.12).

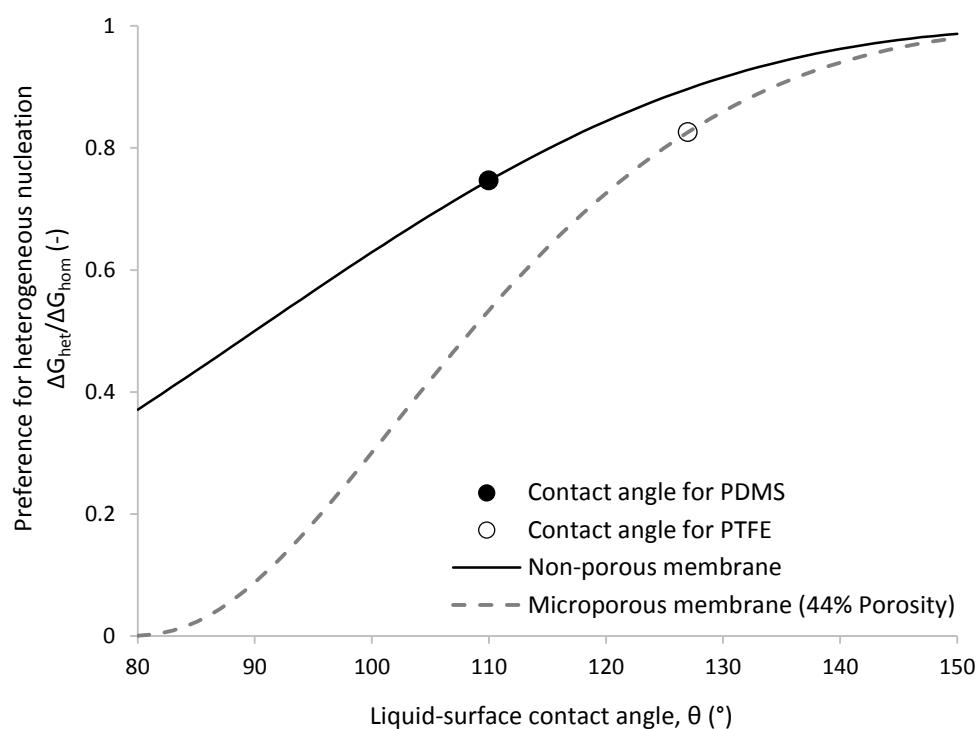


Figure 6.12 Impact of liquid-surface contact angle on the thermodynamic favourability of heterogeneous vs. homogeneous nucleation calculated for the non-porous PDMS membrane and PTFE micro-porous membrane used (Appendix, A1).

The contact angle reflects the three phase line at the perimeter of the pore mouth, where the CO_2 gas phase, aqueous ammonia phase and PTFE solid phase interact (Figure 6.1; Curcio *et al.*, 2006)

and accounts for the proximity of nucleation sites relative to the pore mouth. It is proposed that the nucleation mechanism is analogous to that underpinning evaporation-migration-condensation as seen in MCr which is thought to follow: (1) surface adsorption through non-specific attractive interaction; (2) hindrance of lateral migration by the irregular pore structure causing packing; and (3) molecular entrapment which induces relatively higher supersaturation (Di Profio *et al.*, 2010). However, within the gas crystallisation process proposed, CO₂ will migrate from the gas phase through the stagnant region of the solvent meniscus resident within the pore to the nucleation site, the rate of which will be determined by the reactivity of the solvent.

Growth of ABC crystals on the shell-side of the membrane was demonstrated following recirculation of the ammonia absorbent (Table 6.2). Crystals grown within 3 and 5 mol_{NH₃} L⁻¹ absorbents differed from those grown within 2 mol_{NH₃} L⁻¹ absorbent which were characterised by growth perpendicular to the membrane surface and from a comparatively limited number of nucleation points. Lowering the aqueous ammonia concentration to 2 mol_{NH₃} L⁻¹ results in two effects: (1) this is close to the nominal limiting saturation concentration for the reactant product (ABC, 2.24 mol L⁻¹); and (2) the flux of CO₂ into the aqueous phase is reduced due to the lower absorbent reactivity. The crystal orientation identified at low fluxes is indicative of conditions favouring crystal growth over nucleation, and is analogous to observations made previously when employing low solvent fluxes for evaporative MCr (Zhang *et al.*, 2008) which results in production of fewer larger crystals.

Following extensive solvent recirculation, crystal growth was observed on the lumen side of the PTFE fibre (Figure 6.7). In a preliminary evaluation of CO₂ absorption into aqueous NH₃ using oxyphan® micro-porous hollow fibres, Makhoulfi *et al.* (2014) postulated that the CO₂ flux decline observed was due to lumen-side (gas-side) crystallisation which was initiated through high ammonia slip into the humidified gas phase. To investigate this mechanism, in this study, glycerol (1 %) was added to the aqueous ammonia absorbent used with the micro-porous PTFE membranes as this is commonly employed to suppress NH₃ volatility by the glycerol hydroxyl group bonding to the free

ammonia (Shuangchen *et al.*, 2013). However, with the inclusion of glycerol, CO₂ flux declined more rapidly than without glycerol addition suggesting that glycerol-ammonia bonding also retarded mass transfer (Cheng *et al.*, 2003) and that the organic glycerol may act as a membrane and actively increasing pore wetting (Goh *et al.*, 2013). Direct measurement of ammonia slip could not be made in this study due to scale. However, ammonia slip has been measured by this group using a larger contactor scale (0.79 m²) and similar process conditions (5 mol_{NH3} L⁻¹ aq. NH₃; G/L 7.5) and a slip of only 0.015 % NH₃ was noted which is ostensibly insufficient to cause the crystal growth observed within the fibre. The low slip can be explained by the low liquid velocities imposed, for which the depletion of ammonia through reaction with CO₂ extends radially away from the fibre wall toward the bulk (Figure 6.13). This presents a barrier of non-volatile NH₄⁺ ions that inhibit direct contact between the bas and the free ammonia bulk, thereby limiting volatilisation of NH₃. This is experimentally corroborated at high G/L ratios where high CO₂ fluxes are coincident with diminished CO₂ removal efficiency (Figure 6.4) due to the decrease in mole ratio between NH₃ and CO₂ in the reaction zone (Zeng *et al.*, 2013). At a G/L of 3, the methane content in the outlet gas exceeding the CH₄ content of North Sea natural gas (Persson *et al.*, 2007) which indicated that the gas treatment objective can be met whilst limiting the NH₃ concentration (and slip) at the gas-liquid interface.

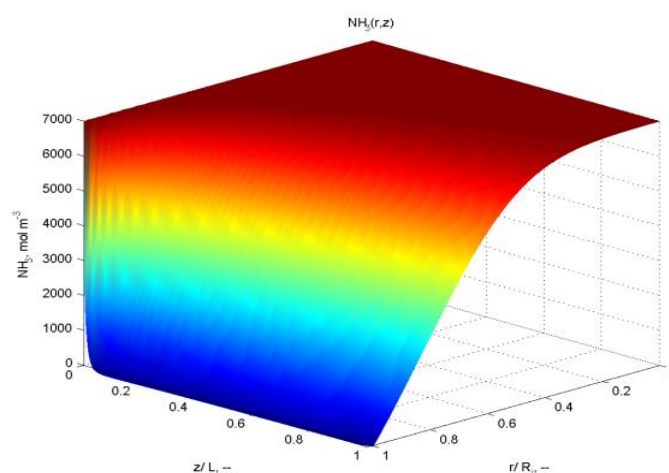


Figure 6.13 An illustration of NH₃ depletion by chemical reaction with CO₂, where volatile free ammonia concentration at the interface with the gas is exceptionally low across the membrane length (z) due to rapid reaction, thereby inhibiting NH₃ volatilisation in to the gas phase.

Higher aqueous ammonia concentrations were demonstrated to lower absorbent surface tension (γ , mN m^{-1}) considerably (Figure 6.11). Lower surface tension is known to decrease breakthrough pressure ($\Delta P_{B.P.}$) for a cylindrical pore (Franken *et al.*, 1987) which notably enhances the probability for wetting (4):

$$\Delta P_{B.P.} = \frac{-4B\gamma \cos \theta}{d_{\max}} \quad 4$$

where d_{\max} is the maximum pore size. It is suggested that the reduction in surface tension observed at high aqueous ammonia concentration enables penetration of the ammonia rich absorbent into the pore and into the CO_2 rich gas phase initiating crystal nucleation in the lumen side of the micro-porous membrane. This was evidenced by the faster onset of lumen-side (gas phase) crystal growth within aqueous ammonia concentrations greater than 3 M, which were characterised by a relatively large reduction in surface tension ($\Delta\gamma$ -5.6 to -9.6 mN m^{-1} , Figure 6.11). For comparison, whilst shell-side crystallisation was noted within the lower concentration 2 $\text{mol}_{\text{NH}_3} \text{ L}^{-1}$ absorbent, lumen-side crystal growth was absent. However, the progressive and gradual decline in CO_2 flux noted for the 2 $\text{mol}_{\text{NH}_3} \text{ L}^{-1}$ absorbent remains indicative of progressive pore wetting (Bougie and Lliuta, 2013); it is therefore asserted that the lower surface tension change measured at 2 $\text{mol}_{\text{NH}_3} \text{ L}^{-1}$ was insufficient to enable complete breakthrough into the lumen side. The role of surface tension in inhibiting both lumen-side crystallisation and wetting was confirmed through the addition of 5 % wt. sodium chloride which counteracted the transition in surface tension introduced by the aqueous ammonia. Whilst the inclusion of NaCl increased surface tension of the aqueous ammonia by only 2.8 mN m^{-1} , a marked increase in CO_2 flux stability was observed (Figure 6.10, Figure 6.11).

Dense PDMS hollow fibre membranes were also evaluated as an approach to diminish lumen side crystallisation observed with micro-porous membranes at high aqueous concentrations, as they prevent absorbent breakthrough due to a lack of micro-pores. Whilst some crystal growth was observed on the shell-side of the PDMS membrane, crystal growth predominated on the lumen-side of the membrane within the gas phase (Figure 6.9). To generate analogous flux rates to those of the

PTFE membrane, a high liquid velocity was used (G/L 0.39) which enhances surface renewal of free ammonia at the absorbent-membrane boundary and hence the potential for ammonia slip. Furthermore, since ammonia is a smaller and more condensable molecule than CO₂, it is more permeable through PDMS (Makhloufi *et al.*, 2014). Consequently co-permeability of both free ammonia and water vapour in the dense PDMS membrane promoted crystal growth within the fibre lumen and within the dynamic free volume network of the rubbery PDMS membrane which induced fibre wall distortion. Wetting and subsequent lumen-side crystallisation can be ascribed to the stretched pore shape of the micro-porous membrane in this study in addition to the surface tension of the absorbent. Stretched pores are a common feature of several commercially available hydrophobic polymeric micro-porous membranes (d/L 0.48, Heile *et al.*, 2014) but was exacerbated within the PTFE fibre studied (d/L 0.065). Franken *et al.* (1987) introduced a pore geometry coefficient (B) to the Laplace-Young equation (4) where non-cylindrical pore shape was classified by a coefficient of between $0 < B < 1$. This emphasises that pore wetting is exacerbated as pore shape tends away from that of a cylinder (Bougie and Lliuta, 2013). Consequently, micro-porous membranes with tighter pore shape together with surface tension regulation of the solvent are recommended to encourage preferential shell-side crystallisation and enhanced CO₂ flux stability in gas-liquid membrane absorption crystallisation reactors.

6.5 Conclusions

The use of microporous hollow fibre membrane contactors has been introduced to enable the nucleation and growth of crystalline reaction products initiated through chemical absorption of CO₂ from a synthetic biogas. This represents the first membrane crystallisation reactor where the solubility limit to initiate nucleation is reached through counter diffusion of solutes from the solvent bulk to the membrane and of solutes from the 'permeate-side' through the membrane micropores into the membrane-solvent boundary. Lumen-side crystallisation can be avoided in favour of preferential shell-side nucleation and more stable CO₂ fluxes by: (1) raising surface tension of the

absorbent through either limiting aqueous ammonia concentration or addition of a surface tension regulator; and, (2) selection of a membrane with a more regulated pore shape than the PTFE membrane used (d/L 0.065) as both actions can diminish solvent ingress into the pore. Although limiting aqueous ammonia concentration will diminish solvent reactivity and CO_2 flux, which suggests a larger process scale, the value ascribed to controlled production of the reaction product must also be weighted. Further refinement is required to ensure that longer term CO_2 flux stability can be ascertained simultaneously with ammonium bicarbonate growth. However, the progressive decline in CO_2 flux with the lower ammonia absorbent concentration was notably a result of wetting rather than interference of shell-side crystal growth. Whilst a high initial aqueous ammonia concentration initiated a large number of nucleation sites, the absorbent ammonia concentration also influenced morphology of crystals formed on the shell-side. Crystals formed within lower absorbent ammonia concentration (and lower CO_2 fluxes) possessed fewer nucleation sites and are characteristic of crystals preferentially grown under low flux conditions to favour growth over nucleation. This represents a potentially favourable characteristic for the continued detachment (and hence recovery) of the ammonium bicarbonate crystals formed, where the low shear stresses applied in continuous MCr have been shown sufficient to enable detachment and downstream recovery of the crystalline product (Di Profio *et al.*, 2010).

Acknowledgments

The authors would like to thank the Engineering and Physical Sciences Research Council (EPSRC, V/N: 08001923), Anglian Water, Northumbrian Water, Severn Trent Water and Yorkshire Water for their financial support, and Markel Corporation for their kind donation of the micro-porous PTFE hollow fibre membranes.

Appendix A – Nucleation model

The likelihood of preferential heterogeneous nucleation of a crystal on the membrane surface can be assessed by comparison of the free energy of this process versus that of the homogeneous alternative:

$$\frac{\Delta G_{het}}{\Delta G_{hom}} = 0.25(2 + \cos\theta)(1 - \cos\theta)^2 \left[1 - \varepsilon \frac{(1 + \cos\theta)^2}{(1 - \cos\theta)^2} \right]^3 \quad A1$$

where ΔG_{het} and ΔG_{hom} are the free energies of heterogeneous and homogeneous nucleation respectively, θ is the contact angle between liquid and membrane surface and ε is the fractional porosity of the membrane (Curcio *et al.*, 2006).

Appendix B – NH₃ depletion model

The model developed by Wang *et al.* (2004) enables estimation of 3 dimensional chemical reactant concentration co-ordinates within the lumen of a hollow fibre, using the diffusivity of CO₂ and chemical reactant, and the reaction rate with CO₂ as inputs. Although originally developed for organic amine solutions, the model can be used for an NH₃ chemical reactant by substitution of the relevant transport and kinetic data (Table 6.B1) (Derks and Versteeg, 2009). The viscosity of water can be calculated as a function of temperature and used to determine the viscosity of NH₃ solutions as a function of both temperature and NH₃ concentration:

$$\eta^{H_2O} = 1.18 \times 10^{-6} \exp\left(\frac{16400}{RT}\right) \quad B1$$

$$\eta^{NH_3(aq.)} = (0.67 + 0.78x_{NH_3}) \times 10^{-6} \exp\left(\frac{17900}{RT}\right) \quad B2$$

where η is the liquid viscosity (Pa s), x_{NH_3} is the mole fraction of NH₃ in aqueous solution, R is the molar gas constant (8.314 m³ Pa K⁻¹ mol⁻¹) and T is temperature (K). These viscosity values can be used in conjunction with the diffusivity of CO₂ in water to determine the CO₂ diffusion coefficient NH₃ solution. The diffusivity of CO₂ in water can be determined as a function of temperature:

$$D_{CO_2}^{H_2O} = 2.35 \times 10^{-6} \exp\left(\frac{-2119}{T}\right) \quad B3$$

where $D_{CO_2}^{H_2O}$ is the diffusivity of CO₂ in the water (H₂O) solvent (m² s⁻¹). Subsequently the diffusivity of CO₂ in NH₃ solution can be calculated:

$$D_{CO_2}^{NH_3(aq.)} = D_{CO_2}^{H_2O} \left(\frac{\eta^{H_2O}}{\eta^{NH_3(aq.)}} \right)^{0.8} \quad B4$$

where $D_{CO_2}^{NH_3(aq.)}$ is the diffusion coefficient of CO₂ in the respective aqueous NH₃ solution. Kinetic data given for reaction between CO₂ and NH₃ at 283.15 was re-assessed for reaction at 298.15 K:

$$k_i = k_{i-283} \exp\left(\frac{A_i}{283.15} - \frac{A_i}{T}\right) \quad B5$$

where k_i is the respective kinetic component and A_i is an associated constant (Table 6.B1). Using these kinetic parameters the rate of reaction of CO₂ (R_{CO_2} , mol m⁻² s⁻¹) upon absorption in to the liquid is calculable:

$$R_{CO_2} = \frac{k_2[CO_2][NH_3]}{1 + (k_{-1}/k_{H_2O}[H_2O]) + (k_{-1}/k_{OH^-}[OH^-]) + (k_{-1}/k_{NH_3}[NH_3])} \quad B6$$

where [CO₂], [NH₃], [H₂O] and [OH⁻] are the liquid phase concentrations of CO₂, NH₃, H₂O and OH⁻ respectively (mol m⁻³). Due to the relatively low concentration of hydroxide in solution this term can be assumed to yield negligible contribution and can be neglected. The transport and kinetic information for CO₂ in a given solution can be used to estimate the liquid phase concentration of molecular CO₂ for any given 3 dimensional coordinate within the fibre lumen (where liquid is fed lumen-side):

$$v_r \frac{\partial C_{CO_2}}{\partial z} = D_{CO_2} \left(\frac{\partial^2 C_{CO_2}}{\partial r^2} + \frac{1}{r} \frac{\partial C_{CO_2}}{\partial r} \right) - R_{CO_2} \quad B7$$

where C_{CO_2} is the liquid phase molecular CO₂ (mol m⁻³), r and z are the radial and axial (fibre width and length) coordinates respectively (m) and v_r describes the parabolic radial velocity profile within the fibre (m s⁻¹):

$$v_r = 2V_L \left[1 - \left(\frac{r}{R_i} \right)^2 \right] \quad \text{B8}$$

where V_L is the superficial liquid velocity (m s^{-1}) and R_i is the inner fibre radius (m). Similarly the liquid phase concentration of NH_3 (C_{NH_3} , mol m^{-3}) can be determined for any given 3 dimensional coordinate within the fibre lumen:

$$v_r \frac{\partial C_{\text{NH}_3}}{\partial z} = D_{\text{NH}_3} \left(\frac{\partial^2 C_{\text{NH}_3}}{\partial r^2} + \frac{1}{r} \frac{\partial C_{\text{NH}_3}}{\partial r} \right) - R_{\text{NH}_3} \quad \text{B9}$$

where R_{NH_3} is the rate of reaction of NH_3 ($\text{mol m}^{-2} \text{s}^{-1}$), assumed to be equivalent to R_{CO_2} for a 1:1 reaction, and D_{NH_3} is the diffusivity of NH_3 within the NH_3 solution. This is a function of solution concentration and was determined for the solutions used in the present study by interpolation of data given for a concentration range up to saturation (Table 6.B1) (Frank *et al.*, 1996). Initial and boundary conditions are given:

$$z = 0, \quad C_{\text{CO}_2} = 0, \quad C_{\text{NH}_3} = C_{\text{NH}_3,0} \quad \text{B10a}$$

$$r = 0, \quad \frac{\partial C_{\text{CO}_2}}{\partial r} = 0, \quad \frac{\partial C_{\text{NH}_3}}{\partial r} = 0 \quad \text{B10b}$$

$$r = R, \quad D_{\text{CO}_2} \left(\frac{\partial C_{\text{CO}_2}}{\partial r} \right) = k_{\text{ex}} (C_{\text{CO}_2g} - C_{\text{CO}_2g,i}), \quad \frac{\partial C_{\text{NH}_3}}{\partial r} = 0 \quad \text{B10c}$$

where $C_{\text{CO}_2, g}$ is the bulk gas phase CO_2 concentration (mol m^{-3}), $C_{\text{CO}_2, g, i}$ is the gas phase CO_2 concentration at the liquid-gas interface (mol m^{-3}) and k_{ex} is the external mass transfer coefficient (m s^{-1}). Interfacial concentration of CO_2 can be determined on the basis of physical absorption under the influence of Henry's law:

$$C_{\text{CO}_2,i} = m C_{\text{CO}_2g,i} \quad \text{B11}$$

where $C_{\text{CO}_2, i}$ is the liquid phase CO_2 concentration at the liquid-gas interface (mol m^{-3}) and m is the liquid-gas partition coefficient for CO_2 equivalent to the dimensionless Henry's constant (0.83 in water at 25 °C). Henry's constants for CO_2 in reactive systems are routinely determined by analogy with that of nitrous oxide (N_2O), which was virtually unchanged from its value in water in NH_3

solutions up to 5 mol_{NH3} L⁻¹. Consequently the Henry's constant for CO₂ in water was assumed applicable in all NH₃ solutions examined presently. The value of k_{ex} can be completely determined by mass transfer resistance in the membrane phase ($1/k_m$) when resistance in the gas phase ($1/k_g$) is zero due to a pure CO₂ gas phase:

$$\frac{1}{k_{ex}} = \frac{1}{k_g} + \frac{1}{k_m} \quad \text{B12}$$

All calculations and subsequent surface plots were executed using the Matlab® software.

References

Atchariyawut, S., Jiraratananon, R. and Wang, R. (2007), "Separation of CO₂ from CH₄ by using gas-liquid membrane contacting process", *Journal of Membrane Science*, vol. 304, no. 1-2, pp. 163-172.

Bougie, F. and Lliuta, M. C. (2013), "Analysis of Laplace-Young equation parameters and their influence on efficient CO₂ capture in membrane contactors", *Separation and Purification Technology*, vol. 118, pp. 806-815.

Budzianowski, W. M. (2011), "Mitigating NH₃ vaporization from an aqueous ammonia process for CO₂ capture", *International Journal of Chemical Reactor Engineering*, vol. 9, Article number A58.

Cheng, W. L., Chen, Z. S., Akisawa, A., Hu, P. and Kashiwangi, T. (2003), "Theoretical and experimental study on surface tension and dynamic surface tension of aqueous lithium bromide and water with additive", *Science in China, Series E: Technological Sciences*, vol. 46, no. 2, pp. 191-203.

Curcio, E., Criscuoli, A. and Drioli, E. (2001), "Membrane crystallizers", *Industrial and Engineering Chemistry Research*, vol. 40, no. 12, pp. 2679-2684.

Curcio, E., Fontananova, E., Di Profio, G. and Drioli, E. (2006), "Influence of the structural properties of poly(vinylidene fluoride) membranes on the heterogeneous nucleation rate of protein crystals", *Journal of Physical Chemistry B*, vol. 110, no. 25, pp. 12438-12445.

Derks, P. W. J. and Versteeg, G. F. (2009), "Kinetics of absorption of carbon dioxide in aqueous ammonia solutions", *Energy Procedia*, vol. 1, no. 1, pp. 1139-1146.

Di Profio, G., Curcio, E. and Drioli, E. (2010), "Supersaturation control and heterogeneous nucleation in membrane crystallizers: Facts and perspectives", *Industrial and Engineering Chemistry Research*, vol. 49, no. 23, pp. 11878-11889.

Di Profio, G., Curcio, E., Cassetta, A., Lamba, D. and Drioli, E. (2003), "Membrane crystallization of lysozyme: kinetic aspects", *Journal of Crystal Growth*, vol. 257, no. 3-4, pp. 359-369.

Drioli, E., Curcio, E., Criscuoli, A. and Di Profio, G. (2004), "Integrated system for recovery of CaCO_3 , NaCl and $\text{MgSO}_4 \cdot 7\text{H}_2\text{O}$ from nanofiltration retentate", *Journal of Membrane Science*, vol. 239, no. 1, pp. 27-38.

Esquiroz-Molina, A., Georgaki, S., Stuetz, R., Jefferson, B. and McAdam, E. J. (2013) "Influence of pH on gas phase controlled mass transfer in a membrane contactor for hydrogen sulphide absorption", *Journal of Membrane Science*, vol. 427, pp. 276-282

Frank, M. J. W., Kuipers, J. A. M. and Van Swaaij, W. P. M. (1996), "Diffusion coefficients and viscosities of $\text{CO}_2 + \text{H}_2\text{O}$, $\text{CO}_2 + \text{CH}_3\text{OH}$, $\text{NH}_3 + \text{H}_2\text{O}$, and $\text{NH}_3 + \text{CH}_3\text{OH}$ liquid mixtures", *Journal of Chemical and Engineering Data*, vol. 41, no. 2, pp. 297-302.

Franken, A. C. M., Nolten, J. A. M., Mulder, M. H. V., Bargeman, D. and Smolders, C. A. (1987), "Wetting criteria for the applicability of membrane distillation", *Journal of Membrane Science*, vol. 33, no. 3, pp. 315-328.

Goh, S., Zhang, J., Liu, Y. and Fane, A. G. (2013), "Fouling and wetting in membrane distillation (MD) and MD-bioreactor (MDBR) for wastewater reclamation", *Desalination*, vol. 323, pp. 39-47.

Heile, S., Rosenberger, S., Parker, A., Jefferson, B. and McAdam, E. J. (2014), "Establishing the suitability of symmetric ultrathin wall polydimethylsiloxane hollow-fibre membrane contactors for enhanced CO₂ separation during biogas upgrading", *Journal of Membrane Science*, vol. 452, pp. 37-45.

Herzog, H. and Falk-Pedersen, O. (2000), "The kvaerner membrane contactor: lessons from a case study in how to reduce capture costs", *In: Proceedings of the 5th International Conference on Greenhouse Gas Control Technologies, Cairns, 13–16 August*.

Li, K., and Tan, X. (2000), "Design of hollow fibre membrane modules for soluble gas removal", *Chemical Engineering Science*, vol. 55, pp. 5579-5588.

Makhloufi, C., Lasseuguette, E., Remigy, J. C., Belaisaoui, B., Roizard, D. and Favre, E. (2014), "Ammonia based CO₂ capture process using hollow fiber membrane contactors", *Journal of Membrane Science*, vol. 455, pp. 236-246.

Ofgem (2014) <https://www.ofgem.gov.uk/publications-and-updates/full-tariff-tables> (accessed 1st September 2014).

Persson M., Jonsson O. And Wellinger A. (2007), "Task 37 – Biogas upgrading to vehicle fuel standards and grid injection", *IEA Bioenergy*, pp 20-21.

Shuangchen, M., Huihui, S., Bin, Z. and Gongda, C. (2013), "Experimental study on additives inhibiting ammonia escape in carbon capture process using ammonia method", *Chemical Engineering Research and Design*, vol. 91, no. 12, pp. 2775-2781.

Thornton, A. (2007), "The Application of Ion Exchange for Ammonium Removal from Municipal Wastewaters", *PhD Thesis, Cranfield University*.

Thurston, R. V., Russo, R. C. and Emerson, K. (1979), "Aqueous ammonia equilibrium – tabulation of percent un-ionised ammonia", *United States Environmental Protection Agency, EPA-600/3-79-091*.

Wang, R., Li, D. F. and Liang, D. T. (2004), "Modeling of CO₂ capture by three typical amine solutions in hollow fiber membrane contactors", *Chemical Engineering and Processing: Process Intensification*, vol. 43, no. 7, pp. 849-856.

Weissenborn, P. K. and Pugh, R. J. (1995), "Surface tension and bubble coalescence phenomena of aqueous solutions of electrolytes", *Langmuir*, vol. 11, no. 5, pp. 1422-1426.

Zeng, Q., Guo, Y., Niu, Z. and Lin, W. (2013), "The absorption rate of CO₂ by aqueous ammonia in a packed column", *Fuel Processing Technology*, vol. 108, pp. 76-81.

Zhang, X., Zhang, P., Wei, K., Wang, Y. and Ma, R. (2008), "The study of continuous membrane crystallization on lysozyme", *Desalination*, vol. 219, no. 1-3, pp. 101-117.

Chapter 7

Discussion

7.1 Discussion

The investigations comprising this thesis have supported the initial hypothesis: *the regulated design and non-dispersive liquid-gas contact of HFMCs, shown to offer excellent specific surface area very high mass transfer, can be applied to biogas upgrading to provide an effective, viable and potentially preferable alternative to existing upgrading technologies in a wastewater treatment context.* The contributions to knowledge comprised in this thesis extend to broad gas absorption applications but also introduce findings that are specific to water utilities. For example, one of the key contributions from the literature review (Chapter 2) was the knowledge transfer from the physical chemistry literature and application to a broad physical gas absorption theme, which enables gas solubilities to be derived from first principle parameters. The parameters introduced, such as G_{cav} , allow for correlation of empirically derived gas solubilities such that the underlying chemistry controlling selective absorption from binary gases can be discussed, where previous absorption literature did not possess the tools to explain this adequately. Whilst this is applicable to a large range of gas separations it is also specifically pertinent to the CO_2/CH_4 separation necessary for biogas upgrading. Whilst the contributions to knowledge have the potential to significantly impact traditional wastewater flowsheets in the future, many of the findings in this thesis possess less grand but more immediately applicable value. To illustrate, the chemically enhanced CO_2 absorption enabled by real ammonia rich wastewaters has the potential to simultaneously make chemical absorption more amenable to water utilities, add value to the inert CO_2 portion of the raw biogas via recovery as ammonium bicarbonate, act as a return liquor treatment via reduction of the ammonia return to the front of the treatment works or totally eliminate the requirement for nitrification. Although significantly increasing the potential benefits of upgrading at WWTWs, the additional requirements of ion exchange and solvent pre-treatment technologies means a complex pathway to implementation. Alternatively the determination that molar concentration of electrolyte can reduce methane slip by 25% versus pure water, without inhibiting CO_2 absorption, is much more readily usable knowledge contribution since secondary effluents comparatively low in electrolyte

concentration are known to currently be applied as the physical solvent during upgrading at WWTW. The contributions to knowledge supplied within this thesis are presented within three key categories that support the practical implementation of HFMCs for upgrading biogas generated during municipal wastewater treatment to biomethane:

1. The practical and operational advantages presented by membrane contactors for biogas upgrading versus traditional scrubbing technology?

Water scrubbing is the most popular method of biogas upgrading and is conventionally performed using random packed columns (Persson *et al.*, 2007; Kohl and Nielsen, 1997). This technology has been scrutinised in the broader gas absorption literature due to common practical problems such as flooding at high solvent flow rate (Q_L) and channelling at low Q_L with subsequent loss of surface area for mass transfer. Investigations of micro-porous hollow fibre membrane contactors (HFMCs) as an alternative demonstrate that their non-dispersive method of contacting and independent fluid flows prevent flooding and maintain a fixed area for mass transfer regardless of Q_L or gas flow rate (Q_G). Additionally, the regulated design of HFMCs typically enables an order of magnitude greater specific surface area than random packed columns (Table 7.1) (Reed *et al.*, 2003).

Table 7.1 Typical specific surface areas for several liquid-gas contactors (adapted from Reed et al., 2003).

Contactor type	Specific surface area $\text{m}^2 \text{m}^{-3}$
Free dispersion columns	3 - 33
Packed/tray columns	33 - 330
Mechanically agitated columns	164 - 500
HFMCs (general)	1640 - 6500
HFMC Liqui-Cel 1.7x5.5 (this thesis)	3618

Comparison of the mass transfer of CO₂ determined in this thesis using a HFMC and DI water as a physical absorbent with data compiled within the literature review adds detail to the known advantages of HFMCs versus packed column technology with respect to process intensification (Table 7.2) (McLeod *et al.*, 2013; Karoor and Sirkar, 1993; Evren and Özdural, 1999; Rixon, 1948). The HFMC data demonstrate up to an order of magnitude greater volumetric mass transfer coefficients than those achieved within the packed columns, particularly for the HFMC data by Karoor and Sirkar (1993).

Table 7.2 Mass transfer and G/L data for CO₂ absorption by water in HFMCs and packed columns.

	CO ₂ partial pressure P_{CO_2} atm	Liquid velocity Q_L $10^6 \text{ m}^3 \text{ s}^{-1}$	Gas velocity Q_G $10^6 \text{ m}^3 \text{ s}^{-1}$	G/L ratio -	Volumetric mass transfer coefficient $k_L a$ 10^3 s^{-1}	References
HFMC	0.4	1.4 – 6.7	4.2	3.0 – 0.63	10.1 – 47.9	McLeod <i>et al.</i> (2013)
HFMC	0.4	0.12 – 1.3	1.3	10.8 – 1.0	130 – 250	Karoor and Sirkar (1993)
Column	0.2	83.3 – 150	1170 – 583	14.0 – 3.9	12.7 – 19.5	Evren and Özdural (1999)
Column	2.2	16,623	5071	0.31	14.0	Rixon (1948)

The $k_L a$ observed for both HFMC studies exceeded the full scale mass transfer recorded by Rixon (1948) whilst operating at consistently superior G/L even with the column operating a pressurised system. Direct comparison between studies is complicated by operational variables, however, direct comparison of HFMCs and packed columns under normalised conditions have confirmed greater $k_L a$ and superior solvent efficiency for HFMCs, where approximately forty times more solvent was required by a column to match the CO₂ removal efficiency of a HFMC (deMontigny *et al.*, 2005; Nii *et al.*, 1992). The superior $k_L a$ of HFMCs is advantageous to water utilities attempting to integrate new biogas upgrading apparatus within existing wastewater treatment assets and infrastructure due to a reduced physical footprint compared to a packed column operating at the equivalent output of biomethane. Also, implementation of large packed columns (or towers) may even be problematic

due to the planning permissions required for tall structures. The substantially greater G/L exhibited by HFMCs will be reflected in a reduced electrical cost for pumping of the water solvent versus a packed column operating under comparable conditions. Furthermore, HFMCs can be orientated horizontally to minimise the pumping head and reduce pressure drop (and therefore pumping energy), whereas packed columns are necessarily vertical due to the gravity fed nature of the solvent input.

A key finding in this thesis was the causal correlation between Q_L and the loss of methane by co-absorption with CO_2 during upgrading, known as methane slip (McLeod *et al.*, 2013). Determination of this mechanism, previously unavailable within the literature, can significantly impact the decision of water utilities to opt for water scrubbing versus chemical scrubbing technologies. Methane slip must be minimised in order to obtain a high yield of upgraded biomethane and restrict the carbon footprint of the upgrading process to maintain carbon neutrality. Water utilities operating upgrading plants are largely dependent upon government subsidy, such as the renewable heat incentive (RHI) in the UK, which can be impacted by methane slip. For example, in Germany, some incentives are only activated below a methane slip of 0.5 % (Wolf and Nettelbreker, 2011). Also, the ordinance on gas network access (gasNZV) only allows access to the natural gas grid if methane slip below 0.2 % is demonstrated (Strauch and Krassowski, 2012). However, the physical absorption of CO_2 in water necessarily demands high Q_L to maximise the liquid controlled mass transfer and permit a feasible process scale, thereby encouraging higher methane slip. HFMCs can better manage this effect due to their greater solvent efficiency compared to packed columns, with a methane slip of 5.2 % observed using a HFMC during experiment. This is only an additional 0.5 % methane slip to that quoted during operation of commercial packed column scrubbers of 4.7 %, although manufacturers commonly quote methane slip of 1-2 % (Patterson *et al.*, 2011). This is possible in packed columns due to the inclusion of abatement technologies, described as crucial to reduce CH_4 losses, which superficially improve the methane slip data for packed column water scrubbers (Läntelä *et al.*, 2012). For example; flash tanks recover dissolved CH_4 in pressured

systems but consume additional energy for re-compression of the flashed gas before re-entering the packed column. Alternatively, any CH_4 in the gas exiting the re-boiler upon desorption can be thermally oxidised to CO_2 , which technically reduces CH_4 emissions but at the expense of biomethane yield and without addressing the causal issue (Wolf and Nettelbreker, 2011). A fairer comparison for the HFMC in the present thesis is a pilot study of landfill gas upgrading using packed column without add-on abatement technologies, where the HFMC and packed column generated comparable methane purity of 85 % and 86.5 % respectively (Läntelä *et al.*, 2012). Methane slip up to 13.1 % was observed using the packed column, approximately 252 % that observed in the present thesis using a HFMC.

2. The benefits of chemical absorption versus physical absorption in water and amenable application for water utilities using membranes?

During absorption using a physical solvent, e.g. water, selective gas absorption is imparted by a combination of solubility, diffusivity and hydrodynamics, as discussed within the literature review. However addition of a chemical reactant to the solvent introduces an additional method for imparting selectivity by preferential absorption of chemically reactive gases (i.e. CO_2) versus chemically inert gases (i.e. CH_4). Upon dissolution the chemical reaction of CO_2 produces highly soluble ionic carbonate species, allowing effective CO_2 absorptive capacity in excess of predictions based on Henry's law, whereas CH_4 solubility remains comparable to that of the pure water solvent. Greater CO_2 solubility corresponds to a greater CO_2 mass transfer potential, allowing a reduction of the process scale necessary to upgrade a fixed Q_G and therefore a lower capital expenditure by scaling down the membrane surface area required. A key finding of this thesis was the mechanism by which chemical absorption can significantly reduce methane slip versus physical absorption. It was determined that a high rate of chemical reaction (using $1 \text{ mol L}^{-1} \text{ NaOH}$) is more efficient at re-establishing the concentration gradient driving force for CO_2 mass transfer compared to physical transport of dissolved CO_2 at high Q_L during physical absorption. Due to an excess of reactive

chemical within the liquid boundary layer, the liquid phase no longer limits mass transfer, allowing CO₂ flux to be maintained at substantially lower Q_L than in pure water. This inhibits CH₄ absorption, which remains liquid phase limited, and thereby reduces slip in the chemical absorbent compared to the DI water physical solvent. HFMCs can maximise the advantage of chemical absorption because they allow precise and responsive Q_L control to consistently allow only the minimum necessary Q_L. Coupled with the high solvent efficiency of HFMCs, chemical absorption substantially reduces methane slip from the 5.2 % observed using DI water to just 0.1 %. This was further lowered to 0.03 % by using a high ionic strength chemical solvent (by addition of 1 mol L⁻¹ NaCl) to further lower physical solubility of CH₄.

A key principle advanced within this thesis was the application of ammonia-rich wastewaters as sustainable chemical solvents within the HFMC. Despite the advantages of chemical absorption, the conventional amines used as chemical reactant (e.g. monoethanolamine, MEA) incur an additional chemical cost, increase the energy demand for reversal of chemical reactions during solvent regeneration and increase maintenance costs due to corrosion. For example, the energy required to upgrade biogas by chemical absorption using amine has been quoted as 1.5 times greater than that for upgrading by water scrubbing (although chemical absorption was lower if methane slip was accounted for) and the annual maintenance costs are quoted as almost 4 times greater for chemical absorption (59,000 € y⁻¹ vs 15,000 € y⁻¹) (Patterson *et al.*, 2011). This dissuades water utilities from adopting chemical absorption, where the current philosophy is to avoid chemically intensive treatments. However, ammonia (NH₃) has received attention as a potential alternative to amines (i.e. MEA) for CO₂ absorption due to its greater loading capacity, reduced corrosive properties and lower energy for solvent regeneration (Yeh *et al.*, 2005; Budzianowski, 2011; Darde *et al.*, 2011). These advantages may be further extended by utilising ammonia-rich wastewaters because water utilities already receive, handle and treat such liquids. For example, return (sludge) liquor possesses ca.1000 g_{NH4-N} m⁻³ whilst ion exchange technology produces regenerant liquids, with concentrations >10000 g_{NH4-N} m⁻³ cited (Mackinnon *et al.*, 2003). Therefore

this presents a unique opportunity for water utilities to capitalise on the advantages of chemical absorption, whilst simultaneously eliminating the cost of chemicals and solvent regeneration. For example, the regeneration of MEA used to upgrade biogas from Minworth wastewater treatment works (WWTW) was estimated to cost 2.2 M£ y⁻¹, whereas the nitrification of NH₄-N is performed already anyway, at a lower estimated aeration cost of approximately 1 M£ y⁻¹.

However, two issues arise from the use of NH₃ derived from wastewater as a chemical absorbent:

1. Low NH₃ concentration – studies using NH₃ chemical absorbents typically use concentration of ca.10 % wt. (100,000 g_{NH3} m⁻³); an order of magnitude above the maximum concentration anticipated from IEX regenerants.
2. NH₃ volatility – transfer of NH₃ in to the gas phase is problematic because biomethane has a low limit of consent for NH₃ content (0.02g_{NH3} m⁻³) (Environmental Agency UK, 2012). Investigations of CO₂ absorption by NH₃ solutions typically use chilled solvent to limit the volatility of NH₃, which adds complexity and additional costs to the process.

The present thesis has demonstrated that these issues can be well managed by using a HFMC as the liquid-gas contacting device. HFMCs have demonstrated highly efficient chemical usage, such that large chemical enhancement may be achieved using relatively low chemical concentration (Esquiroz-Molina *et al.*, 2013). This is because a precise stoichiometric excess of chemical reactant can be maintained within the liquid boundary layer during laminar flow through the hollow fibres, which cannot be similarly managed by random packed columns. Therefore lower chemical concentrations can be used since a lower proportion of unreacted chemical can be lost during the blow-down step of solvent recirculation. Additionally, the solvent efficiency exhibited by HFMC versus column contactors for a water physical absorbent is also exhibited during chemical absorption (deMontigny *et al.*, 2005; Nii *et al.*, 1992). Consequently, in this thesis, CO₂ flux in a synthetic 10000 g_{NH4-N} m⁻³ was chemically enhanced by 25 times that observed in DI water, whilst a real return liquor solution (2325 g_{NH4-N} m⁻³) demonstrated an enhancement factor of 15 and good parity with synthetic NH₃ solutions.

It has also been posited that HFMC are well adapted to minimise NH_3 loss (or slip) by back-transfer from the chemical solvent in to the gas phase (Budzianowski, 2011). Measurement of NH_3 stripping in to the gas phase during the present thesis demonstrated very low volatilisation at the NH_3 concentrations expected from wastewaters ($\leq 10000 \text{ g}_{\text{NH}_4\text{-N}} \text{ m}^{-3}$), with $0.002 \text{ g}_{\text{NH}_3} \text{ m}^{-3}$ in the gas phase. This is a factor of 10 below the limit of consent for NH_3 in biomethane applied to the gas grid, despite non-optimal hydrodynamic conditions. By comparison, a packed column operating with the same NH_3 liquid phase concentration exhibited considerably greater volatilisation in to the gas phase, with approximately $3.5 \text{ g}_{\text{NH}_3} \text{ m}^{-3}$ observed in the gas exiting the column contactor (Niu *et al.*, 2012). Critically this demonstrates that the use of HFMCs can allow water utilities to employ chemical absorption using NH_3 -based chemical solvents of low concentration without the need to pre-chill the solvent or additional post treatment of the upgraded gas, for example by using acid to chemically absorb the gaseous NH_3 .

3. Recovery of the product of reaction between NH_3 and CO_2 during upgrading by chemical absorption impact upon the broader wastewater flowsheet?

The recovery of nitrogen (N) and phosphorus (P) nutrients from wastewater is of increasing interest to water utilities seeking to augment conventional destructive treatment methods due to the rising cost of energy and the anticipation of more stringent limits of consent for discharge in the future. Non-destructive treatment techniques also provide the opportunity to generate value from waste. For example, the recovery of P as struvite can remove > 80 % of dissolved P from return (or sludge) liquor whilst generating a valuable fertiliser product (Britton and Baur, 2010). A key concept developed within this thesis was the recovery of the ammonium bicarbonate (ABC) product of reaction between NH_3 and CO_2 during biogas upgrading. HFMCs can facilitate the recovery of ABC by stimulating heterogeneous nucleation of crystals on the membrane surface. The controllability of the liquid boundary layer in the laminar flow regime enables ABC production to be confined within close proximity to the membrane surface where nucleation is desired. By this method it has been

posited that the local concentration gradients generated could enable nucleation and growth of crystals in solutions below the solubility constant of the crystalline product in the liquid bulk. This mechanism is less feasible in packed column contactors possessing greater turbulent mixing of the liquid boundary layer and the liquid bulk. The flow of NH_3 and CO_2 constituents through a large conventional WWTW are feasibly close to the 1:1 stoichiometry of the ABC product, with figures published for the Minworth WWTW (UK) indicating approximately $0.9 \text{ Mmol}_{\text{NH}_4\text{-N}} \text{ d}^{-1}$ and $1.3 \text{ Mmol}_{\text{CO}_2} \text{ d}^{-1}$. This provides the opportunity to enhance the biogas not just by upgrading but by adding value to the CO_2 'waste' component of the gas due to the potential of ABC as a sustainable fertilizer product, and by lowering or eliminating aeration demand for nitrification by precipitation of dissolved N. This concept could be feasibly applied at differing scales within two scenarios:

1. At a reduced scale for use as a dedicated return liquor treatment, with a lower impact upon the conventional flowsheet but requiring reduced investment and risk
2. At maximum scale, using the entirety of $\text{NH}_4\text{-N}$ available within the flowsheet, with the potential for greater financial reward but requiring significant investment in both membrane and ion exchange (IEX) technology.

The greatest concentration of $\text{NH}_4\text{-N}$ available at conventional WWTW is within the return liquors generated by dewatering of digested sludge, which may contain up to 25 % of the total $\text{NH}_4\text{-N}$ load of the WWTW but contribute only approximately 10 % of the liquid flow (Thornton, 2007). For example, $2325 \text{ g}_{\text{NH}_4\text{-N}} \text{ m}^{-3}$ was determined for the real return liquor used in this thesis. Water utilities are interested in installing dedicated return liquor treatments to eliminate this return of $\text{NH}_4\text{-N}$ to the front of the WWTW and reduce the load upon the activated sludge process (ASP). These include, flow control for dilution, dedicated nitrification/de-nitrification, methanol addition, struvite precipitation, air stripping and a combined Sharon/Anammox process (Table 7.3) (Thornton, 2007).

Table 7.3 Total costs for known return liquor treatments compared to the potential gain by using ABC recovery.

Return liquor treatment	Total cost £ kg ⁻¹ (NH ₄ -N)
Flow control (dilution)	-4.80
Nitrification/de-nitrification	-2.50
Methanol addition	-2.25-2.45
Struvite precipitation	-5.40-9.65
Air stripping	-7.45
Sharon/Anammox	-0.90
	Potential gain £ kg ⁻¹ (NH ₄ -N)
ABC recovery	+0.45

Based upon the G/L for maximum CO₂ flux using return liquor in this thesis, approximately 13 % of raw biogas flow could be upgraded using only the return liquor as a chemical absorbent, with the remainder directed towards conventional CHP. This may be desirable for water utilities seeking to minimise the capital investment for upgrading technology whilst maximising the utility of existing CHP assets. Assuming a 25 % reduction in aeration for nitrification, an increased value for 13 % of the raw biogas due to upgrading and the potential revenue from ABC; a +0.45 £ kg_{NH4-N}⁻¹ gain is presented for return liquor treatment by ABC recovery, approximately 1.7 M£ y⁻¹ in excess of a conventional flowsheet. This is achieved with only an 30000 £ y⁻¹ capital investment for membrane surface area based upon the maximum CO₂ flux determined within this thesis for return liquor (Figure 7.1b), thereby minimising the impact of membrane technology within the overall capital investment for upgrading (including pumps, tanks etc.).

By utilising 100 % of the ammonia available across the entire flow sheet, significantly greater profit might be generated (Figure 7.1a).

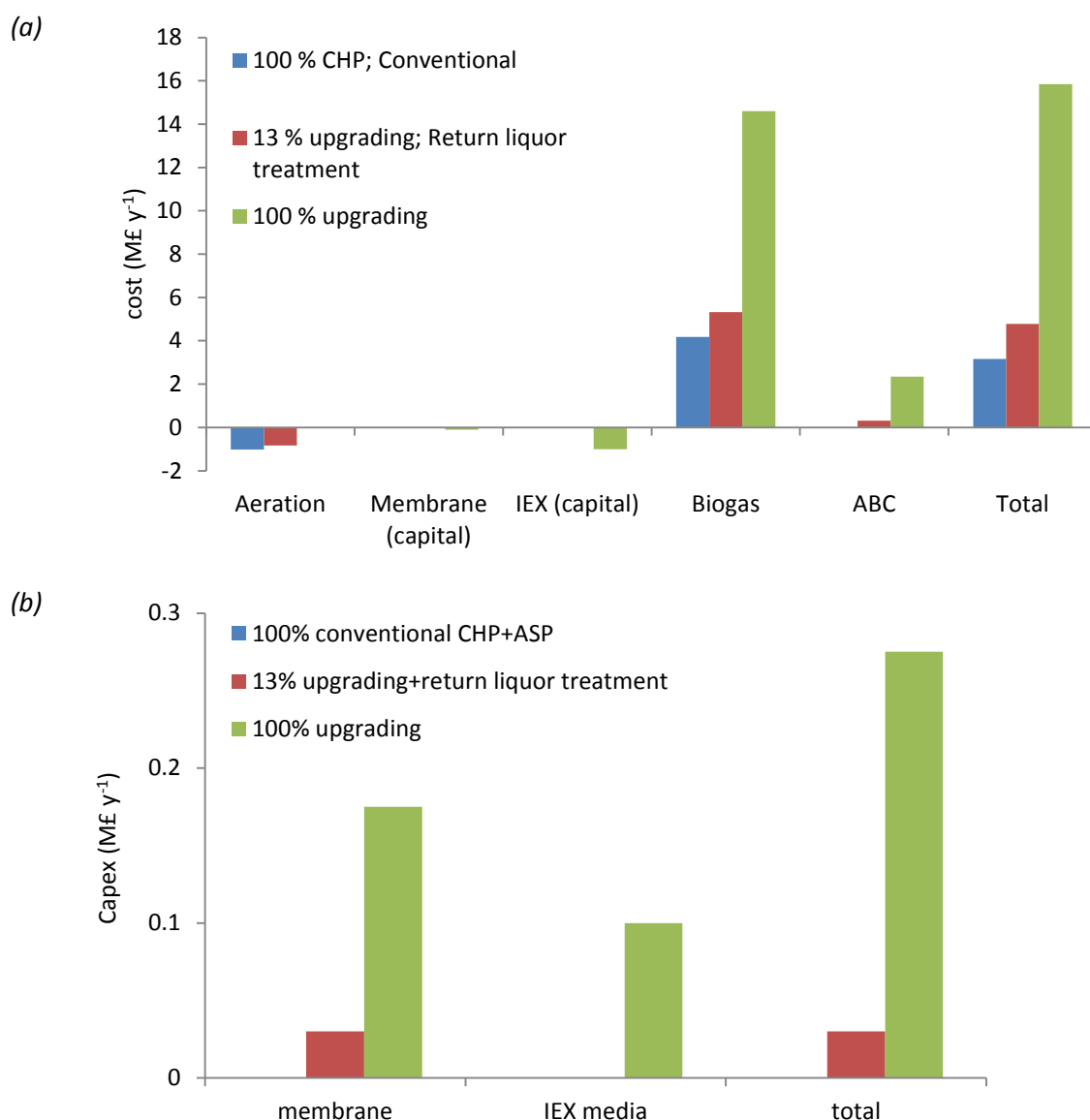


Figure 7.1 Breakdown of key operational (a) and capital expenditures (b) and monetary gains associated with a conventional WWTW with 100 % biogas application to CHP, and hypothetical WWTW with 13 % biogas applied to upgrading for return liquor treatment and 100 % applied to upgrading necessitating investment in ion exchange technology.

Assuming total $\text{NH}_4\text{-N}$ recovery as ABC, the profitability of upgrading + ABC sales + reduced aeration is approximately 250 % greater compared to sole application of biogas to CHP, generating approximately 15.9 M£ y^{-1} (12.7 M£ y^{-1} surplus). This approach has the advantage of fully enhancing the worth of the biogas beyond its direct application as a fuel gas by sequestering the CO_2 component within an intrinsically valuable solid. The 21 % surplus gained versus the conventional flowsheet due to ABC revenue and elimination of aeration for nitrification can act as a sizeable

buffer against the dependency of upgrading upon governmental incentivisation schemes. This would reduce the financial risk and provide protection against changes in the political landscape, which may impact upon the future profitability of biogas upgrading versus CHP. Conversely it is speculated that the ABC itself could become subsidised to promote the production of sustainable fertilisers, due to the high dependency of synthetic nitrogen fertilisers upon fossil fuels. Despite these positives, utilisation of $\text{NH}_4\text{-N}$ across the entire flowsheet presents many foreseeable risks associated with a greater capital investment. It was determined within this thesis that the concentration of $\text{NH}_4\text{-N}$ typical for settled sewage of secondary effluent (ca. $10\text{-}100 \text{ g}_{\text{NH}_4\text{-M}} \text{ m}^{-3}$) was too low for sufficient chemical enhancement of CO_2 , necessitating IEX technology to remove the dissolved $\text{NH}_4\text{-N}$ and provide a more concentrated solvent by regeneration of the exhausted IEX media. The cation exchange capacity (CEC) of $0.54 \text{ kg}_{\text{NH}_4^+} \text{ t}^{-1}$ and cost of common clinoptilolite IEX media (168 £ t^{-1}), under the conditions for Minworth WWTW, were determined from the literature (Aiyuk *et al.*, 2004). Approximately $\text{£}1,000,000$ of capital investment would be required for IEX technology using clinoptilolite at this scale, corresponding to a bed volume of approximately 3000 m^3 . The small process scale of HFMCs is critical here to minimise the feasibility installing a large scale plant in addition to upgrading apparatus. Based upon the flux observed for the IEX regenerant within this thesis ($477 \text{ g}_{\text{NH}_4\text{-N}} \text{ m}^{-3}$) the capital cost for the membrane would be approximately $\text{£}100,000$, corresponding to a single industrial scale HFMC (approximately $1.5 \text{ m} \times 0.6 \text{ m}$). IEX can only be feasible if ABC can be totally recovered from the regenerant, or the efficacy of used regenerant can be otherwise re-established, due to the exorbitant cost of purchasing and disposing of chemicals for single-pass regenerations. In this thesis it was estimated that the cost of sodium chloride (NaCl) and disposal of used regenerant would total approximately 54 M£ y^{-1} , assuming that a fixed regenerant volume could be used twice before a critical loss of efficacy. Within the present thesis, ABC was formed *in situ* on the membrane surface using concentrated synthetic ammonia solutions ($34000 \text{ g}_{\text{NH}_4\text{-N}} \text{ m}^{-3}$ - $85000 \text{ g}_{\text{NH}_4\text{-N}} \text{ m}^{-3} / 2 \text{ mol L}^{-1}$ - 5 mol L^{-1}) but not using return liquor or IEX regenerant, where instead calcium carbonate (CaCO_3) was formed *in situ* upon absorption of CO_2 . This may be

expected based upon bulk NH_3 concentrations due to the high solubility of ammonium salts; however optimisation of the IEX process, including use of higher CEC zeolites could improve the concentration of the regenerant. Alternatively it was suggested during a research and development meeting of several Water utilities that industrial sources of NH_3 , traditionally rejected by municipal waste water treatment works, could be accepted to increase the dissolved concentration and aid preferential ABC crystallisation (Moore, 2013). The suitability of membrane types must be further scrutinised to prevent the gas-side formation of ABC due to pore wetting when using the polytetrafluoroethylene (PTFE) membrane. This was attributed to the relatively large pore size ($> 0.2 \mu\text{m}$) and elongated shape, compared to the smaller ($0.03 \mu\text{m}$) circular pores of the polypropylene (PP) membrane in the commercial contactor where gas-side crystallisation was not observed. It was also observed that wetting could be managed by increasing the ionic strength of the solvent, which presents IEX regenerants as good candidates to inhibit this undesirable phenomenon.

Since even application of 100 % of the biogas to upgrading would necessitate only a single industrial scale HFMC, water utilities may wish to invest in oversized HFMC technology for initial application to return liquor treatment only (using 13 % of biogas flow). This will allow time for further work on IEX technology and for the idea of an ABC subsidy to be clarified to de-risk the 100 % upgrading strategy whilst the upgrading technology necessary to handle 100 % of biogas flow will already have been commissioned.

References

- Aiyuk, S., Xu, H., van Haandel, A. and Verstraete, W. (2004), "Removal of ammonium nitrogen from pretreated domestic sewage using a natural ion exchanger", *Environmental technology*, vol. 25, no. 11, pp. 1321-1330.
- Britton, A. and Baur, R. O. B. (2010), "Phosphorus: A resource in decline", *Journal / American Water Works Association*, vol. 102, no. 9, pp. 117-118.

Budzianowski, W. M. (2011), "Mitigating NH₃ vaporization from an aqueous ammonia process for CO₂ capture", *International Journal of Chemical Reactor Engineering*, vol. 9., Article number A58.

Bujedo, J. and Peterson, P. A. (1997), "Removing Dissolved Oxygen from Ultrapure Water", *Semiconductor International*.

Dang, T., Huntsberger, D. S. and Kitteringham, B. A. (2003), "Using Membrane Contactors for CO₂ Removal to Extend Resin Bed Life", *Ultrapure Water*, July/August, pp. 20-23.

Darde, V., Van Well, W. J. M., Stenby, E. H. and Thomsen, K. (2011), "CO₂ capture using aqueous ammonia: Kinetic study and process simulation", *Energy Procedia*, Vol. 4, pp. 1443-1450.

deMontigny, D., Tontiwachwuthikul, P. and Chakma, A. (2005), "Comparing the absorption performance of packed columns and membrane contactors", *Industrial and Engineering Chemistry Research*, vol. 44, no. 15, pp. 5726-5732.

Environmental Agency (2013), "http://www.environment-agency.gov.uk/static/documents/Revised_Draft_Quality_Protocol_for_biomethane.pdf", pp. 17-18. (accessed 2nd January 2014).

Esquiroz-Molina, A., Georgaki, S., Stuetz, R., Jefferson, B. and McAdam, E. J. (2013) "Influence of pH on gas phase controlled mass transfer in a membrane contactor for hydrogen sulphide absorption", *Journal of Membrane Science*, vol. 427, pp. 276-282

Evren, V. and Özdural, A. R. (1995), "A new technique for the determination of mass transfer coefficients in packed columns for physical gas absorption systems", *The Chemical Engineering Journal and The Biochemical Engineering Journal*, vol. 57, no. 1, pp. 67-71.

Karooor, S. and Sirkar, K. K. (1993), "Gas absorption studies in microporous hollow fiber membrane modules", *Industrial and Engineering Chemistry Research*, vol. 32, no. 4, pp. 674-684.

Kohl, A. and Nielsen, R. (1997), "Gas Purification, Fifth Edition", *Gulf Publishing Company*.

Läntelä, J., Rasi, S., Lehtinen, J. and Rintala, J. (2011), "Landfill gas upgrading with pilot-scale water scrubber: Performance assessment with absorption water recycling", *Applied Energy*, vol. 92, no. 1, pp. 307-314.

Mackinnon, I.D.R., Barr, K., Miller, E., Hunter, S. and Pinel, T., (2003), "Nutrient removal from wastewaters using high performance materials", *Water Science and Technology*, vol. 47, no. 11, pp. 101-107.

McAdam, E. J., Lüffler, D., Martin-Garcia, N., Eusebi, A. L., Lester, J. N., Jefferson, B. and Cartmell, E. (2011), "Integrating anaerobic processes into wastewater treatment", *Water Science and Technology*, vol. 63, no. 7, pp. 1459-1466.

McLeod, A., Jefferson, B. and McAdam, E. J. (2013), "Quantifying the loss of methane through secondary gas mass transport (or 'slip') from a micro-porous membrane contactor applied to biogas upgrading", *Water research*, vol. 47, no. 11, pp. 3688-3695.

Moore, A., Northumbrian Water, 9th December 2013, *Cranfield University*.

Nii, S. and Takeuchi, H. (1992), "Removal of CO₂ by gas absorption across a polymeric membrane", *Journal of Chemical Engineering of Japan*, vol. 25, no. 1, pp. 67-72

Niu, Z., Guo, Y., Zeng, Q. and Lin, W. (2012), "Experimental studies and rate-based process simulations of CO₂ absorption with aqueous ammonia solutions", *Industrial and Engineering Chemistry Research*, vol. 51, no. 14, pp. 5309-5319.

Patterson, T., Esteves, S., Dinsdale, R. and Guwy, A. (2011), "An evaluation of the policy and techno-economic factors affecting the potential for biogas upgrading for transport fuel use in the UK", *Energy Policy*, vol. 39, no. 3, pp. 1806-1816.

Persson M., Jonsson O. And Wellinger A. (2007), "Task 37 – Biogas upgrading to vehicle fuel standards and grid injection", *IEA Bioenergy*, pp 20-21.

Reed, W. B., Semmens, M. J. and Cussler, E. L. (1995), "Membrane contactors", in *Membrane Separations Technology Principles and Applications*, Elsevier.

Rixon, F. F. (1948), *Transactions of the Institute of Chemical Engineers London*, vol. 26, pp. 119-130.

Rooksby J. (2007), "Guidance for the Treatment of Landfill Leachate", *Environment Agency*, Chapter 2, pp. 39.

Strauch, S. and Krassowski, J. (2012), "Overview of biomethane markets and regulations in partner countries"
www.greengasgrids.eu/fileadmin/greengas/media/Downloads/Documentation_from_the_GreenGas_Grids_project/120529_D2_2_Overview_of_biomethane_markets_rev1.pdf (accessed 26th February 2014).

Thornton, A. (2007), "The Application of Ion Exchange for Ammonium Removal from Municipal Wastewaters", *PhD Thesis, Cranfield University*.

Wolf M. and Nettelbreker, U. (2011), "Method for Biogas Treatment and Biogas Installation", *United States patent Application publication*, US20110245572.

Yeh, J. T., Resnik, K. P., Rygle, K. and Pennline, H. W. (2005), "Semi-batch absorption and regeneration studies for CO₂ capture by aqueous ammonia", *Fuel Processing Technology*, vol. 86, no. 14-15, pp. 1533-1546.

Chapter 8

Conclusions and further work

8.1 Conclusions

The unique non-dispersive liquid-gas contact facilitated by HFMCs, in addition to a highly regulated design, present several key advantages applicable to biogas upgrading at wastewater treatment work (WWTW). Many of these advantages relate to the ability of HFMCs to manage methane slip. This is critical since the largest financial benefit of the wastewater flowsheets proposed within this thesis is the value of the upgraded biogas, with the potential recovery of ammonium bicarbonate (ABC) and subsequent reduction in aeration for nitrification contributing secondary benefits.

It is determined in this thesis that methane slip is maximised as liquid flow rate (Q_L) is increased and it is also known that HFMCs operate using a greater liquid efficiency compared to column technology. This suggests that methane slip can be reduced by simple substitution of the basic absorption technology from conventional water scrubbers to HFMCs. This was demonstrated by the comparable methane slip for the HFMC using water as a physical solvent (5.2 %) to that quoted for commercial water scrubbers ostensibly operating with additional slip abatement technologies (i.e. flash tanks). It was shown that methane slip is significantly inhibited by the low Q_L permissible under the gas-phase controlled CO_2 mass transfer facilitated by chemical absorption. The novel use of ammonia-rich wastewaters are presented as alternative chemical solvents that are more amenable to water utilities that have rejected conventional amine scrubbers in favour of physical absorption using water. HFMCs provide the opportunity to maximise the potential of these novel wastewater chemical solvents. For example; an exceptionally low back flux of volatile NH_3 in to the biogas was observed using a HFMC at concentrations pertaining to wastewater, in stark contrast to studies of packed columns using comparable NH_3 concentrations, thereby preventing the need for post-conditioning of the gas phase or pre-chilling of the ammonia solvent that would likely increase both capital and operational expenditures.

Although the greatest proportion of the potential value affiliated with biogas upgrading is associated with the generation of biomethane, it is proposed in this thesis that recovery of ABC can have sizeable additional benefits across conventional wastewater flowsheets. It was proposed that

HFCs can provide the unique opportunity to preference the recovery of ABC, even in the presence of cations offering products with greater thermodynamic stability, by manipulation of concentration gradients within the liquid boundary layer. Demonstration of this hypothesis was impeded by membrane wetting by the synthetic ammonia solutions, however solutions to this problem were provided such that this proposal may be further examined. Recovery of ABC would be an attractive prospect to water utilities not only because of the intrinsic worth of ammonium salts as fertiliser products, but also due to the reduction in aeration for nitrification. This additional source of revenue (approximately 26 % of the additional value due to biogas upgrading versus conventional flowsheets with application of biogas to CHP alone) can act as a substantial buffer to the risk of changes to governmental subsidy that presently makes biogas upgrading viable for water utilities in the UK. This would also improve the resilience of wastewater treatment itself since a large demand upon the biological processes is alleviated, allowing suitable treatment even in the event of shock loads or during very low temperature conditions.

8.2 Further work

Several key areas from this thesis have been identified that would most benefit from further work to produce the most valuable development of biogas upgrading at WWTW.

- Can pre-treatments of return (sludge) liquor be effectively developed/implemented to prevent rapid fouling of the membrane by organic contaminants and how would this additional cost compare to the capital investments required to provide ion exchange regenerants, which did not so rapidly foul the membranes?
- To what extent does the greater buffering capacity of hard waters (high calcium carbonate, CaCO_3) increase the chemical cost of the pH swing necessary to maximise chemical enhancement using real wastewater solvents and to what extent does this detrimentally affect economic viability?

- Which method is the most cost effective to reduce the buffering capacity of wastewaters and minimise the issue of chemically intensive pH swing? CO_2 degassing is known to be able reduce the acidity but may require additional assets, whilst a simple substitution of NaOH for $\text{Ca}(\text{OH})_2$ to perform the pH swing may precipitate out the bicarbonate/carbonate acidity as CaCO_3 .
- To what extent can the prospects of biogas upgrading using wastewater solvents and ABC formation processes devised and discussed in this thesis be improved by the provision of more concentrated industrial sources of ammonia?
- To what extent can gas-phase limited mass transfer be further imposed by low Q_G during CH_4 degassing to maintain simultaneous high removal efficiency and maximum CH_4 concentration within the recovered gas using full scale HFMC designs, where the sweep gas is fed through the fibre lumen and shell-side spacers and baffles force total contact membrane with the liquid?
- Can the problem of wetting by ammonia solutions be completely prevented whilst using micro-porous membranes to allow examination of the concept that concentration gradients within the liquid boundary layer can be manipulated to produce ABC product in the presence of competition with other cations and even below the solubility product of ABC in the liquid bulk.